FREQUENCY AND TIME DOMAIN MOTION AND MOORING ANALYSES FOR A FPSO OPERATING IN DEEP WATER

BY

TAI-PIL HA

A THESIS SUBMITTED

FOR

THE DEGREE OF DOCTOR OF PHILOSOPHY

SCHOOL OF MARINE SCIENCE AND TECHNOLOGY
FACULTY OF SCIENCE, AGRICULTURE AND ENGINEERING
NEWCASTLE UNIVERSITY

2011

ABSTRACT

An investigation on the motion responses of a Floating Production, Storage and Offloading (FPSO) vessel moored in irregular waves has been carried out based on both frequency- and time-domain approaches. In the frequency-domain approach a three-dimensional panel method was employed in order to calculate the first-order hydrodynamic forces and moments such as added masses, potential damping and wave excitation forces and moments and of the resulting the first-order motions and mean second-order forces and moments on the vessel in six degrees of freedom behaviour. A spectral analysis was carried out in order to estimate both the significant and the extreme values of the first-order motions. Additionally Pinkster's approximation was used to find the mean-square values of slow drift motions, in order to calculate wave-induced extreme excursions and the resulting tensions on the mooring lines of the vessel.

Two different methods were used in the time-domain approach for undertaking a mooring analysis. One method used a fast practical time-domain technique that calculates the first-order motion responses in random waves based on the frequency-domain response amplitudes and simulated seas, and also solves the uncoupled second-order motion responses of the FPSO induced by second-order forces, based on Newman's approximation in irregular seas. The other method is by solving six coupled equations of motion based retardation functions transformed from potential damping for the FPSO and induced by the first-order and second-order wave excitations in random seas. The results of the wave-induced extreme excursions and the mooring line tensions obtained by means of the frequency- and time-domain methods are compared and discussed.

As the selected FPSO is operating in deep water, the effect of the mooring line inertia may be significant. The equations of motion of line dynamics were formulated and numerically solved to investigate the importance of line dynamics for deep water mooring. Comparisons between the results of the line tensions both with and without the effects of line dynamics are made and discussed.

CONTENTS

LIST OF FIGURES

LIST OF TABLES

NOMENCLATURE

A_{ii}	Added mass of the vessel in the ii direction
A_w	Water plane area
$\overline{BM_L}$	Metacentric radius
C	Restoring coefficient
C_C	Critical damping
C_D	Drag coefficient
C_i	Mooring stiffness in i direction
F_i^{moor}	Force in the i-th mooring line
F_i^{wave}	First order wave force
$F_i^{(1)}$	Wave exciting force in the i-th motion
$F_i^{(2)}$	Second-order force in the i-th motion
F_2^{SV}	Slowly varying drift force
F_{V0}	Vertical external force
GM_L	Metacentric height in the longitudinal direction
GM_T	Metacentric height in the transverse direction
H_S	Significant wave height
I_{ii}	Moment inertia of the vessel in the ii direction
I_{WA}	Moment of inertia of the water plane area
I_Z	Mass moment of inertia of the vessel about z-axis
K_{kj}	Retardation function in k-direction due to the motion in the j-direction
L	Length of vessel
MTA	First-order motion R.A.O
MTP	First-order motion phase angle
M_{ii}	Mass of the vessel in the ii direction
N	Number of responses in a given storm
N_W	Wave making damping
N_V	Viscous damping

P	Annual probability that the event will not occur
RAO	Response amplitude operator
$S(\omega)$	Wave spectrum density
S_{Fj}	Spectral density of the low frequency drift force
S_{ω}	ITTC wave spectrum
T	Mean time period
T	Duration of storm in hours
T_{draft}	Draught of the vessel
T_H	Horizontal mooring forces applied at the attached point to the vessel
T_V	Vertical mooring forces applied at the attached point to the vessel
T_{max}	Maximum tension of the mooring line
TT_n^{ii}	Natural period of motion in the ii direction
VCG	Volume centre of gravity
X	Horizontal distance of the total mooring line
Z	Vertical distance of the total mooring line
a_m	Wave amplitude at m-th frequency
$b_{breadth}$	Breadth of the vessel
c_{ii}	Restoring coefficient due to the mooring lines in the ii direction
d	Damping ratio
g	Gravitation constant
h	Depth of the water
m_0	Area of response spectrum
m_2	Second moment of the area of response spectrum
k	Stiffness
k_{ii}	Restoring coefficient due to the fluid pressure in the ii direction
k_{θ}	Pitch restoring moment coefficient
k_m	Wave number
k_{xx}	Radius of gyration about x-axis
k_{yy}	Radius of gyration about y-axis

ℓ	Total mooring line length
$\ell_{\min}$	Minimum length of the mooring line
ℓ_S	Wetted mooring line length
n	Platform life in years
x	Horizontal distance of the wetted mooring line
x_i	Coordinates of the attach point for x-axis
y_i	Coordinates of the attach point for y-axis
z_b	Centre of buoyancy
Δ	Displacement of the vessel
∇	Volumetric displacement of the vessel
α	Phase angle relative to the wave
$\alpha_1(x, y, z, \omega)$	Phase angle in the first order motion
β	Heading angle
λ_{kj}	Damping coefficient in k-direction due to the motion in the j-direction
μ_{ij}	Frequency independent added mass coefficient
ξ	Motion response amplitude operator
$\xi_j^{(1)}(x, y, z, t)$	First order motion of vessel in the j-direction
$\xi_j^{(2)}(x, y, z, t)$	Second order motion of vessel in the j-direction
$\xi_1(x, y, z, \omega)$	1st order motion amplitude
ρ	Density of sea water
σ_x^2	Mean square value of the motion
ε_m	Phase angle on m-th frequency
ε_n	Phase angle on n-th frequency
$\zeta(x, y, t)$	Wave elevation
ψ_i	Angle of a mooring line about x-axis
ω_m	Circular frequency
ω_m	Wave frequency in m-th
ω_n	Natural frequency

ACKNOWLEDGEMENTS

I would like to thank my supervisor Dr. Hoi Sang Chan for his excellent encouragement, valuable advice and continuous instruction throughout the course of this research. I could not complete my work successfully without his great comments.

I also want to thank Prof. Atilla Incecik for his motivation about mooring analysis.

I appreciate Mr. John Garside for his assistance for proofreading from his plentiful experience.

I am thankful to Prof. Seung-Keon Lee in the Department of Naval Architecture and Ocean Engineering of Pusan National University for his guidance to study on the motion analysis of the floating structure while I was master course.

I am greatful to Dr. Yoo Kim for her good counsel.

I would like to express gratitude for my parents Mr. Kyu Yong Ha and Mrs. Young Do Lee, my brother Mr. Tae Hark Ha for their patience with constant support.

DECLARATION

EXCEPT WHERE REFERENCE IS MADE TO THE WORK OF OTHERS,
THIS THESIS IS BELIEVED TO BE ORIGINAL

CHAPTER

1

Introduction

1.1 General Overview

The oil and gas production industry was grown due to the increasing demand for energy and this trend is expected to continue in the future for decades. The demand for oil and gas is proportional to the size of population and growing economy. United Nations forecasted that the world population will be increased up to eight billion by the year 2025. The coming quarter of the century will have more increased industrial development than any earlier period. The world consumption of oil is currently at about more than 75 million barrels of oil daily. However future consumption will be increased continuously due to the national development in both industrially advanced nations and in developing countries. Technical development make it possible to produce oil and gas on deeper off-shore sites which will be discovered in order to take advantage of the energy from a new or the abandoned area of otherwise difficult access today. The deep water development is likely to be indispensable to oil and gas production. Deepwater is said to be about 400~1500m while ultra-deepwater is about 1500~3000m normally. The deep water technical developments have evolved with the increase of the depth year by year gradually. The recorded water depths of the recent FPSO operations are 1,290m in 2002 (Brazil by BP), 1,350m in 2006 (Capixaba by BP), 1,462 in 2008 (Agbami by Chevron) and a water depth of 1,780m is supposed to be developed in 2010 (Parque das Conchas by Shell). FPSOs are adequate for the deep sea operations with a large capacity and flexible in order to disconnect the turret and mooring lines in extreme harsh environmental conditions. However, the accurate prediction of their motion responses to waves is indispensible for FPSOs in safe operational purposes.

The number of the offshore developments is more than hundred sites in the water depth of deep and ultra deep water in recent years. There are many in the fields off the UK, Ireland and Norway. For the new UK fields normally the water depth is between 400-600m while for the

fields offshore Ireland depths can be more than 1500m. In West Africa there are six deep water areas (West Africa transform margin, 2 areas in Niger delta, Gabon, Lower Congo Basin, Angola) in the water depth of 1800-3000m and in US Gulf of Mexico there are more than 180 sites where the water depth is over 500m. The current sites of ultra deep water are mostly in Brazil and the US Gulf of Mexico. The reservoir of oil in those deep water sites (US, Norway, Brazil, West of Shetland, West of Africa) is estimated at more than 40 billion barrels of oil. More than 200 billion barrels of oil are expected in the case that the reservoirs of ultra deep water sites (West of Ireland, the Caspian Sea, Falkland Islands, Alaska, Canada's arctic waters, Sakhalin Island waters, Norway's & Russia's Barent sea) are added to the amount in the deep water sites. The development of the ultra deep water sites will be significant operations. There are many developing methods for each water depth range. The conventional platforms are used for the water depths under 450m, such as bottom mounted steel space frame jackets and concrete gravity platforms. There are about 7,000 conventional platforms in the world and roughly 90 percent of them are small steel jackets under the water depth of 75m and only 10 percent are fixed bottom structures over a water depth of 75m. However several other platforms for deep water are beneficial for each purpose. FPSOs (Floating Production Storage and Offloading Systems) are used for the mobile systems and the oil production facilities in a limited area on far operating sites at sea. FPSOs are particularly advantageous for marginal oil fields, avoiding the need for pipelines, etc. FPSOs have the advantages of the unified storage and offloading system, relatively low cost, shorter lead time in conversion and reusability. The system of FPSOs has the potential to provide an important role for the development of deep water production in a water depth range of 150-1500m.

1.2 Deepwater Mooring Systems

The use of floating platforms has been increased to produce oil and gas for recent decades. Most of these floating systems are moored by cable and chain lines having a catenary form. Safe mooring systems thus become important in proportion to the use of floating vessels for the production. The wave-induced motions of a moored FPSO must be considered in deep water conditions.

The development of the ocean resources, oil and gas, is progressing lively according to the exhaustion of the natural resources recently. This trend will be continued to the exploitation of the deep and ultra-deep water in future. The floating ocean structures, FPSOs, have a vessel form

for the operation and storage with the mooring line systems in place in order to keep the position in an operational area. This floating production and storage offloading unit requires a long time operational period, thus both estimates and analyses are very significant for the motion responses of the FPSO due to the wave environmental loads from a working point of view. The design and analysis of the installed mooring systems are also very important field for the keeping positions with respect to the safe operation. Therefore, the wave forces and the motion analysis of a floating structure have become the centre of interest in the department of the ocean engineering in order to meet certain design criteria for mooring systems. Furthermore, the slowly varying surge, sway, and yaw motions of the moored FPSO in deep water caused by wave drift forces need to be estimated in a mooring analysis since they are significant and occur at the natural frequencies of the FPSO in these modes.

The quasi-static approach has been taken as the most suitable approach for the mooring arrangement design application. The basic principle of the quasi-static design approach assumes that mean drift forces are accounted for as static loads leading to a mean quasi-static displacement where the mooring system is balanced to equilibrium condition. Figure 1.1 illustrates the mooring arrangement for the selected FPSO Schiehallion, which is a very large vessel of its type in the world.

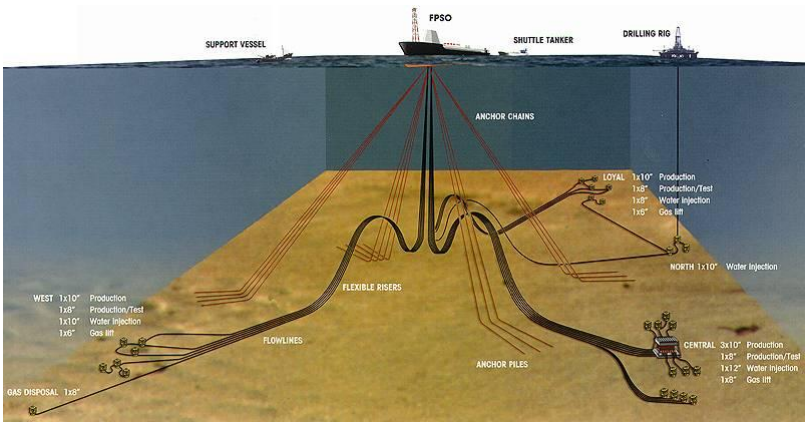

Figure 1.1 Layout of mooring lines connected to the FPSO

The maximum mooring line loads due to the first-order and second-order motions have to be kept below the minimum breaking strength of the mooring components for operations in the safe condition. The required safety factors are dependent upon the various loaded conditions of the vessel and the other adjacent offshore structure as well as allowing implicitly for various uncertainties in the calculation processes, etc. Mooring analysis is carried out in order to optimize the mooring system and to prevent excessive lateral motions of the vessel. The mooring

system should limit vessel motions without leading to a failure of the lines themselves.

The dynamic responses of mooring lines to the excitations of deep water offshore platforms can be important in the case that the water depth is deep and the floater which is connected to the mooring line is relatively small against the effect of the mooring lines regarding to added mass and damping.

1.3 Literature Review and Present Position

A floating body is considered to be rigid and oscillating sinusoidally with small amplitude in six degrees of freedom due to small incident waves. The wave-body interaction problem can be decomposed into a radiation and a diffraction problem in condition that the fluid flow is assumed to be incompressible and irrotational so that velocity potential exists (Newman 1977).

The radiation problem leads to the calculation of hydrodynamic coefficients such as added masses and damping in the frequency domain while the diffraction problem leads to the computation of the first-order wave excitation forces and moments at different wave frequencies. The unknown velocity potentials of radiation waves due to the motions of the oscillating body in calm water and of diffraction waves due to the fixed body attacked by incident waves may be sought by means of source distribution method (Faltinsen 1990). Then, the equations of motion can be solved to obtain the response amplitude operators RAOs in the frequency domain. Furthermore, the second-order forces and moments on the floating body can be calculated by means of direct pressure integration method (Pinkster 1979).

Although computer simulation is now used widely for the motions analysis of floating structures, there is a difference in the output among many of the programs. The results of surge and sway motion of a semi-submersible obtained from these programs show a small deviation in values while the heave, roll and pitch motion results show a large scatter (ITTC 1984). A good correlation can be found in the motions of surge and sway while not so for other motions and also force calculations in the case of a tension leg platform (ISSC 1985). The comparisons of the first and second order forces obtained from 23 different institutions (Floating Production Systems Report 2000) show that the results of the first-order forces and added-mass for a turret moored ship are better than those for a deep draft floater. The damping values are in poor agreement in both the ship and floater. The calculated results of the second-order different frequency forces are scatter among all of the different programs.

Despite poor correlations shown between the results obtained from in different programs, we may use a validated computer software for the motions analysis of the floating offshore structures because it is considered that these different results are not due to the hydrodynamic theory but attributable to inaccurate modelling.

The frequency domain analysis is an attractive approach due to its efficiency while the linearised frequency domain analysis is not expected to be as accurate as the time domain analysis since resonant nonlinear second order responses can be considerable and result in geometric nonlinearities of the lines (Low and Langley 2006).

The stiffness of the mooring lines affects the natural periods of the horizontal motions of a floating structure and its slow drift motions, while wave frequency motions are little affected by mooring loads. Thus, the mean, low and wave frequency motion responses can be decoupled in the frequency domain analysis (Luo et al 2003). The motions of a moored FPSO in irregular waves can be considered as a combination of the first order wave induced motion and a second order low frequency motion. The first order wave force is applied in the time domain equations of wave frequency motion, in which the added mass matrix is calculated at infinite frequency, and the velocity term is argued with retardation function. The retardation function is the influence of the memory effect on the free-surface and it can be found with the cosine transform of damping coefficient in the frequency domain (Oortmerssen 1976). On the other hand, the second order low frequency motion may be sought by solving uncoupled equations of motion induced by second order forces and moment in surge, sway and yaw modes. The effects of low frequency damping from mooring lines on slow drift motions may be significant while the wave frequency damping is negligible at the natural periods of the slow drift motions. However, the effects of damping and stiffness due to mooring lines in this kind of time domain analysis are still linear if the mooring lines are not coupled to the body to account for changes in position and shape of the mooring lines. Fully coupled time domain simulations need many approximated methods in order to consider the coupling effects of mooring lines on the motions of floating systems in a cost efficiency manner (Ormberg and Larsen 1998). Several of these methods incorporate the dynamic influence of the lines as equivalent linear inertia and damping coefficients in a time domain analysis (Senra et al 2002).

FPSO motions can be large due to extreme wave excitations on its large hull body and are also sensitive to wave directions to the vessel. A turret mooring system is usually employed in FPSOs sited in harsh environments for its ability to allow the FPSOs to weathervane into the

least loading while spreading mooring system cannot.

A static mooring analysis is considered to be beneficial in order to find the static offset of a floating unit caused by environmental forces such as the first and second-order forces from irregular waves. However, the dynamic features cannot be considered in this method as added mass and damping effects are absent. The static analysis ignores the effect of line dynamics that may be significant when the inertia is important in the mooring line (DNV 1996).

If the natural frequencies of horizontal motions of a moored vessel are away from the frequency range of the wave exciting forces in the mooring system, the dynamic motion of the mooring lines can be negligible and then the lines are thought to be responding statically to the motions of the vessel. In this condition, the resulting maximum line tensions can be found as the motion responses of the vessel are thought to be employed in the static catenary mooring system within a quasi-static analysis approach (Ansari 1980, Schellin et al 1982). Although the quasi-static method is generally applicable for the analysis related to the frequency domain or time domain, this method disregards the effect of line dynamics and that is particularly important for the realistic behaviour of the mooring line motions as it becomes significant when the line inertia is important. This is clearly important in deep water systems. In the approach for the mooring line dynamics, the motion equations of the line dynamics are formulated and numerically solved in order to decide the tension-displacement characteristics and these can also be used as non-linear restoring forces in the motion response analysis of the moored vessel (Ansari and Khan1986).

The coupled time domain analysis is adequate when mooring lines have a significant influence to the motion responses (Luo and Baudic 2003). Kim 2004 considered the motion responses of a FPSO coupled with mooring line dynamics and found that the dynamic mooring tension can be underestimated with truncated mooring system when mooring dynamic effects are significant. The mooring line damping can also be significantly underestimated depending on the level of mooring-line truncation. In mooring tension spectra, slowly varying components are generally greater than wave-frequency components, and therefore, the mooring lines behave mostly in a quasi-static manner. It is why the discrepancy was not so large in that case. In the case of semi-taut mooring system, greater dynamic effects are expected (Kim et al 2004), which may result in greater error in dynamic mooring tension measurement with truncated mooring system. The above argument can be observed in the mooring-tension spectra, where the taut-side mooring has negligible wave-frequency component, while the slack-side mooring has

appreciable wave-frequency component. Therefore, dynamic effects are less important in taut side.

The coupling effects between the mooring line dynamics and the behaviour of the moored floater can be negligible for the wave frequency motions in the case of a FPSO which has a large displacement with low frequency damping effects on the coupling. However, Cozijn and Bunnik 2004 argued that these coupling effects can be significant for small water plane area floaters such as Catenary Anchor Leg Mooring (CALM) buoys as dynamic behaviour of the mooring lines affects the inertia and damping for the CALM buoy. They found that the fully dynamic coupled simulations with interaction between the CALM buoy motions and the dynamic mooring line loads show better agreement with experiments for the buoy motions than the quasi-static simulations in which only the nonlinear static restoring force from the mooring system was considered. The dynamic mooring line loads were found based on a lumped mass method.

Although the static influence of mooring lines upon the wave frequency motions of a large displacement floating structure is not significant, the motions of the floating structure do affect the dynamic responses of mooring lines. Hence, the dynamic analysis of mooring lines is usually separated from the motion analysis of moored floating structures. Most popular methods used in the line dynamic analysis are the finite element method (Skop and O'Hara 1969) and the lumped mass method (Nakajima et al 1982). Furthermore, the line dynamic analysis can be carried out either in the time domain or in the frequency domain. All nonlinear terms such as stretching and shape deformation and damping are properly accommodated in the time domain analysis based on either the finite element method or the lumped method, whereas they are approximated by equivalently linearised ones in the frequency domain (Low and Langley 2006).

The dynamic behaviour and tension of multi-component mooring lines subjected to forced oscillation at their upper end were studied by Nakajima et al (1982) using a lumped mass method, which takes into account the elastic deformation and viscous drag damping of the mooring lines. Good correlations between numerical and experimental results of dynamic tensions on different configurations of mooring lines were found. This development could be applied for the dynamic analysis of various types of mooring line arrangements A time domain simulation for the dynamic analysis of mooring lines in irregular waves can be produced based on this method.

In this research, the feature of a turret moored FPSO, weathervane, was not considered and thus any fishtailing effect will not be taken into account for the motion responses of the selected FPSO. This limitation may give rise to an unrealistic behaviour of a FPSO, However, this typical

analyses of vessel's motions and mooring line tensions at a particular wave direction are valuable for the academic purpose to investigate how the mooring systems are influenced by environmental forces which lead to different resulting motions of a FPSO and tensions of a moored line.

1.4 Objectives of Current Research

The aim of the thesis is to develop overall system design tools for deep water offshore moored platforms. This research will take into account the response analysis of deep water offshore platforms to waves for the performance, behaviour and the integrated technology of the overall design.

Therefore, the objectives of the present study are

- To develop modelling and analysis programs making possible more accurate assessment of motion response caused by external environmental wave forces and meeting the needs for the development of deep water offshore platforms in the interests of both the accurate estimation of the overall motions and of the mooring line tensions as necessary for the safety of FPSO vessels.
- To investigate and compare the motions of a turret moored FPSO predicted by the frequency domain method and time domain simulations.
- To investigate and compare the tensions of the mooring lines estimated by the frequency domain analysis and time domain simulations with and without line dynamics.

It is to be noted that wind loading and current effects are not included in this study. This research will contribute to not only the extensive use of the marine energy but also to the development of the marine industry.

1.5 Selection of FPSO Example and Approach

The FPSO vessel selected for the present study, shown in Figure 1.2, is the Schiehallion FPSO moored by wire/chain mooring legs in a water depth of 395m and located at the Schiehallion oil

field in the north east Atlantic ocean. The total recoverable reserves of Schiehallion oil field was estimated at approximately 425 million barrels and discovered in 1993. The FPSO Schiehallion is 245m long with a fully laden dead-weight of 154,000t and her turret mooring systems are subject to harsh North East Atlantic weather conditions.

Figure 1.2 FPSO Schiehallion

The sea area in which the Schiehallion oil field is located is shown in Figure 1.3.

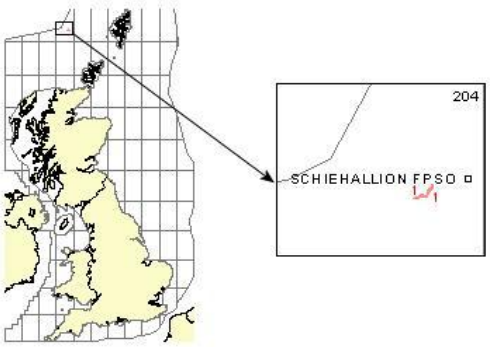

Figure 1.3 Schiehallion oil field

1.6 Layout of Thesis and Chapter Overview

This thesis is basically arranged in accordance with the methods used for motion and mooring analyses. They are a fast time domain method, a retardation function based time domain method and a frequency domain method.

Chapter 1 introduces a general overview of this study and the deepwater mooring systems

including mooring dynamics. A summarised literature review is presented regarding the motion analysis of the floating structures and the mooring line analysis. The aim and objectives of the present study are introduced and a brief layout is presented in accordance with the each chapter.

Chapter 2 presents the summary of the selected FPSO, Schiehallion, and describes the numerical analysis procedures that are quasi-static cable analysis and mooring line dynamics of the mooring line systems. The characteristics of Schiehallion oil field are introduced and the arrangement of 14 mooring lines is described. The catenary equations employed for single component and multi-component mooring lines are presented and their applications for static and quasi-static mooring analyses are discussed. Furthermore, several configurations of a multi-component mooring line are reviewed in addition to the static and quasi-static mooring analyses, line dynamic analysis based on a lumped mass method is discussed.

Both quasi-static and dynamic mooring line analyses can be performed after the motion responses of the FPSO vessel are determined by means of the fast time domain method presented in Chapter 3 or by the retardation function based time domain method in Chapter 4 for North Sea environmental conditions.

In Chapter 3, the generation of irregular wave time series and its corresponding spectrum are discussed and a fast practical time domain method for the first-order wave frequency motions and wave excitations of a floating structure is presented. In addition to the first-order wave frequency motions, the uncoupled second-order motion responses of a moored floating structure to second-order forces obtained from Newman's approximation are determined. The results of time series of the first-order motion responses of the FPSO vessel at different mooring line attachment points in six degrees of freedom, the first-order and second-order wave excitations, the second-order motions and the combined first- and second-order motions are discussed for different wave heading angles. The corresponding motion spectra are also reviewed.

Based on the catenary equations given in Chapter 2, the results of the variation of horizontal mooring force at the attachment point on the FPSO vessel against excursion and of the variation of vertical mooring force at the attachment point against its vertical distance above seabed are presented and discussed in Chapter 4 in connection with nonlinear mooring forces and moments used in a time domain simulation of the moored FPSO motions. Chapter 4 presents the time domain coupled motion equations based on retardation function associated with motion velocity for the simulation of the FPSO motion responses to irregular waves. . The results of the retardation functions obtained from the cosine transform of potential damping coefficients are

presented and reviewed. The simulated time series of the first order motions of the FPSO vessel in six degrees of freedom and their corresponding motion spectra are discussed for three different heading angles. Comparisons between the FPSO motions in irregular waves obtained from the fast time domain method and the retardation function based time domain technique are made.

The quasi-static frequency domain mooring analysis is also presented in Chapter 4 and the results of maximum surge and sway excursions due to the first- and second-order motions obtained from the frequency domain and fast time domain analyses are compared.

Comparisons of the motions and the tensions at the attachment points of the four mooring line no. 1, 4, 8 and 12 obtained from two different time domain approaches are made for three different wave directions and their corresponding spectra are discussed in Chapter 4. The effects of line dynamics on cable tensions are investigated by comparing the tension results obtained from the quasi-static frequency method, fast time domain technique, retardation function based time domain simulation and line dynamic analysis.

Chapter 5 investigated the safety factor accounting for the applied tensions for the mooring system. The proven method is selected as the fast time domain analysis for the validation of the resulting motions and tensions and these results are compared with the other methods that are frequency, quasi-dynamic and dynamic analysis.

In Chapter 6 conclusions are drawn from the comparisons among the fast time domain and frequency analyses, and retardation function based time domain motion equation analysis. Recommendations are proposed for further study.

CHAPTER

2

Analysis of FPSO Mooring Lines

2.1 Introduction

This chapter reviews the selected FPSO and the Schiehallion oil field. The adopted mooring analyses are introduced for the mooring static and dynamic method. Following this introduction, Section 2.2 reviews the principal details and characteristics of the candidate FPSO, the Schiehallion, and its operational site. Section 2.3 presents the general mooring line arrangement regarding application for a turret moored FPSO. Section 2.4 reviews the quasi-static cable analysis including multi-component mooring system and Section 2.5 reviews the mooring line dynamic analysis by using the lumped mass method. Finally, conclusions are given in Section 2.6.

2.2 Schiehallion Oil Field and FPSO

The Schiehallion oil field was discovered in 1993 while the semi-submersible drilling rig Ocean Alliance was exploring the seafloor off the Shetlands around the Northwest Atlantic ocean as shown in Figure 1.2. It is estimated that there are recoverable reserves of about 350-500 million barrels (approximately 425 million barrels for the maximum) of oil and lie approximately 175 km west of Shetland Islands (UK) in a water depth of between 350 to 450 metres. The Schiehallion FPSO, see Figure 1.1 in Chapter 1, was at the time the largest newly built vessel of her type and started production in mid 1998. Table 2.1 summarizes the principal particulars of the Schiehallion oil field and Figure 2.1 shows the hull external surface panel model of the FPSO used for computer based hydrodynamic analysis. The mean wetted surface of the FPSO was modelled by 1034 flat panels. The vessel has been designed to maintain station, in winds up to

130 mph and an extreme design wave height of 33m, by means of a top-mounted internal turret mooring system, which allows the vessel to weathervane around its anchored position according to the directional changes of the external forces. Anchoring is achieved using 14 line anchor legs, each consisting of 6.25in (15.9cm) stud-less chain (Quality R3S) which has a 1650m radius. Each chain has a proof load to 13,733kN and a minimum breaking load to 19,652kN.

Table 2.1 Schiehallion oil field

Discovery	1993
Participants	BP, Shell, Amerada Hess, Statoil, Murphy and OMV
Development cost	£1,000 million
Start up	July 1998
Location	175km West of Shetland Islands
Water Depth	400m average
Size of Field	350-500 million barrels of oil
Peak production	199,000 bpd

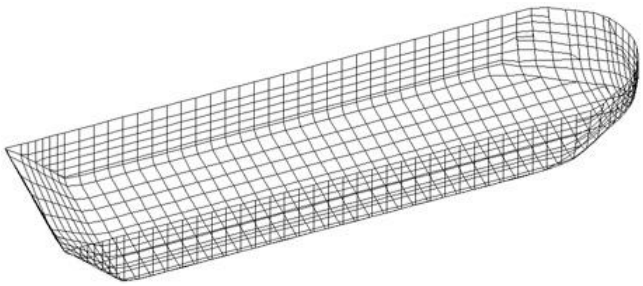

Figure 2.1 Discretisation of Schiehallion FPSO hull envelope

In operating the Schiehallion field it was possible to use the maximum availability of sharing helicopters and supply vessels with the adjacent Foinaven and Loyal fields which lie within 15 kilometres around and the recoverable oil was estimated to be about 600 million barrels from the three fields combined. The production life is estimated to be 17 years and the daily output is peaking at about 142,000 barrels/day.

The Schiehallion field mostly relies on subsea wellhead technology due to the water depth which means the requirement for a floating production system rather than a fixed system and this was the best solution among various considered solutions for the development. This field had a system for oil flowing from subsea pipelines into the Schiehallion, the floating production storage and offloading (FPSO) vessel, through risers.

The subsea technology is equipped with 42 wells in five clusters which were drilled into the reservoir. Of these a number of 29 subsea wells drain the field in four producing clusters. 16 horizontal production wells drain the flat-lying reservoir formations, while 12 non-horizontal wells inject water into the other reservoir sites in order to maintain the pressure in the reservoir and 1 well deals with gas to prevent it from flaring. The oil is moved into the tanks of the FPSO when the inflowing liquids are separated into oil, gas and water. The two gas-oil-water separation processes can carry out their operations for the peak oil capacity of 154,000 barrels a day. The three main drilling centres, Schiehallion Central, Schiehallion West and Loyal, have production and water injection wells while the fourth, Schiehallion North, has a separated gas disposal well that has only water-injection wells. The production wells cluster and send the produced fluids from the wells to the FPSO through flow lines. These fluids are moved along to the turret in the bow region of the vessel to the on-board plants for the processing via 15 dynamic risers.

The production facilities have 3 steps for the processes. The one is for the recovery of the reservoir products. The second is for the cleaning and re-injection of gas and water. The third is for the chemical treatment of the reservoir and associated facilities.

The Schiehallion FPSO, a new type of platform operated by BP, was designed and developed to sustain extreme sea conditions. She was built at Harland and Wolff of Belfast and was the largest new building of a FPSO at that time.

The vessel has an internal turret having a 14m diameter for the size of the cylinder, installed in the bow region of the vessel with a condition to support at the upper deck level on the turret collar. The FPSO vessel has the length of 246m and the design life is 25 years for environmental loads while the theoretical fatigue life is 50 years. The entire crude oil storage capacity is contained mainly in combined seven pairs of cargo tanks in the middle body region of the vessel and also one pair of tanks under the forecastle, with the combined amount of 950,000 barrels. This purpose built FPSO is able to take on board both crude oil and gas up to 154,000 barrels of oil per day. Table 2.2 summarises the principal particulars of Schiehallion FPSO vessel.

Table 2.2 Specification of Schiehallion FPSO

Length between perpendiculars	228.4 m
Breadth	45 m
Depth	27 m
Draught (full load condition)	19.7 m
Dead-Weight	154,000 t
Displacement	194,785 t
LCG from AP	108.359 m
VCG from BL	15.83 m
GM_T	3.129 m
GM_L	227.311 m
Natural surge period	125.54 sec
Natural sway period	169.28 sec
Natural heave period	11.65 sec
Natural roll period	15.53 sec
Natural pitch period	10.46 sec
Natural yaw period	92.37 sec
Storage capacity	950,000 barrels
Peak	154,000 barrels of oil/day
Design Life	25 years
Operating Depth	395 m
Turret	14m diameter with 360 rotation
Mooring	14 anchor chain legs in groups
Type	6.25 inch studless chain and wire rope

The station keeping system is thus maintained with the weathervane turret, which can rotate according to the changes of wind, waves and currents, and connect the mooring lines rising from seabed to the vessel. The export of oil from the FPSO is completed by the associated shuttle tanker, the Loch Rannoch, which is an effective means in the circumstances for FPSOs. The Loch Rannoch, constructed at Daewoo's shipyard in South Korea and operated by BP, delivers the processed crude from the Schiehallion FPSO to the Sullom Voe terminal in Shetland and maintains the transportation link on the basis of a 4~5 day cycle. Offloading of oil from the FPSO to Loch Rannoch takes place every three to six days. The activity of the shuttle tanker helps to prevent the overall through-put oil supply from decreasing in production. Loch Rannoch shuttle tanker which is a ship designed for oil transport is equipped with DP (Dynamic Positioning) system compatible with the Schiehallion oil field. DP system is used to keep the

tanker in position with two or three bow thrusters and stern thrusters. In another case a shuttle tanker can be equipped with mooring system which can be a Single Point Mooring (SPM) or a Multi Buoy Mooring (MBM). The dynamic, the mean and the low frequency motions of a shuttle tanker must keep the safe position preventing from colliding with a moored FPSO in both the moored or Dynamically Positioned (DP) vessels however the effects of the shuttle tanker are not considered since the offloading takes place in calm weather conditions.

It is important to find out the natural periods of the motions as the resonance motion conditions occur when excitation frequency is near the natural period. The natural periods T_n and natural frequencies ω_n of surge, sway, heave, roll, pitch and yaw motions are basically obtained by the following formulae for the moored FPSO:

$$T_n^{ii} = \frac{2\pi}{\omega_n} = 2\pi\sqrt{\frac{(M + A_{ii})}{k_{ii}}} \tag{2.1}$$

$$T_n^{Surge} = \frac{2\pi}{\omega_n^{Surge}} = 2\pi\sqrt{\frac{(M + A_{11})}{k_{11}}} \qquad \left\{k_{11} = \sum_{l=1}^{14} C_l \cos^2\theta_l\right\} \tag{2.2}$$

$$T_n^{Sway} = \frac{2\pi}{\omega_n^{Sway}} = 2\pi\sqrt{\frac{(M + A_{22})}{k_{22}}} \qquad \left\{k_{22} = \sum_{l=1}^{14} C_l \sin^2\theta_l\right\} \tag{2.3}$$

$$T_n^{Yaw} = \frac{2\pi}{\omega_n^{Yaw}} = 2\pi\sqrt{\frac{(I_{66} + A_{66})}{k_{66}}} \qquad \left\{k_{66} = \sum_{l=1}^{14} C_l \left(x_l \sin\theta_l - y_l \cos\theta_l\right)^2\right\} \tag{2.4}$$

$$\omega_n^{Heave} = \sqrt{\frac{\rho g A_W}{(M + A_{33})}} \tag{2.5}$$

$$\omega_n^{Roll} = \sqrt{\frac{\rho g \nabla G M_T}{(I_{44} + A_{44})}} \tag{2.6}$$

$$\omega_n^{Pitch} = \sqrt{\frac{\rho g \nabla G M_L}{(I_{55} + A_{55})}} \tag{2.7}$$

where M is the displacement of the FPSO; A_{ii} and k_{ii} are the added mass and stiffness respectively in i-th direction due to i-th mode of motion; I_{44}, I_{55} and I_{66} are the moment of inertia for roll, pitch and yaw motions respectively; ρ is the water density; g is the acceleration due to gravity; A_w is the waterplane area; ∇ is the volume of displacement of the FPSO; GM_T and GM_L are respectively the transverse and longitudinal metacentre heights; C_l is the horizontal stiffness

of the *l*-th mooring line; θ_l is the angle of the *l*-th mooring line measured from the *x*-axis shown in Figure 2.2. The moment of inertia I_{ii} is the product of ship mass M and the square of radius of gyration γ_i. In the present study, the radii of gyration for roll and pitch were taken as 39% of ship breadth and 25% of ship length respectively, and the radius of gyration for yaw was assumed to be the same as for pitch.

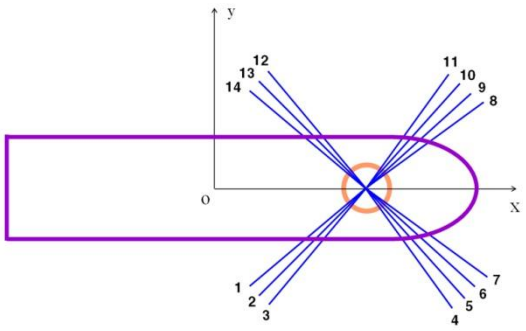

Figure 2.2 Turret-mooring arrangement

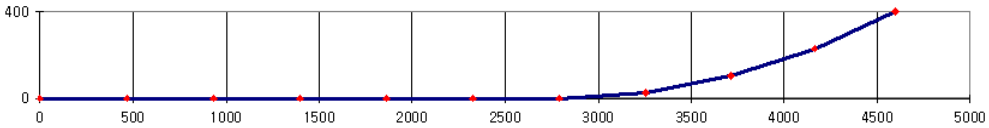

Figure 2.3 Mooring line configuration (10 segments)

Figure 2.2 shows the arrangement of the 14 spread mooring lines with the global o-xy coordinate system. Figure 2.3 shows the profile of a typical mooring line. The water depth is about 400m and anchor position is at 0m position while the attachment position to the turret is at 4,652m in the local line coordinate system for the initial static condition. The still water pre-tension of each line is set to be 2,297kN which is applied force to hold the weight of the line at the attachment point and the weight per unit length of the chain in water is 504N/m. It is for this purpose that each line is represented by 10 segments, of each length, as illustrated in Figure 2.3.

2.3 Single Component Mooring Line Analysis

The integrity evaluation requirement of its mooring system is essential for a deep water floating production platform. In this research, a non-linear analysis of the mooring lines will be progressed on the turret mooring system for the selected FPSO. The floating structure requires

some form of a mooring system to hold the vessel within imposed operational positional constraints for the range of sea states and environmental forces to be expected during its required life.

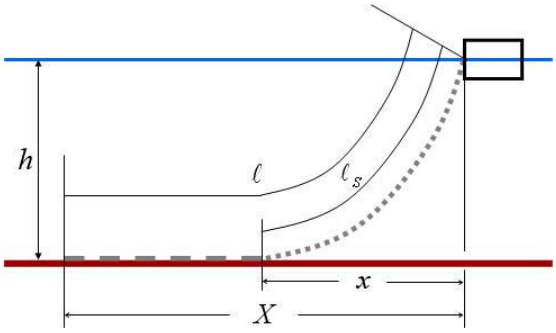

Figure 2.4 Single point mooring line

Figure 2.4 is basically for a simple mooring system in that only single mooring line is used to constrain the floating structure. In this figure, a uniform cable segment is hanging freely under the water:

ℓ = total mooring line length
ℓ_S = hanged mooring line length
h = water depth
w = weight per unit length of chain in water
T_H = horizontal mooring force applied at the attached point on the vessel
X = horizontal distance of the total mooring line from the attached point to the anchor point
x = horizontal distance of the mooring line from the attached point to the touch down point

In this case there is only a single line and a horizontal external force greater than the horizontal mooring force T_H would cause the floating body to move laterally until some stable position is reached and T_H is equal to the horizontal external force. The horizontal force is determined in Eq. (2.14) on the condition that all other values are obtained without the horizontal tension. However, the mooring line arrangement is actually composed of 14 mooring lines as shown in Figure 2.5 that indicates sets of 4 mooring lines spreading to the starboard and port forwards side while 3 mooring lines spreading to the starboard and port aftward direction.

The geometry of a caternary mooring line is given by (Faltinsen 1990):

$$\ell_S = a\sinh\left(\frac{x}{a}\right) \tag{2.8}$$

$$h = a\left[\cosh\left(\frac{x}{a}\right) - 1\right] \tag{2.9}$$

where

$$a = \frac{T_H}{w} \tag{2.10}$$

Combining equations (2.9) and (2.10) yields

$$\ell_S^2 = h^2 + 2ha \tag{2.11}$$

Substituting equations (2.11) and (2.9) for l_s and x into the expression $X = l - l_s + x$ gets

$$X = \ell - h\left(1 + 2\frac{a}{h}\right)^{\frac{1}{2}} + a\cosh^{-1}\left(1 + \frac{h}{a}\right) \tag{2.12}$$

The maximum tension $T_{\max}$ which occurs at the upper end of the mooring line is given by

$$T_{\max} = \left(\frac{wh}{2}\right)\left[1 + \left(\frac{\ell_S}{h}\right)^2\right] = T_H + wh \tag{2.13}$$

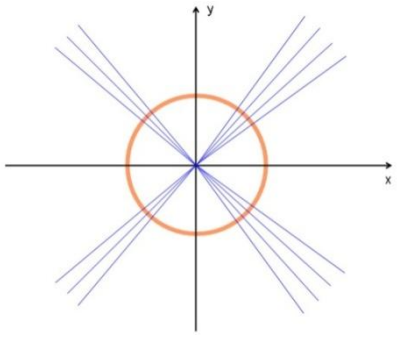

Figure 2.5 Arrangement of mooring system

The above equations for a single component mooring line in a slack condition can be applied for static analysis or quasi-static analysis. Static tensions on the mooring lines due to steady current loads on the lines and the FPSO and/or due to steady wind load on the FPSO can be calculated in a static analysis but are not considered in the present study. On the other hand, mean tensions on the lines caused by mean second-order loads on the FPSO can be obtained by means of a quasi-static analysis and will be considered in subsequent chapters.

2.4 Multi-Component Mooring Line Analysis

The equations given in the previous section for a single component mooring line cannot be applied to a multi-components mooring line, which is made up of combinations of anchors, clump weights, chains and cables as illustrated in Figure 2.6. Moreover, they are also not applicable for taut mooring, where the touch point of the mooring line is not tangent to the sea bed. In order to deal with multi-component mooring line and taut mooring, different geometric configurations of the mooring line are considered.

In deriving the various geometric configuration equations, use is made of the catenary relationships pertaining to a static mooring system configuration. w_1, w_2 and w_3 indicate three different types of cable, which have different weights per unit length (Ansari 1980).

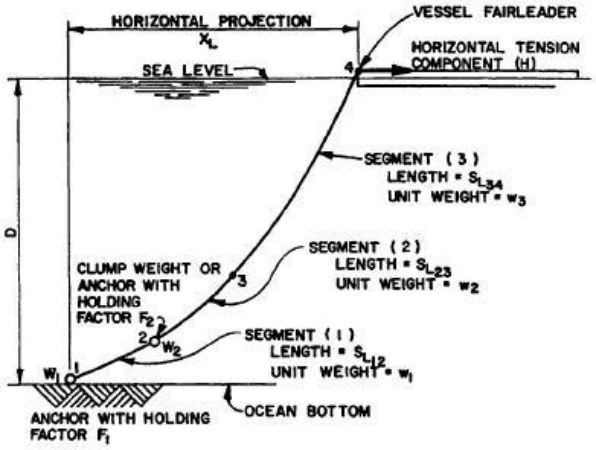

Figure 2.6 Typical multi-component mooring line

2.4.1 Catenary Equations

For a uniform cable segment between arbitrary points *A* and *B* hanging freely under its own constant weight *w* per unit length allowing for buoyancy per unit length as shown in Figure 2.7, the governing differential equation is given by

$$\frac{d^2\mathbf{z}}{\mathbf{d}x^2} = \frac{\mathbf{w}}{\mathbf{H}}\frac{\mathbf{ds}}{\mathbf{dx}} \qquad \textbf{(2.14)}$$

where H = horizontal component of the cable tension

ds = an infinitesimal element of the cable

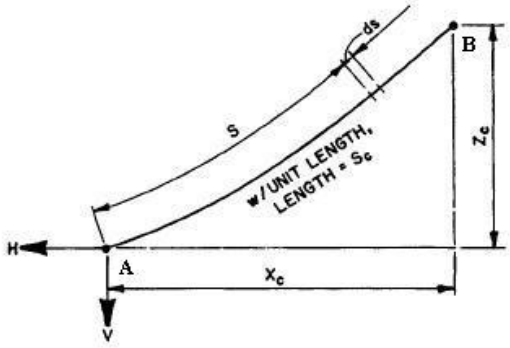

Figure 2.7 Uniform cable hanging freely under its own weight

Upon integration and inclusion of boundary conditions, the following relationships for the horizontal projection X_C and the catenary height Z_C can be derived as

$$X_c = \frac{H}{w}\left[\sinh^{-1}\frac{wS_c + V}{H} - \sinh^{-1}\frac{V}{H}\right] \qquad \textbf{(2.15)}$$

$$Z_c = \frac{H}{w}\left[\cosh\left(\frac{wX_c}{H} + \sinh^{-1}\frac{V}{H}\right) - \cosh\left(\sinh^{-1}\frac{V}{H}\right)\right]$$

where S_C = cable length

V = vertical component of the cable tension at *A*

V/H = the slope at *A*

It is noted that the horizontal tension component H is constant for a given line configuration while the vertical tension component V varies along the line.

2.4.2 Configuration Equations

Depending on the movement of the upper attachment point, several configurations of a multi-component mooring line that can occur are as shown in Figures 2.8 ~ 2.12 (Ansari 1980). Configuration 1 shown in Figure 2.8 illustrates that all of segments 1 and 2 and part of segment 3 lie on sea bottom with both anchors at nodes 1 and 2 holding. Even though w_1, w_2 and w_3 are not identical, the segment 3 in configuration 1 corresponds to a slack single component mooring line discussed in Section 2.3.

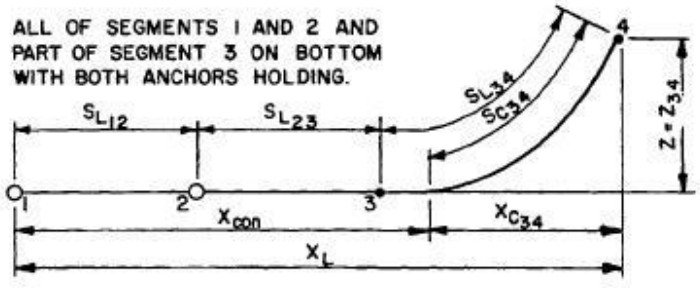

Figure 2.8 Multi-component line in configuration 1

Shown in Figure 2.9 is configuration 2 that all of segment 1 and part of segment 2 lie on the sea bottom with both anchors holding. If segments 2 and 3 have the same unit weight, this configuration also corresponds to the configuration of a slack single component mooring line as carried out in this study in condition that the clump weight is eliminated.

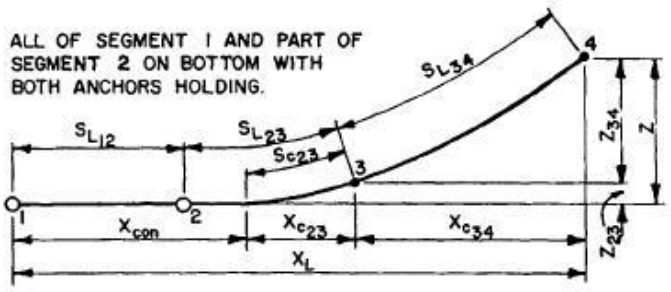

Figure 2.9 Multi-component line in configuration 2

Configuration 3 shown in Figure 2.10 demonstrates segment 1 only on the sea bottom with both anchors holding. This configuration indicates a kind of taut mooring.

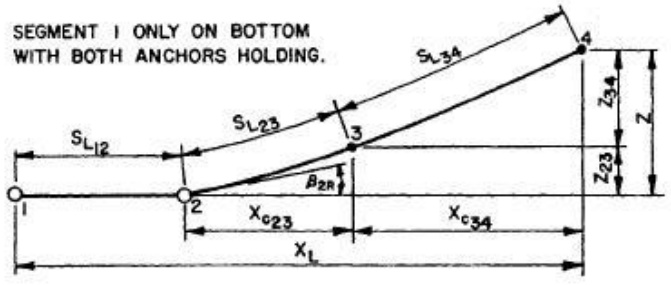

Figure 2.10 Multi-component line in configuration 3

Figure 2.11 shows configuration 4 in which only part of segment 1 lies on the sea bottom with anchor 1 holding. The anchor at node 2 is lifted up and may represent a clump weight. Since the slope of the line at node 2 is not equal to zero, this configuration is a taut mooring.

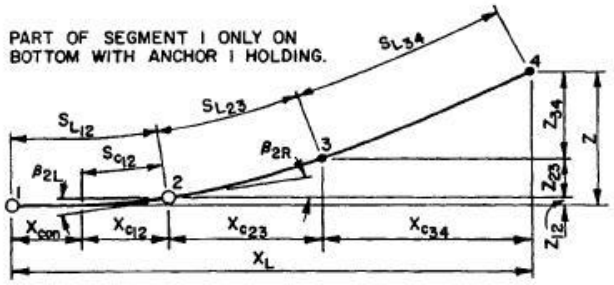

Figure 2.11 Multi-component line in configuration 4

Configuration 5 shown in Figure 2.12 presents a taut mooring of multi-component line. No cable lies on the sea bottom but with anchor 1 holding. The slope of the line at node 1 is not equal to zero.

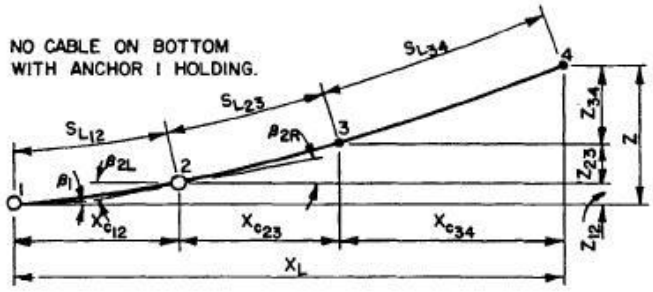

Figure 2.12 Multi-component line in configuration 5

Using Eq. (2.15), the governing system equations can be given by (Ansari 1980)

$$
\begin{aligned}
&X_{c_{12}} = C_1\left[\sinh^{-1}\left(\frac{S_{c_{12}}}{C_1}+\tan\beta_1\right)-\sinh^{-1}(\tan\beta_1)\right]\\
&Z_{12} = C_1\left[\cosh\left\{\frac{X_{c_{12}}}{C_1}+\sinh^{-1}(\tan\beta_1)\right\}-\cosh\left\{\sinh^{-1}(\tan\beta_1)\right\}\right]\\
&V_1 = H\tan\beta_1,\ V_{2L} = V_1 + w_1 S_{c_{12}},\ V_{2R} = W_2 + V_{2L},\ \beta_{2L} = \tan^{-1}\frac{V_{2L}}{H}\\
&\beta_{2R} = \tan^{-1}\frac{V_{2R}}{H},\ X_{c_{23}} = C_2\left[\sinh^{-1}\left(\frac{S_{c_{23}}}{C_2}+\frac{V_{2R}}{H}\right)-\sinh^{-1}\frac{V_{2R}}{H}\right]\\
&Z_{23} = C_2\left[\cosh\left(\frac{X_{c_{23}}}{C_2}+\sinh^{-1}\frac{V_{2R}}{H}\right)-\cosh\left(\sinh^{-1}\frac{V_{2R}}{H}\right)\right]\\
&V_3 = V_{2R} + w_2 S_{c_{23}},\ X_{c_{34}} = C_3\left[\sinh^{-1}\left(\frac{S_{c_{34}}}{C_3}+\frac{V_3}{H}\right)-\sinh^{-1}\frac{V_3}{H}\right]\\
&Z_{34} = C_3\left[\cosh\left(\frac{X_{c_{34}}}{C_3}+\sinh^{-1}\frac{V_3}{H}\right)-\cosh\left(\sinh^{-1}\frac{V_3}{H}\right)\right]\\
&V_4 = V_3 + w_3 S_{c_{34}},\ Z = Z_{12} + Z_{23} + Z_{34},\ X_L = X_{c_{12}} + X_{c_{23}} + X_{c_{34}} + X_{con}
\end{aligned}
\tag{2.16}
$$

with the following applicable to specific configurations as given (Ansari 1980).

Configuration 1 (Figure 2.8):

$$
\begin{aligned}
&S_{c_{12}} = S_{c_{23}} = \beta_1 = \beta_{2L} = \beta_{2R} = V_1 = V_{2L} = V_{2R} = V_3 = 0\\
&S_{c_{23}} = \sqrt{2Z\left(C_3+\frac{Z}{2}\right)},\ X_{con} = S_{L_{12}} + S_{L_{23}} + S_{L_{34}} - S_{c_{34}}
\end{aligned}
\tag{2.17}
$$

Configuration 2 (Figure 2.9):

$$
\begin{aligned}
&S_{c_{12}} = \beta_1 = \beta_{2L} = \beta_{2R} = V_1 = V_{2L} = V_{2R} = 0\\
&S_{c_{23}} = S_{L_{12}} + S_{L_{23}} - X_{con},\ S_{c_{34}} = S_{L_{34}}
\end{aligned}
\tag{2.18}
$$

Configuration 3 (Figure 2.10):

$$
\begin{aligned}
&S_{c_{12}} = \beta_1 = V_1 = V_{2L} = \beta_{2L} = 0,\ S_{C_{23}} = S_{L_{23}},\\
&S_{c_{34}} = S_{L_{34}},\ X_{con} = S_{L_{12}},\ V_{2R} = H\tan\beta_{2R}
\end{aligned}
\tag{2.19}
$$

Configuration 4 (Figure 2.11):

$$
\beta_1 = V_1 = 0,\ S_{C_{12}} = S_{L_{12}} - X_{con},\ S_{C_{23}} = S_{L_{23}},\ S_{C_{34}} = S_{L_{34}} \tag{2.20}
$$

Configuration 5 (Figure 2.12):

$$
S_{C_{12}} = S_{L_{12}},\ S_{C_{23}} = S_{L_{23}},\ S_{C_{34}} = S_{L_{34}},\ X_{con} = 0 \tag{2.21}
$$

In the above equations, C_k is the same as H/w_K (where K=1, 2, 3) and V_K denotes the resolved

vertical tension component at the point K on the mooring line. The subscripts 2R and 2L refer to points on the line just to the right or the left, respectively, of anchor 2 position, and the quantity C_{con} refers to the length of line lying on the ocean bottom, which, in the analysis, is considered to be flat. H can be determined in condition that V is determined at each node position by Eq. (2.16) as part of the catenary analysis. It is noted that a clump weight or a multi-component line are not used in this study. The mooring line is divided into ten segments and treated as a single-component line which is stud-less chain in the present study although the whole length of the line is of a constant geometry chain.

The foregoing equations for different configurations of a multi-component mooring line can be used to determine the tension-displacement relationships in static mooring analysis or quasi-static mooring analysis. Furthermore, the quasi-static mooring analysis based on either a single component line or multi-component line can be carried out in conjunction with a frequency domain approach, a fast time domain approach or a time domain retardation function based approach as discussed in the subsequent chapters.

2.5 Mooring Line Dynamics

Mooring line dynamics should be investigated when the line inertia is important. In accordance with DNV rules for classification of mobile offshore units (DNV 1996), dynamic analyses are recommended for deeper water than 450 m or for floating production and/or storage units at location with water depth more than 200 m. Since the Schiehallion FPSO vessel is operating in deep water about 400 m, the dynamic analysis of mooring lines is required.

2.5.1 Lumped Mass Method

In the present study a lumped mass method developed by Walton and Polachek (1959) for a inelastic line and extended by Nakajima et al (1982) for a elastic multi-component mooring line will be used for line dynamic analysis. The continuous distribution of the mooring line's mass is replaced by a discrete distribution of lumped masses at a finite number of points on the line. This replacement amounts to idealizing the system as a set of point masses and non-mass linear springs. Therefore the line is idealised into a number of lumped masses connected by a mass-less elastic line taking drag and elastic stiffness into account.

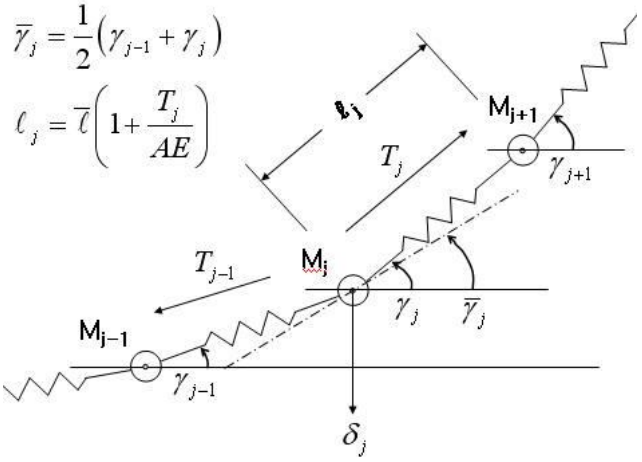

Figure 2.13 Coordinate systems of the lumped mass model

A schematic diagram of the idealised lumped mass model is given in Figure 2.13. The masses are lumped at the node points in the discretised mooring line in the case that j-1, j and j+1 represent three nodes. M_{j-1}, M_j and M_{j+1} represent the mass of the mooring line idealised into a series of discrete lumps. The forces that have an effect on the lines are gravity, hydrodynamic forces and tensions. The motion equations of mooring lines are written as (Nakajima et al 1982)

$$\begin{aligned}
&[M_j + A_{nj}\sin^2\bar{\gamma}_j + A_{tj}\cos^2\bar{\gamma}_j]\cdot\ddot{x}_j + [A_{tj} - A_{nj}]\cdot\ddot{z}_j \sin\bar{\gamma}_j\cos\bar{\gamma}_j = F_{xj} \\
&[M_j + A_{nj}\cos^2\bar{\gamma}_j + A_{tj}\sin^2\bar{\gamma}_j]\cdot\ddot{z}_j + [A_{tj} - A_{nj}]\cdot\ddot{x}_j \sin\bar{\gamma}_j\cos\bar{\gamma}_j = F_{zj}
\end{aligned} \qquad \text{for j = 2, 3, …N} \qquad \textbf{(2.22)}$$

where

M_j, $A_{nj,}$ A_{tj} : Mass, normal and tangential added masses of j-th lump respectively

$\ddot{x}_j$, $\ddot{z}_j$: Acceleration components of j-th lump in horizontal and vertical direction respectively

The external forces F_{xj} and F_{zj} in horizontal and vertical directions are respectively given by

$$\begin{aligned}
F_{xj} &= T_j\cos\gamma_j - T_{j-1}\cos\gamma_{j-1} - f_{dxj} \\
F_{zj} &= T_j\sin\gamma_j - T_{j-1}\sin\gamma_{j-1} - f_{dzj} - \delta_j
\end{aligned} \qquad \textbf{(2.23)}$$

where

T_j : Tension of line in the middle of j-th and (j+1)-th lump

δ_j : Weight of lumped mass under water

γ_j : Angle of j-th line segment at node j with respect to the horizon

The drag forces f_{dxj} and f_{dzj} in horizontal and vertical directions respectively are proportional to the square of the flow velocity relative to the lines as

$$\begin{aligned} f_{dxj} &= -\frac{\rho}{2} D_C \bar{\ell} \left[C_{dn} \sin\bar{\gamma}_j \left| u_{nj} \right| u_{nj} - C_{dt} \cos\bar{\gamma}_j \left| u_{tj} \right| u_{tj} \right] \\ f_{dzj} &= \frac{\rho}{2} D_C \bar{\ell} \left[C_{dn} \cos\bar{\gamma}_j \left| u_{nj} \right| u_{nj} + C_{dt} \sin\bar{\gamma}_j \left| u_{tj} \right| u_{tj} \right] \end{aligned} \qquad \text{for j = 2, 3, …N} \qquad \textbf{(2.24)}$$

where

D_C : Equivalent diameter of mooring line

ρ : water density

$\bar{\ell}$: Original length of line segment

C_{dn}, C_{dt} : Drag force coefficient in normal and tangential direction respectively as shown in Eq. (2.40)

Equivalent diameter is to enable drag calculations to be made that assume a cable of a simple diameter instead of a chain. Drag force coefficient is assumed as that for a simple circular section. The normal and tangential velocity components u_{nj}, u_{tj} of fluid with respect to j-th line segment are respectively written as

$$\begin{aligned} u_{nj} &= -\left(\dot{x}_j - c_j \right) \sin\gamma_j + \dot{z}_j \cos\gamma_j \\ u_{tj} &= \left(\dot{x}_j - c_j \right) \cos\gamma_j + \dot{z}_j \sin\gamma_j \end{aligned} \qquad \textbf{(2.25)}$$

where c_j is the horizontal current velocity at j-th lumped mass. Horizontal current velocity may be either uniform or varying over depth. However, current velocity was not considered as the directional relation was not taken into account to the plane of the catenary for 3-D geometry in this study.

The elastic deformation of mooring line due to tension is governed by

$$\left(x_j - x_{j-1} \right)^2 + \left(z_j - z_{j-1} \right)^2 = \bar{\ell}^2 \left(1 + \frac{T_{j-1}}{AE} \right)^2 \qquad \text{for j = 2, 3, …N+1} \qquad \textbf{(2.26)}$$

where

A : Cross-sectional area of line (Equivalent diameter is used in the case of a chain)

E : Modulus of elasticity of the line material

The elasticity of mooring line is conservative however if the material is steel like chain, it is likely to show a little bit difference against others as fiber or polyester rope.

The previous governing equations (2.22) can be reduced to (Nakajima et al 1982)

$$\begin{aligned} \ddot{x}_j &= \left(R_j T_j - P_j T_{j-1} + U_j\right)/\Delta t^2 \\ \ddot{z}_j &= \left(S_j T_j - Q_j T_{j-1} + V_j\right)/\Delta t^2 \end{aligned} \qquad \text{for j = 2, 3, …N} \qquad \textbf{(2.27)}$$

The related values are obtained in the following equations :

$$\begin{aligned} I_1 &= M_j + A_{nj}\sin^2\bar{\gamma}_j + A_{tj}\cos^2\bar{\gamma}_j \\ I_2 &= \left[A_{tj} - A_{nj}\right]\sin\bar{\gamma}_j\cos\bar{\gamma}_j \\ I_3 &= M_j + A_{nj}\cos^2\bar{\gamma}_j + A_{tj}\sin^2\bar{\gamma}_j \end{aligned} \qquad \textbf{(2.28)}$$

$$\begin{aligned} R_j &= \Delta t^2\left[I_3\cdot\cos\bar{\gamma}_j - I_2\cdot\sin\bar{\gamma}_j\right]/\lambda \\ P_j &= \Delta t^2\left[I_3\cdot\cos\bar{\gamma}_{j-1} - I_2\cdot\sin\bar{\gamma}_{j-1}\right]/\lambda \\ S_j &= \Delta t^2\left[I_1\cdot\sin\bar{\gamma}_j - I_2\cdot\cos\bar{\gamma}_j\right]/\lambda \\ Q_j &= \Delta t^2\left[I_1\cdot\sin\bar{\gamma}_{j-1} - I_2\cdot\cos\bar{\gamma}_{j-1}\right]/\lambda \end{aligned} \qquad \textbf{(2.29)}$$

$$\begin{aligned} U_j &= \Delta t^2\left[I_2\left(f_{dzj} + \delta_j\right) - I_3\cdot f_{dxj}\right]/\lambda \\ V_j &= \Delta t^2\left[I_2\cdot f_{dxj} - I_1\left(f_{dzj} + \delta_j\right)\right]/\lambda \end{aligned} \qquad \textbf{(2.30)}$$

$$\lambda = I_1\cdot I_3 - I_2^{\,2} \qquad \textbf{(2.31)}$$

The velocity and acceleration of the node can be found by Houbolt Method (Dukkipati et al 2000) as follows

$$\begin{aligned} \ddot{x}_j^{n+1} &= \frac{1}{\Delta t^2}\left(2x_j^{n+1} - 5x_j^n + 4x_j^{n-1} - x_j^{n-2}\right) \\ \dot{x}_j^{n+1} &= \frac{1}{6\Delta t}\left(11x_j^{n+1} - 18x_j^n + 9x_j^{n-1} - 2x_j^{n-2}\right) \end{aligned} \qquad \textbf{(2.32)}$$

The vertical values of those can be obtained in a similar method.

The nodal displacements of next time step are derived as

$$x_j^{n+1} = \frac{5}{2}x_j^n - 2x_j^{n-1} + \frac{1}{2}x_j^{n-2} + \left(R_j^{n+1}\cdot T_j^{n+1} - P_j^{n+1}\cdot T_{j-1}^{n+1} + U_j^{n+1}\right)/2$$
$$z_j^{n+1} = \frac{5}{2}z_j^n - 2z_j^{n-1} + \frac{1}{2}z_j^{n-2} + \left(S_j^{n+1}\cdot T_j^{n+1} - Q_j^{n+1}\cdot T_{j-1}^{n+1} + V_j^{n+1}\right)/2 \quad \textbf{(2.33)}$$

The line tension at the next time step is found by the Newton-Raphson Method as

$$T_j^{n+1} = \tilde{T}_j^{n+1} + \Delta T_j^{n+1} \quad \textbf{(2.34)}$$

where

$\tilde{T}_j^{n+1}$: Tentative value of the tension

ΔT_j^{n+1} : Correction value

The equation of the mooring line tension at the next time step is given by

$$\psi_j^{n+1} = -\overline{\ell}^2\left(1 + T_{j-1}^{n+1}/E\cdot A\right)^2 + \left(x_j^{n+1} - x_{j-1}^{n+1}\right)^2 + \left(z_j^{n+1} - z_{j-1}^{n+1}\right)^2 \quad \text{for j = 2, 3, …N} \quad \textbf{(2.35)}$$
$$= \psi_j^{n+1}\left(T_{j-2}^{n+1}, T_{j-1}^{n+1}, T_j^{n+1}\right) = 0$$

A Taylor series expansion of ψ_j^{n+1} about $\left(\tilde{T}_{j-2}^{n+1}, \tilde{T}_{j-1}^{n+1}, \tilde{T}_j^{n+1}\right)$ is given as

$$\psi_j^{n+1} = \tilde{\psi}_j^{n+1} + \frac{\partial\tilde{\psi}_j^{n+1}}{\partial T_{j-2}^{n+1}}\cdot\Delta T_{j-2}^{n+1} + \frac{\partial\tilde{\psi}_j^{n+1}}{\partial T_{j-1}^{n+1}}\cdot\Delta T_{j-1}^{n+1} + \frac{\partial\tilde{\psi}_j^{n+1}}{\partial T_j^{n+1}}\cdot\Delta T_j^{n+1} + \ldots = 0 \quad \textbf{(2.36)}$$

The equation for the differential correction ΔT_j^{n+1} is found as the higher order is neglected on the condition that the tentative value $\tilde{T}_j^{n+1}$ is close to the correct value T_j^{n+1} relating to the following equations (Nakajima et al 1982).

$$\tilde{E}_j^{n+1}\cdot\Delta T_{j-2}^{n+1} - \tilde{F}_j^{n+1}\cdot\Delta T_{j-1}^{n+1} + \tilde{G}_j^{n+1}\cdot\Delta T_j^{n+1} = -\tilde{\psi}_j^{n+1} \quad \text{for j = 2, 3, …N+1} \quad \textbf{(2.37)}$$

$$
\begin{aligned}
\tilde{\psi}_j^{n+1} &= -\bar{\ell}^2\left(1+\tilde{T}_{j-1}^{n+1}/E\cdot A\right)^2+\left(\tilde{x}_j^{n+1}-\tilde{x}_{j-1}^{n+1}\right)^2+\left(\tilde{z}_j^{n+1}-\tilde{z}_{j-1}^{n+1}\right)^2 \\
\tilde{E}_j^{n+1} &= \frac{\partial\tilde{\psi}_j^{n+1}}{\partial T_{j-2}^{n+1}}=\tilde{P}_{j-1}^{n+1}\left(\tilde{x}_j^{n+1}-\tilde{x}_{j-1}^{n+1}\right)+\tilde{Q}_{j-1}^{n+1}\left(\tilde{z}_j^{n+1}-\tilde{z}_{j-1}^{n+1}\right) \\
\tilde{F}_j^{n+1} &= \frac{\partial\tilde{\psi}_j^{n+1}}{\partial T_{j-1}^{n+1}}=\left(\tilde{P}_j^{n+1}+\tilde{R}_{j-1}^{n+1}\right)\left(\tilde{x}_j^{n+1}-\tilde{x}_{j-1}^{n+1}\right)+\left(\tilde{Q}_j^{n+1}+\tilde{S}_{j-1}^{n+1}\right)\left(\tilde{z}_j^{n+1}-\tilde{z}_{j-1}^{n+1}\right) \\
&\quad +2\bar{\ell}^2\left(1+\tilde{T}_{j-1}^{n+1}/E\cdot A\right)/\left(E\cdot A\right) \\
\tilde{G}_j^{n+1} &= \frac{\partial\tilde{\psi}_j^{n+1}}{\partial T_j^{n+1}}=\tilde{R}_j^{n+1}\left(\tilde{x}_j^{n+1}-\tilde{x}_{j-1}^{n+1}\right)+\tilde{S}_j^{n+1}\left(\tilde{z}_j^{n+1}-\tilde{z}_{j-1}^{n+1}\right)
\end{aligned}
\qquad \textbf{(2.38)}
$$

for j = 2, 3, …N+1

$$
\begin{aligned}
\tilde{x}_j^{n+1} &= \frac{5}{2}x_j^n-2x_j^{n-1}+\frac{1}{2}x_j^{n-2}+\left[\tilde{R}_j^{n+1}\cdot\tilde{T}_j^{n+1}-\tilde{P}_j^{n+1}\cdot\tilde{T}_{j-1}^{n+1}+\tilde{U}_j^{n+1}\right]/2 \\
\tilde{z}_j^{n+1} &= \frac{5}{2}z_j^n-2z_j^{n-1}+\frac{1}{2}z_j^{n-2}+\left[\tilde{S}_j^{n+1}\cdot\tilde{T}_j^{n+1}-\tilde{Q}_j^{n+1}\cdot\tilde{T}_{j-1}^{n+1}+\tilde{V}_j^{n+1}\right]/2
\end{aligned}
\qquad \textbf{(2.39)}
$$

for j = 2, 3, …N

$\tilde{R}_j^{n+1}$, $\tilde{S}_j^{n+1}$, $\tilde{P}_j^{n+1}$, $\tilde{Q}_j^{n+1}$, $\tilde{V}_j^{n+1}$, $\tilde{U}_j^{n+1}$ is the tentative values that is of R_j^{n+1}, S_j^{n+1}, P_j^{n+1}, Q_j^{n+1}, V_j^{n+1}, U_j^{n+1}.

The iteration has to be processed with some known quantity employed as the iteration convergence parameter as a direct solution can not be obtained.

The computational process is as follows :

1) The initial form for the equilibrium condition of mooring system and idealisation into a reasonable number of segments

2) Calculate the upper end point movement from the motions of the vessel in 6-DOF

3) The correction for the weight of the lumped mass that is close to the bottom

4) The hydrodynamic drag forces affecting on the lines

5) Calculate line tensions with an initial tentative and an incrementally corrected value

6) Calculate nodal displacement of the next time step

7) Undertake an iteration for the instantaneous convergence

8) The repeat of the calculations for the next time step

The principal characteristics of the chain are shown in Table 2.3.

Table 2.3 Principal particulars of chain

Material	Steel (without stud)
Weight per Length in water (W_W)	504 N/m
Equivalent Diameter	22.45 cm
Modulus of elasticity	2.1 X 10^6 kg/cm^2

The motion of the upper end point of the line is a full 3-D motion according to the behaviour of the moored FPSO in irregular waves. In the present study, the number of nodes is 11 for 10 line segments used and this is adequate number for the configuration of a mooring line as 10 nodes were used for 9 line segments as shown in the reference (Nakajima et al 1982).

The added mass and viscous damping coefficients of a mooring line can be found by experiments (Nakajima et al 1982). In the present study, the following values of these coefficients were used.

$$
\begin{aligned}
C_{hn} &= (added\ mass\ in\ normal\ direction)\times\left(\frac{4}{\rho D_C^2\pi\bar{\ell}}\right)=1.98\\
C_{ht} &= (added\ mass\ in\ tangential\ direction)\times\left(\frac{4}{\rho D_C^2\pi\bar{\ell}}\right)=0.2\\
C_{dn} &= (drag\ \ force\ in\ normal\ direction)\times\left(\frac{3\pi}{4\rho D_C\bar{\ell}u_n^2}\right)=2.18\\
C_{dt} &= (drag\ \ force\ in\ tangential\ direction)\times\left(\frac{3\pi}{4\rho D_C\bar{\ell}u_t^2}\right)=0.17
\end{aligned}
\qquad \textbf{(2.40)}
$$

The drag force is assumed to be applied at the node points although it is obtained along the segments by Eq. (2.24). In the same way the added mass is lumped at the nodes.

The correction increment of the tension is expressed as

$$
\begin{aligned}
-F_2^{n+1}\Delta T_1^{n+1}+G_2^{n+1}\Delta T_2^{n+1} &= -\psi_2^{n+1}\\
G_3^{n+1}\Delta T_1^{n+1}-F_3^{n+1}\Delta T_2^{n+1}+G_3^{n+1}\Delta T_3^{n+1} &= -\psi_3^{n+1}\\
G_4^{n+1}\Delta T_2^{n+1}-F_4^{n+1}\Delta T_3^{n+1}+G_4^{n+1}\Delta T_4^{n+1} &= -\psi_4^{n+1}\\
&\cdots
\end{aligned}
\qquad \textbf{(2.41)}
$$

The matrix form of Eq. (2.41) for unknown tension increments is shown as (Nakajima et al 1982)

$$\begin{bmatrix} -F_2^{n+1} & G_2^{n+1} & 0 & 0 & 0 & 0 \\ E_3^{n+1} & -F_3^{n+1} & G_3^{n+1} & 0 & 0 & 0 \\ 0 & E_4^{n+1} & -F_4^{n+1} & G_4^{n+1} & 0 & 0 \\ \cdots & \cdots & \cdots & \cdots & \cdots & \cdots \\ 0 & 0 & 0 & E_{10}^{n+1} & -F_{10}^{n+1} & G_{10}^{n+1} \\ 0 & 0 & 0 & 0 & E_{11}^{n+1} & -F_{11}^{n+1} \end{bmatrix} \begin{Bmatrix} \Delta T_1^{n+1} \\ \Delta T_2^{n+1} \\ \Delta T_3^{n+1} \\ \cdots \\ \Delta T_9^{n+1} \\ \Delta T_{10}^{n+1} \end{Bmatrix} = \begin{bmatrix} -\psi_2^{n+1} \\ -\psi_3^{n+1} \\ -\psi_4^{n+1} \\ \cdots \\ -\psi_{10}^{n+1} \\ -\psi_{11}^{n+1} \end{bmatrix} \quad \textbf{(2.42)}$$

2.5.2 Correction of Lumped Mass at Bottom of Catenary

The weight of the lumped mass close to the seabed needs to be modified in order to prevent it from moving unrealistically. The two lumped masses are revised over the seabed (Nakajima et al 1982).

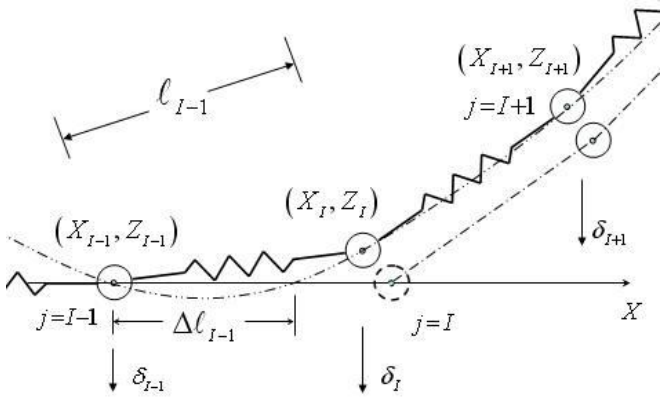

Figure 2.14 Correction of lumped mass model

There are two cases for the consideration of the correction of the weight of a line segment. The first case is given in Eq. (2.43) in condition that $\Delta\ell_{I-1}$ is larger than zero and smaller than ℓ_{I-1} as shown in Figure 2.14.

$$\begin{aligned} &if\ \ 0 \le \Delta\ell_{I-1} < \ell_{I-1} \\ &\delta_I = 1.5W_C\left(1-\Delta\ell_{I-1}/\ell_{I-1}\right) \\ &\delta_{I+1} = W_C\left(1+0.5\Delta\ell_{I-1}/\ell_{I-1}\right) \end{aligned} \quad \textbf{(2.43)}$$

where

W_C = weight per unit length in sea water

$$\Delta\ell_{I-1} = -a_{I-1} / b_{I-1}$$

$$a_{I-1} = \frac{x_{I+1} \cdot z_I - x_I \cdot z_{I+1}}{x_I \cdot x_{I+1}\left(x_I - x_{I+1}\right)}$$

$$b_{I-1} = \frac{x_I^2 \cdot z_{I+1}^2 - x_{I+1}^2 \cdot z_I}{x_I \cdot x_{I+1}\left(x_I - x_{I+1}\right)}$$

$$\ell_{I-1} = \overline{\ell}\left(1 + \frac{T_{I-1}}{AE}\right)$$

The second case is given in Eq. (2.44) in the condition that $\Delta\ell_{I-1}$ is smaller than zero as referred to in Figure 2.14.

$$if\ \Delta\ell_{I-1} < 0,\ \delta_I = 1.5W_C\ \ and\ \ \delta_{I+1} = W_C \qquad \textbf{(2.44)}$$

The nodal displacement for the next time step (n+1) is given by Eq. (2.26). The local lumped mass is then adjusted accordingly.

2.6 Concluding Remarks

The specification of a FPSO stationed in Schiehallion field, approximately 140km to the west of the Orkney Islands UK has been described. In particular, the arrangement and the characteristics of the 14 mooring lines attached at the bottom of the turret of the FPSO have been reviewed.

The catenary equations for a single component mooring line and multi-component line respectively have been presented. These equations can be used for static mooring analysis or quasi-static analysis. The static analysis is to find the maximum static lateral offset of the vessel caused by the total steady environmental forces in association with a load-excursion curve of the mooring system itself, and to find the resulting tensions on the mooring lines. Since the static mooring analysis cannot account for dynamic effects of the first-order and second-order motions of the FPSO on the mooring lines, a quasi-static mooring analysis is required. The dynamic lateral offset of the FPSO due to the first-order and second-order wave excitations, which will be discussed in Chapters 3 and 4, needs to be determined in the quasi-static analysis in order to find the corresponding maximum line tension.

For the mooring line dynamics, the lumped mass method developed by Nakajima et al 1982 has been presented. In this method a mooring line is divided into a number of segments. The larger the number of segments the more accurate will be the computed results. Segments are connected to each other by lumped masses. The lumped masses represent the local value of the mass of the adjacent line segments and the line segments are themselves assumed to be weightless. The distribution of the lumped masses equates to that of the line. Thus the summation of all of the lumped masses is equal to the mass of the whole mooring line. The mooring line segments, although massless still have axial stiffness properties related to the cross-sectional area of the cable and of the modulus of elasticity of its material.

The equivalent diameter of the cable is used in order to determine the drag forces and added masses due to the oscillations of the cable in the water.

The lumped masses are at the discretised line node points and the coordinates of these node points are determined to match the shape of the catenary before the equations of motion of mooring dynamics are solved. Moreover, each massless line segment is a straight line between the two associated node points.

CHAPTER

3

Free Floating Body Motions by Frequency-Domain and Fast Time-Domain Methods

3.1 Introduction

The motions of a moored FPSO can be divided into wave frequency motions induced by the first-order wave exciting forces and moments, and the slowly varying low frequency motions due to second-order different frequency wave excitations. These motions can be calculated either in frequency domain or in time domain. In a frequency-domain motion analysis, the linear wave theory assumes that the amplitudes of the waves and the resulting floating structure motions are small so the simple superposition of these values at different wave frequencies is allowed in order to determine the motions of the structure in irregular waves. On the other hand, a time-domain motion analysis, which may account for some nonlinear effects due to large amplitude motions, mooring line stiffness, etc, is more time consuming than the frequency-domain analysis. Since a random wave simulation can be carried out by means of superposition principle, the motion responses of the FPSO vessel to irregular waves may also be performed in a similar manner. Thus, instead of solving the time-domain motion equations in six degrees of freedom a fast time-domain method based on the response amplitude operators RAOs can be used to predict the motions at the attachment points of the mooring lines in order to estimate the mooring line tensions in extreme weather conditions.

Following this introduction, Section 3.2 reviews irregular waves and their spectra, and the simulation of random waves. The frequency domain analysis is carried out to determine motion RAOs and mean second-order forces and moments on the FPSO vessel in Section 3.3. The fast time-domain motion method for the prediction of the first- and second-order motions of a floating structure is presented in Section 3.4 and the results of the first- and second-order forces

and motions are discussed. Section 3.5 investigates the motion spectra of the combined first- and second-order motions obtained in Section 3.4 and conclusions are given in Section 3.6.

3.2 Wave Spectrum

The influences of ocean waves on the motion responses of a moored offshore structure and the line tensions of its mooring system can be determined by means of a spectral analysis method, in which wave spectrum must be specified. A wave spectrum is obtained from the transformation of the time series of wave elevation measurement to its spectrum description. The significant waves in a sea state are established from the long period collected statistics of waves by measurements and the wave spectrum is set up in the form of the significant wave height and mean zero crossing wave period.

The waves that are experienced provide the cause for making floating structures to move at sea. Those motions are due to the external forces resulting from the waves making contact with the floating structure. A single regular wave system of a given height and period may be used to predict the general response motion of a FPSO but this behaviour will be different from that of a real complex sea state which is composed of an almost unlimited number of waves that have different wave heights and periods leading to a random behaviour. A wave energy spectrum can be used to describe and consider those irregular waves. The waves are made from a wave spectrum can be seen as the composition of numerous waves travelling from the far distance. That is to say that the ocean waves seem to be irregular waves created by the superposition varying numbers of regular waves of various heights and periods. Compiled wave data are available in several forms and time bases for many sea and ocean areas in the world.

The advantage of the wave spectrum is that it can be used not only to simulate random seas and the resulting motion responses of a floating structure in time domain but also to predict various short-term and long-term statistical properties of a dynamic response. When the number of the embedded wave components is taken as 15~20, a satisfactory calculated wave spectrum has been shown to be obtained for a normal sea state. In this research, 80 wave components are used for obtaining the more detailed results in the computer simulation of wave elevation. There are several formulae that can be used to apply to the wave spectrum for the wave profile simulation. The Pierson-Moskowitz spectrum, P-M, has two forms in that the first formula was developed by using a wind speed parameter, while the second formula is produced with respect

to the significant wave height. The JONSWAP spectrum, another well used formula, was developed especially to represent North Sea sea state conditions also with a wind speed parameter. The ISSC spectrum was normally introduced with both significant wave height and mean wave period in the formula and this was modified from the P-M spectrum. The appropriate wave spectrum may be taken to apply for modelling sea state in the specific operational area.

Wave spectrum represents the highly complex distribution of the wave height-period surface variance of a particular sea state for a given period of elapsed time. The total wave energy is represented as ρgE where E is the area under the curve of the wave spectrum.

The specific parameters of a wave spectrum are the significant wave height and the mean zero crossing wave period. A significant wave height of 16 m and a mean time period of 14.5 sec was used in the present study for the extreme conditions for the North East Atlantic area whose position is at latitude 60 degrees North and at longitude 4 degrees West. This corresponds to the near sea area in Brent field selected as location model for the extreme weather condition representing a 100 year return period as given in Appendix D. The definition of return period given in the U.K. DEn Guidance Note is:

The return period of a stated value of a metocean variable is the average period of time between exceedance of that value.

The extreme wave conditions in Appendix D are used in order to cover 100 year exposure conditions for the practical application in the design of offshore structures. A return period of 100 years stands for an annual probability of occurrence of 1/100 = 0.01, or a probability of non-occurrence of $1-1/100=0.99$. In this study, the probability P of occurrence is expected to be about 0.22 in order to experience this extreme wave condition at least one time in its life as the design life of Schiehallion FPSO is required to be 25 years.

The probability P of occurrence can be found as follows:

$$P = 1 - p^n \tag{3.1}$$

p = annual probability that the event will not occur

n = platform design life in years

Thus:

$$P = 1 - (0.99)^{25} = 0.22 \quad \textbf{(3.2)}$$

However, there are different formulae for describing the wave spectrum. ISSC spectrum as used in this study is a two parameter spectrum with respect to significant wave height H_s and mean time period T and is function of wave frequency ω:

$$S(\omega) = 0.11 \frac{H_S{}^2 T}{2\pi} \left(\frac{T\omega}{2\pi} \right)^{-5} \exp\left(-0.44 \left(\frac{T\omega}{2\pi} \right)^{-4} \right) \quad \textbf{(3.3)}$$

This spectrum of significant wave height 16 m and mean period 14.5 sec is shown in Figure 3.1, and the rectangular points represent the spectral density obtained by Fourier transform (Appendix A) from the simulated time series of irregular waves while the solid line represents the spectral density from the ISSC formula. A good correlation between the spectral density obtained from the Fourier transform and the ISSC spectrum formula indicates that the simulated irregular waves meet the target ISSC spectrum.

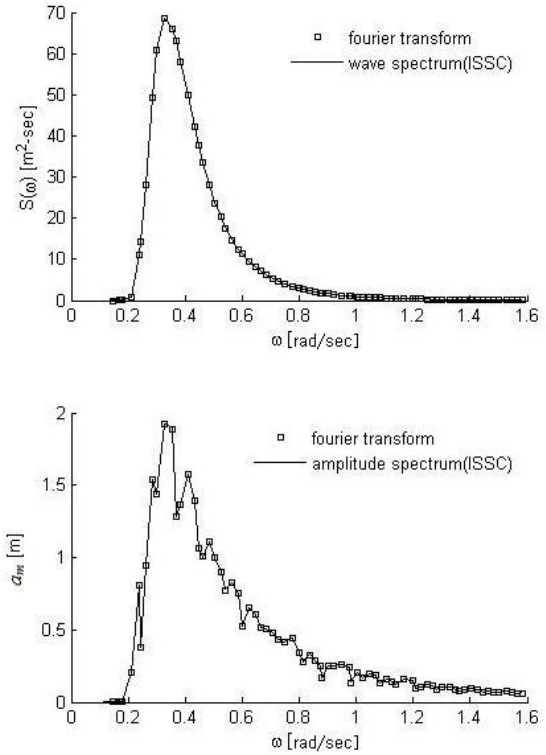

Figure 3.1 ISSC wave spectrum and amplitude spectrum

The wave frequencies for the simulation of random waves were taken as the random frequencies (see Table 3.1) for the irregularity of the wave profile. The numerical simulation of irregular waves can be achieved by the superposition of different wave amplitude component

$a(\omega)$ at different random wave frequencies as given by Eq. (3.5). The amplitude component so called amplitude spectrum $a(\omega)$ is given by :

$$a(\omega) = \sqrt{2S(\omega)\Delta\omega} \qquad \textbf{(3.4)}$$

where $\Delta\omega$ is the random frequency interval.

Table 3.1 ISSC Wave spectrum, random frequency and random phase angle

ω [rad/sec]	S(ω) [m^2-sec]	a [m]	ε [rad]	Δω [rad/sec]
0.011	0.000	0.000	2.593	0.011
0.033	0.000	0.000	2.626	0.022
0.063	0.000	0.000	-1.463	0.030
0.066	0.000	0.000	0.490	0.003
0.081	0.000	0.000	2.373	0.015
0.101	0.000	0.000	-1.304	0.020
0.126	0.000	0.000	-0.946	0.025
0.147	0.000	0.000	-1.623	0.021
0.167	0.000	0.001	3.126	0.020
0.180	0.002	0.007	-1.979	0.013
0.209	0.733	0.206	-3.049	0.029
0.239	10.965	0.811	-3.084	0.030
0.244	14.427	0.380	0.858	0.005
0.260	28.035	0.947	-0.140	0.016
0.284	49.504	1.541	0.582	0.024
0.301	60.713	1.437	0.366	0.017
0.328	68.458	1.923	2.099	0.027
0.355	66.304	1.892	-1.578	0.027
0.368	63.136	1.281	-2.405	0.013
0.384	58.260	1.365	-0.177	0.016
0.409	49.831	1.578	-1.323	0.025
0.432	42.269	1.394	0.875	0.023
0.447	37.721	1.064	0.587	0.015
0.462	33.557	1.003	0.385	0.015
0.484	28.176	1.113	-3.020	0.022
0.505	23.814	1.000	2.707	0.021
0.525	20.295	0.901	-1.876	0.020
0.542	17.734	0.777	1.728	0.017
0.565	14.809	0.825	2.063	0.023
0.588	12.406	0.755	2.565	0.023
0.600	11.328	0.521	0.800	0.012
0.622	9.614	0.650	-0.298	0.022
0.645	8.131	0.612	-2.448	0.023
0.664	7.102	0.519	-1.600	0.019
0.685	6.135	0.508	0.179	0.021
0.707	5.282	0.482	-3.024	0.022
0.727	4.625	0.430	0.067	0.020
0.749	4.009	0.420	3.093	0.022
0.779	3.318	0.446	-2.347	0.030

0.799	2.935	0.343	1.028	0.020
0.813	2.698	0.275	0.977	0.014
0.836	2.355	0.329	-2.724	0.023
0.856	2.099	0.290	2.765	0.020
0.873	1.906	0.255	0.376	0.017
0.881	1.823	0.171	0.556	0.008
0.900	1.642	0.250	-2.263	0.019
0.921	1.466	0.248	-0.859	0.021
0.948	1.272	0.262	0.212	0.027
0.974	1.113	0.241	-1.632	0.026
0.983	1.064	0.138	1.238	0.009
1.005	0.954	0.205	-0.284	0.022
1.021	0.882	0.168	2.244	0.016
1.046	0.783	0.198	2.534	0.025
1.071	0.696	0.187	2.126	0.025
1.085	0.653	0.135	-2.274	0.014
1.106	0.594	0.158	0.772	0.021
1.125	0.546	0.144	1.562	0.019
1.140	0.511	0.124	2.948	0.015
1.168	0.453	0.159	1.800	0.028
1.198	0.399	0.155	2.624	0.030
1.210	0.380	0.096	2.285	0.012
1.225	0.357	0.104	3.066	0.015
1.248	0.326	0.122	-0.511	0.023
1.269	0.300	0.112	2.854	0.021
1.282	0.285	0.086	-1.113	0.013
1.303	0.263	0.105	1.718	0.021
1.328	0.239	0.109	-0.716	0.025
1.345	0.224	0.087	-1.890	0.017
1.360	0.212	0.080	2.912	0.015
1.380	0.198	0.089	1.491	0.020
1.404	0.181	0.093	-0.074	0.024
1.428	0.167	0.089	0.926	0.024
1.443	0.158	0.069	1.098	0.015
1.464	0.147	0.079	1.576	0.021
1.483	0.138	0.072	1.634	0.019
1.501	0.130	0.068	2.887	0.018
1.526	0.120	0.077	2.084	0.025
1.546	0.112	0.067	-1.400	0.020
1.564	0.106	0.062	2.990	0.018
1.585	0.099	0.064	-1.588	0.021

A satisfactory simulation of irregular waves can be obtained with a limited number of wave amplitude and frequency components although the most desirable method to replicate complex irregular waves is by selecting the number of wave components to be as a large as an unlimited value and this means the frequency interval becomes closer to zero. In this research, 80 wave frequencies were used for the generation of irregular waves. This is assumed to be sufficiently accurate for the purposes of this study.

The resulting form of the amplitude spectrum shown in Figures 3.1, 3.2 and 3.4 is not a smooth line and this is due to the adaptation of random frequency.

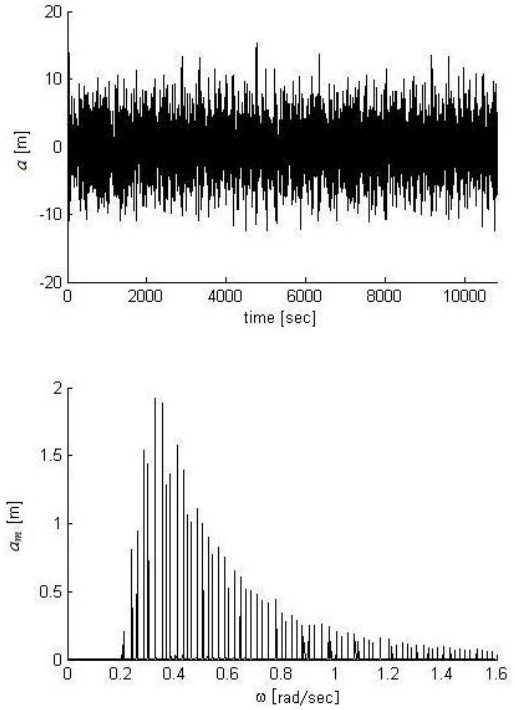

Figure 3.2 Wave profile and Fourier spectrum

The time series of wave elevation ζ at a point (x, y) on mean free surface can be simulated by

$$\zeta(x,y,t)=\sum_{m=1}^{N} a_m \cos\left[k_m\left(x\cos\beta+y\sin\beta\right)-\omega_m t+\varepsilon_m\right] \qquad \textbf{(3.5)}$$

where a_m is the wave amplitude component given by Eq. (3.4) at wave frequency component ω_m and k_m is the corresponding wave number. β is the incident wave angle that is taken by convention as for following seas ($0°$), beam seas ($90°$) and head seas ($180°$). The angle ε_m is a random phase. N is the number of wave components, which was taken as 80 in the present

investigation.

Figure 3.2 shows the simulated time series of irregular wave elevation at $x = 0$, $y = 0$ and $\beta = 150^\circ$ for significant wave height = 16 m and mean time period = 14.5 sec, and the corresponding wave amplitude components at different wave frequencies. This approach to generating time histories of random variable has been proven to be useful when investigating the effects of the motion responses of the FPSO on mooring line tensions in random seas.

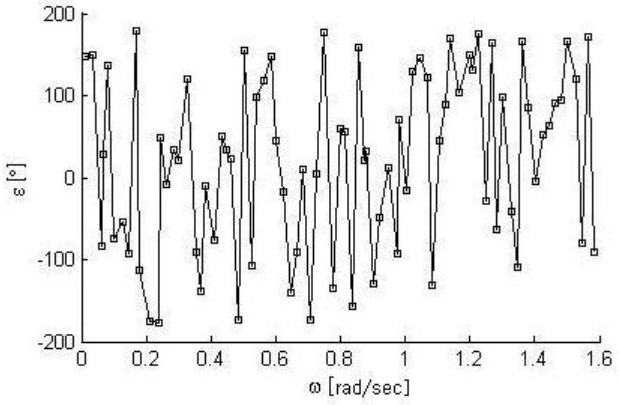

Figure 3.3 Random phase angle

The result of the corresponding random phase angle ε_m is shown in Figure 3.3 and this has an effect on the irregularity of the simulated wave elevation. The values of amplitude components calculated by means of Eq. (3.4) with random frequencies given in Table 3.1 and obtained by the Fourier transform of the simulated wave elevation time series are compared and shown in Figure 3.4. They are correlated to each other. The null values of the amplitude components that take place near to the horizontal axis of the upper graph in Figure 3.4 are due to the irregular intervals of the original wave frequencies. The Fourier transform uses regular interval in the process while the simulated amplitude components are based on irregular frequency intervals. Some of the random intervals are near zero and so the corresponding amplitude components become very small. These null amplitude components do not have any effect on the simulated random waves since the amplitude spectrum obtained by the Fourier transform correlates with the input amplitude spectrum from ISSC. Thus these null amplitude components should be ignored. The peak values shown in the lower graph of Figure 3.4 were determined by the Fourier transform of the simulated random wave profile without the effects of null amplitude components and also agree with the values of the input amplitude components. This good agreement may not occur in

the spectrum obtained by the Fourier transform of irregular waves simulated with a large number of components or of a real measured sea data because the wave signal from the real seas contains not only noise data but also nearly an unlimited number of wave components.

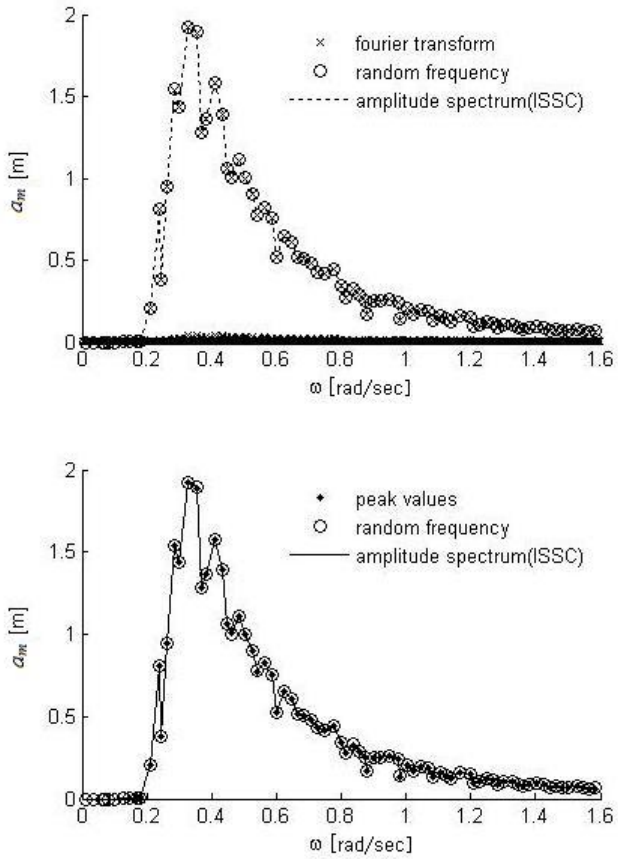

Figure 3.4 Fourier transform and amplitude spectra

Figure 3.5 shows a good agreement between the ISSC wave spectral densities obtained from Eq. (3.3) and calculated by the Fourier transform of simulated wave elevation time series given in Figure 3.2.

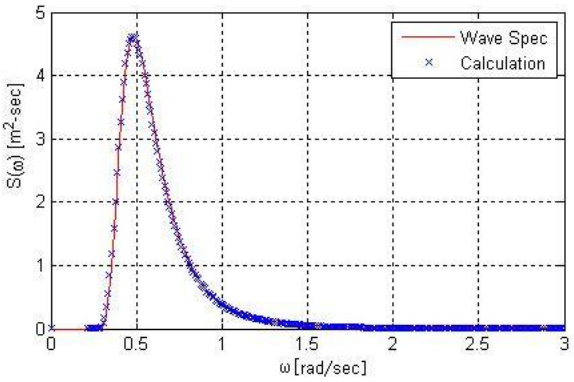

Figure 3.5 Comparison of ISSC wave spectrum and Fourier transform

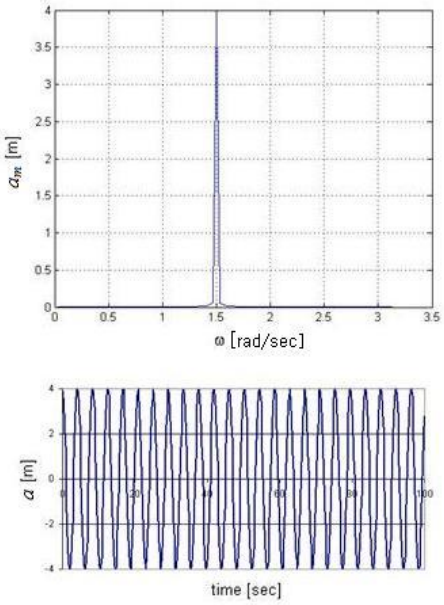

Figure 3.6 Amplitude spectrum and single wave

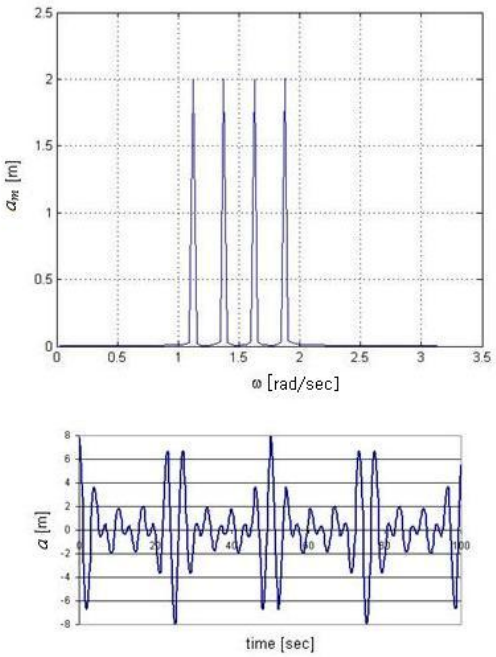

Figure 3.7 Amplitude spectrum and irregular waves

The mechanism of a single regular wave is shown in Figure 3.6, where a regular wave of amplitude 4m at wave frequency 1.5 rad/sec can be made by a single component, and the corresponding amplitude spectrum from the Fourier transform is just 4m. On the other hand, an irregular wave pattern made of four components with amplitude 2m at different wave frequencies 1.125, 1.375, 1.625 and 1.875 rad/sec respectively and its corresponding amplitude spectrum are shown in Figure 3.7. This irregular wave pattern is not random at all because of repetition after several cycles in a given time period. Such repetition is due to the small number of frequency components in the simulation. This problem can be resolved by increasing the number of frequency components. Then the period of repetition will become longer and the repetition will be overcome by using random frequency and random phase angle properties.

The time histories of random wave elevations at the attachment points of No.1 to No.14 mooring lines are shown in Figures 3.8 to 3.10 for three different wave heading angles of the incident waves as shown in Eq. (3.5). There are 15 plots as the 15^{th} plot is for the origin of the global coordinate system which means the wave elevations at the centre of FPSO. The coordinates of the attachment points are given in Table 4.1 (Chapter4). These irregular waves were derived from Eq. (3.5) with 80 components of random amplitude, frequency and phase respectively.

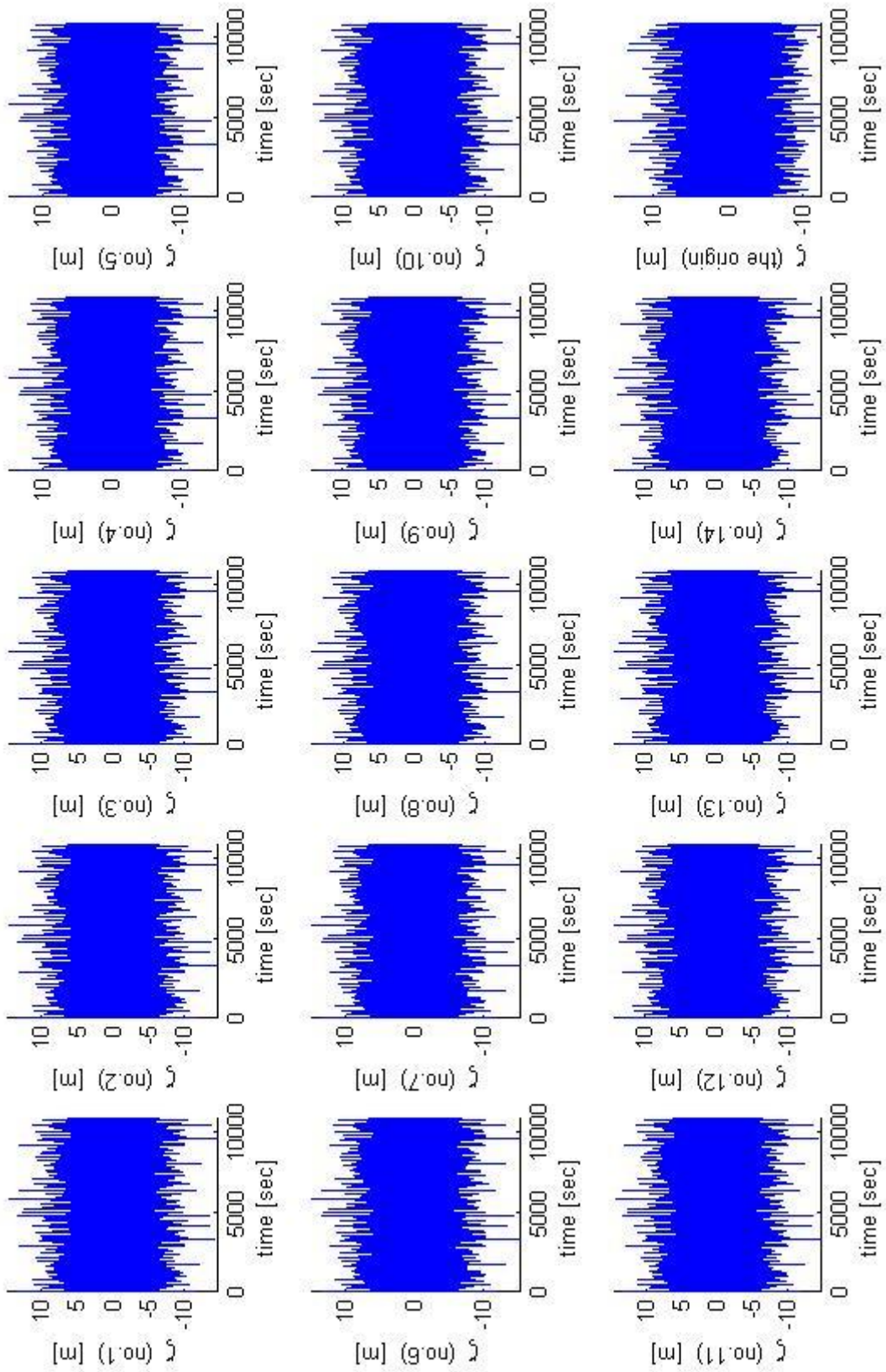

Figure 3.8 Wave elevation at mooring line attachment points and at origin of coordinate system (β=150 degrees)

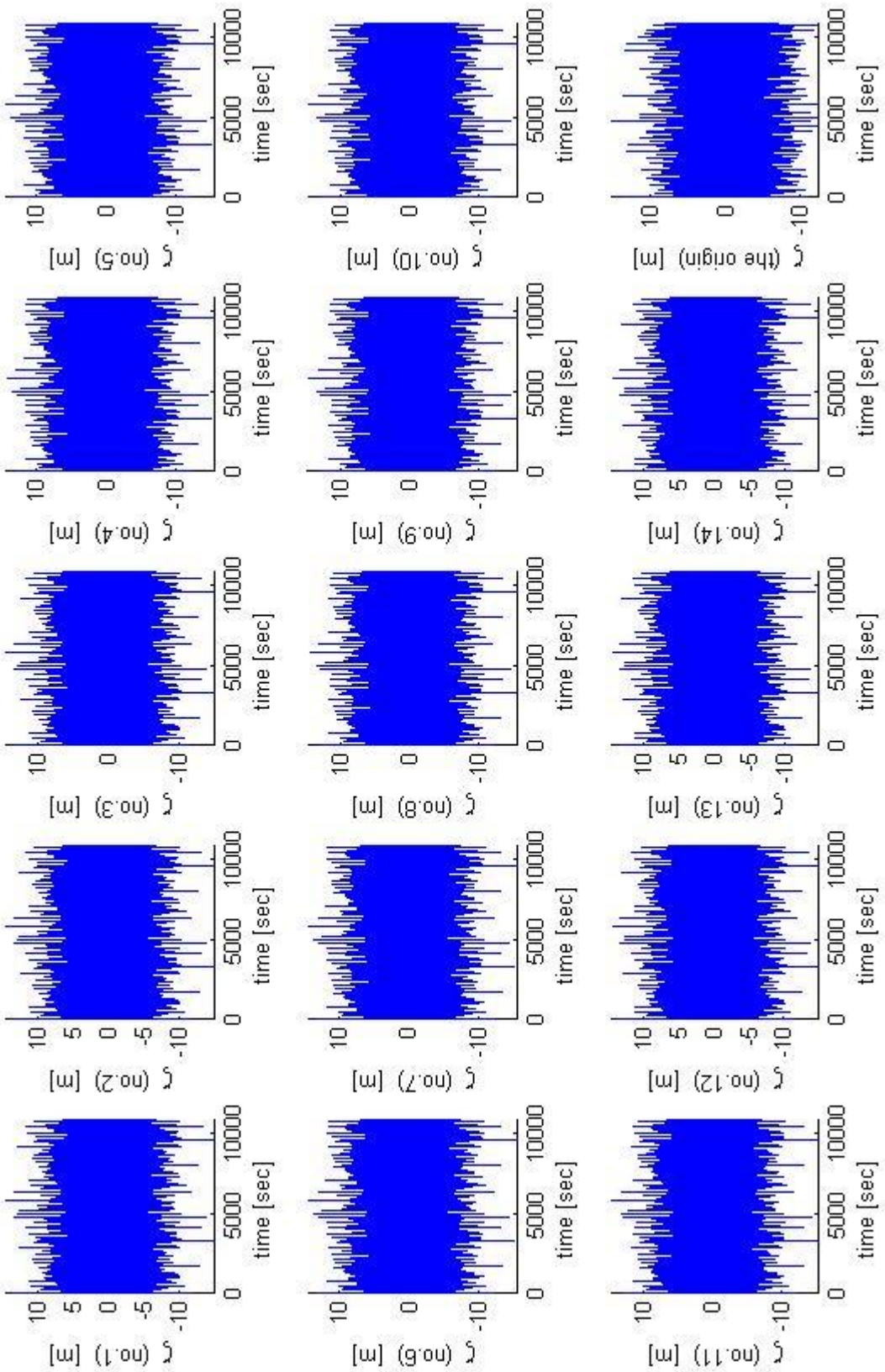

Figure 3.9 Wave elevation at mooring line attachment points and at origin of coordinate system (β=165 degrees)

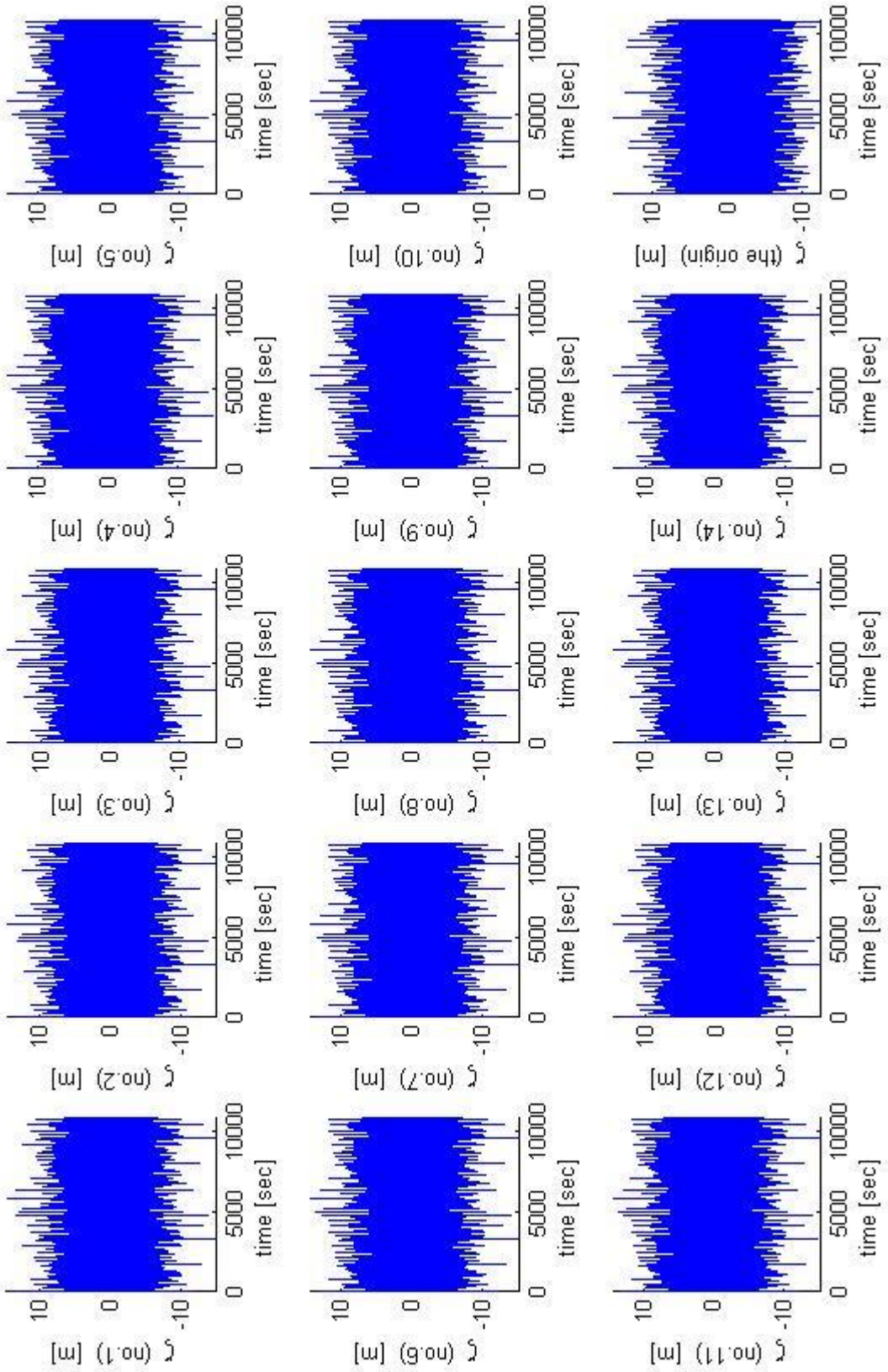

Figure 3.10 Wave elevation at mooring line attachment points and at origin of coordinate system (β=180 degrees)

3.3 Frequency-Domain Analysis

Suppose that a moored FPSO oscillates as a rigid body in six degrees of freedom about its mean position with complex amplitudes ξ_k with respect to the origin of the rectangular co-ordinate system o-xyz. Here k = 1, 2, 3, 4, 5, 6, refer to surge, sway, heave, roll, pitch and yaw modes of motion respectively. The z-axis is vertically upward through the centre of gravity of the body with the origin o on the mean free surface and the x-axis is longitudinally pointing to the bow as shown in Fig. 2.2. In general, the coupled linear motions of a moored FPSO can be expressed as

$$\sum_{k=1}^{6}\left[\left(M_{jk}+A_{jk}\right)\ddot{\xi}_k+B_{jk}\dot{\xi}_k+\left(C_{jk}+K_{jk}\right)\xi_k\right]=F_j^W+F_j^V \qquad \text{for } j=1,2,\ldots 6 \qquad \textbf{(3.6)}$$

where $\ddot{\xi}_k$ and $\dot{\xi}_k$ are the motion acceleration and velocity respectively. M_{jk} is the element of mass matrix, A_{jk} is the added mass, B_{jk} is the damping, C_{jk} is the restoring coefficient due to change in buoyancy, K_{jk} is the stiffness due to mooring system, F_j^W is the wave exciting force (moment is understood hereafter) and F_j^V is the viscous excitation force. The indices j and k indicate the direction of the fluid force and the mode of motion respectively. The hydrodynamic coefficients in the equations of motion may be considered as linear dependence of fluid forces due to non-lift potential flow and viscous flow such that $B_{jk}=b_{jk}+\hat{b}_{jk}$, etc.: b_{jk} is the wave damping coefficient and $\hat{b}_{jk}$ is the viscous damping coefficient.

The viscous effects on damping, restoring and excitation forces may be found using the Froude-Krylov approach together with the cross-flow and the pseudo-steady state assumptions (Chan 1992). It is noted that the terms in the equations of motion due to viscous effects depend upon the amplitudes of motion responses. As a consequence, the equations of motion are solved iteratively until a reasonable convergence of motion amplitudes is obtained.

The unsteady motions of the stationary FPSO and the fluid are assumed to be small so that the unsteady body boundary and free surface conditions can be linearised. The solution of the linearised unsteady motion problem is constructed by means of the three-dimensional Green's function integral equation method. Thus the domain of the problem is reduced from the infinite fluid domain to the hull surface on which oscillating source singularities are distributed. The Green's function satisfies the three-dimensional Laplace's equation, the linearised free surface condition, the sea bottom condition and the far-field radiation condition. Hydrodynamic

coefficients and wave exciting forces given in Eq. 3.6 can be obtained after solving the integral equation which satisfies the linearised body boundary conditions (Chan 1992). This is accomplished by the discretisation of the mean wetted body surface into a finite but large number of flat panels (Hess & Smith 1962).

Numerical computations have been carried out to predict the first-order motion responses of the Schiehallion FPSO to regular waves at different wave frequencies and three heading angles and the resulting mean second-order forces and moment in the frequency domain.

Figs. 3.11 and 3.12 show the motion response amplitude operators (RAOs) and phase angles of Schiehallion FPSO at different wave frequencies in three different wave heading angles 150°, 165° and 180° (head waves). The motion RAOs are non-dimensionalised by wave amplitude ζ and wave number κ. A positive phase of the motion response indicates that a motion reaches its positive maximum value before the crest of the undisturbed incoming regular wave passes the ship's centre of gravity.

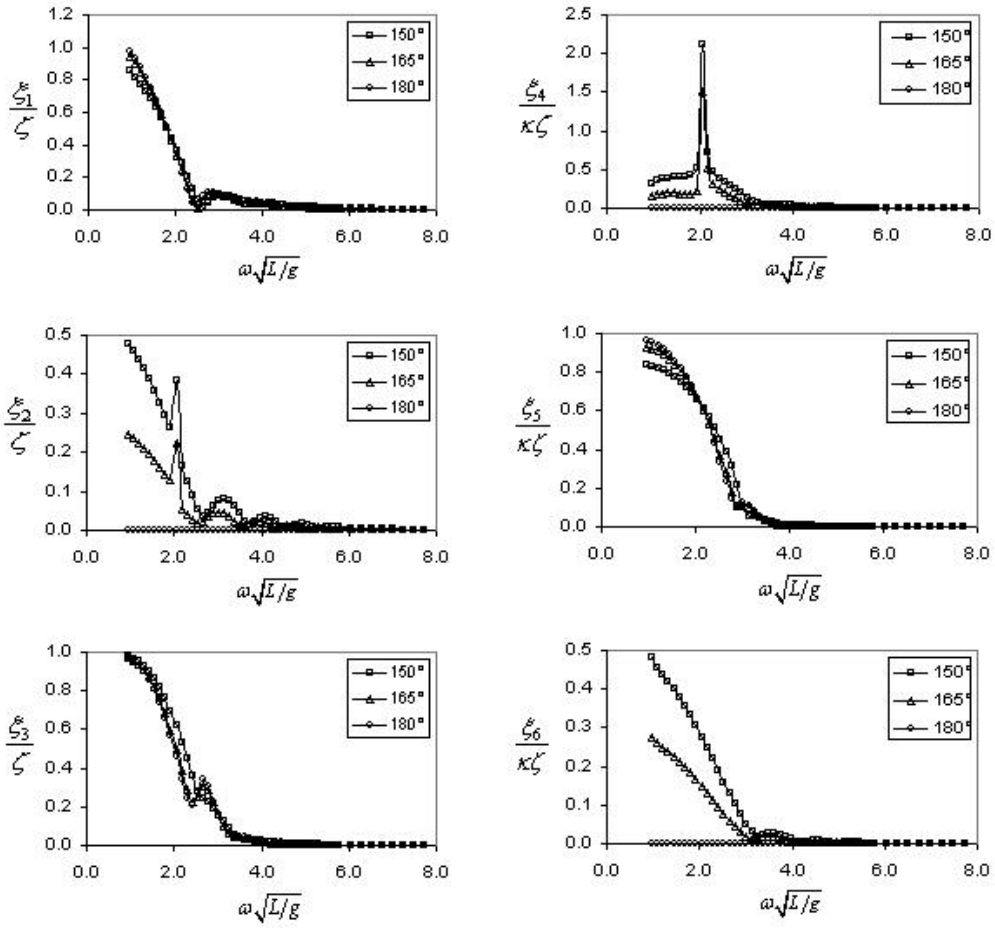

Figure 3.11 Motion RAOs of Schiehallion FPSO

The sway, roll and yaw motions of the FPSO in bow waves 150^{o} are larger than those in 165^{o} but vanish in head seas as expected. Similarly, the heave motion is slightly larger in bow waves 150^{o} than that in 165^{o} and head waves. On the other hand, the FPSO experiences slightly larger surge and pitch motions in long head waves than in bow waves.

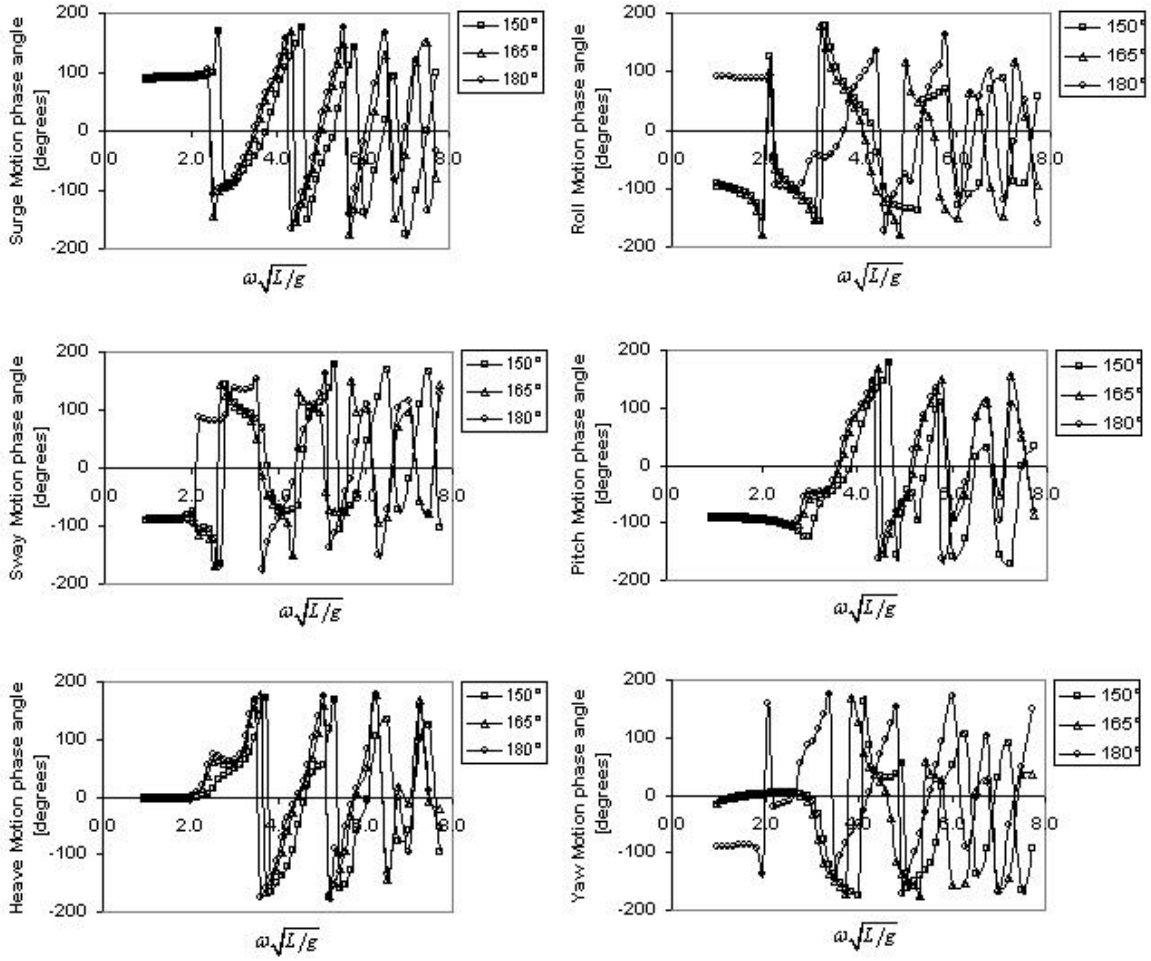

Fig. 3.12 Motion phase angles of Schiehallion FPSO

After the first-order motions have been obtained, the surge and sway mean second-order forces and yaw moments on the Schiehallion FPSO can be calculated by means of near-field method (Pinkster 1979) or far-field method (Maruo 1961, Newman 1967). In the present study, the mean second-order surge force $\overline{F}_1^{(2)}$, sway force $\overline{F}_2^{(2)}$ and yaw moment $\overline{F}_6^{(2)}$ are calculated by integrating the first-order hydrodynamic pressures (near-field method) and are expressed in the form:

$$\bar{F}_1^{(2)} = -\tfrac{1}{4}\rho g\oint_{L_0}\zeta_r\zeta_r' n_1 dl + \tfrac{1}{4}\rho\iint_{S_0}\nabla\Phi\bullet\nabla\Phi' n_1 ds + \tfrac{1}{2}\rho\iint_{S_0}\alpha\bullet\nabla\Phi_t' n_1 ds + \tfrac{1}{2}\left(\xi_5 F_3' - \xi_6 F_2'\right) \quad \textbf{(3.7)}$$

$$\bar{F}_2^{(2)} = -\tfrac{1}{4}\rho g\oint_{L_0}\zeta_r\zeta_r' n_2 dl + \tfrac{1}{4}\rho\iint_{S_0}\nabla\Phi\bullet\nabla\Phi' n_2 ds + \tfrac{1}{2}\rho\iint_{S_0}\alpha\bullet\nabla\Phi_t' n_2 ds + \tfrac{1}{2}\left(\xi_6 F_1' - \xi_4 F_3'\right) \quad \textbf{(3.8)}$$

$$\bar{F}_6^{(2)} = -\tfrac{1}{4}\rho g\oint_{L_0}\zeta_r\zeta_r' n_6 dl + \tfrac{1}{4}\rho\iint_{S_0}\nabla\Phi\bullet\nabla\Phi' n_6 ds + \tfrac{1}{2}\rho\iint_{S_0}\alpha\bullet\nabla\Phi_t' n_6 ds + \tfrac{1}{2}\left(\xi_1 F_2' - \xi_2 F_1'\right) + \tfrac{1}{2}\left(\xi_4 F_5' - \xi_5 F_4'\right) \quad \textbf{(3.9)}$$

where ρ is the water density, g is the acceleration due to gravity, ζ_r is the relative wave elevation, Φ is the unsteady velocity potential due to radiation, diffraction and incident wave systems, α is the first-order displacement vector, n_j is the generalised direction cosine, F_j is the first-order hydrodynamic force in the j-th direction, the prime over a variable denotes the complex conjugate of the variable.

The calculated surge and sway drift forces and mean second-order yaw moments on the Schiehallion FPSO at different wave frequencies and three heading angles are shown in Fig. 3.13. The negative value of surge drift force indicates that the force is in negative x direction, while the positive value of sway drift force means that the force is in positive y direction. The positive yaw moment indicates that the vessel yaws anti-clockwise. The spikes in the drift forces and yaw moment may be caused by irregular frequency phenomenon where no unique solution exists. These spikes are neglected in the process of Newman's approximation method (Newman 1974) to generate the time history of the second-order forces.

The surge drift force on the Schiehallion FPSO does not vary much with wave heading angle and approaches an asymptotic value at high frequencies. However, the sway drift force is sensitive to wave angle of attack and increases with heading angle changing from head waves to beam seas. Furthermore, the asymptotic sway drift force in bow waves 150^{o} appears earlier than that in 165^{o}. Since the lateral area of a vessel is greater than the frontal area, the sway drift force is normally larger than the surge drift force as shown in Fig. 3.13. The mean second-order yaw moment on the FPSO in bow waves 150^{o} is larger than that in 165^{o} but vanishes in head waves as expected.

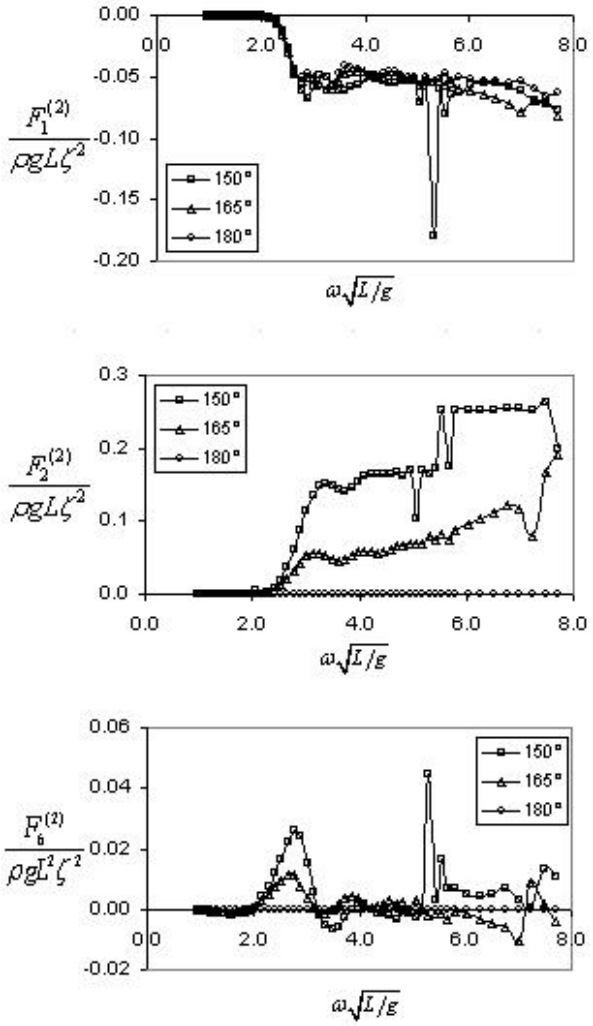

Fig. 3.13 Mean second order forces and yaw moment on Schiehallion FPSO

3.4 First and Second-Order Motions and Forces

Although the frequency-domain method, together with a spectral analysis, is practical and predicts the extreme motions of the vessel with some degree of engineering accuracy, the combination of the extreme value first-order wave-induced motion and the second-order slow-drift motion in the frequency-domain analysis is an engineering approximation that can be used for the design of mooring systems but is however uncertain in its accuracy. In order to eliminate this uncertainty, a time-domain coupled motion and mooring analysis is required.

In general, the equations of motion for the six degrees of freedom of a floating vessel are integrated in the time-domain in which the effects of hydrodynamic added mass, damping and non-linear restoring forces due to the mooring lines on the motions are included. It is, however, computationally intensive to run this kind of time domain simulation in an irregular seas with a storm duration of at least three hours.

In the present study, an alternative time-domain method which integrates motion responses to regular waves of all frequencies is developed. Based on the linear theory of the motion responses of vessels, the wave elevation ζ and the corresponding first-order motion $\xi_j^{(1)}$ at a point (x, y, z) on the floating vessel are the summation of their amplitude components of all frequencies as shown in Eqs. (3.5) and (3.10) respectively.

$$\xi_j^{(1)}(t;x,y,z)=\sum_{m=1}^{N}\sqrt{2S(\omega_m)\left|\xi_j(x,y,z,\omega_m)\right|^2 d\omega}\cdot\cos\left(\omega_m t+\alpha_j(x,y,z,\omega_m)+\varepsilon_m\right) \text{ for } j = 1,2 \ldots 6 \quad \textbf{(3.10)}$$

where $|\xi|$ is the motion amplitude of the attachment point in the *j*-th mode and α_j is the phase angle relative to the waves. They can be calculated from their real and imaginary parts:

$$\left|\xi_j(x,y,z,\omega)\right|=\sqrt{\mathrm{Re}^2\left\{\xi_j(x,y,z)\right\}+\mathrm{Im}^2\left\{\xi_j(x,y,z)\right\}} \quad \textbf{(3.11)}$$

$$\alpha_j(x,y,z,\omega)=\tan^{-1}\frac{\mathrm{Im}\left\{\xi_j(x,y,z)\right\}}{\mathrm{Re}\left\{\xi_j(x,y,z)\right\}} \quad \textbf{(3.12)}$$

The real and imaginary parts of the translational motions $\vec{\xi}$ at an attachment point (*x*, *y*, *z*) can be determined by the translational motions $\vec{\xi}^{OG}$ at the origin of the global coordinate system and the angular motions $\vec{\Omega}$ as follows:

$$\vec{\xi}(x,y,z) = \vec{\xi}^{OG}(0,0,0) + \vec{\Omega} \times \vec{r} \quad \textbf{(3.13)}$$

where $\vec{\xi} = (\xi_1, \xi_2, \xi_3)$ **(3.14)**

$$\vec{\Omega} = (\xi_4, \xi_5, \xi_6) \quad \textbf{(3.15)}$$

$$\vec{r} = (x,y,z) \quad \textbf{(3.16)}$$

The total motion ξ_j of the attachment point can be determined the sum of the first and second order motions as given in Eq. (3.17). $\xi_j^{(1)}$ is the first-order motion while $\xi_j^{(2)}$ is the slowly-varying drift motion of the vessel :

$$\xi_j(x,y,z,t) = \xi_j^{(1)}(x,y,z,t) + \xi_j^{(2)}(t) \quad \textbf{(3.17)}$$

The second-order motion $\xi_j^{(2)}$ of the FPSO in the j-th mode can be found by solving the slow-drift motion equation:

$$(M + A_{jj})\ddot{\xi}_j^{(2)} + B_{jj}\dot{\xi}_j^{(2)}\left|\dot{\xi}_j^{(2)}\right| + C_{jj}\xi_j^{(2)} = F_j^{(2)}(t) \quad \textbf{(3.18)}$$

Using Newman's approximation for the second-order force (Newman 1974), the slow-drift exciting force $F_j^{(2)}$ can be determined as given in Eq. (3.19).

$$F_j^{(2)}(t) = \sum_{m=1}^{N}\sum_{n=1}^{N} a_m a_n \bar{F}_j^{(2)}(\omega_m, \beta)\cos\left[(\omega_m - \omega_n)t + \varepsilon_m - \varepsilon_n\right] \quad \textbf{(3.19)}$$

where a_m and a_n are the wave amplitude determined from Eq. (3.4).

The general scheme of the flow chart is given in Appendix E for the fast-time domain analysis in condition that the 2nd-order motions are obtained from the solution of the 2nd order motion equation (3.18) with the uncoupled mass, added-mass, damping and stiffness coefficients in the process.

Once the displacements of the attachment points on the turret are traced in the time domain, the corresponding maximum tensions on the individual mooring lines can then be obtained.

If the coupled equations of the first-order motions of a floating structure in six degrees of freedom are solved in the time domain as discussed in Chapter 4, the time series of the first-order wave exciting forces on the structure can be calculated by

$$F_j^{(1)}(t) = \sum_{m=1}^{N} \sqrt{2S(\omega_m)\left|F_j(\omega_m)\right|^2 d\omega} \cdot \cos\left(\omega_m t + \alpha_j(\omega_m) + \varepsilon_m\right) \quad \text{for } j = 1,2,\ldots 6 \qquad \textbf{(3.20)}$$

where $\left|F_j(\omega_m)\right|$ and $\alpha_j(\omega_m)$ are respectively the amplitude and phase of the wave exciting force in the j-th mode at random wave frequency ω_m.

3.4.1 Simulated First-Order Wave Exciting Forces

Based on Eq. (3.20), the amplitudes and phases of the wave exciting forces shown in Appendix F and the ISSC wave spectrum of significant wave height 16 m and mean period 14.5 sec, the first order wave exciting forces on the FPSO in wave directions 150, 165 and 180 degrees have been calculated and are shown in Figures 3.14 to 3.16 respectively. The magnitudes of the wave exciting forces in sway, roll and yaw modes vary with the angle of the incident waves while those in surge, heave and pitch modes are much the same. The variation of these forces is related to the changing ratio of the projected area of the underwater hull, as seen by the direction of wave travel. However the projected area related to surge, heave and pitch is not so much different for each of the considered three heading angles from 150 to 180 degrees by the incident waves but those for sway, roll and yaw are changed with a large amount in size to the moving direction of the incident waves.

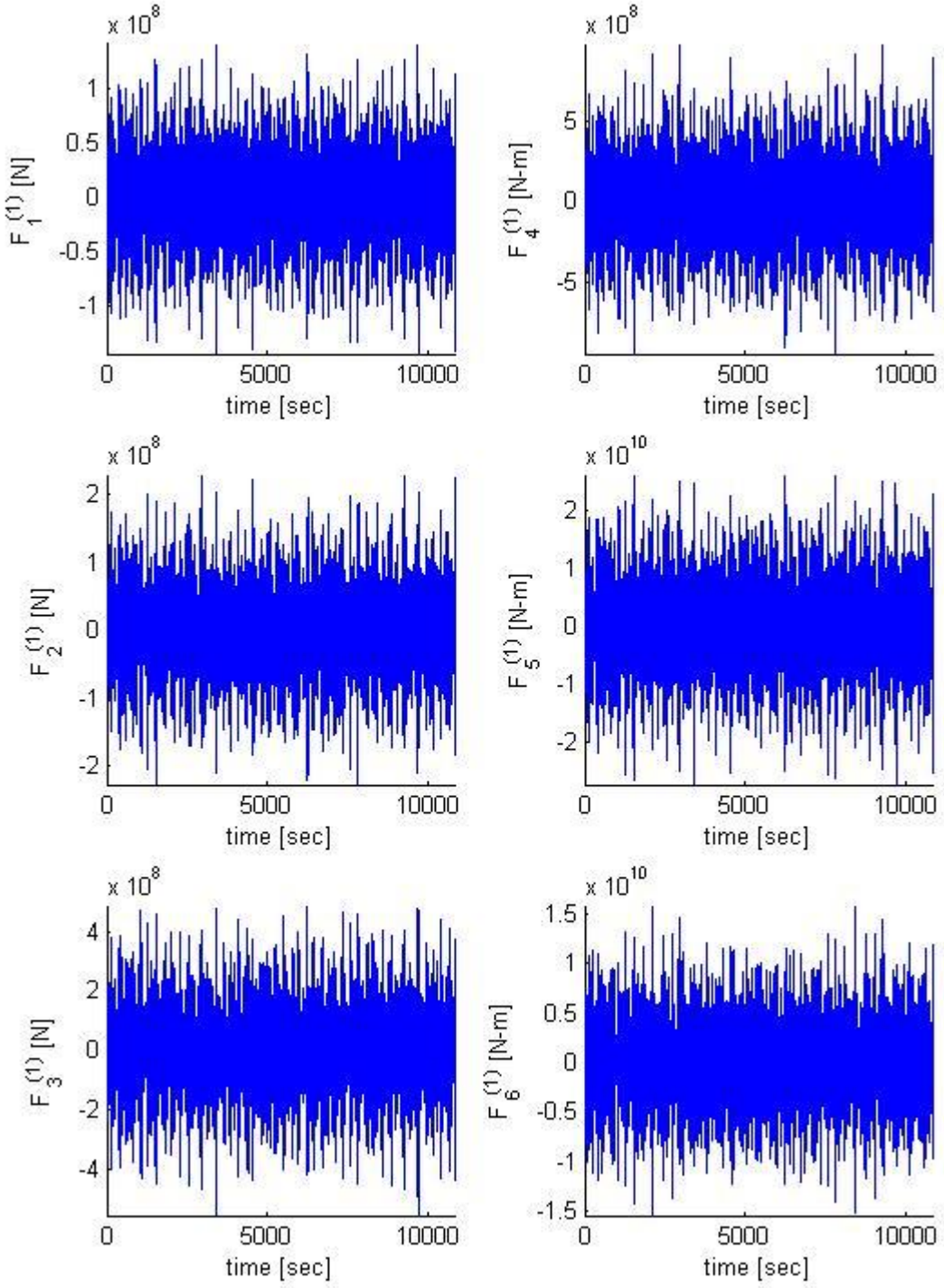

Figure 3.14 Wave exciting forces for surge, sway, heave, roll, pitch and yaw (β=150 degrees)

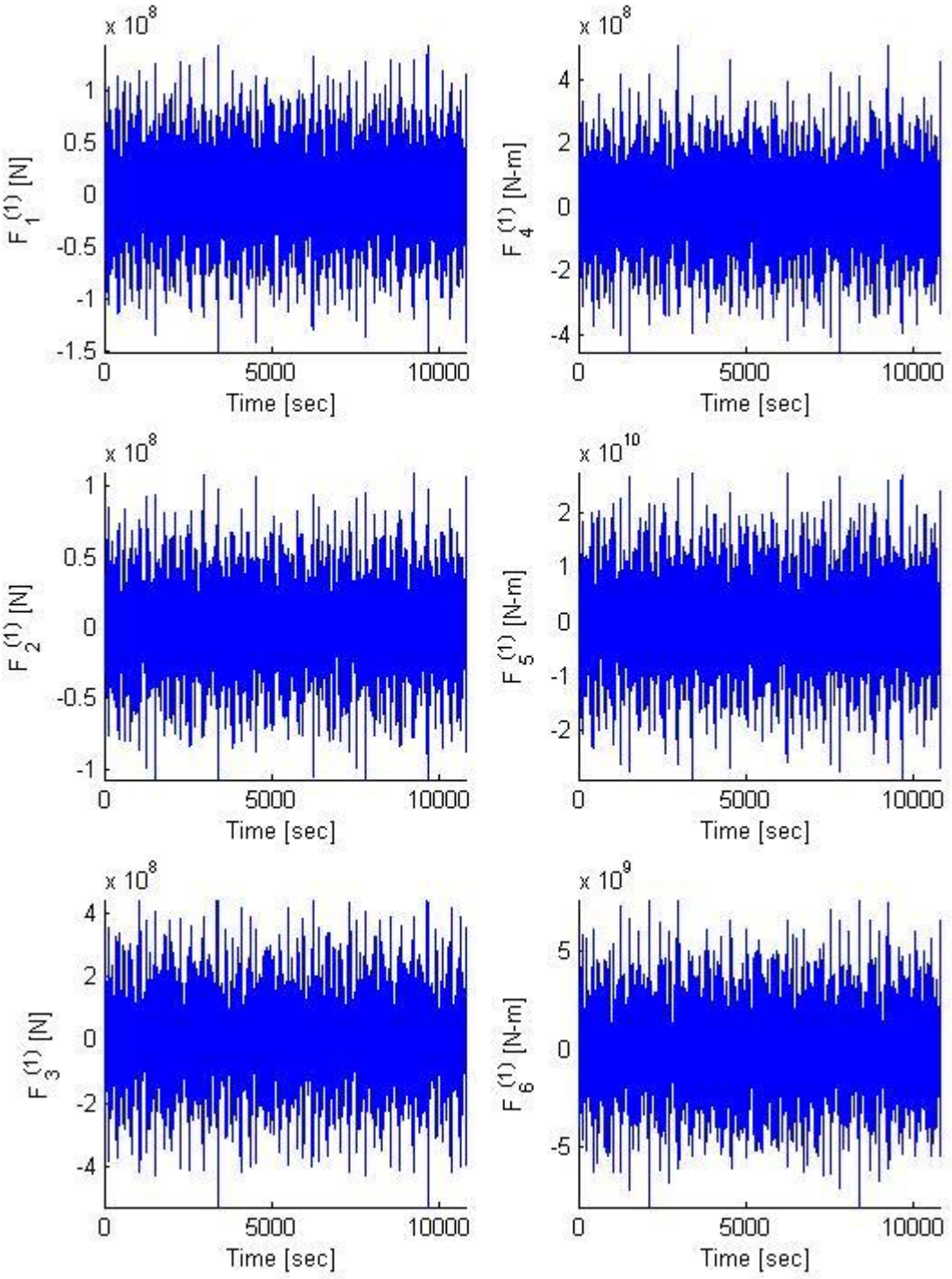

Figure 3.15 Wave exciting forces for surge, sway, heave, roll, pitch and yaw (β=165 degrees)

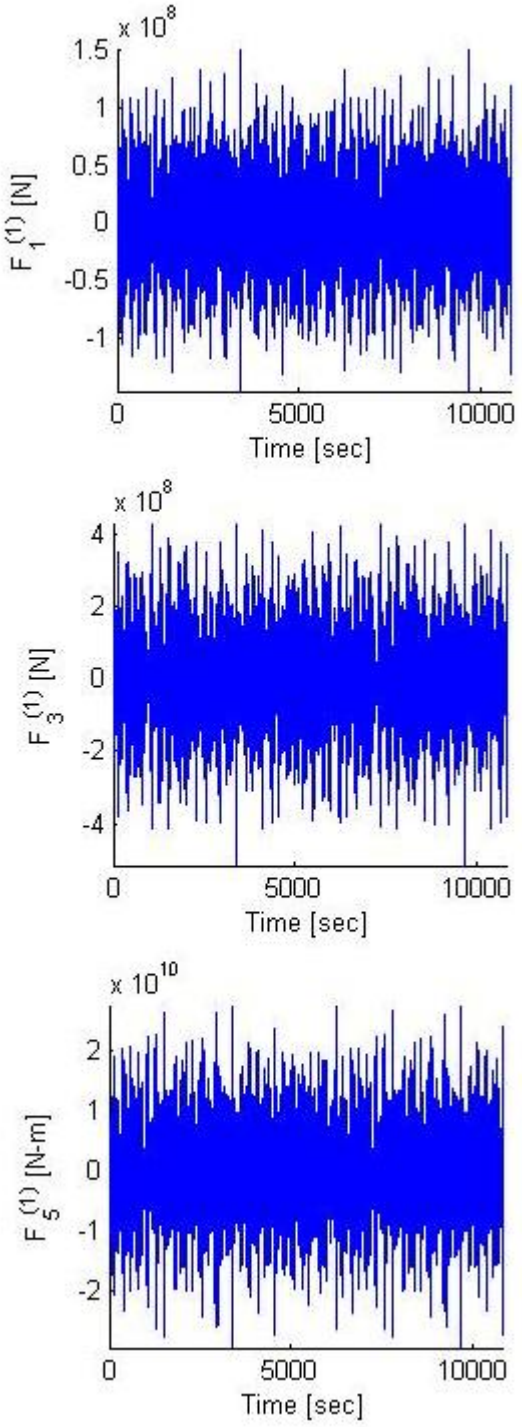

Figure 3.16 Wave exciting forces for surge, heave and pitch (β=180 degrees)

(The values of sway, roll and yaw are zero)

3.4.2 Simulated First-Order Motions

The results of the real parts of transfer functions for surge, sway and heave at 14 attachment points and the origin of the global coordinate system at three different wave heading angles have been obtained by the application of Eq. (3.13) and are shown in Figures 3.17 to 3.19. The real parts of surge transfer functions at No.1~7 attachment points show larger values than those at No.8~14 attachment points while almost same values of sway transfer functions are shown among the attachment points. Some drastic changes occur on No.5 with 165 degrees in the real part of heave transfer function. This may be caused by an irregular frequency problem having no exact solution. The values of the imaginary parts of transfer functions for surge, sway and heave at 14 attachment points and the origin of the global coordinate system in three different wave directions are shown in Figures 3.20 to 3.22 respectively, as obtained by Eq. (3.13). The values are much the same on all of the attachment points from mooring lines No.1 ~ 14.

The first-order motion RAOs for surge, sway and heave at the attachment points in three different wave directions are shown in Figures 3.23 to 3.25 respectively as obtained by Eq. (3.11). The results of surge and heave RAOs at the attachment points are similar in near bow and head waves, but the sway RAOs are different at wave heading angles 150, 165 and 180 degrees. The corresponding phase angles of surge, sway and heave motions at the attachment points in three different wave directions are shown in Figures 3.26 to 3.28 respectively as obtained by Eq. (3.12).

The time series of the first-order surge motions at the attachment points at three different wave heading angles of 150, 165 and 180 degrees are shown in Figures 3.29 to 3.31 respectively as obtained by Eq. (3.10). There is not much difference in the results among the attachment points.

The time histories of the first-order sway motions at the attachment points in three different wave directions are illustrated in Figures 3.32 to 3.34 respectively as obtained by Eq. (3.10). The magnitudes of sway motions are lessen when the heading angle is changing from 150 to 180 degrees. These differences are due to the variation of the projected area in the sway direction to the incoming waves. The values of sway motions are nearly meaningless in the case of a 180 degrees wave direction as there is no sway motion when the FPSO has a frontal symmetrical form.

The variations of the first-order heave motions with time at the attachment points in three different wave directions are demonstrated in Figures 3.35 to 3.37 respectively, as obtained by

Eq. (3.10). The amplitude of heave motion is much the same among the attachment points and the three wave directions.

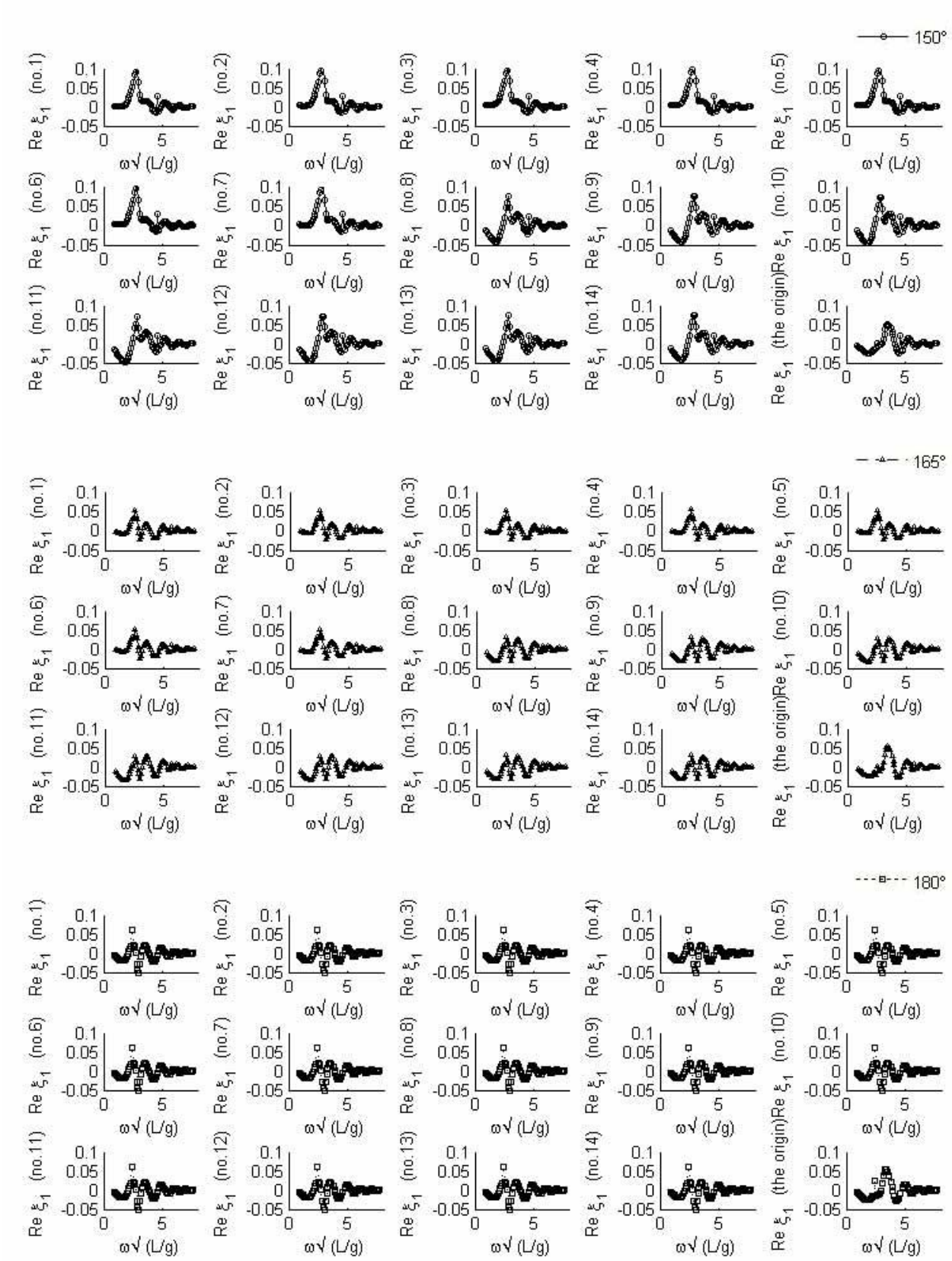

Figure 3.17 Real parts of surge transfer functions at the 14 mooring line attachment points and at the coordinate origin

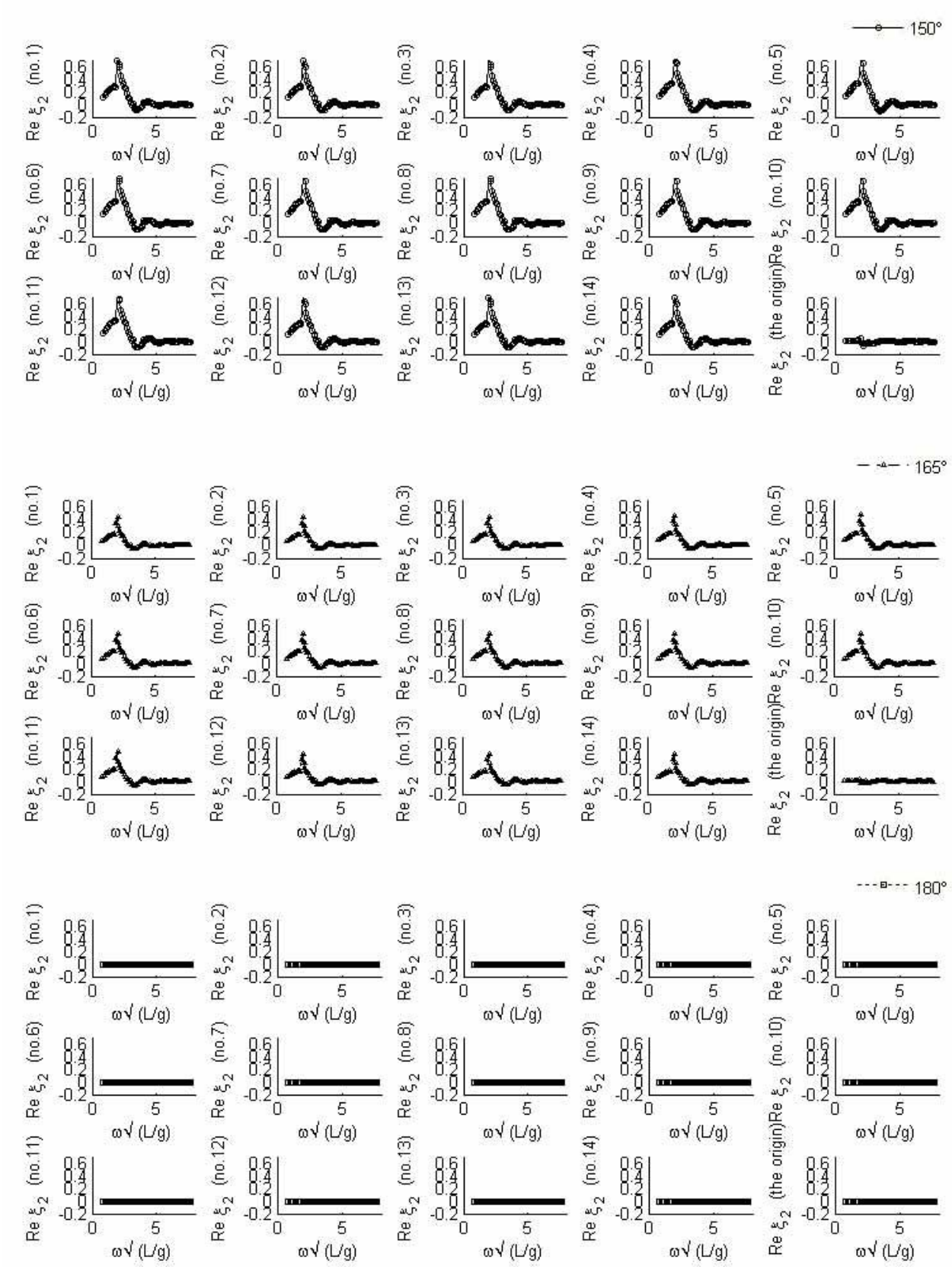

Figure 3.18 Real parts of sway transfer functions at the 14 mooring line attachment points and at the coordinate origin

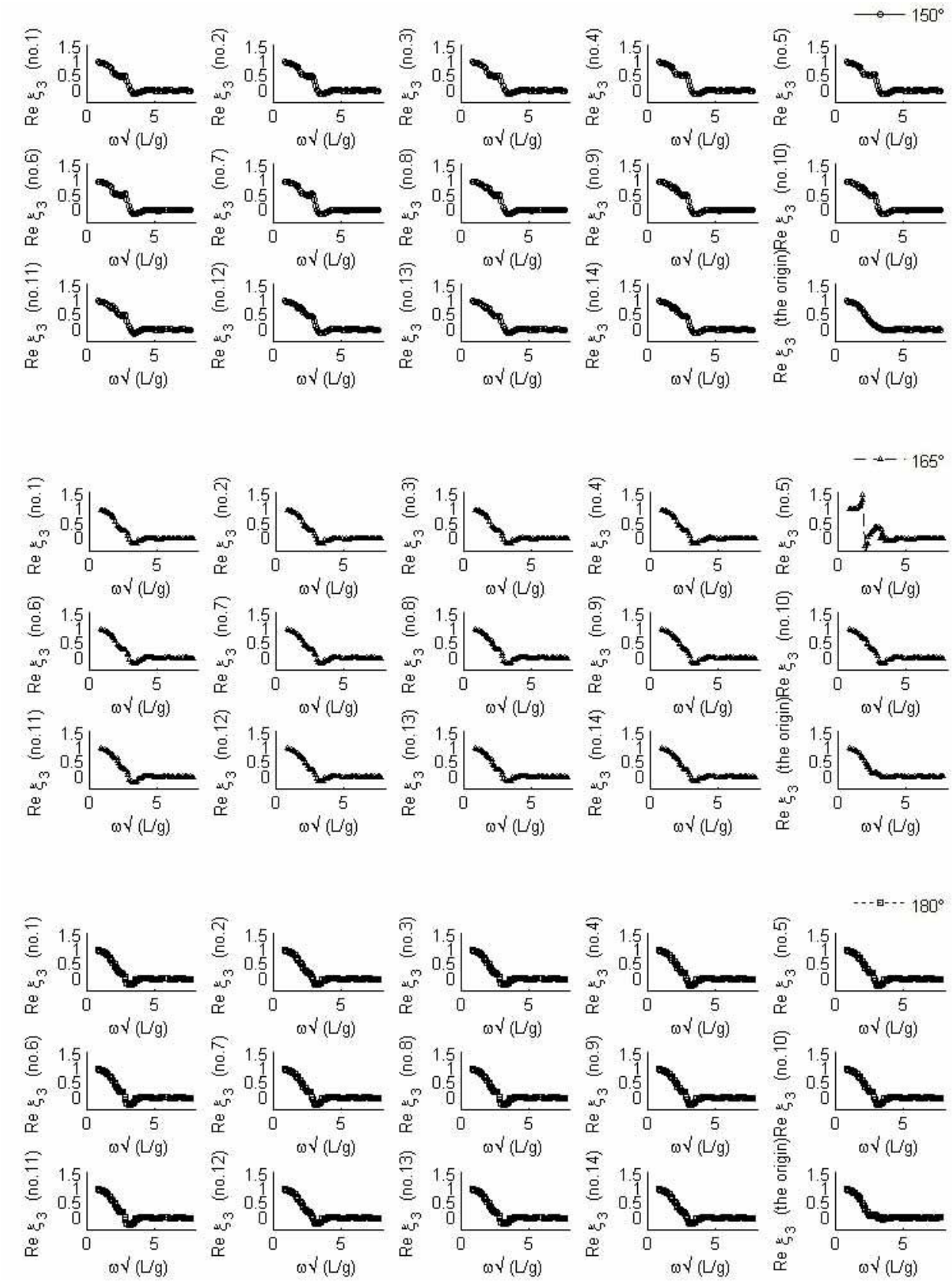

Figure 3.19 Real parts of heave transfer functions at the 14 mooring line attachment points and at the coordinate origin

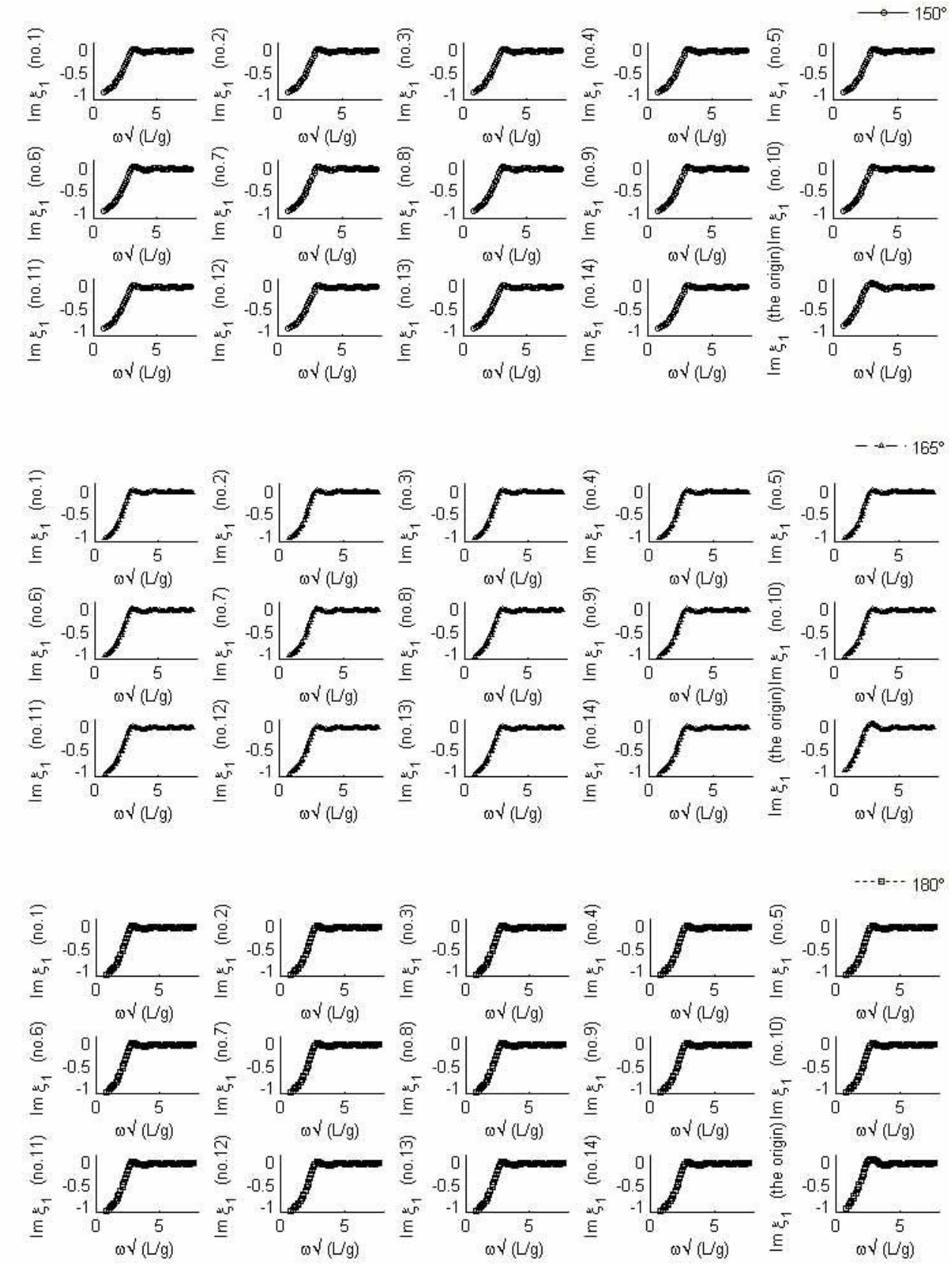

Figure 3.20 Imaginary parts of surge transfer functions at the 14 mooring line attachment points and at the coordinate origin

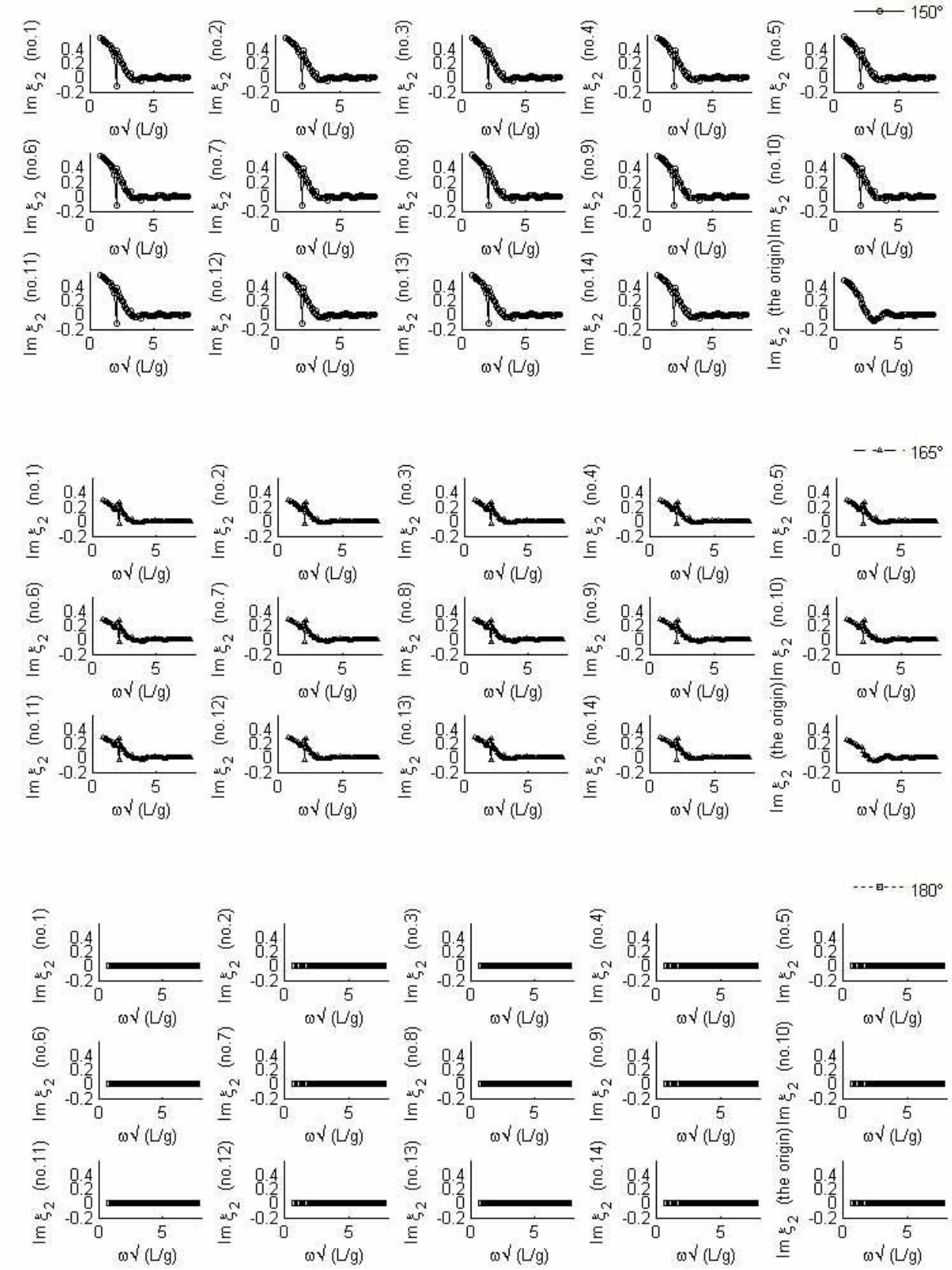

Figure 3.21 Imaginary parts of sway transfer functions at the 14 mooring line attachment points and at the coordinate origin

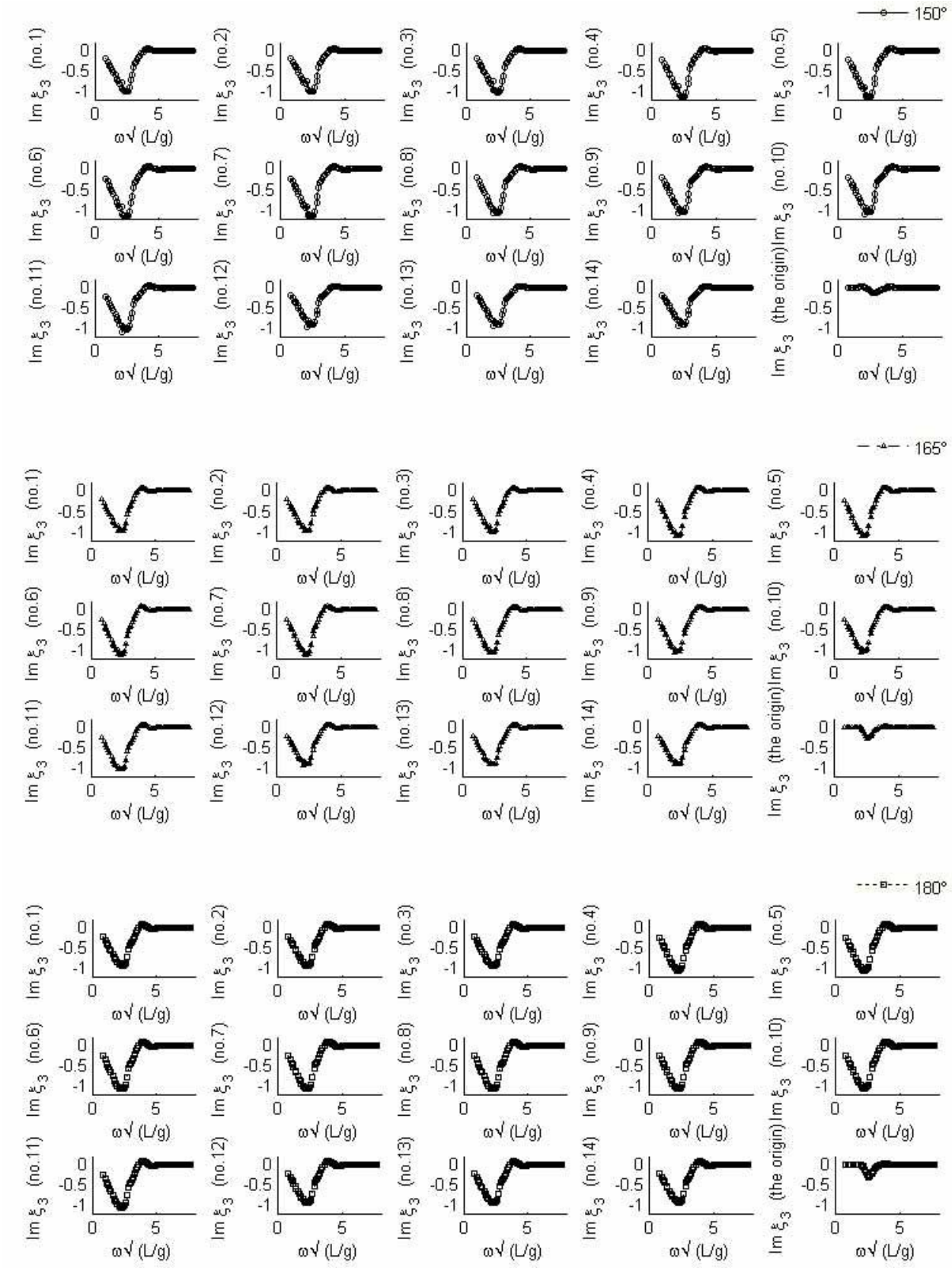

Figure 3.22 Imaginary parts of heave transfer functions at the 14 mooring line attachment points and at the coordinate origin

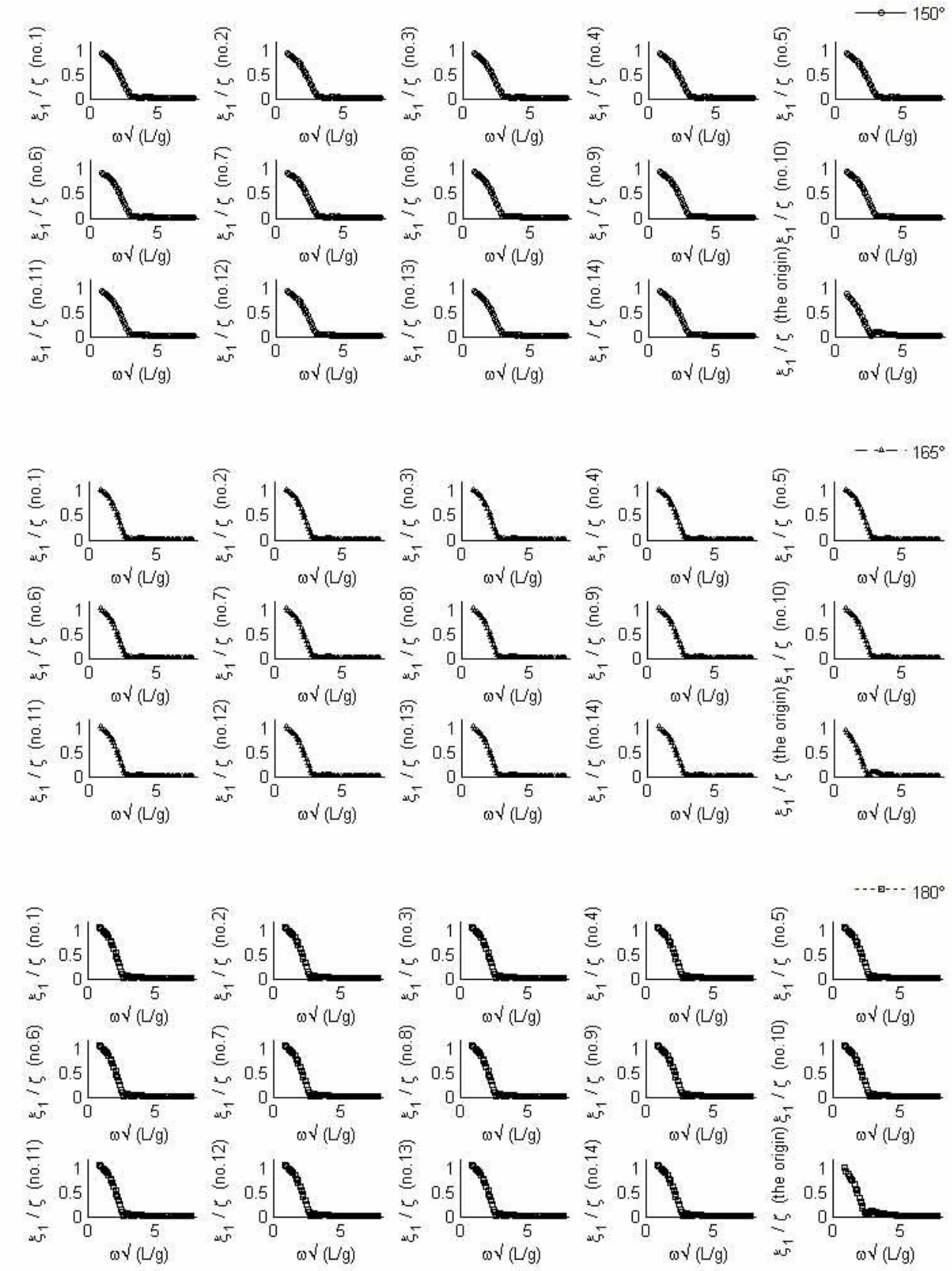

Figure 3.23 First–order surge motion RAOs at the attachment points and the origin

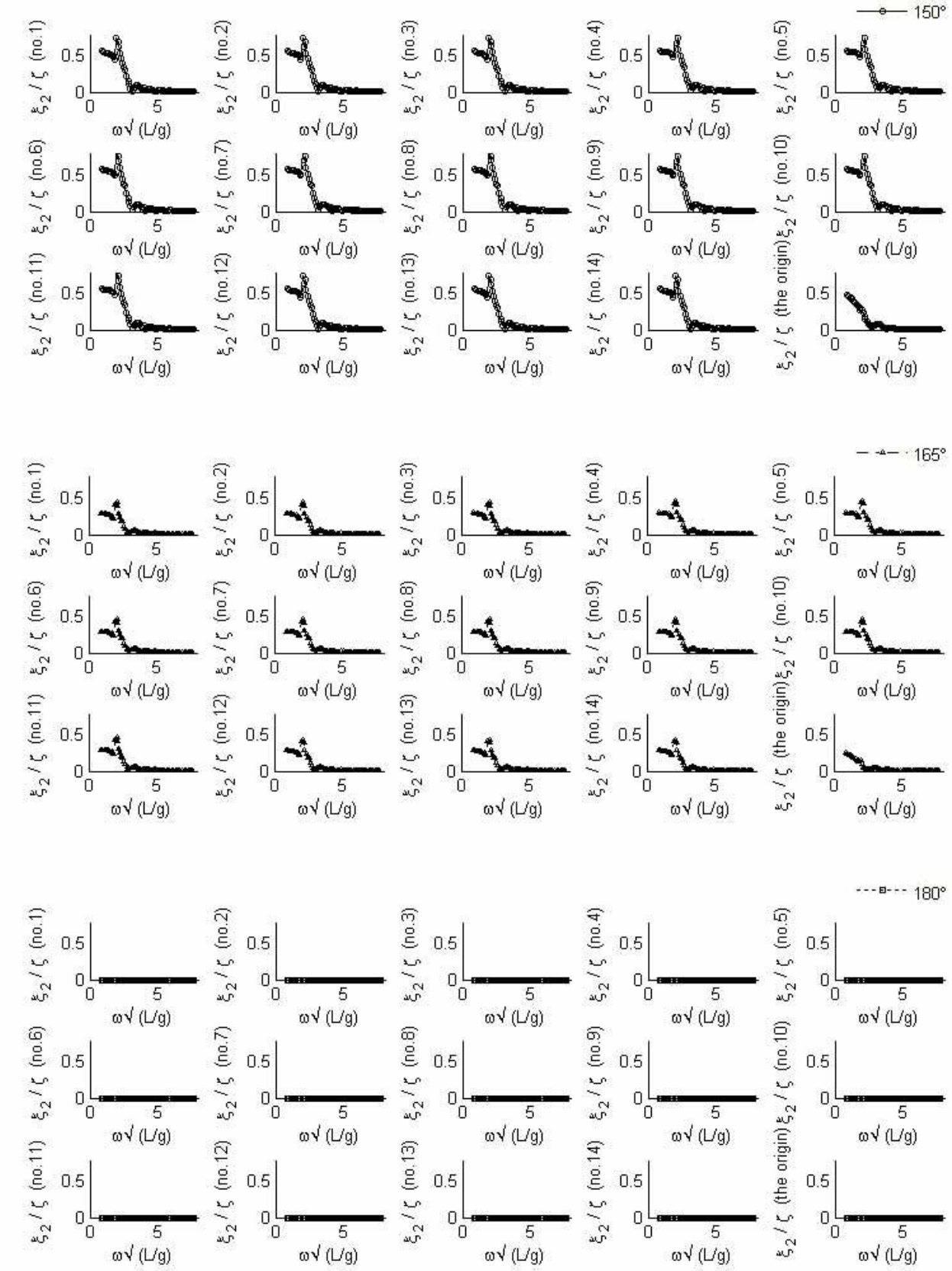

Figure 3.24 First-order sway motion RAOs at the attachment points and the origin

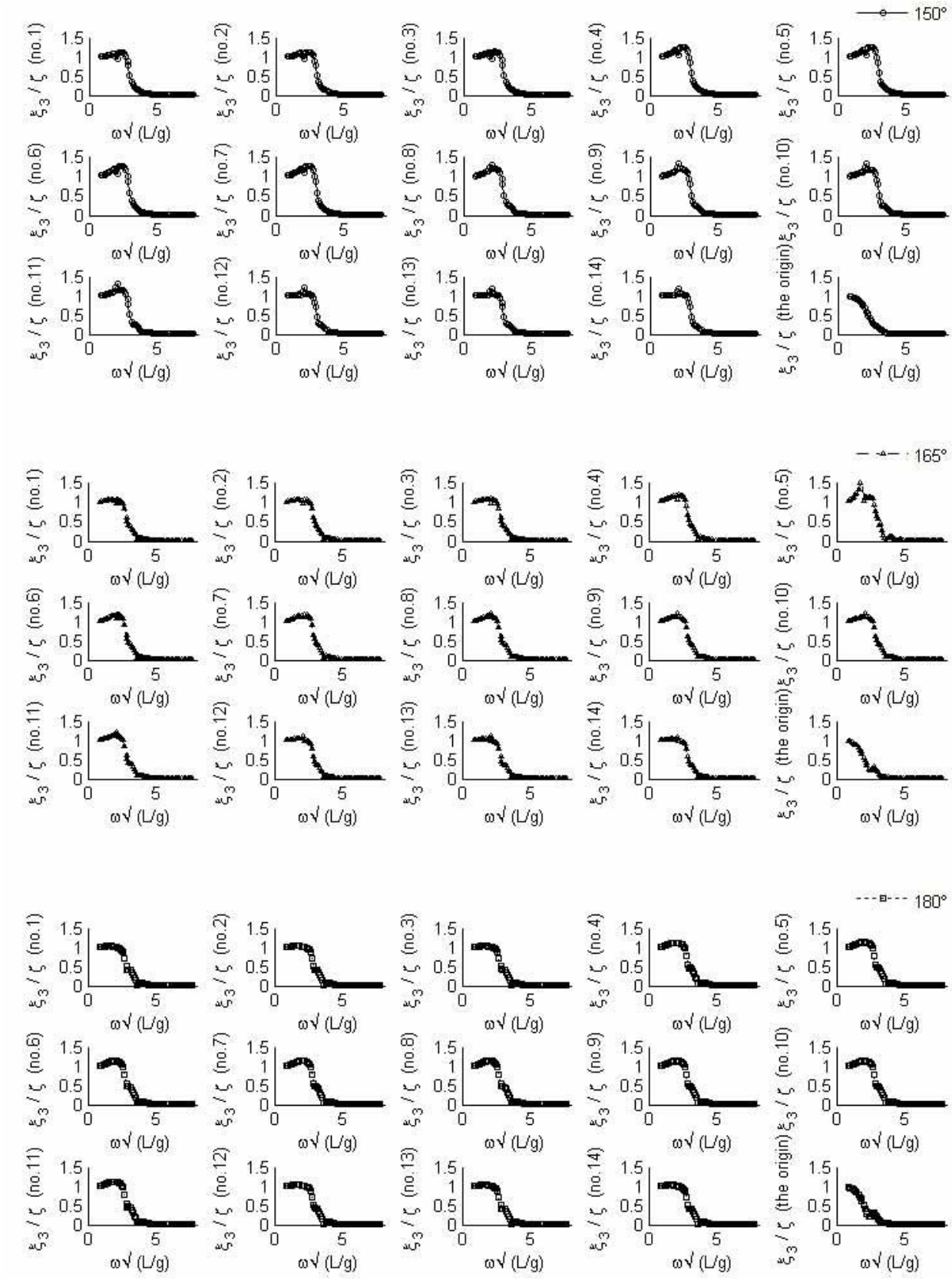

Figure 3.25 First–order heave motion RAOs at the attachment points and the origin

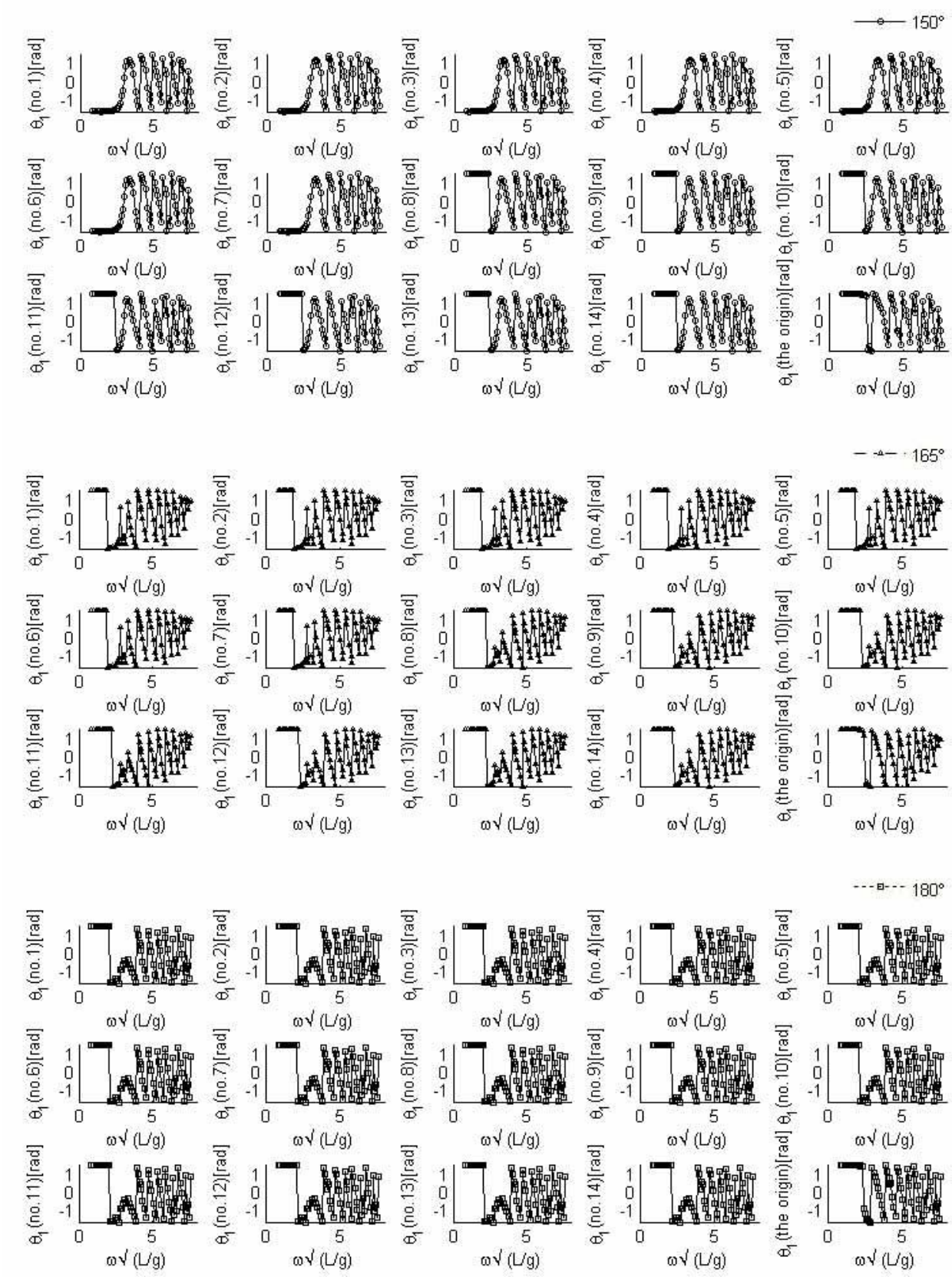

Figure 3.26 Phase angles of surge motions at the attachment points and the origin

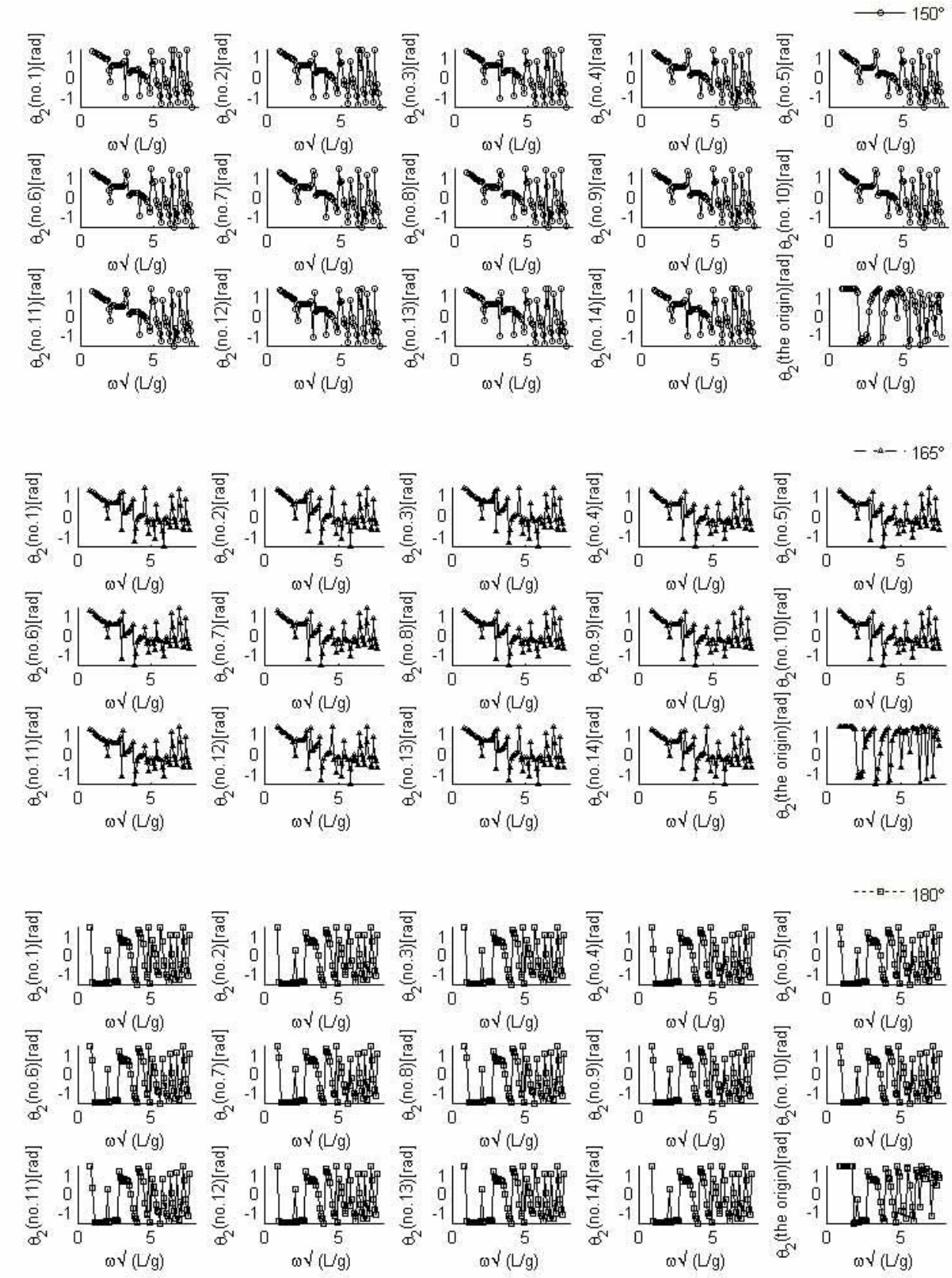

Figure 3.27 Phase angles of sway motions at the attachment points and the origin

Figure 3.28 Phase angles of heave motions at the attachment points and the origin

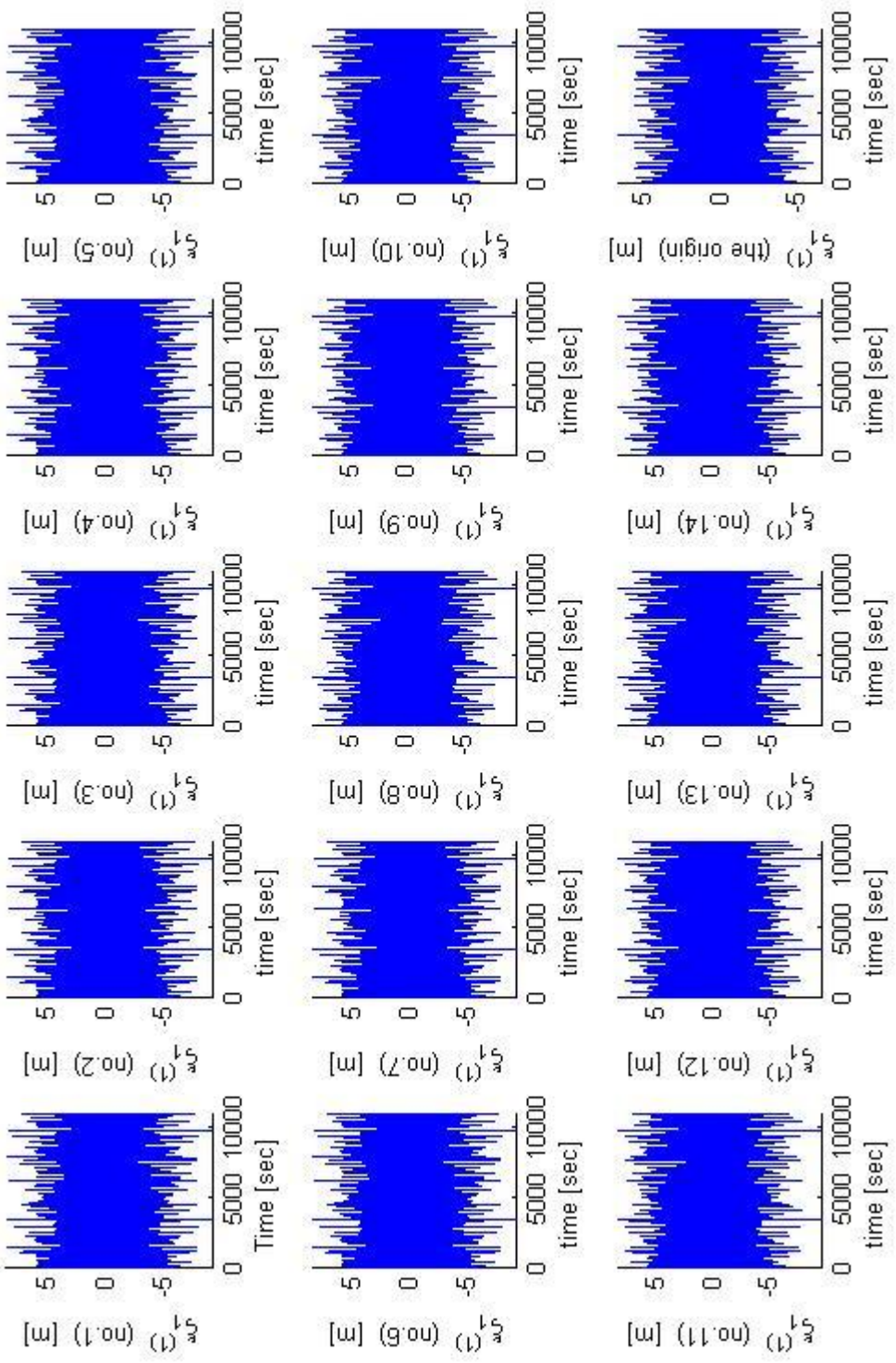

Figure 3.29 First-order surge motions at the attachment points and the origin (β=150 degrees)

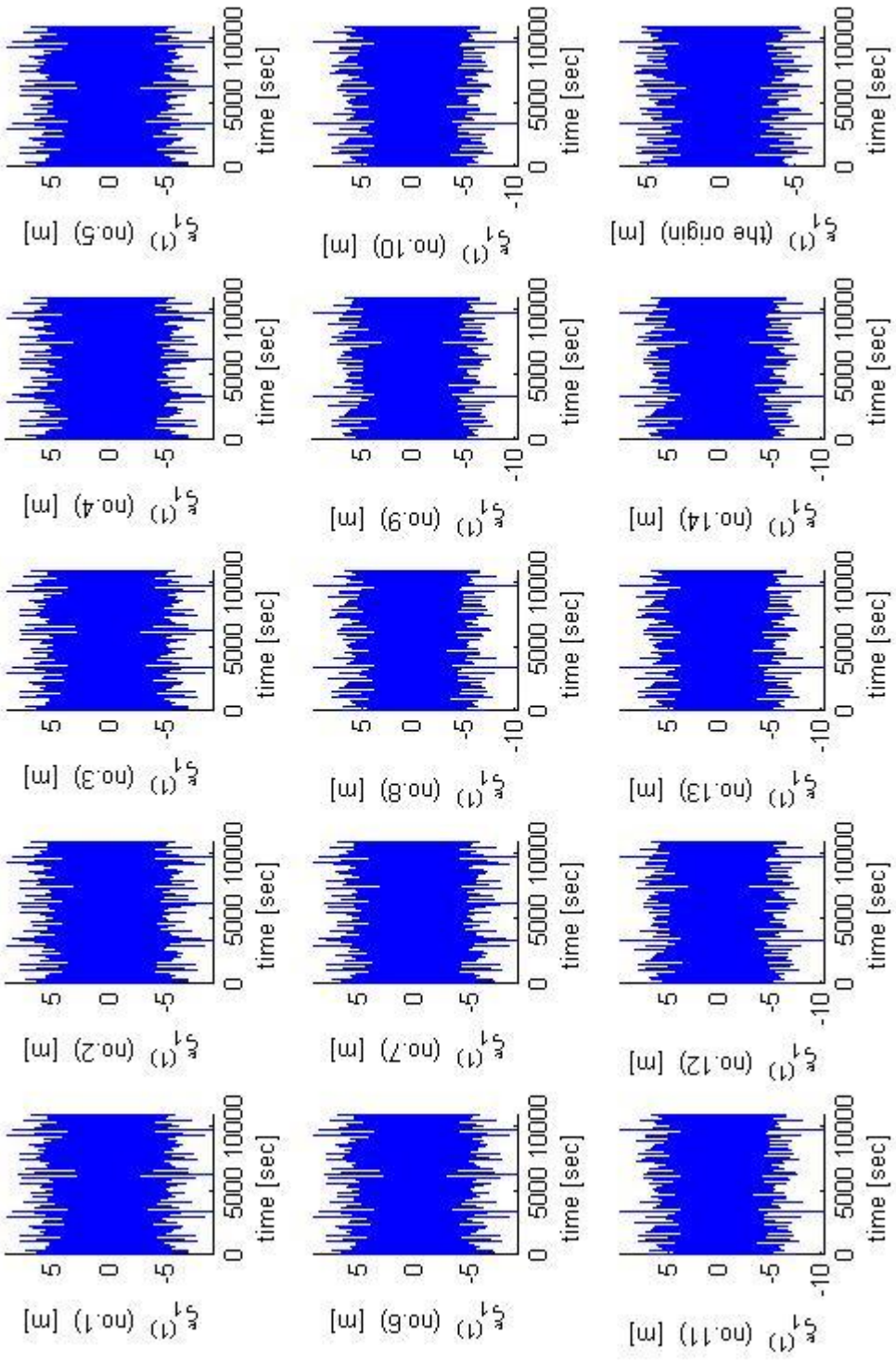

Figure 3.30 First-order surge motions at the attachment points and the origin (β=165degrees)

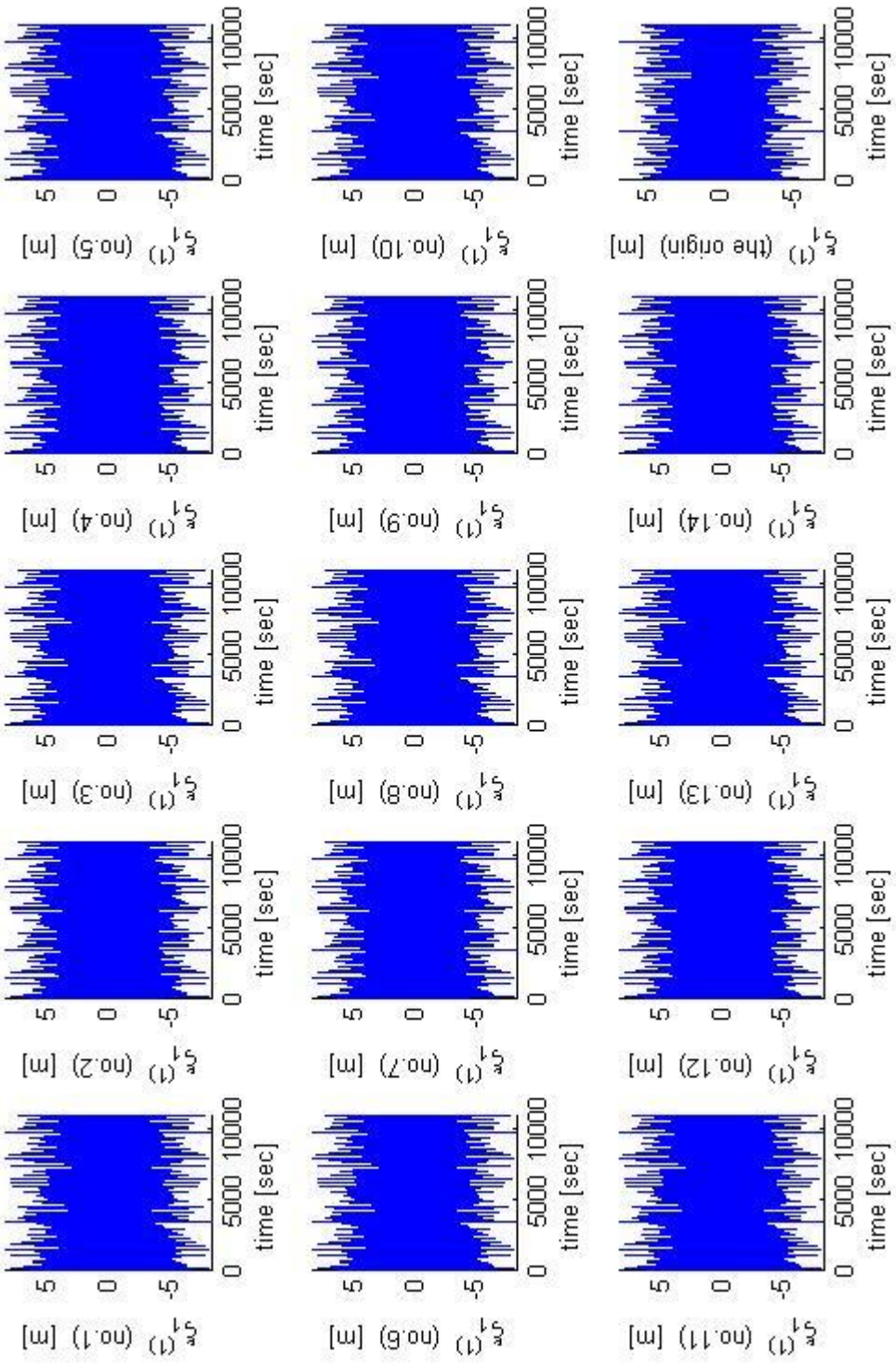

Figure 3.31 First–order surge motions at the attachment points and the origin (β=180 degrees)

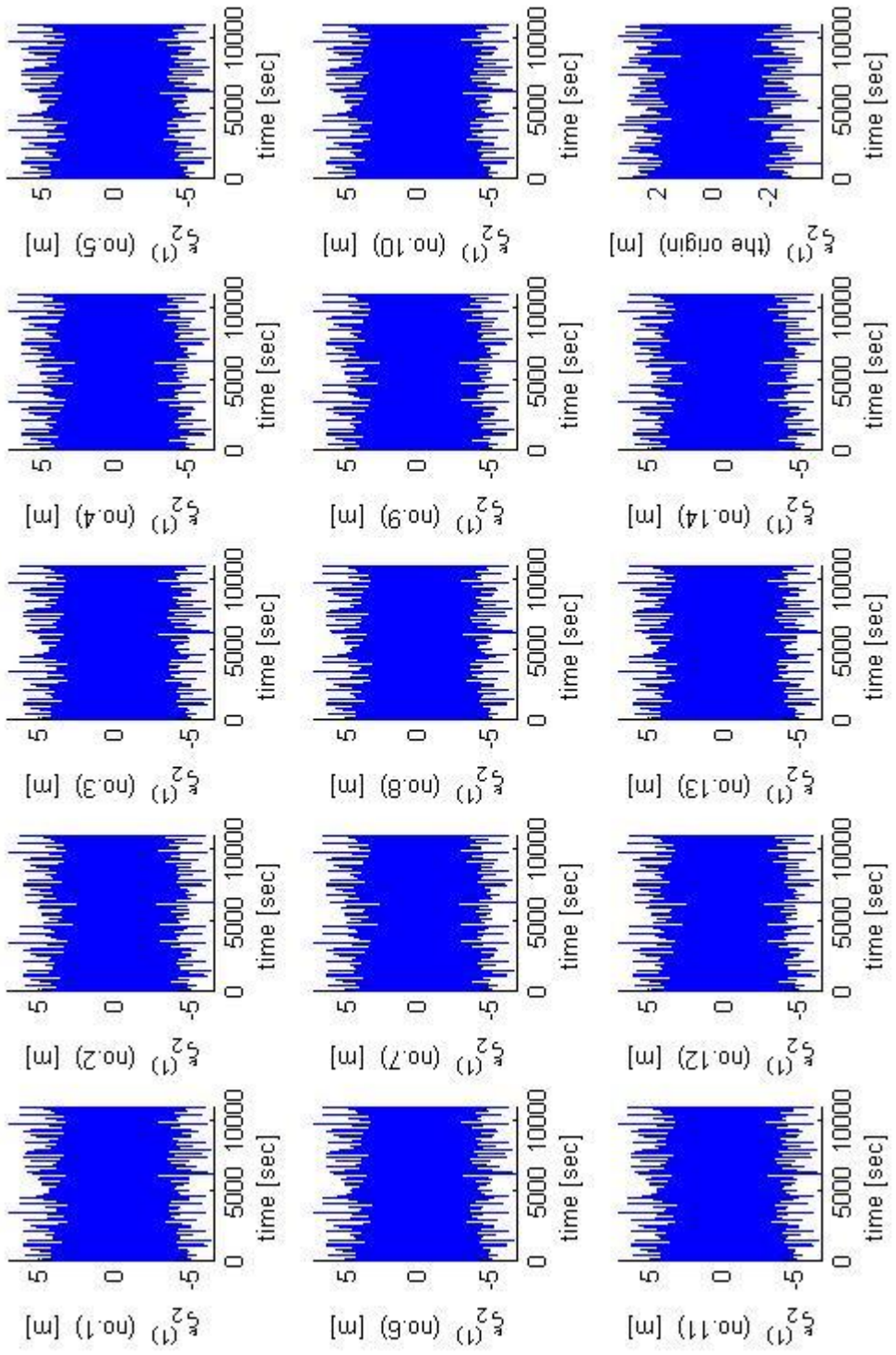

Figure 3.32 First–order sway motions at the attachment points and the origin (β=150 degrees)

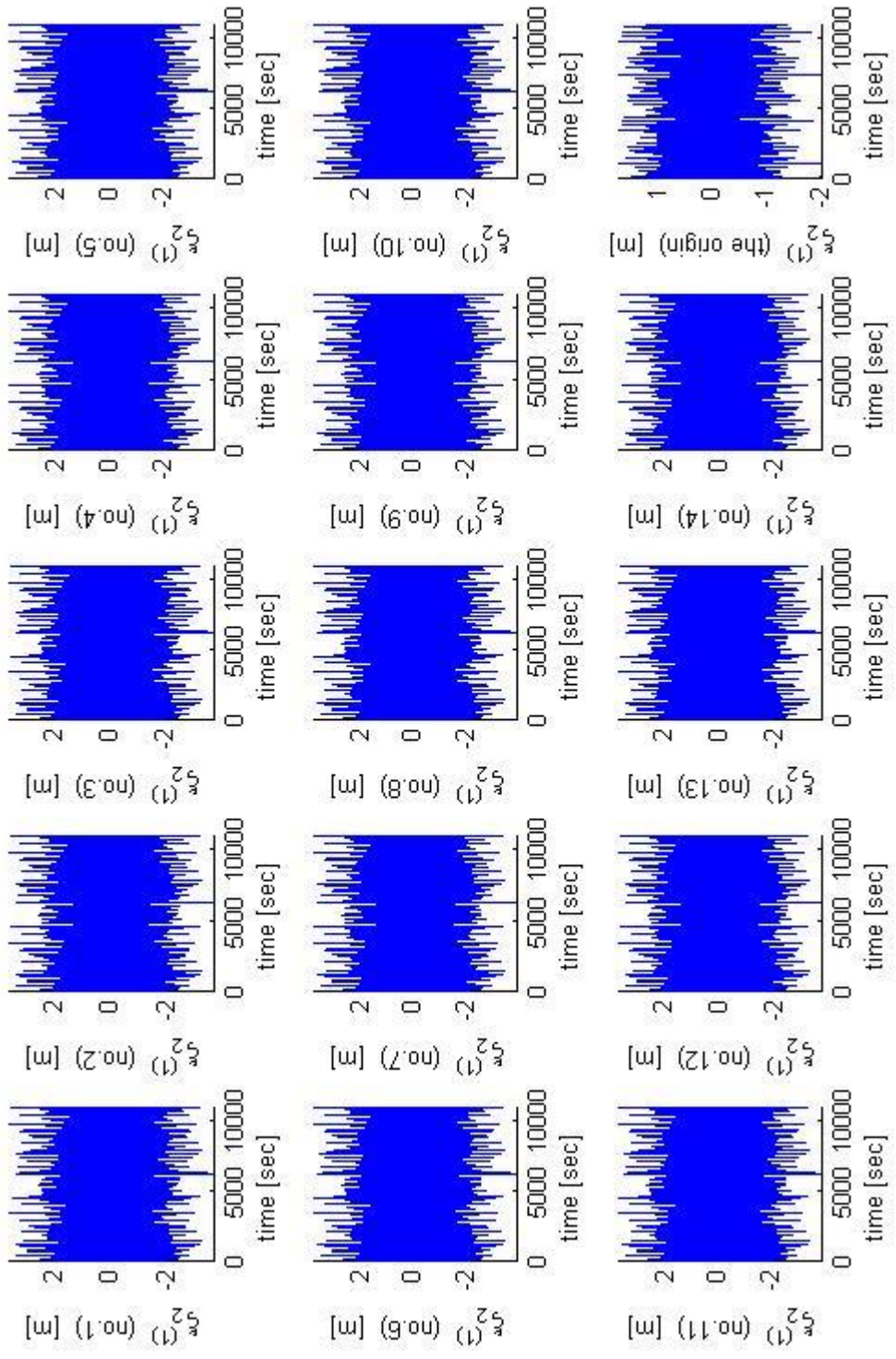

Figure 3.33 First–order sway motions at the attachment points and the origin (β=165 degrees)

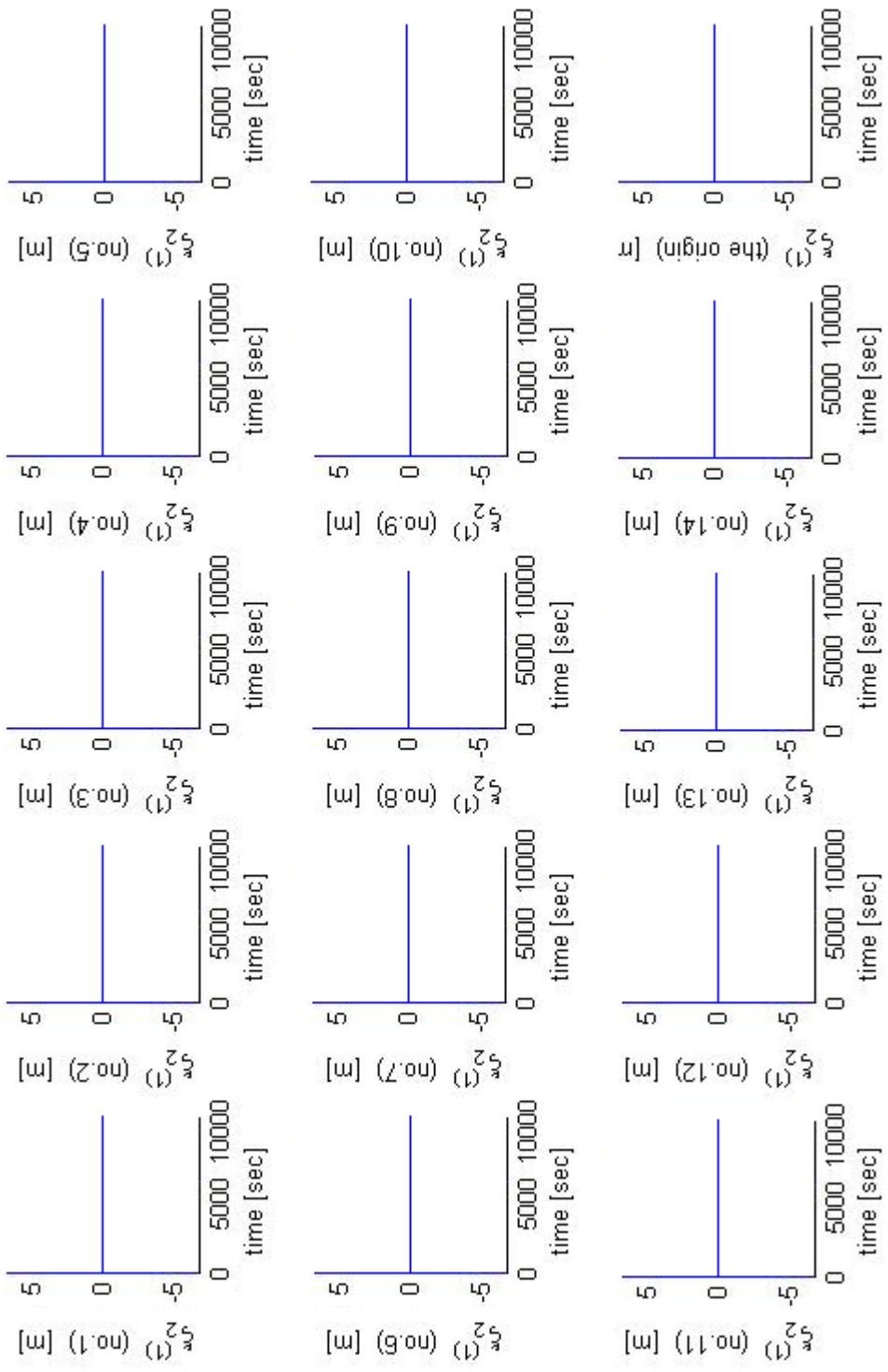

Figure 3.34 First-order sway motions at the attachment points and the origin(β=180 degrees)

(The values of sway are zero in the head sea condition, β=180)

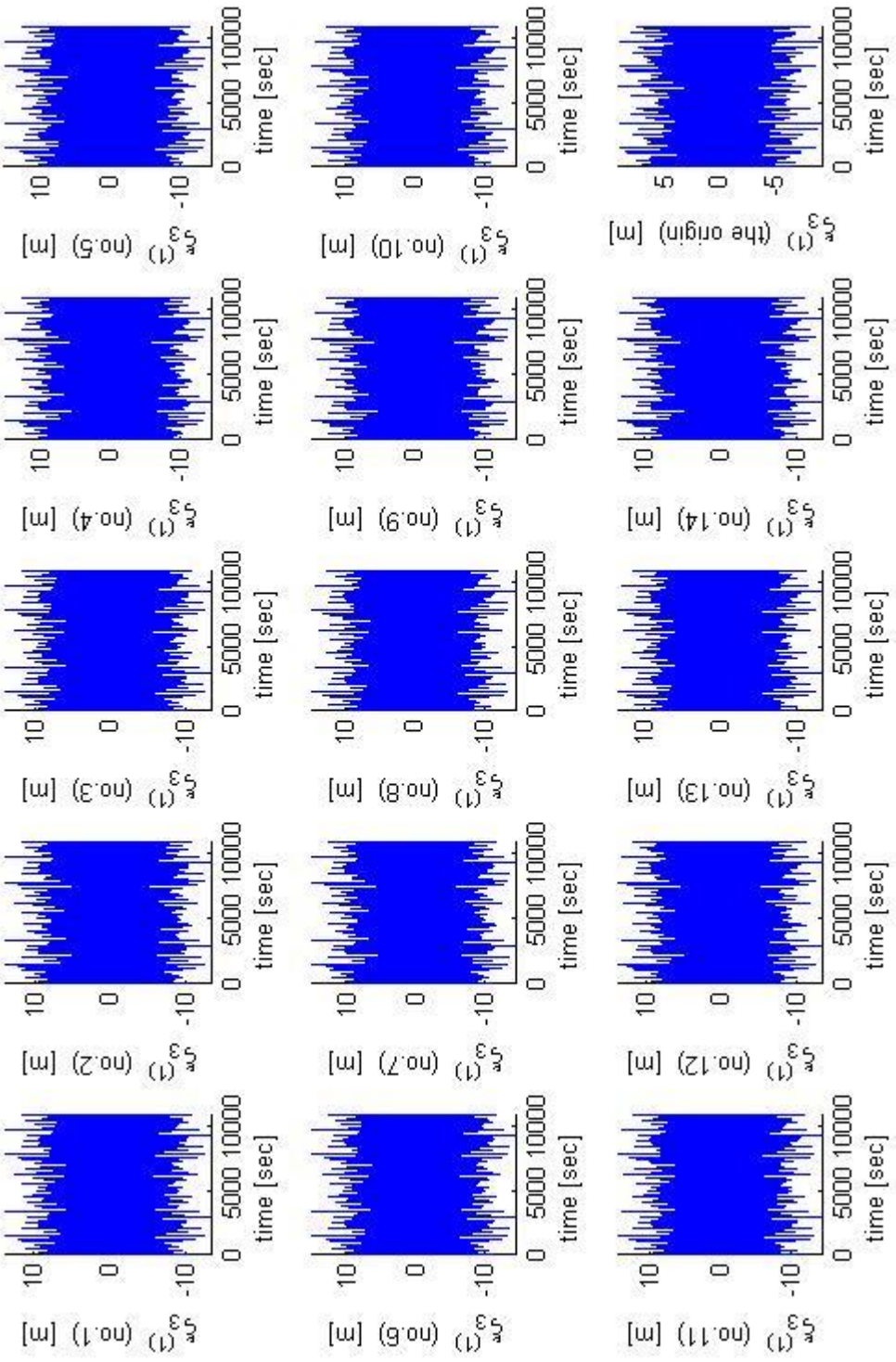

Figure 3.35 First-order heave motions at the attachment points and the origin(β=150 degrees)

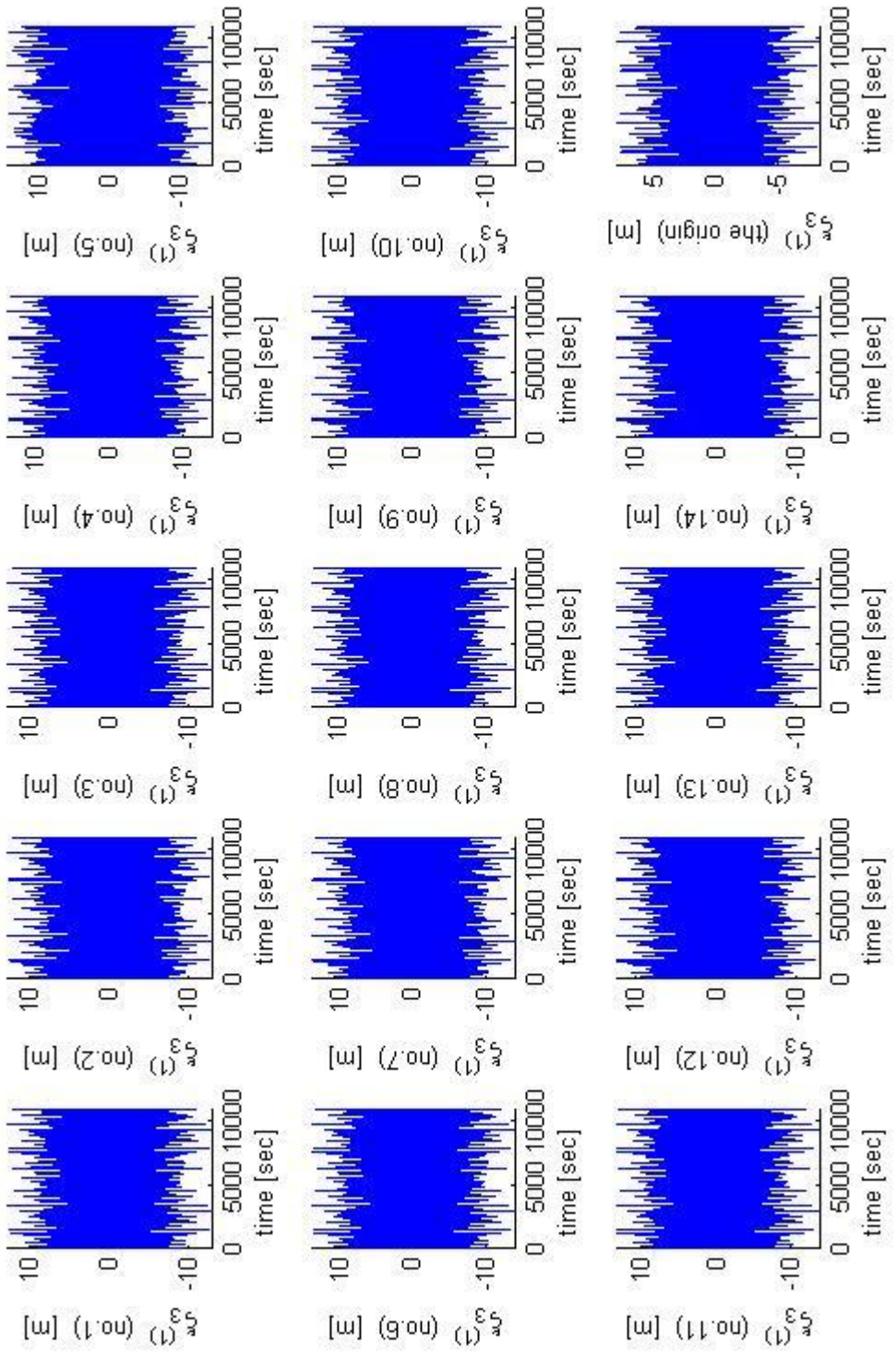

Figure 3.36 First–order heave motions at the attachment points and the origin(β=165 degrees)

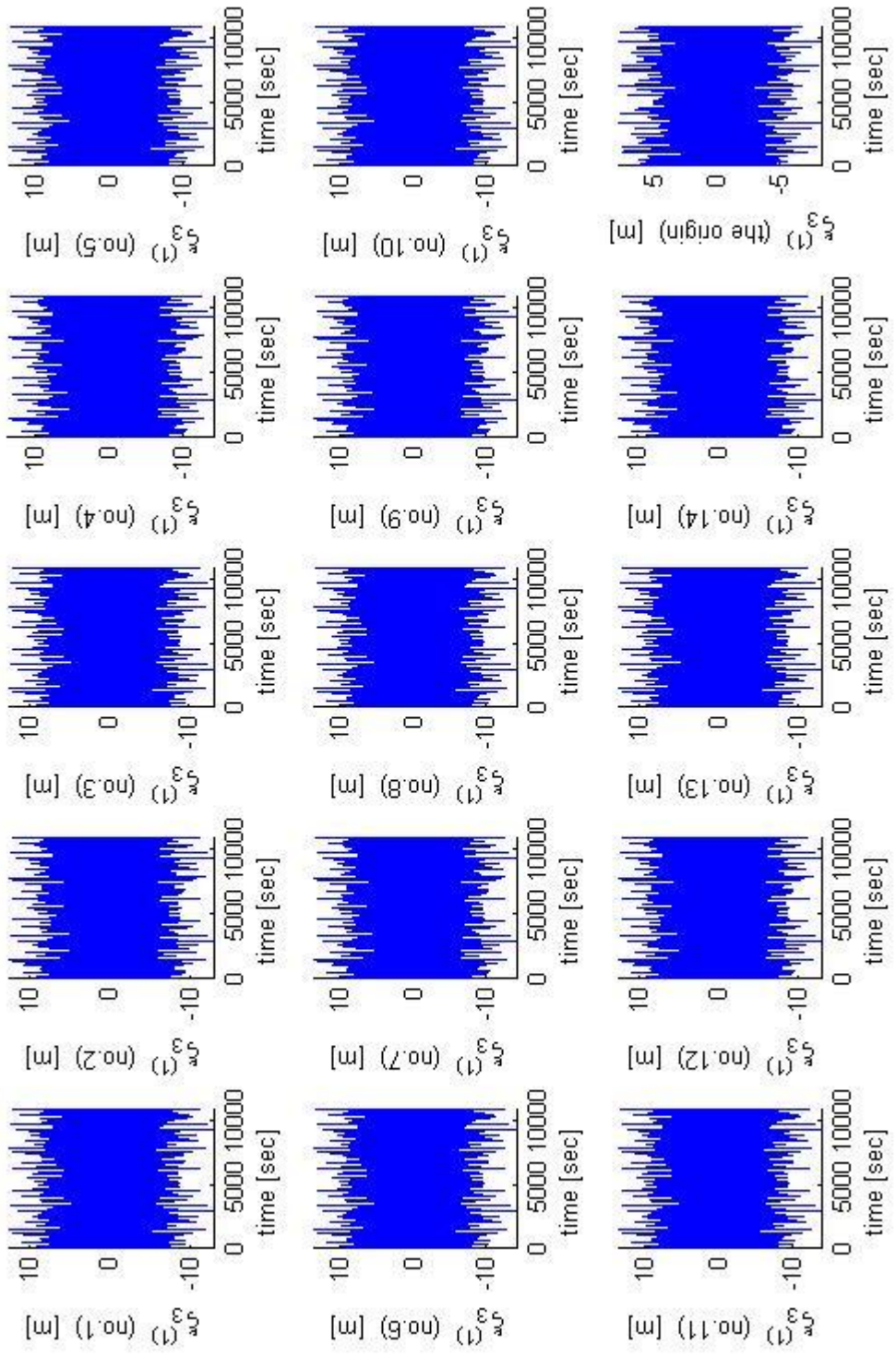

Figure 3.37 First–order heave motions at the attachment points and the origin(β=180 degrees)

Figure 3.38 shows the first-order roll motions of the FPSO at three different wave heading angles. The roll motion amplitudes are decreasing with change in wave direction from 150 to 180 degrees as is the same for the case of sway motions as shown previously in Figures 3.32 to 3.34. Similarly, the time series of the first-order yaw motions of the FPSO shown in Figure 3.40 are also reduced when the wave heading angle increases from 150 to 180 degrees. The time history of the first-order pitch motions of the FPSO are shown in Figure 3.39 and the motion amplitudes are not, however, decreasing with change in wave direction, as also in the case of heave motions shown in Figures 3.35 to 3.37.

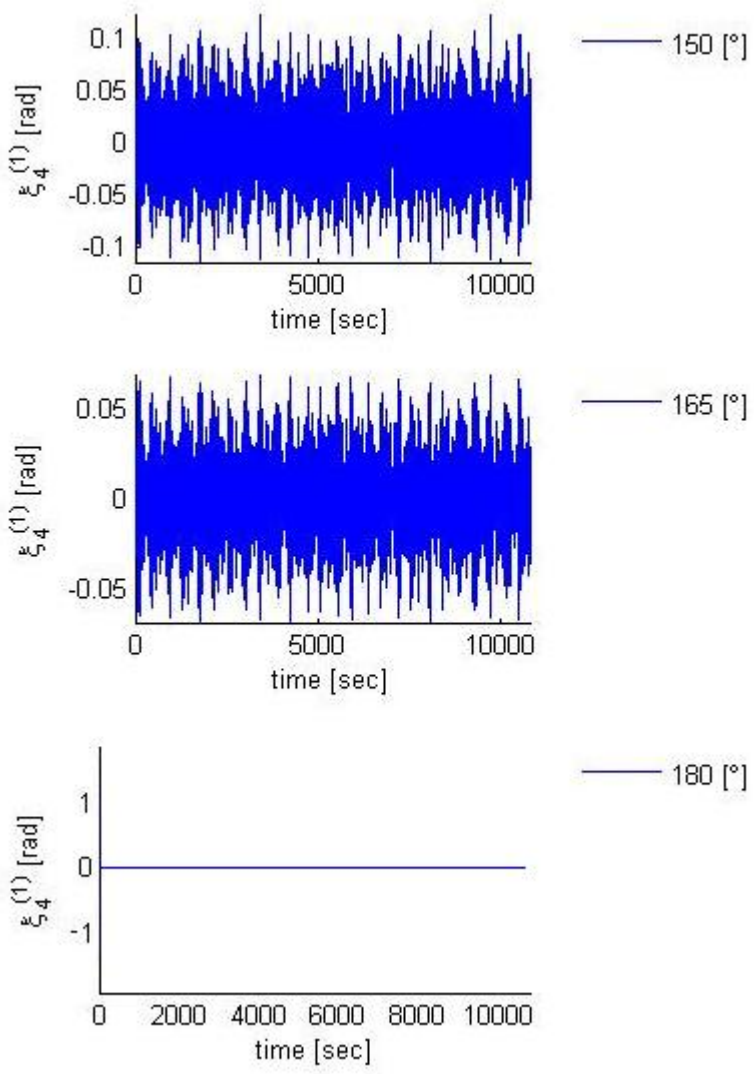

Figure 3.38 First-order roll motion of the FPSO

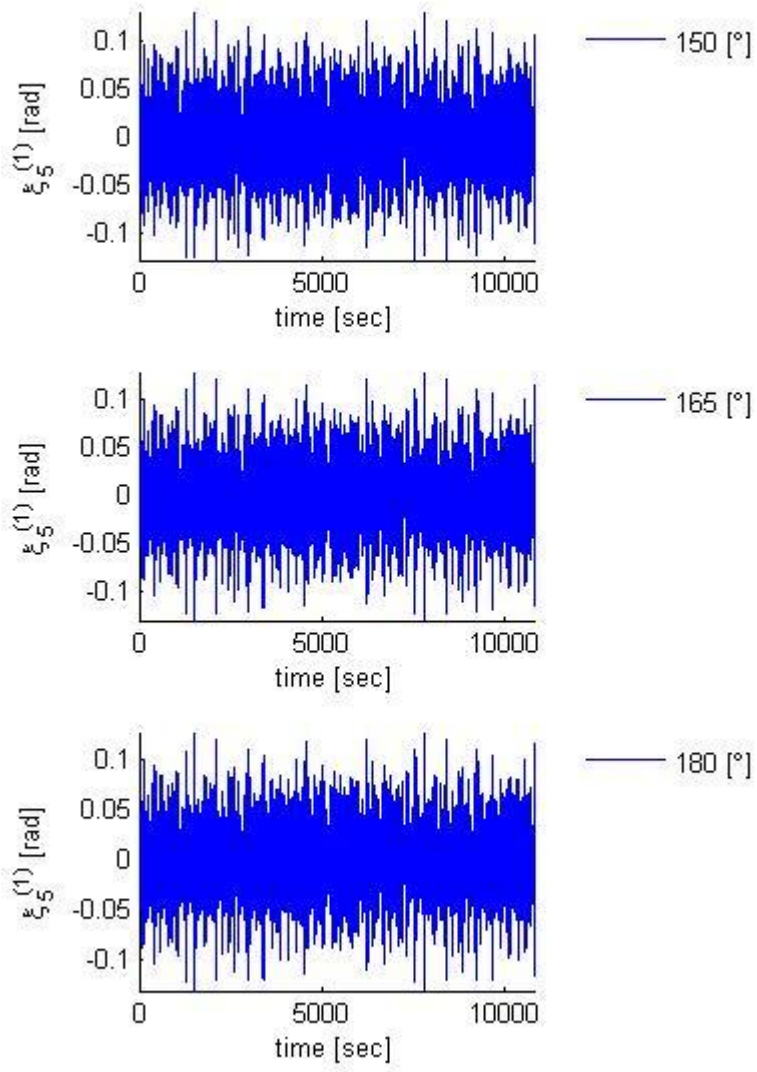

Figure 3.39 First-order pitch motions of the FPSO

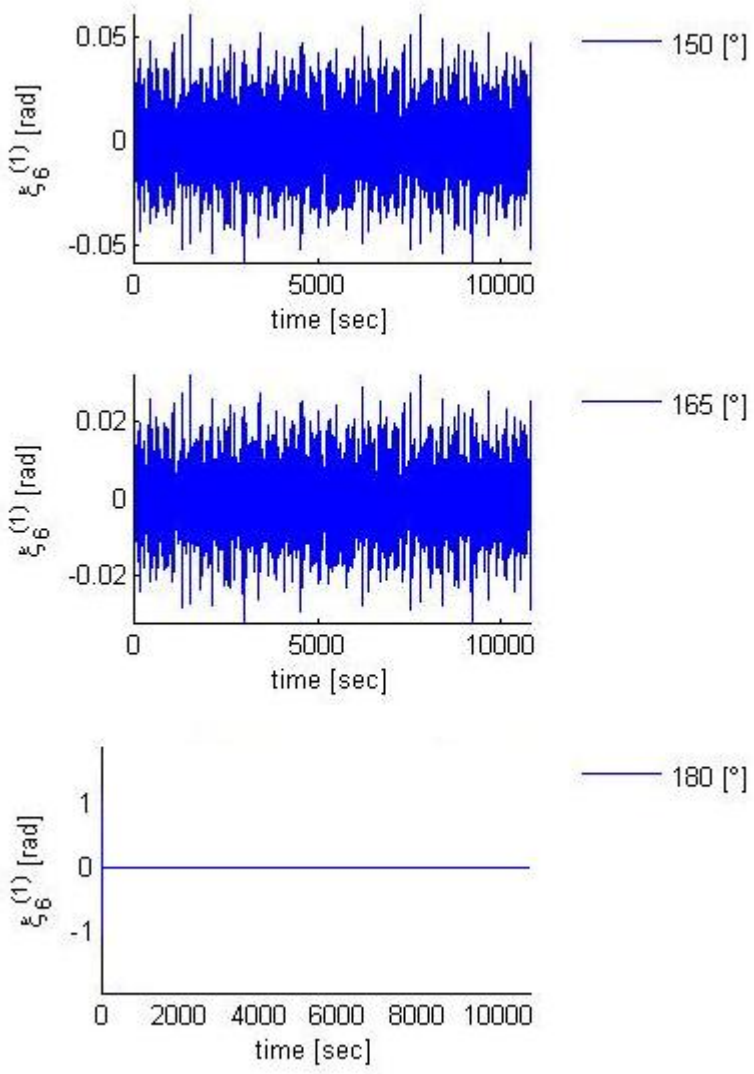

Figure 3.40 First-order yaw motions of the FPSO

3.4.3 Simulated Second-Order Forces

The calculation of the slowly varying low frequency motions of the moored FPSO due to the non-linear wave loads is necessary in order to ensure the operational position and safe design of mooring system. A time-domain simulation is beneficial for the intuitive observation for the vessel's motions.

The time series of the second-order surge and sway forces and yaw moments on the FPSO in three different wave heading angles are shown in Figures 3.41 to 3.43 respectively as obtained by Eq. (3.19). The second-order sway forces and yaw moments decrease largely with change in wave heading angle from 150 degrees to 180 degrees, while the second-order surge forces change little in magnitude. The values of the second-order sway force and yaw moment in head seas are negligible.

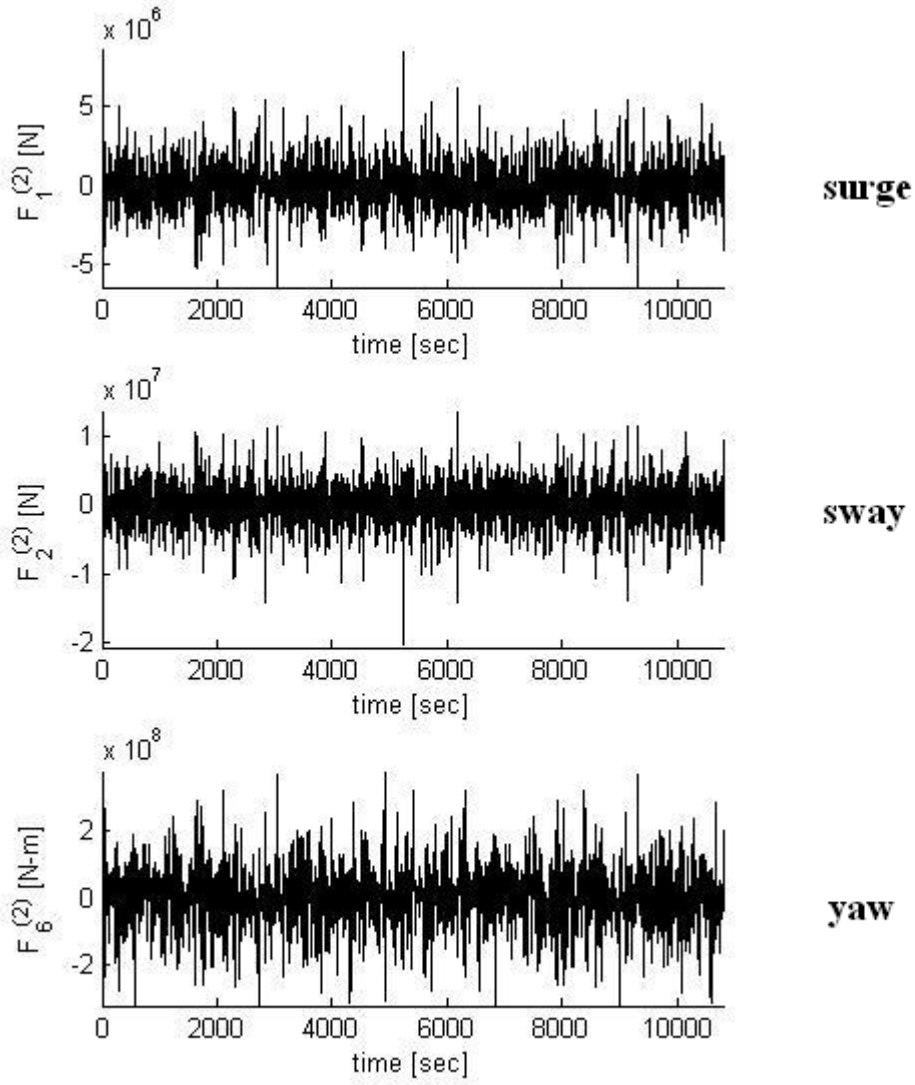

Figure 3.41 Second-order surge and sway forces and yaw moment (β=150 degrees)

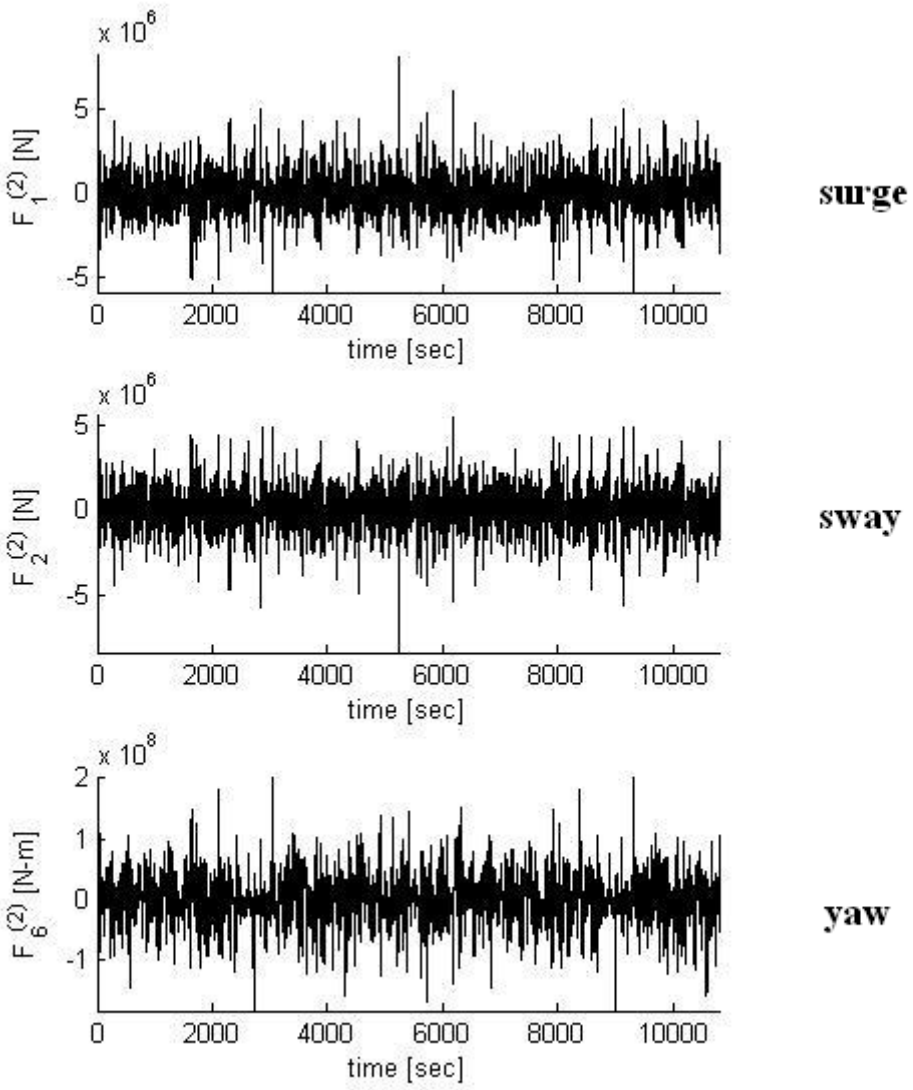

Figure 3.42 Second-order surge and sway forces and yaw moment (β=165 degrees)

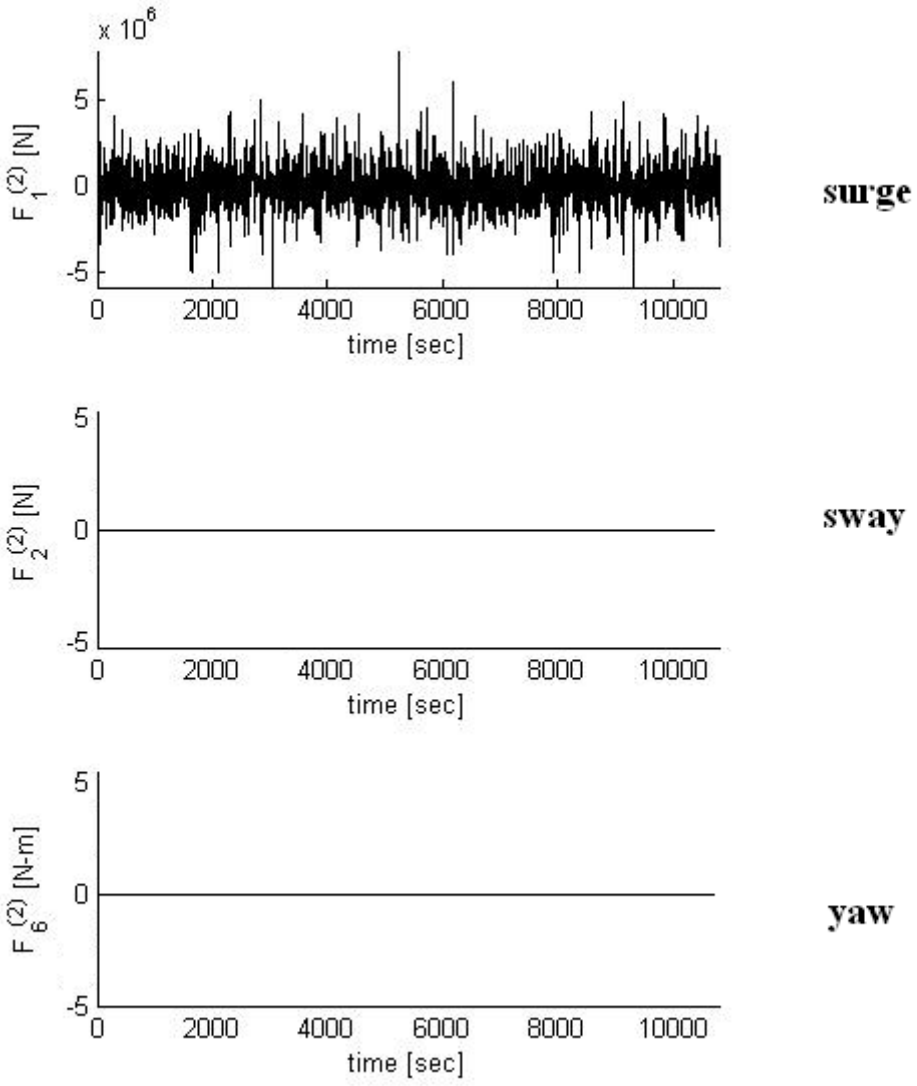

Figure 3.43 Second-order surge and sway forces and yaw moment (β=180 degrees)

3.4.4 Simulated Second-Order Motions

The time series of the second-order surge, sway and yaw motions of the FPSO in three different wave directions are shown in Figures 3.44 to 3.46 respectively as obtained by Eq. (3.18). The sway and yaw motions are significantly reduced according to the changes of the wave directions while the surge motions are not reduced so much as sway and yaw. These motions are to be combined with the first-order motions in order to give rise to the expected total displacement. After that, the corresponding mooring line tensions can be calculated considering all the variations of physical positions with time at line attachment points.

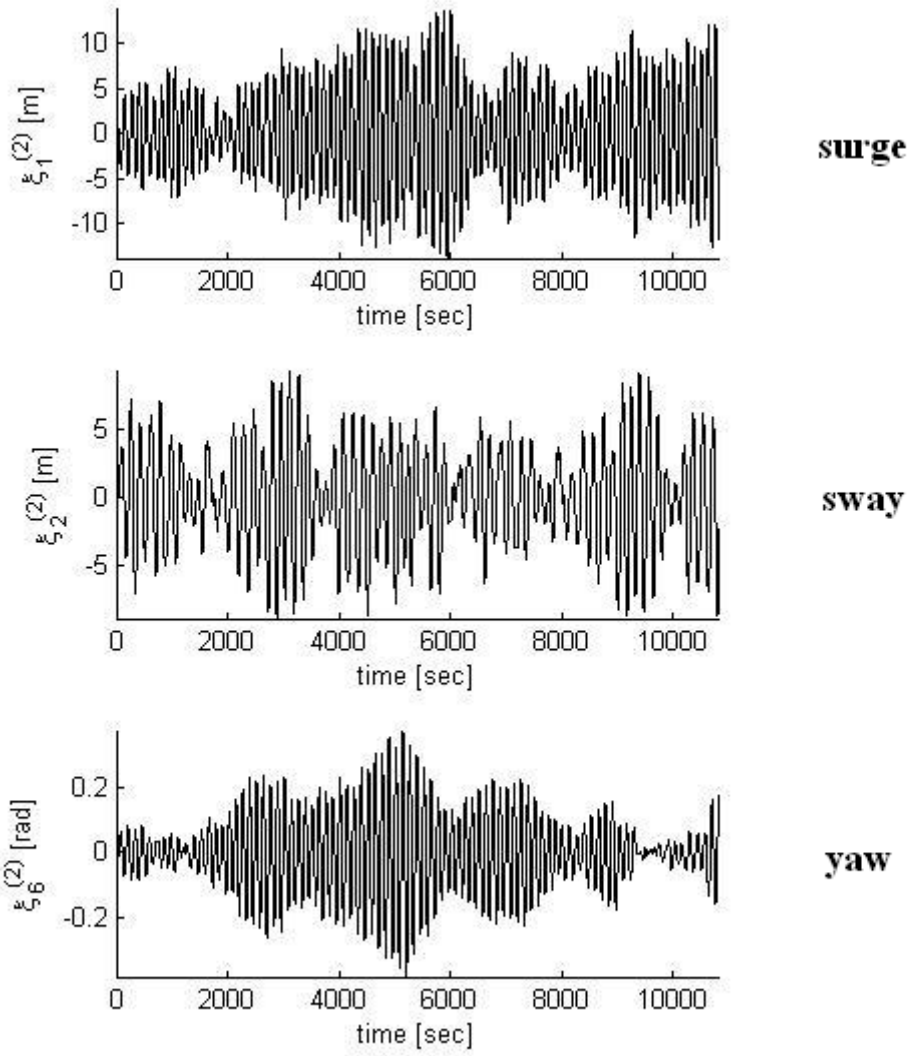

Figure 3.44 Second-order surge, sway and yaw motions of the FPSO (β=150 degrees)

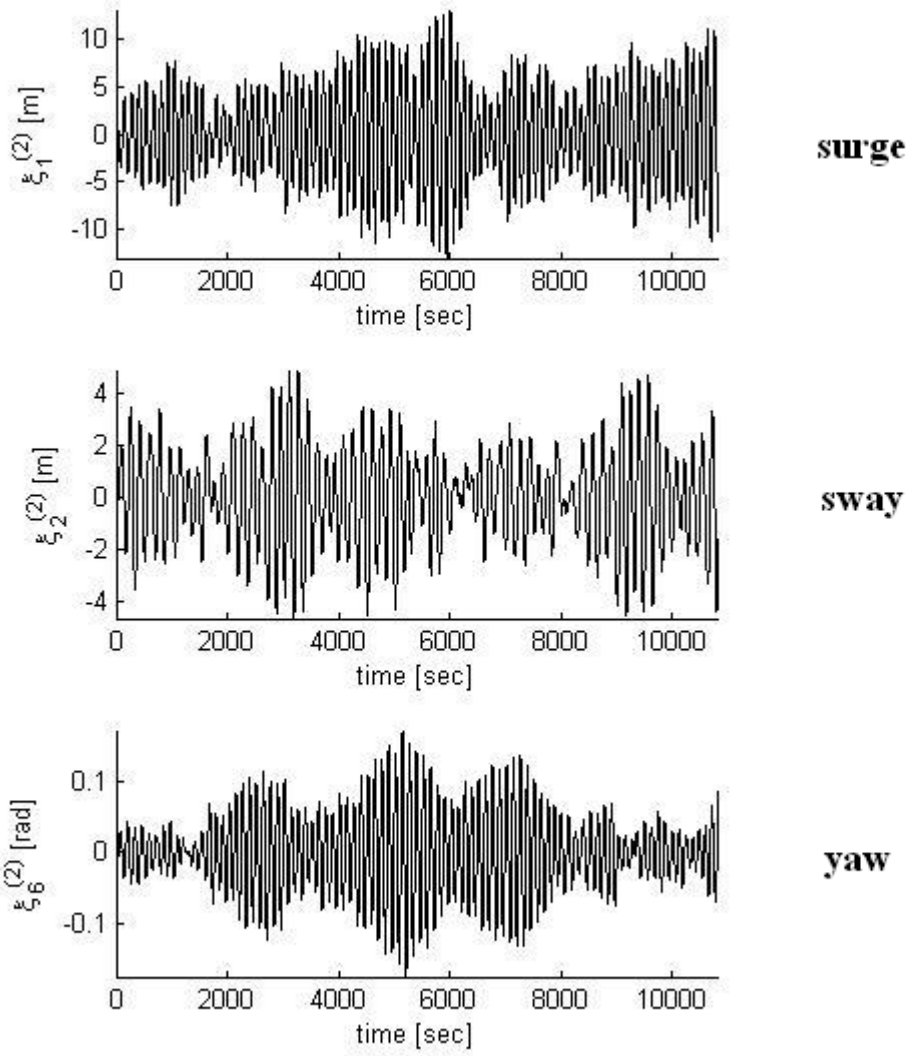

Figure 3.45 Second-order surge, sway and yaw motions of the FPSO (β=165 degrees)

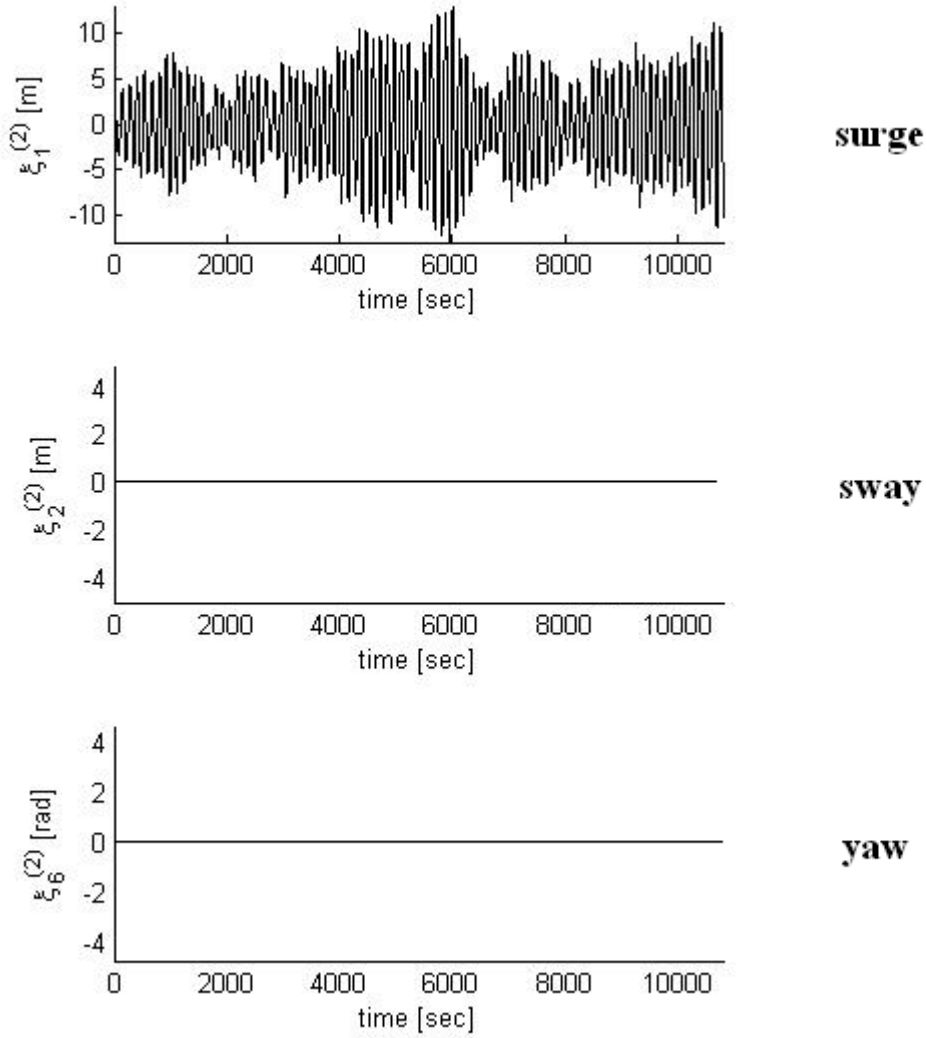

Figure 3.46 Second-order surge, sway and yaw motions of the FPSO (β=180 degrees)

3.4.5 Combined First- and Second-Order Motions

The time series of total surge displacements at the attachment points from No.1 to No.14 mooring lines and the origin of the global coordinate system in three different wave heading angles are shown in Figures 3.47 to 3.49 respectively as obtained by superimposing the first- and second-order motions at each time step. Similarly, the time histories of total combined sway displacements at the attachment points and the origin in three different wave directions are illustrated in Figures 3.50 to 3.52 respectively. The value of the combined sway motions in head waves is negligible.

The time series of total heave displacements at the attachment points from No.1 to No.14 mooring lines and the origin are demonstrated in Figures 3.53 to 3.55respectively for three different wave angles of attack. This heave motion is mainly induced by the first-order waves as the second-order heave forces are effectively small in this case. Similarly, the time histories of total roll motions of the FPSO are shown in Figure 3.56 and the variations of the total pitch motions of the FPSO with time are illustrated in Figure 3.57 respectively for various wave directions. The combined roll motions can be ignored in head seas, as before. The tendency of surge, heave and pitch motions are about the same order in the changing magnitude of motion amplitude with the wave angle β increasing from 150 to 180 degrees.

Figure 3.58 shows the time series of total yaw displacement of the FPSO respectively for various wave angles of attack. The yaw motion amplitudes are seen to decrease with the change of wave angle β from 150 to 180 degrees, as in the case of sway and roll.

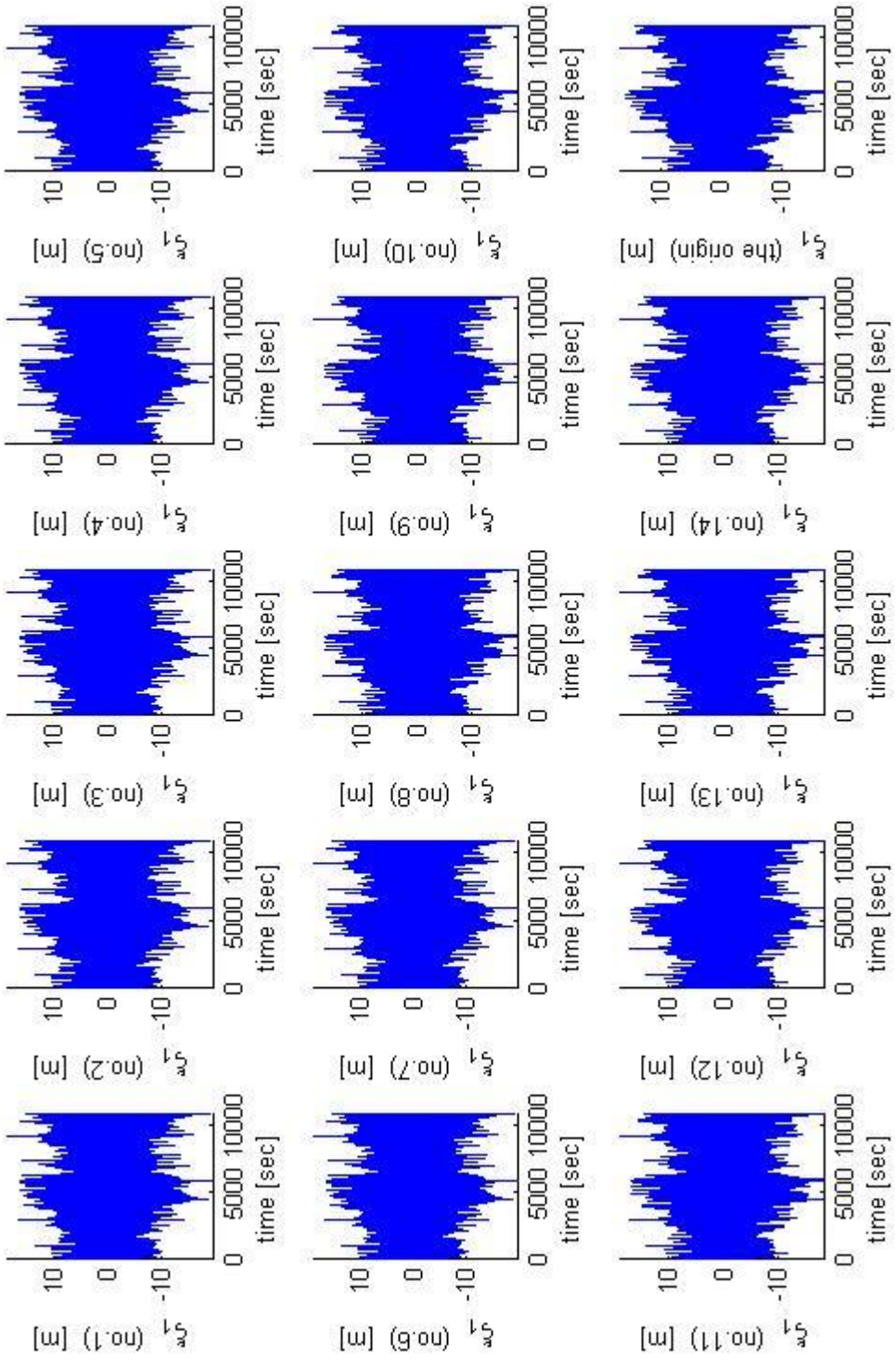

Figure 3.47 Time series of the 1st+2nd order motions combined of surge displacement at each mooring line attachment point and the origin (β=150 degrees)

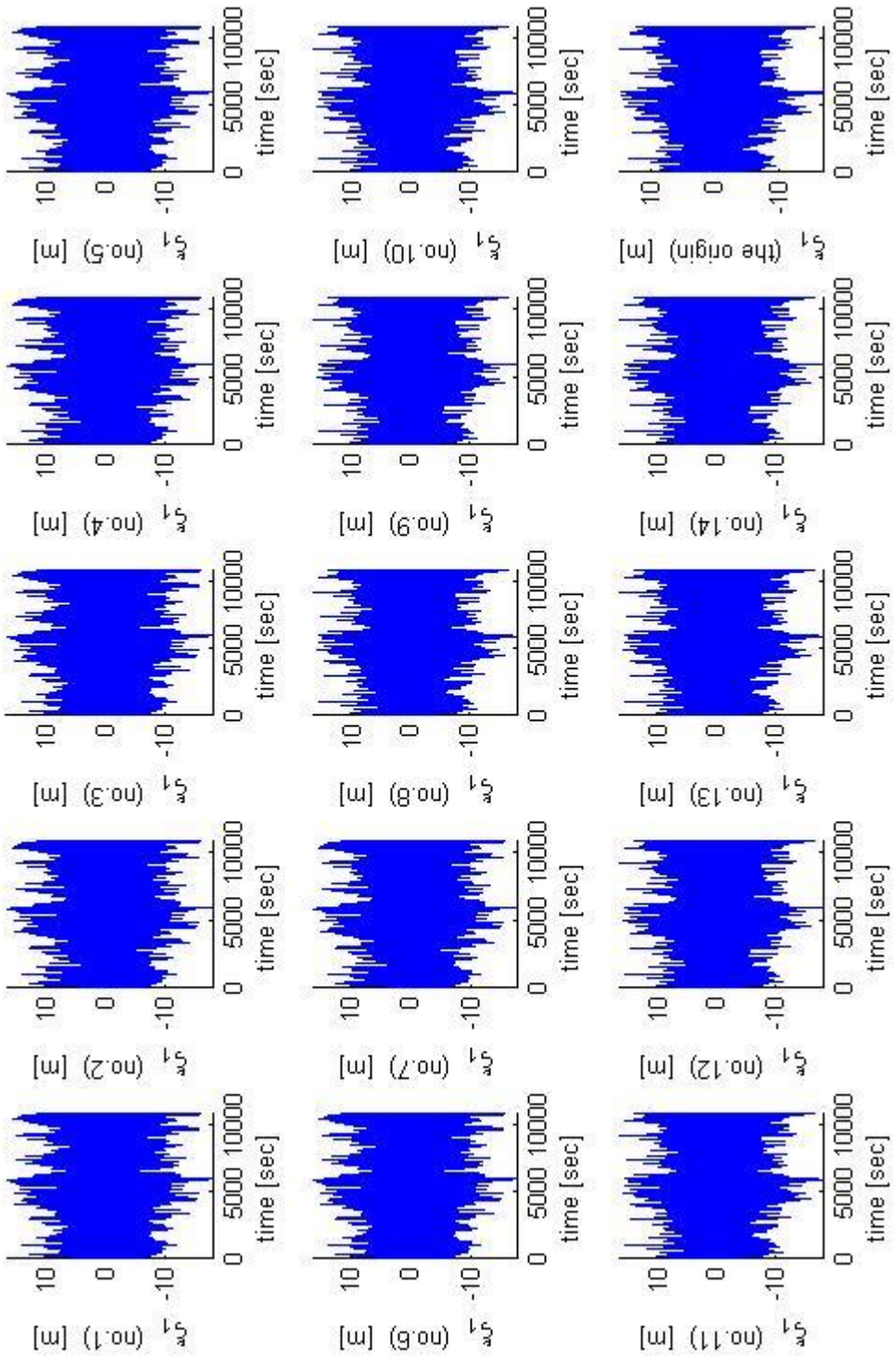

Figure 3.48 Time series of the 1st+2nd order motions combined of surge displacement at each mooring line attachment point and the origin (β=165 degrees)

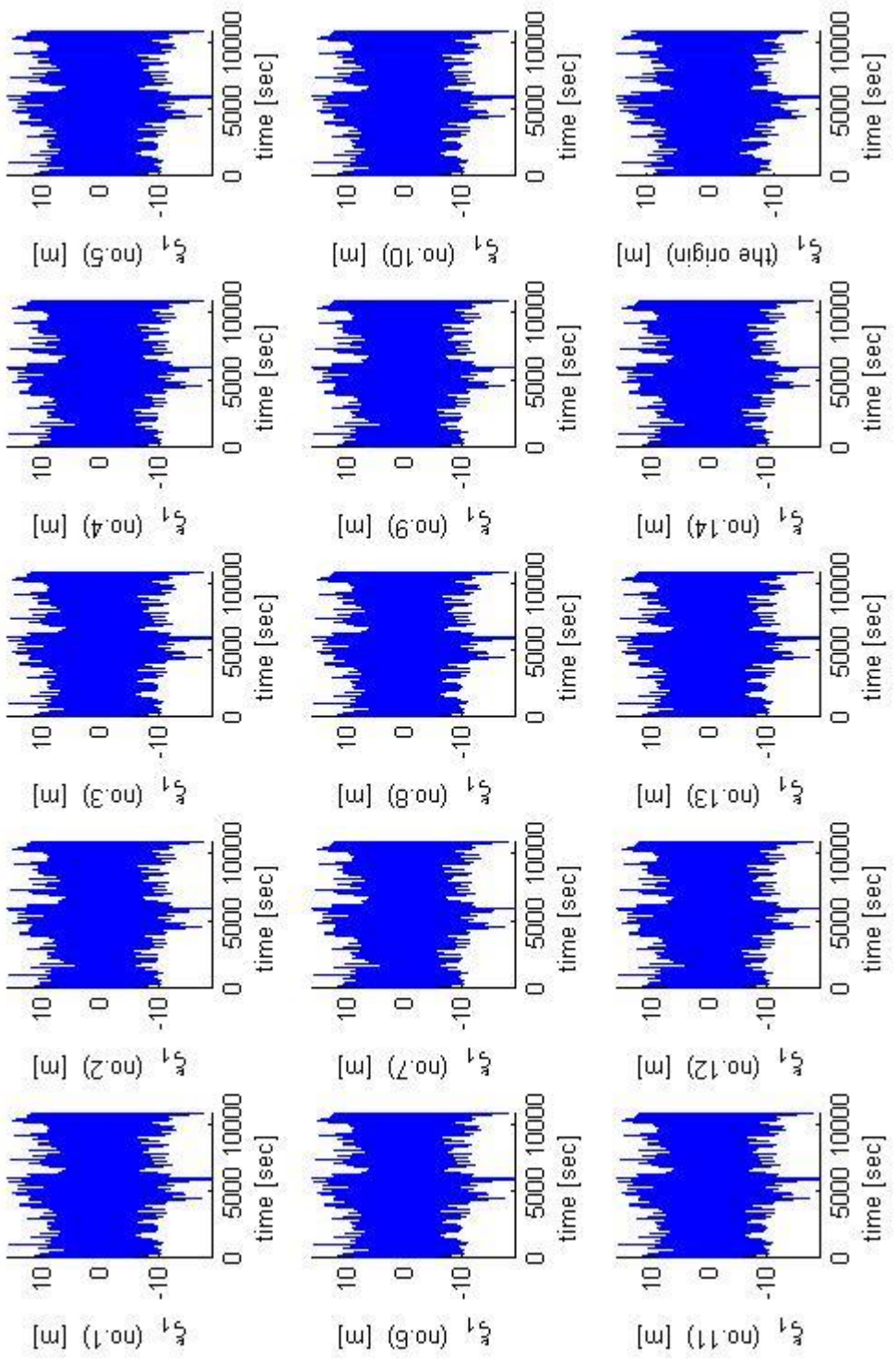

Figure 3.49 Time series of the 1st+2nd order motions combined of surge displacement at each mooring line attachment point and the origin (β=180 degrees)

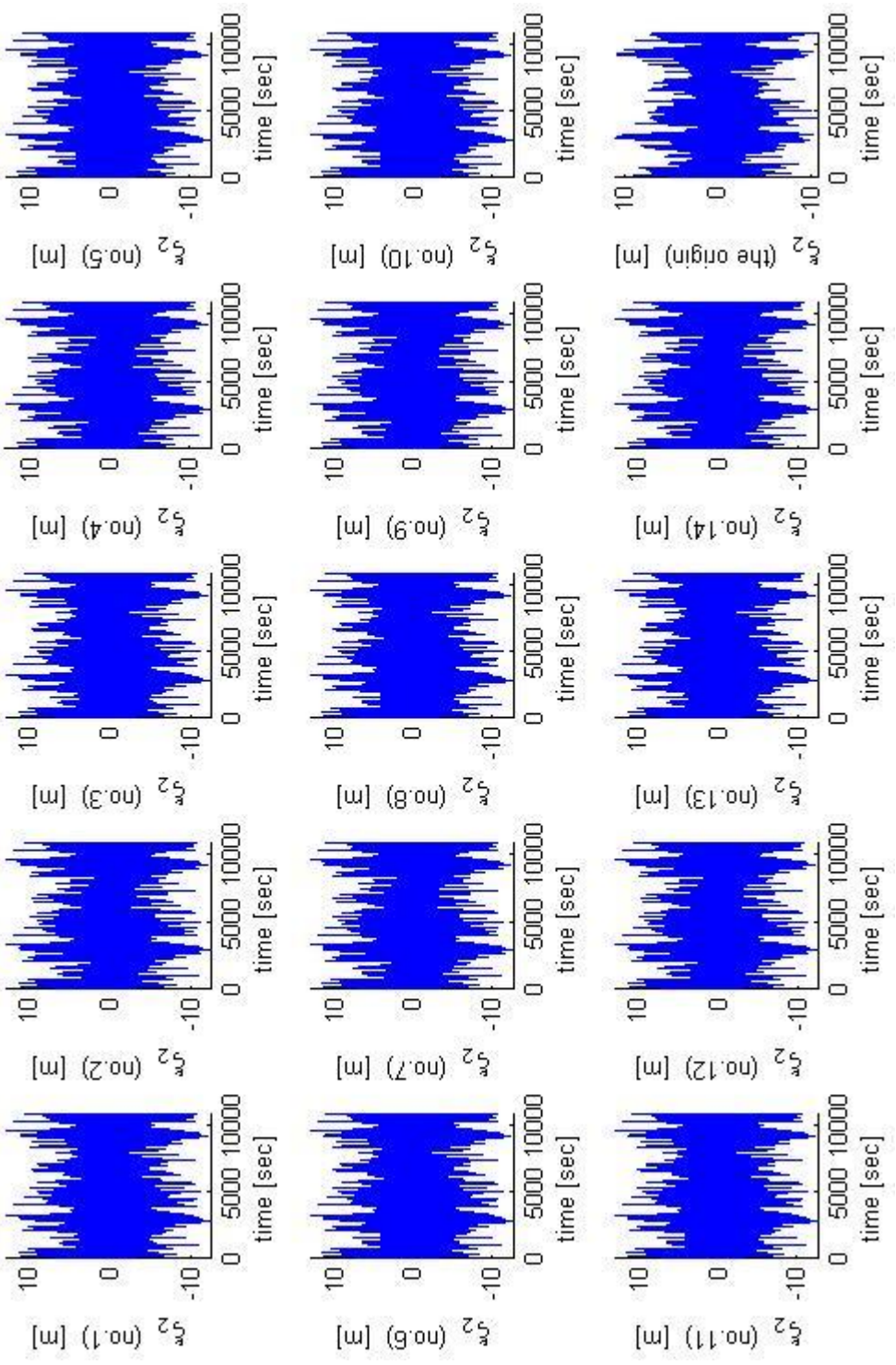

Figure 3.50 Time series of the 1st+2nd order motions combined of sway displacement at each mooring line attachment point and the origin (β=150 degrees)

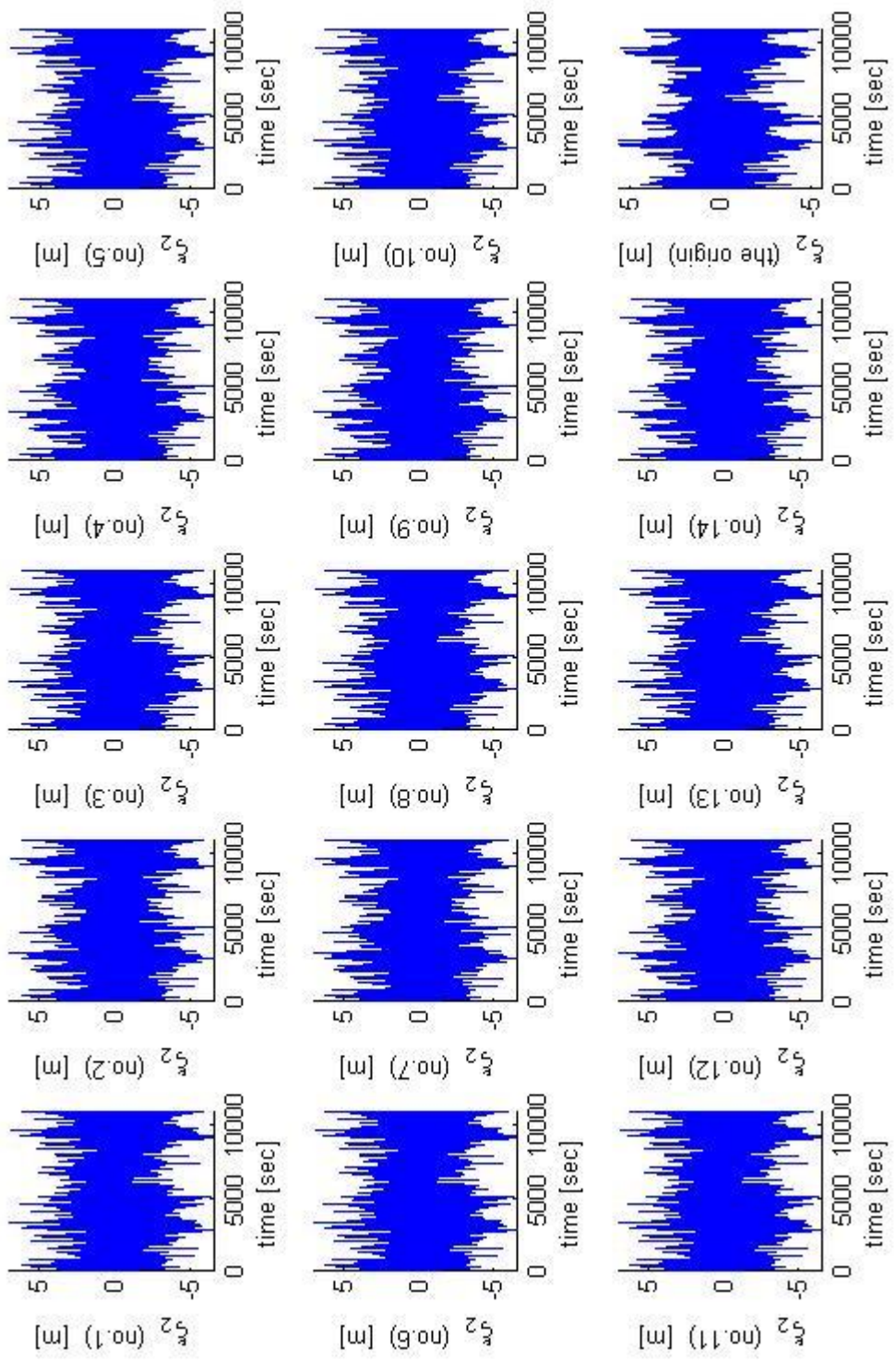

Figure 3.51 Time series of the 1st+2nd order motions combined of sway displacement at each mooring line attachment point and the origin (β=165 degrees)

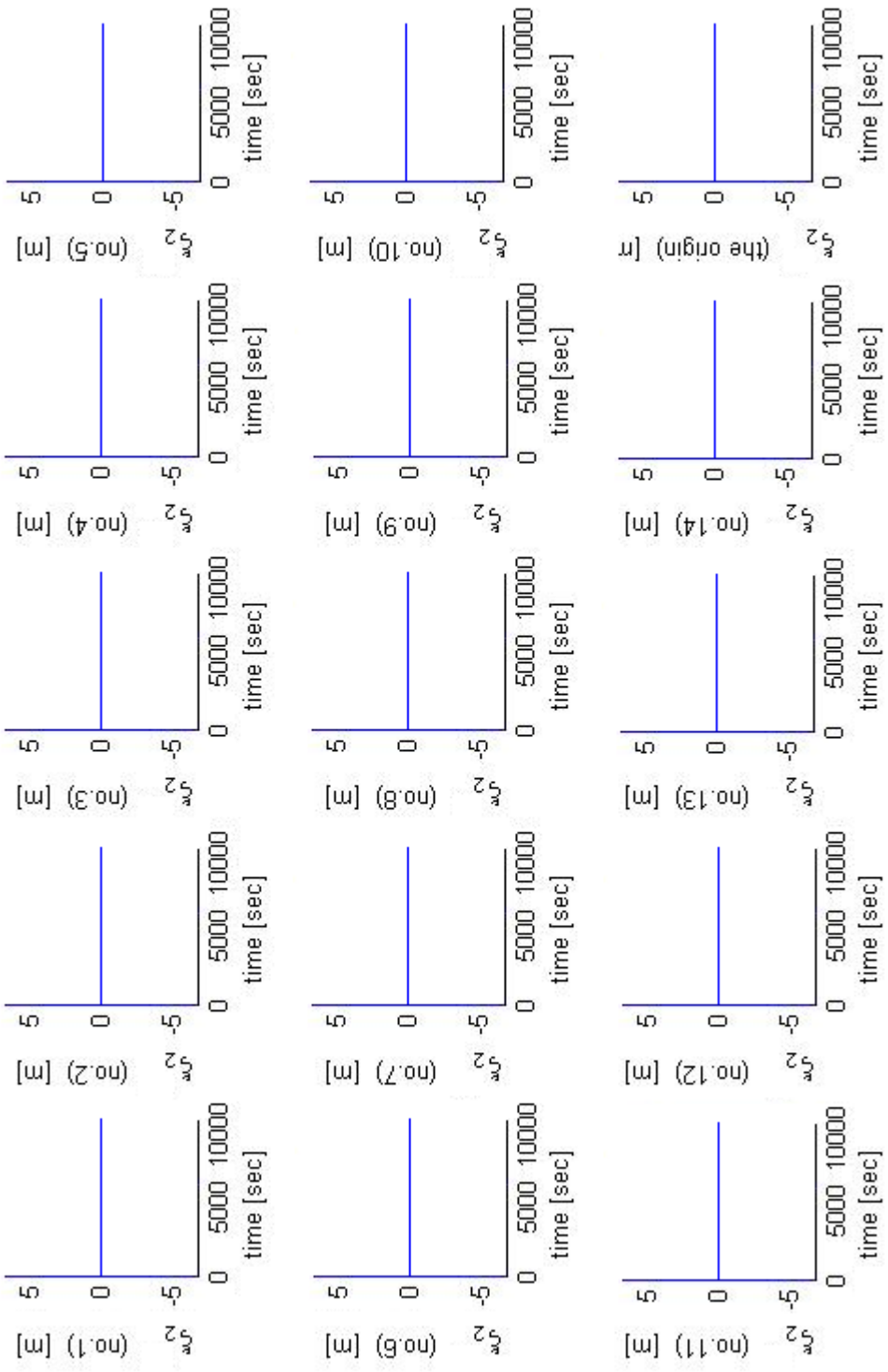

Figure 3.52 Time series of the 1st+2nd order motions combined of sway displacement at each mooring line attachment point and the origin (β=180 degrees)

(The values of sway are zero in the head sea condition, β=180)

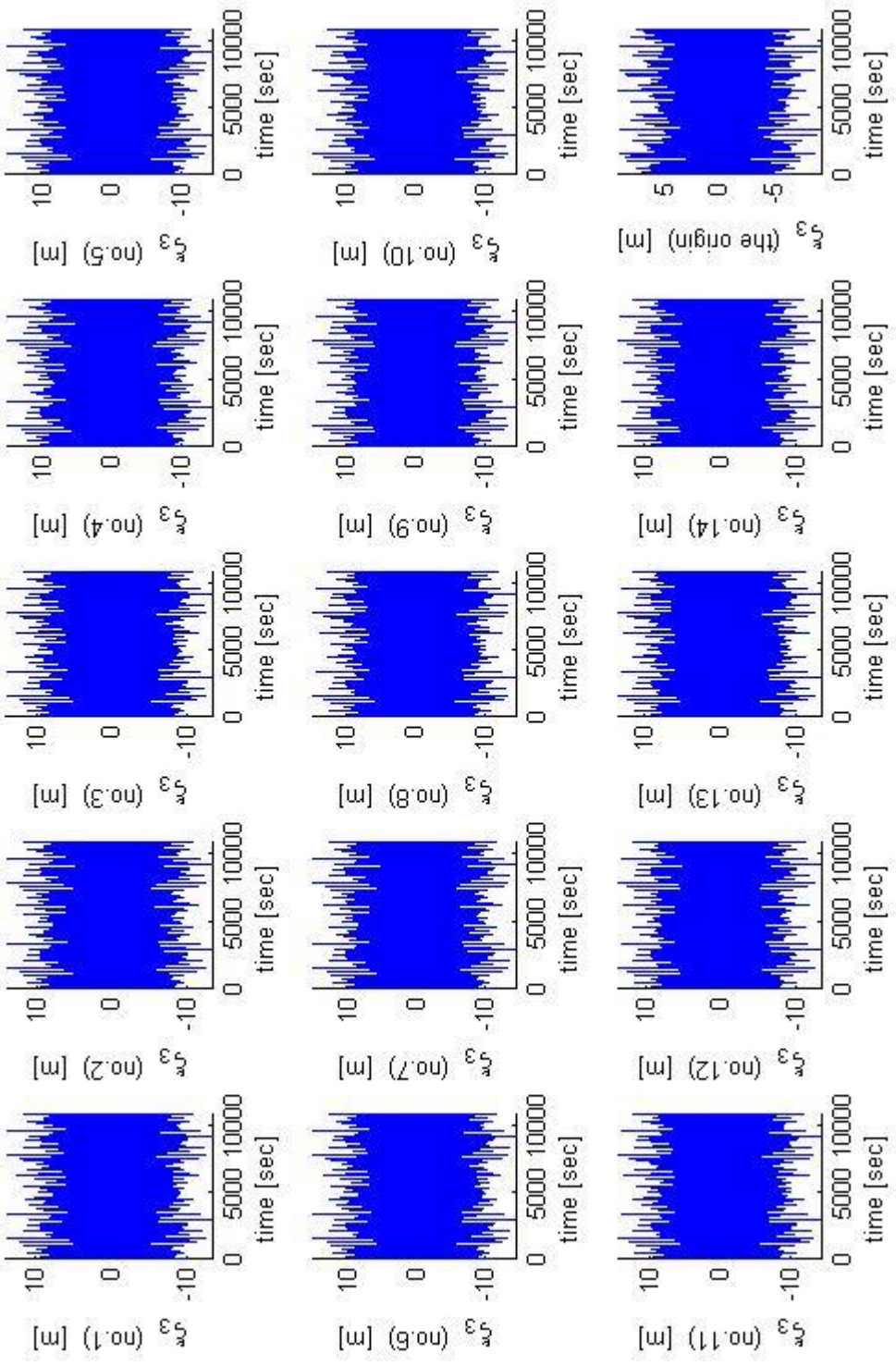

Figure 3.53 Time series of the 1st+2nd order motions combined of heave displacement at each mooring line attachment point and the origin (β=150 degrees)

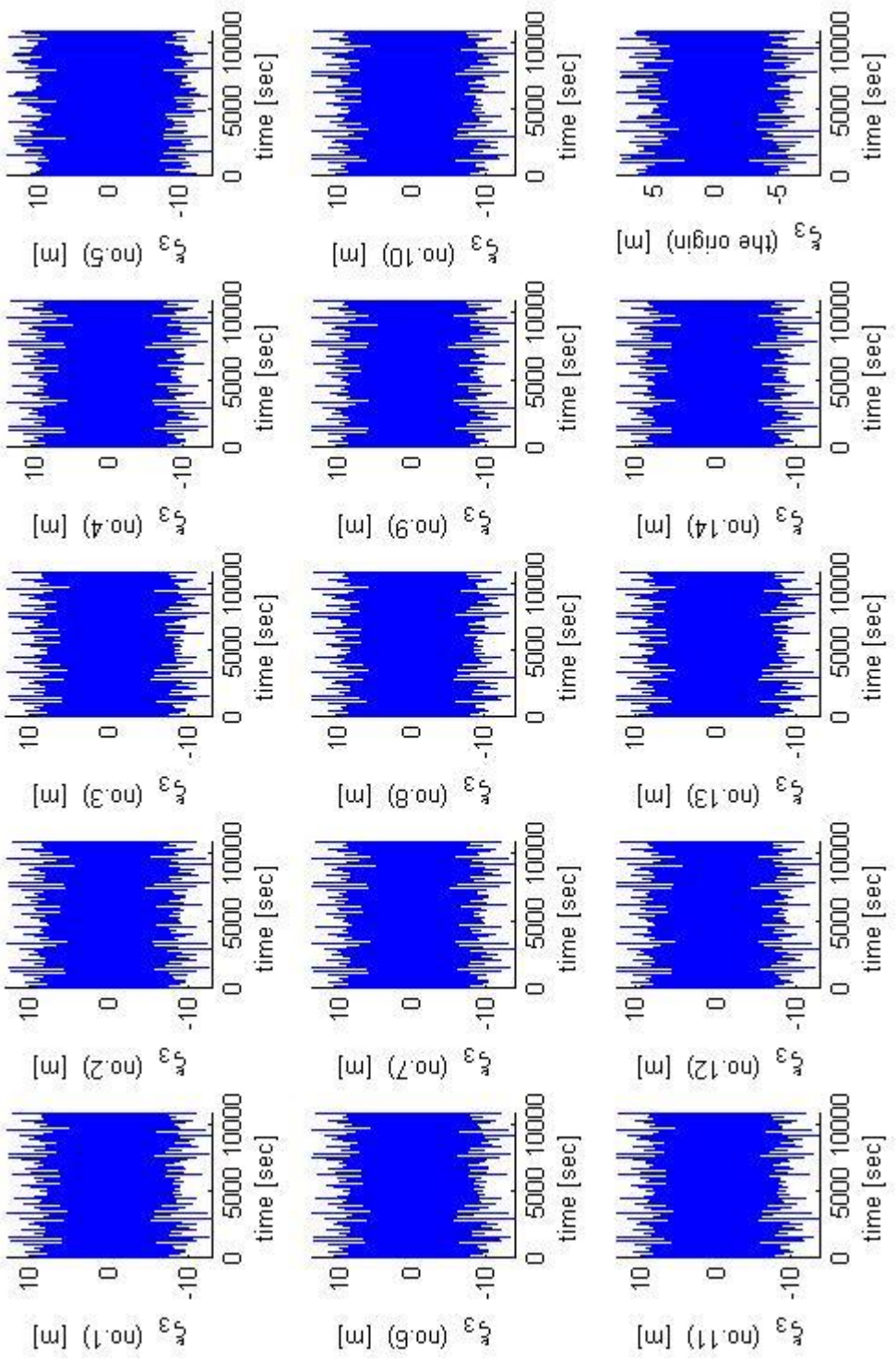

Figure 3.54 Time series of the 1st+2nd order motions combined of heave displacement at each mooring line attachment point and the origin (β=165 degrees)

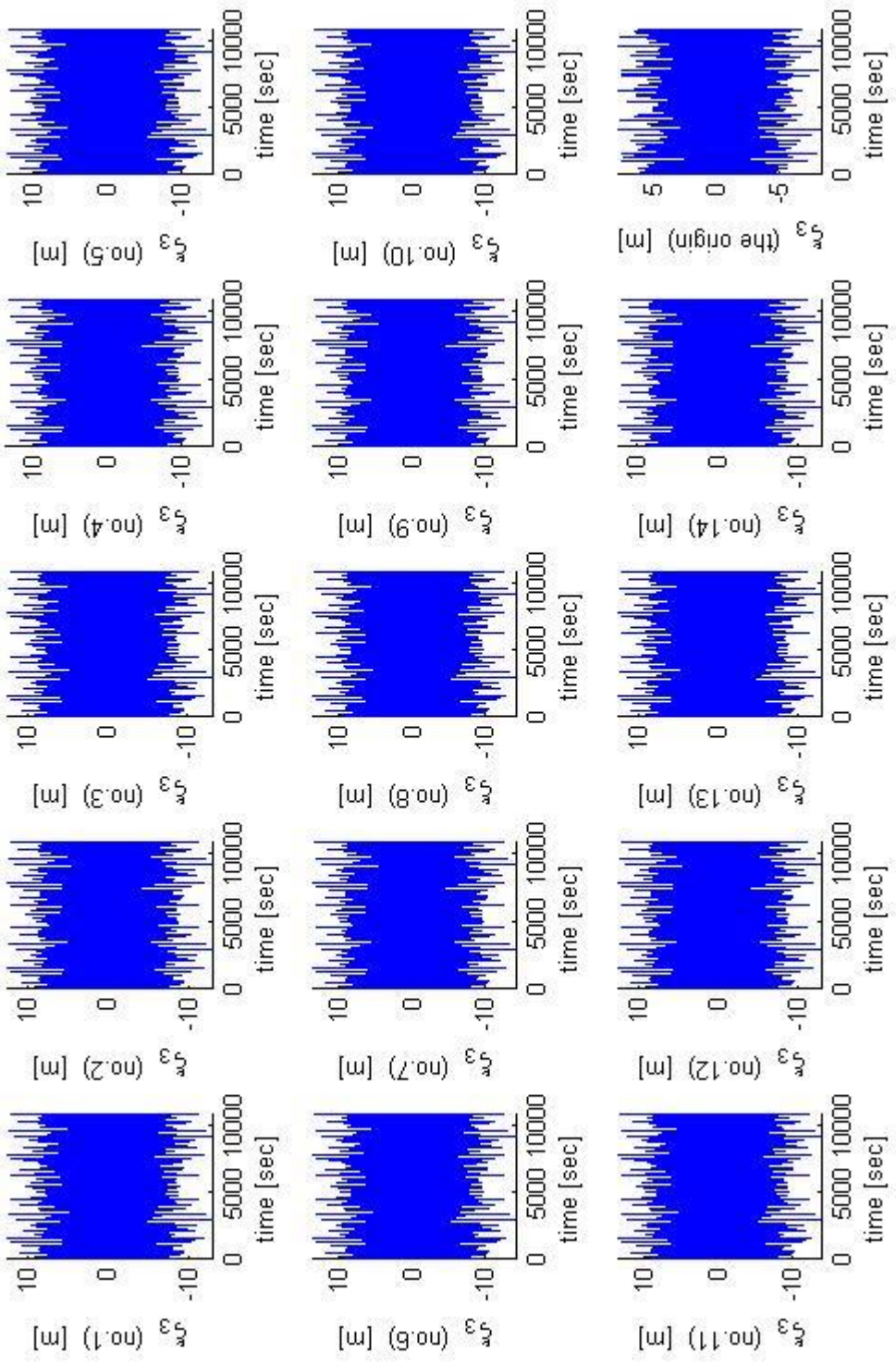

Figure 3.55 Time series of the 1st+2nd order motions combined of heave displacement at each mooring line attachment point and the origin (β=180 degrees)

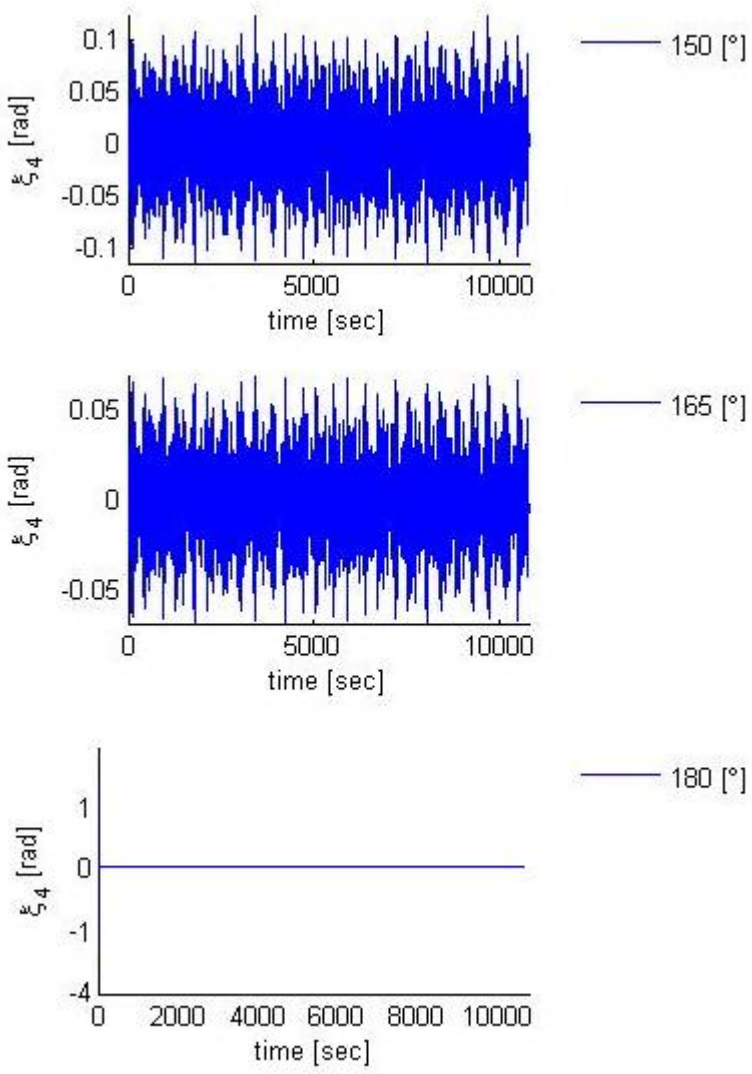

Figure 3.56 Time series of the 1st+2nd order motions combined of roll displacement

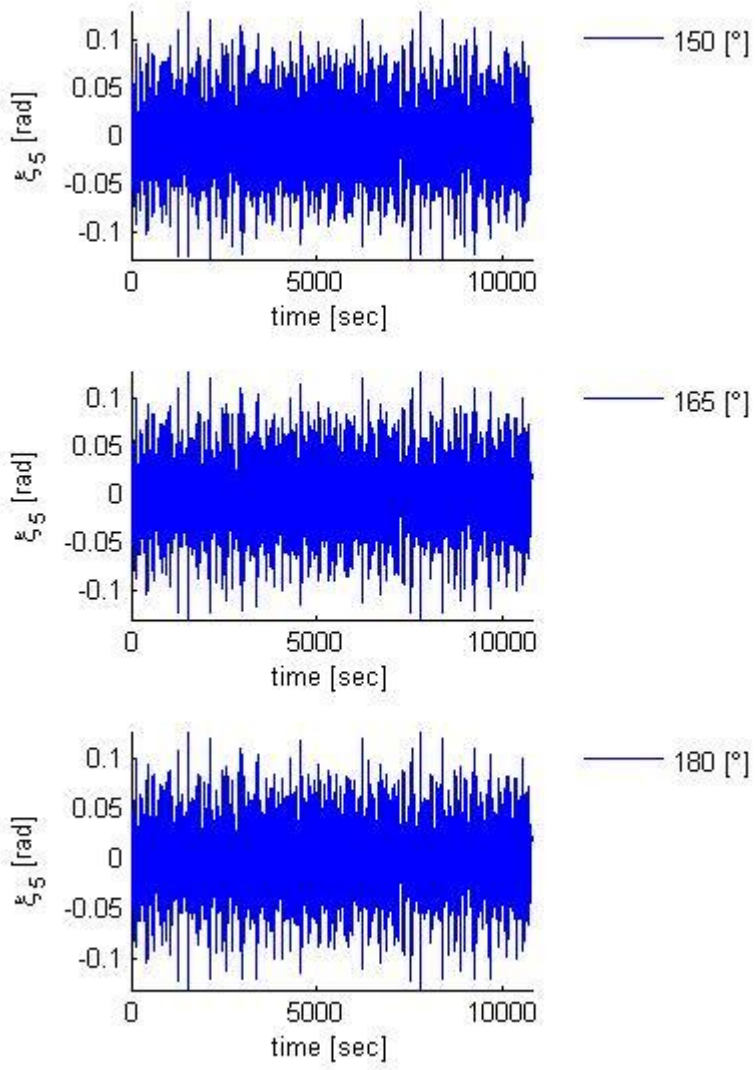

Figure 3.57 Time series of the 1st+2nd order motions combined of pitch displacement

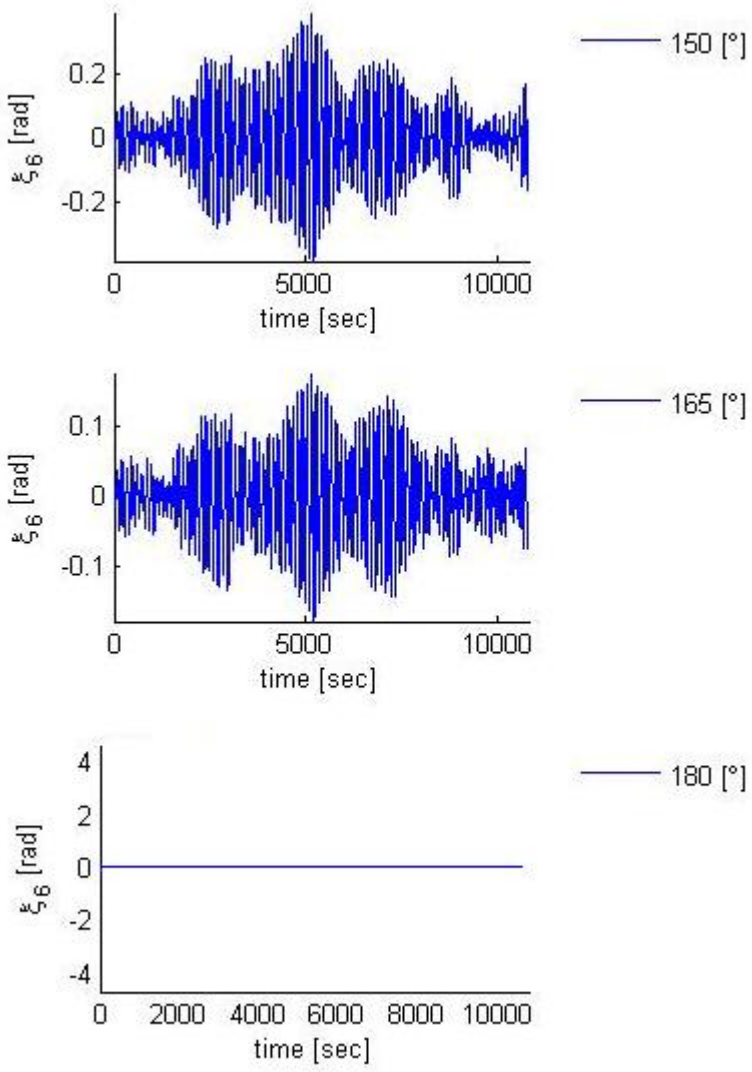

Figure 3.58 Time series of the 1st+2nd order motions combined of yaw displacement

3.5 Spectra of Fast-Time Domain Motion Simulations

The spectra of surge, sway and heave motions simulated by means of the fast time-domain method at the attachment points of mooring line No.1, 4, 8 and 12 and the origin of the global coordinate system in three different wave directions have been obtained by Fourier transform and are shown in Figures 3.59 to 3.61 respectively . The effects of the second-order motion on motion spectra are dominant at the natural frequencies of the FPSO in the case of surge and sway, while the first-order motion governs the heave motion spectrum.

The surge motion spectral density at wave frequency above 0.2 rad/sec at wave direction 150 degrees is larger than that at 165 and 180 while at wave frequency below 0.2 rad/sec it decreases with increasing wave heading angle from 150 degrees to 165 and then increases slightly at 180 degrees. However, the surge motion spectral density is much the same between 165 degrees and 180 degrees. No8 and No12 attachment points that are in the port side of the turret show slightly different surge motion spectrum form from No1 and No4 attachment points in the starboard side when waves are coming from the starboard side at 150 and 165 degrees. Furthermore, the surge motion spectrum of the FPSO at the origin of the global coordinate which is above the centre of gravity of the FPSO is smaller than that at the attachment points.

The sway motion spectral density decreases with increasing wave heading angles from 150 to 180 degrees. This is due to the effect that the projection area of the FPSO hull in the sway direction is diminished rapidly against the increase in angle of the incident wave. The largest peak of the sway motion spectral density at low frequency is caused by the resonance of the second-order sway motion.

On the other hand, the shape of the heave motion spectrum indicates that the first-order motion is dominant entirely. The heave motion spectral densities at the attachment points are larger than those at the origin of the global coordinate systems the attachment points are in the bow region which is susceptible to pitch induced vertical motion. The heave motion density at No.4 attachment point is somewhat larger than that at No.1 and 8 attachment points and that at No. 12 attachment point is the smallest because its position is different relative to the incident wave direction which can make the attachment point to behave in a different degree of displacement especially for pitch.

The motion spectra for roll, pitch and yaw modes are demonstrated in Figure 3.62, where the values of roll motion spectral density go down when the wave direction changes away towards

head seas as in the sway and yaw cases. The pitch motion spectral density is slightly larger in proportion to the heading angles from 150 to 180 degrees. In the yaw case it is shown that both the first- and second-order motion effects are the same as in the sway case.

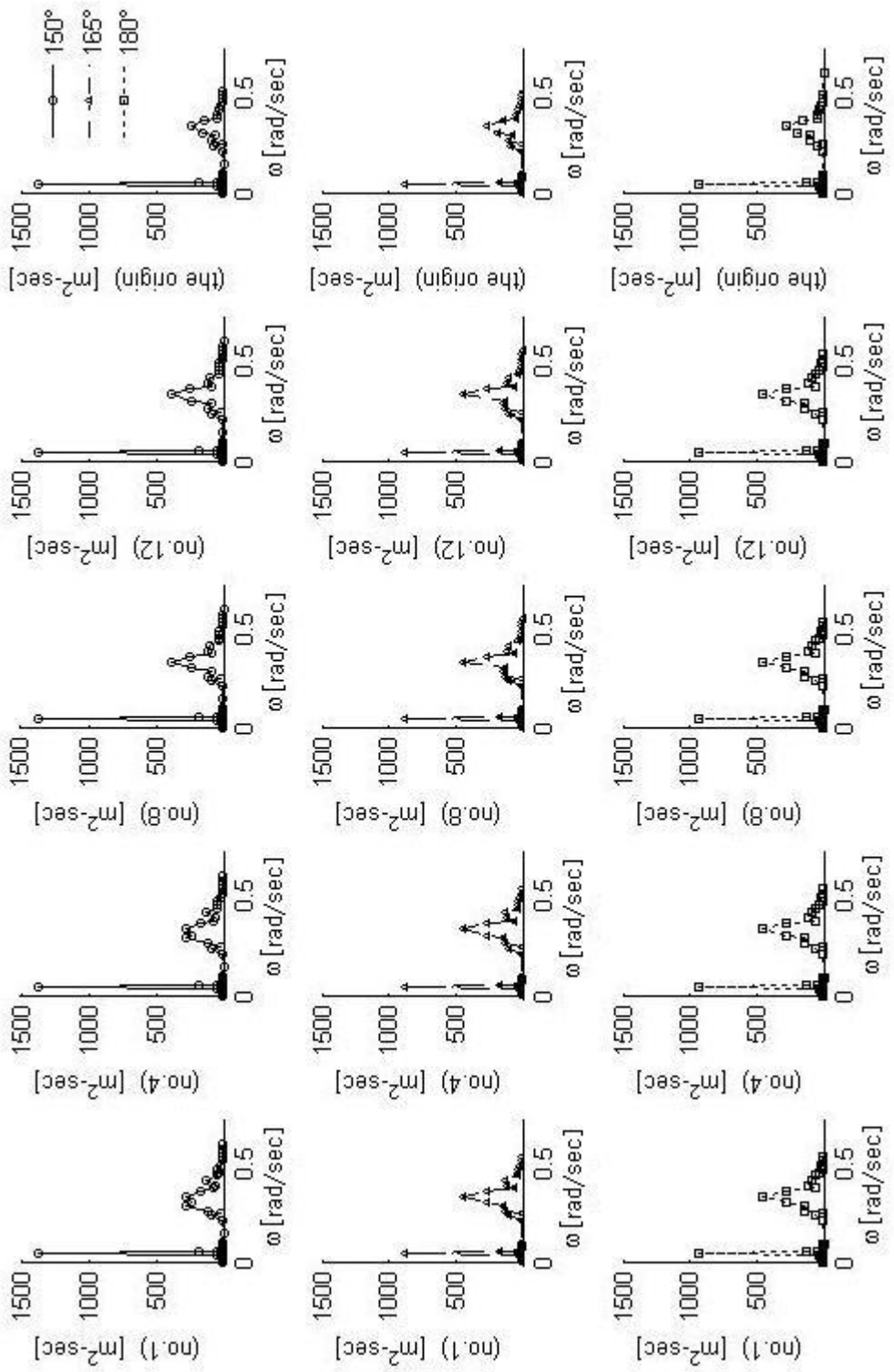

Figure 3.59 Surge motion spectra

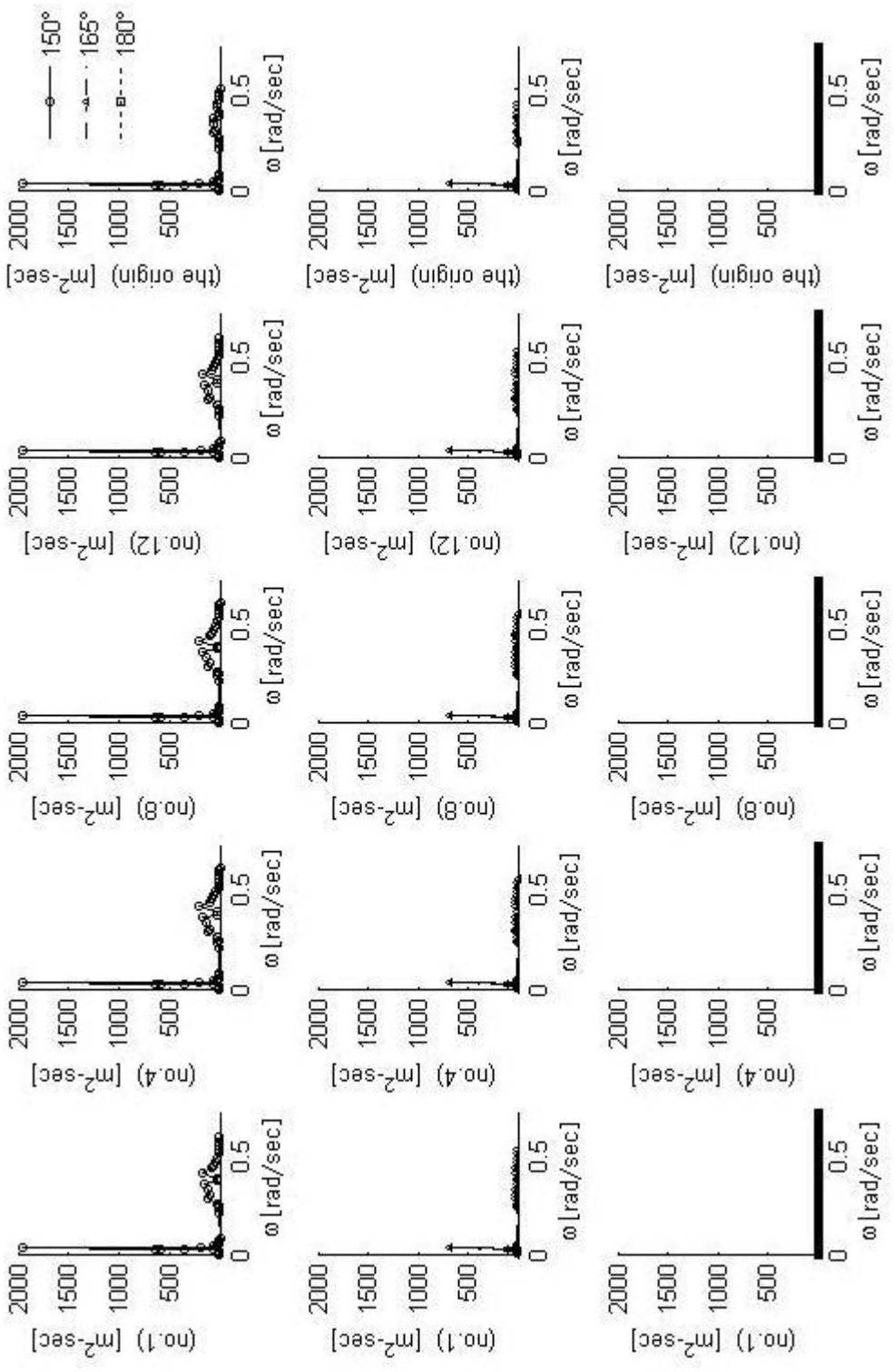

Figure 3.60 Sway motion spectra

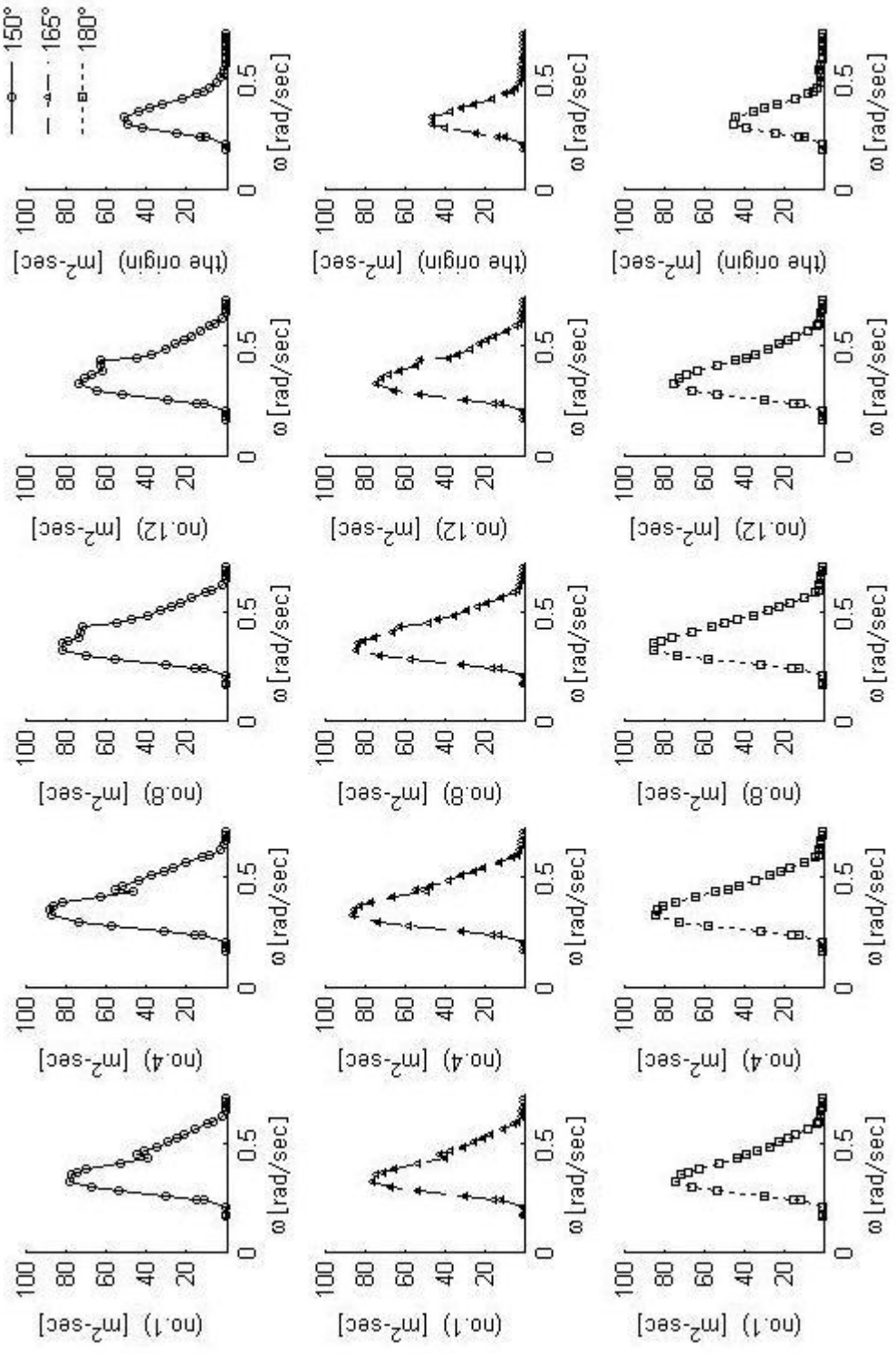

Figure 3.61 Heave motion spectra

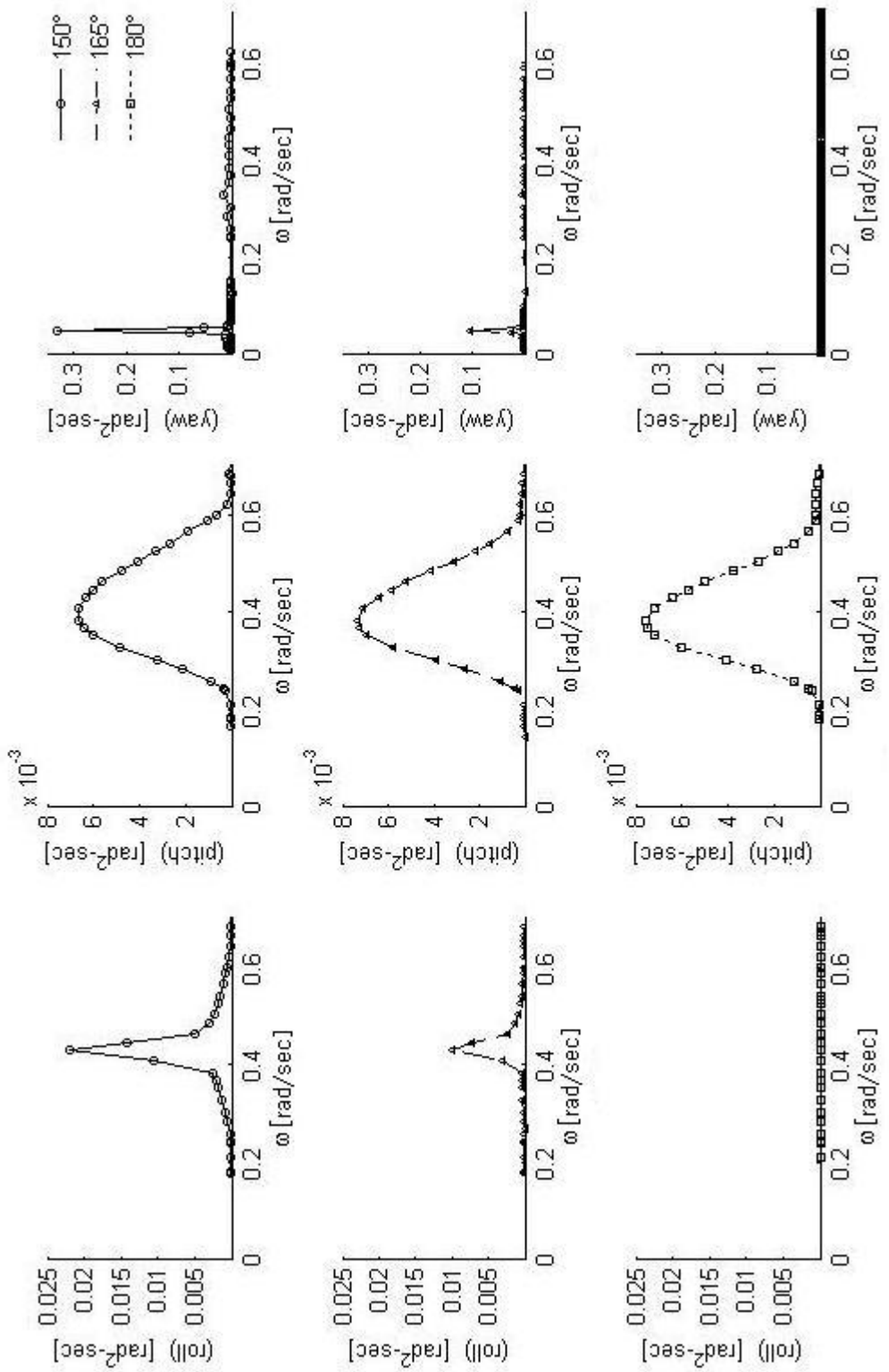

Figure 3.62 Roll, pitch and yaw motions spectra

3.6 Concluding Remarks

The design of a mooring system, in order to ensure the required level of performance, should be assessed by numerical motion simulations at the attachment points of the mooring lines. The characteristics of the motions of the floating structure are complicated owing to the irregularity of the incident waves and the non-linearity effects of the mooring system.

The necessity of the analysis about the mooring system is that the investigation of the stability gives rise to achieving a target value of the overall safety and efficiency during the through-life operation of the mooring system. The 6-DOF (Degree of Freedom) motions can be divided into two characteristics. The one is the characteristics of the motions experienced by mainly freely floating objects and these are the heave, roll and pitch motions. The other is the characteristics of the translational motions experienced by mainly mooring systems and these are caused by the surge, sway and yaw movements of the FPSO, that is, the horizontal plane motions. Translational movements must be constrained within a limited range in order to avoid damage to flow line risers, etc.

The motion responses of the FPSO vessel to regular waves of different frequencies and the resulting mean second-order forces and moments have been calculated by means of source distribution method in the frequency domain analysis. The motion RAOs and their phases at the attachment points of the mooring lines have also been estimated in order to carry out a fast time-domain motion simulation in random seas.

Based on the principle of superposition, the simulations of the first-order wave exciting forces and moments on the FPSO vessel in irregular waves have been performed and presented and will be used in Chapter 4 for the solution of the coupled time-domain motion equations of the FPSO vessel and a time-domain mooring analysis. To obtain practical estimations of motions and resulting mooring line tensions, the fast time-domain motion analysis method has been presented and applied for predicting the first- and second-order motions at the attachment points of the mooring lines in a design extreme wave condition of significant wave height 16 m and mean period 14.5 sec. The fast time-domain analysis is based on the superposition of the first-order response amplitude operator of the motions of the FPSO unit. The variations of the second-order forces and moment with time, which induce the slowly varying low frequency motions of the FPSO in surge, sway and yaw modes, have been obtained from the mean second-order forces and moment based on Newman's approximation. The results of the time series of the combined first- and second-order motions at the attachment points and the origin of the global coordinate

system have been presented and discussed, and will be employed for the time-domain mooring analysis in Chapter 4. The motion spectra of the combined motions in surge, sway and yaw modes indicate that the first-order motions are dominant at wave frequency above 0.2 rad/sec but the second-order motions are significant in long waves. On the other hand, the motion spectra of the combined motions in heave, roll and pitch modes are governed by the first-order motions.

Normally, time-domain simulations of motion responses of a moored vessel in irregular seas are computationally intensive, even in a quasi-static mooring analysis, since the coupled equations of motion are integrated in the time domain and a number of test cases must be considered due to the random nature. Therefore a time domain analysis is more time-consuming than a frequency domain analysis. In the following chapter, both the frequency-domain technique and the time-domain simulation method for coupled wave-induced motions and associated mooring analysis are developed and implemented in order to predict the first-order wave-induced motions and slow-drift motions of a FSPO, and to estimate the resulting maximum line tensions on her turret-mooring system. The maximum excursions and the resulting mooring tensions obtained by the frequency-domain method, the fast time-domain technique and the retardation function based time-domain coupled motion simulation method will be compared and discussed in Chapter 4.

CHAPTER

4

Quasi-Static Mooring Analysis in Frequency and Time Domains and Dynamic Mooring Analysis

4.1 Introduction

The main purpose of a mooring system is to minimize vessel motions by its mooring stiffness, principally in the horizontal plane, not only for the survival of the vessel in extreme weather conditions but also for the operation of the vessel in mild seas. If a FPSO vessel is drifting without any mooring restrain, the vessel will be in a great dangerous situation that grounding/collision may occur. Thus, it is necessary to assess the safety of the mooring system of a FPSO through a mooring analysis. Furthermore, the mooring system plays an important role to ensure the operational envelop of the FPSO vessel within the safety limit of its risers. If the FPSO vessel is often required to shut down its operation due to excessive excursion, it may not be viable to operate it and may result in financial loss.

The mooring analysis of a FPSO vessel may be static, quasi-static or dynamic depending on the motion responses of the FPSO to environmental loads. For static loads due to steady wind, current and mean wave loads, a static mooring analysis is required. In addition to these static loads, the variation of the static tension due to unsteady winds and waves needs to be considered in a quasi-static mooring analysis. The quasi-static mooring analysis can be carried out in the frequency domain or in the time domain. Furthermore, when the FPSO is operating in deep water greater than 100 m (DNV 2008), a dynamic mooring analysis is required. In the present study, static tensions are caused by mean second-order wave loads as current and wind loads are not considered. In this Chapter the quasi-static mooring analysis will be performed by means of a frequency-domain technique, fast time-domain motion analysis method and retardation function based time-domain motion simulation method, while a dynamic mooring analysis based on the

motions of attachment points in the time domain will be carried out by means of the lumped mass method described in Chapter 2.

Having described the catenary equations of single component and multi-component mooring lines in Chapter 2, Section 4.2 presents the results of the variation of horizontal tension with excursion and of the variation of vertical tension with vertical depth for the mooring lines of the Schiehallion FPSO. These variations of tension components with the motions of the attachment points of the mooring lines are employed in the coupled time-domain equations of motion for the FPSO in six degrees of freedom in Section 4.3. The coupled time-domain motion equations are based on the retardation function transformed from damping due to radiation waves. The response motions and motion spectra at the attachment points and the origin of the global coordinate system calculated by the present time-domain analysis for the three different heading angles are discussed in Section 4.4 and compared with those obtained in the previous fast time-domain analysis. Section 4.5 presents the quasi-static frequency-domain mooring analysis and discusses the results of surge and sway excursions of the FPSO. The time series and corresponding spectra of line tensions predicted by two different time-domain approaches are discussed in Section 4.6. Section 4.7 discusses mooring line dynamics and the conclusions are presented in Section 4.8.

4.2 Variations of horizontal and vertical tensions

It is necessary to tension each of the mooring lines which provide restoring forces and moments on the FPSO as the FPSO moves from and around the initial static equilibrium position in which some of the mooring lines are taut while others hang in a relatively slack manner. This equilibrium pretension configuration in which the FPSO vessel and its mooring lines undergo oscillatory motions due to wave excitations is developed through the equilibrium of forces and moments on the FPSO by means of the static catenary equations for each mooring line. It is noted that the effects of winds and currents are not included in this study.

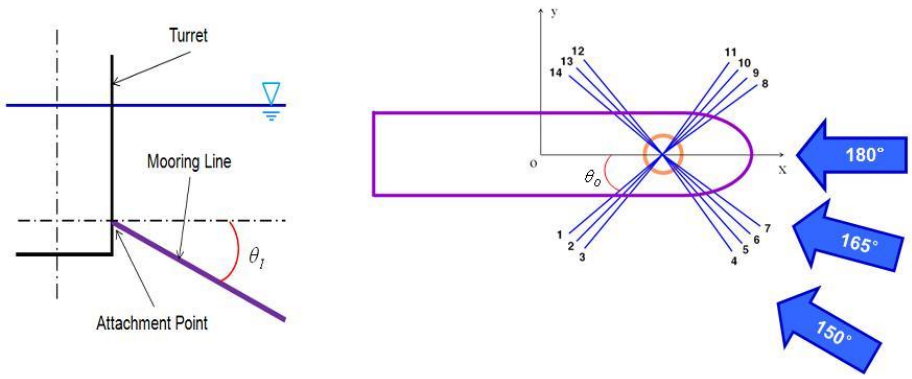

Figure 4.1 Turret-mooring arrangement

Figure 4.1 shows a turret-mooring arrangement in which the Schiehallion FPSO faces to three different wave directions of 150^o, 165^o and 180^o. Since the mooring line arrangement is symmetric centring around the global *x*-axis, the motion and mooring analyses can be performed for waves coming either from port or from starboard side. Table 4.1 summarises the coordinates of the attachment points of 14 mooring lines with respect to the global coordinate system in which the origin lies on the mean free surface with the *x*-axis pointing to the bow, the *y*-axis pointing to the port and the *z*-axis pointing vertically and passing through the centre of gravity of the FPSO. The angle o in Table 4.1 and θ_0 shown in Figure 4.1 mean the angle of each mooring line on the *x*-*y* plane measured from the negative *x*-axis while the angle I in Table 4.1 and θ_I illustrated in Figure 4.1 mean the inclining angle of the last segment of the individual mooring line measured from the waterplane. The value of the inclining angle θ_I was determined by means of the catenary equations presented in Chapter 2 and based on the line length of 4,652 m, the line weight of 504 N/m, and the pretension of 2,297 kN. Both o and I angles will change as the vessel moves, for example the I angle will be larger on slacked side. The data summarised in Table 4.1 will be used as the initial condition for the time-domain motion simulation.

Table 4.1 Coordinates of the attachment points

	x [m]	y [m]	z [m]	o Angle	l Angle
1	178.83	-4.89	0	40.0	21.440
2	179.28	-5.37	0	45.0	21.440
3	179.76	-5.82	0	50.0	21.440
4	189.28	-6.03	0	127.5	21.440
5	189.78	-5.60	0	132.5	21.440
6	190.25	-5.13	0	137.5	21.440
7	190.68	-4.63	0	142.5	21.440
8	190.68	4.63	0	217.5	21.440
9	190.25	5.13	0	222.5	21.440
10	189.78	5.60	0	227.5	21.440
11	189.28	6.03	0	232.5	21.440
12	179.76	5.82	0	310.0	21.440
13	179.28	5.37	0	315.0	21.440
14	178.83	4.89	0	320.0	21.440

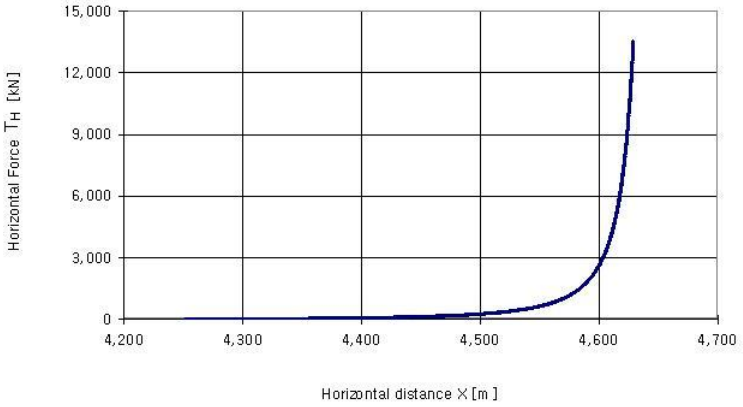

Figure 4.2 Curve of horizontal tension at attachment point against horizontal distance for each mooring line

The larger the mooring stiffness is, the smaller the movement of a moored vessel will be. The horizontal mooring stiffness of a mooring line can be illustrated as the slope of the curve of the horizontal component T_H of line tension at the attachment point against horizontal distance X. The distance X is the horizontal distance between the anchor point and the attachment point shown in Figure 2.4. Figure 4.2 shows the horizontal tensile force component T_H at the attachment point of the mooring line from the bottom anchor to the Schiehallion FPSO vessel as a function of the horizontal distance X. Based on the assumption that the anchor does not move, the horizontal tension component T_H can be obtained from Eq. (2.12) for a slack single component line or from the catenary equations associated with Eq. (2.14) for different configurations of a multi-component line given in Chapter 2. The horizontal tension component T_H increases with increase in the horizontal distance X. In other words, when the attachment point moves away from the anchor point, the line becomes tighter and has higher stiffness and tension. The mooring line stiffness is no longer constant and becomes non-linear when the

horizontal excursion is large. When the motions of the FPSO are large in extreme wave conditions, the mooring system acts as a non-linear spring whose stiffness depends on the lengths and weights of the mooring lines in water and the horizontal and vertical distances of the attachment points respectively from their anchor points and sea bed. The radical increases in horizontal tension and stiffness shown in Figure 4.2 occur at large horizontal distance X or large excursion from its static equilibrium position. The maximum tension of a mooring line must be within some endurable range of tension. The installation pretension needs to be considered for the proper determination of this endurable range of tension as the horizontal tension is very sensitive to the pretension level. The higher pretensions would generate higher line tensions for the same attachment point excursions. However if the pretensions are too low, the restoring forces that are generated in the mooring lines would not be large enough to control lateral displacements within the required operational and survival conditions. The maximum allowable limiting tension can be determined from the line breaking strength associated with an anchor capacity and any required factor of safety.

The curve of the horizontal tension component T_H against the horizontal distance X can be employed for a quasi-static time-domain mooring analysis. When the FPSO vessel is moving from its static equilibrium position, in three dimensions, to some new position in response to waves, the corresponding horizontal distances of the attachment points from their anchor points can be calculated and hence the horizontal tension forces and moments from the mooring lines can be obtained at each time step. In order to facilitate the calculation of the non-linear horizontal restoring forces and moment from the mooring lines in the time domain, the tension-displacement relationship from the static position of a mooring line may be represented, for analysis purposes, in a polynomial form by using a curve-fitting technique from the actual data on each displaced distance and corresponding increased tension.

Figure 4.3 shows the relationship between the vertical tension component T_V at the attachment point and the vertical distance Z of the attachment point above the sea bed. This relationship can be used to calculate the vertical restoring force and moment from the mooring lines in the quasi-static time-domain mooring analysis. It is noted that the vertical tension force T_V is equal to the weight of the mooring line suspended above the sea bed and thus depends on the wetted length ℓ_s of the line. Increasing the vertical distance Z increases the wetted length ℓ_s and the vertical tension T_V. However, the vertical tension and stiffness are not significant when compared with the horizontal tension and stiffness.

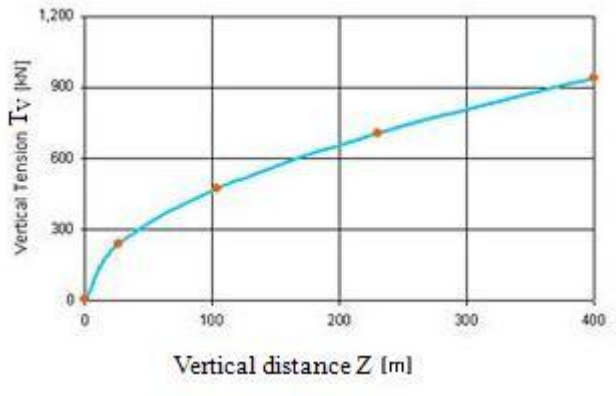

Figure 4.3 Curve of vertical tension at attachment point against vertical distance

After both horizontal and vertical components of the tension at the attachment point are found, the tension can be obtained by $\sqrt{(T_H)^2+(T_V)^2}$. This tension is tangent to the mooring line.

4.3 Motion Equations for Time-Domain Analysis

The time-domain coupled equations of motion of a moored FPSO vessel in six degrees of freedom can be written as (Oortmerssen 1976, Kato et al 1994) :

$$\sum_{k=1}^{6}\left[\left(M_{jk}+A_{jk}(\infty)\right)\ddot{\xi}_k+\int_0^{\infty}K_{jk}(\tau)\,\dot{\xi}_k(t-\tau)d\tau+C_{jk}\xi_k\right]=F_j^{(1)}(t)+F_j^{(2)}(t)-F_j^{m}(t)$$

$$\text{for j = 1, 2, …6} \qquad \textbf{(4.1)}$$

where $A_{jk}(\infty)$ is the added mass at $\omega=\infty$; K_{jk} is the retardation function; C_{jk} is the restoring coefficient due to change in buoyancy; $F_j^{(1)}$ and $F_j^{(2)}$ the first- and second-order forces in the *j*-th mode respectively determined by Eqs. (3.20) and (3.19); $F_j^{m}(t)$ is the mooring force in the *j*-th mode determined by means of the relationship of the horizontal tension component T_H and horizontal distance X and by the vertical tension component T_V against vertical distance Z.

The retardation function is a memory effect on the free surface with the information of the damping coefficient B_{jk} varying with wave frequency ω. The memory effect means that the linear transient motions of the FPSO can be calculated using the convolution integral of the retardation function K_{jk} with the velocity $\dot{\xi}_k$ for the hydrodynamic memory effect. The retardation function K_{jk} can be calculated by the cosine transform of the damping coefficient B_{jk} in the form:

$$K_{jk}(t) = \frac{2}{\pi}\int_0^\infty B_{jk}(\omega)cos(\omega t)d\omega \quad \textbf{(4.2)}$$

Using the damping coefficients calculated by the source distribution method (Chan 1992, 1993) and shown in Appendix F, the retardation functions have been obtained over a duration of 30 sec from Eq. (4.2) and shown in Figures 4.4 and 4.5 and Tables 4.2 and 4.3. This short duration implies that the retardation functions K_{jk} are reduced rapidly and the memory effects affect very near past of the response motions of the FPSO vessel. The retardation function was produced for 30 seconds as the magnitudes of the values are decreased to almost zero. The values can be ignored after 30 seconds for the effect of the retardation function.

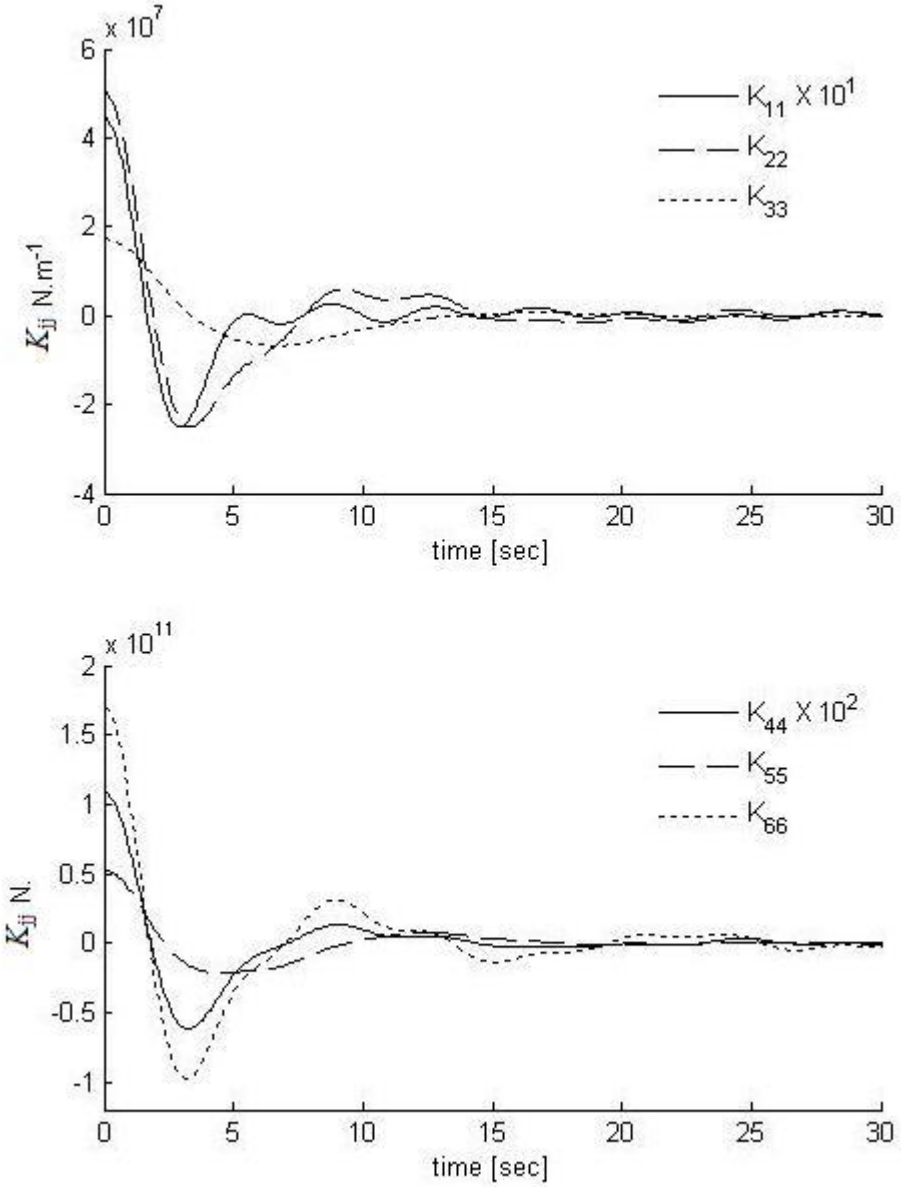

Figure 4.4 Retardation functions for surge, sway, heave, roll, pitch and yaw motions

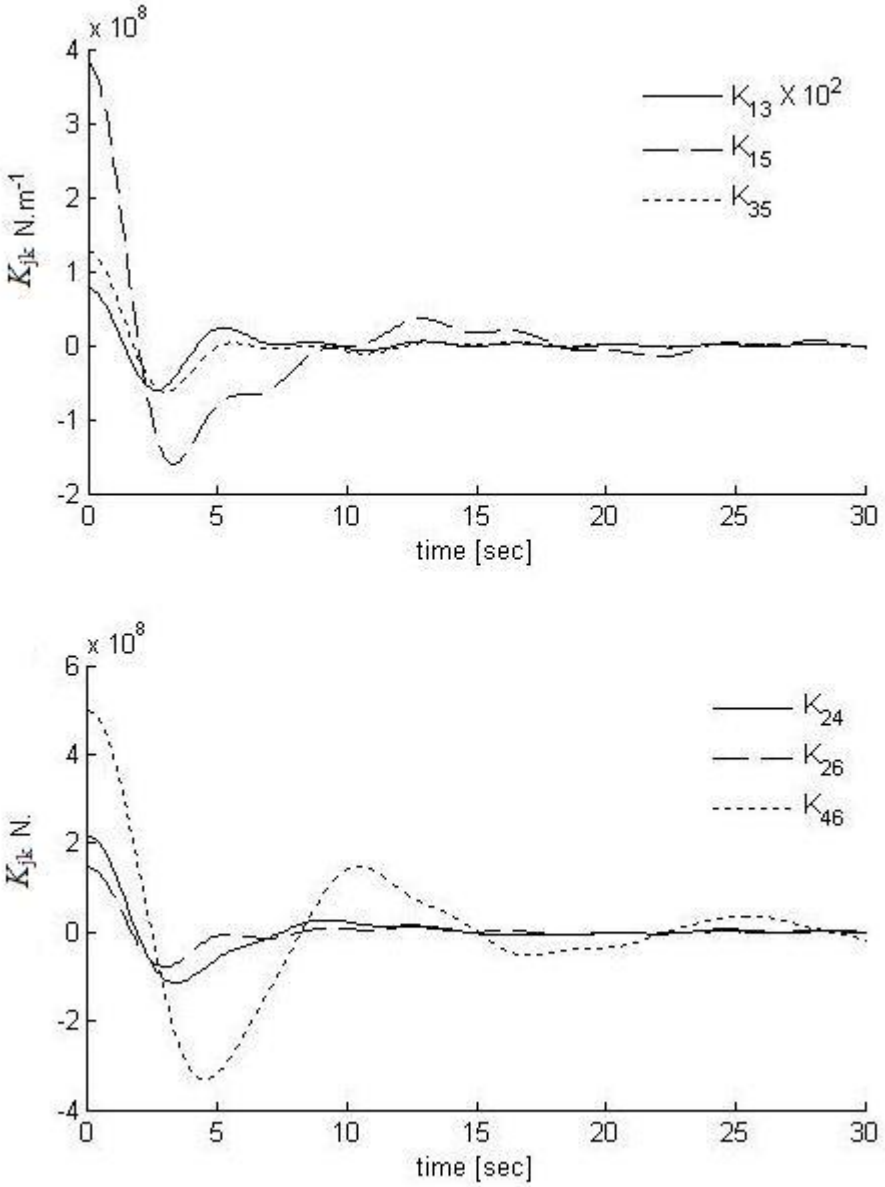

Figure 4.5 Retardation functions for coupled motions

Table 4.2 Retardation function (uncoupled)

Time	K_{11}	K_{22}	K_{33}	K_{44}	K_{55}	K_{66}
0	4.47E+06	5.03E+07	1.73E+07	1.09E+09	5.25E+10	1.70E+11
1	2.48E+06	3.22E+07	1.46E+07	6.71E+08	3.85E+10	1.02E+11
2	-1.10E+06	-3.17E+06	8.36E+06	-1.41E+08	9.31E+09	-2.93E+10
3	-2.50E+06	-2.38E+07	2.00E+06	-6.01E+08	-1.30E+10	-9.68E+10
4	-1.37E+06	-2.21E+07	-2.52E+06	-5.08E+08	-2.06E+10	-7.65E+10
5	-1.38E+05	-1.39E+07	-5.23E+06	-2.33E+08	-2.08E+10	-3.55E+10
6	-4.63E+04	-9.32E+06	-6.60E+06	-8.00E+07	-1.96E+10	-1.57E+10
7	-1.79E+05	-4.87E+06	-6.69E+06	-7.20E+06	-1.59E+10	-6.00E+08
8	1.09E+05	1.84E+06	-5.74E+06	8.15E+07	-8.85E+09	2.15E+10
9	2.61E+05	5.76E+06	-4.39E+06	1.32E+08	-1.97E+09	3.15E+10
10	-3.80E+03	4.75E+06	-3.13E+06	9.69E+07	2.32E+09	2.16E+10
11	-1.35E+05	3.46E+06	-1.99E+06	4.80E+07	5.17E+09	1.09E+10
12	8.37E+04	4.34E+06	-9.85E+05	4.55E+07	7.24E+09	9.22E+09
13	1.86E+05	4.21E+06	-2.84E+05	4.79E+07	7.25E+09	4.67E+09
14	1.09E+04	1.51E+06	1.03E+05	1.52E+07	5.23E+09	-7.18E+09
15	-4.39E+04	-8.08E+05	3.68E+05	-2.01E+07	3.22E+09	-1.39E+10
16	1.25E+05	-9.97E+05	5.81E+05	-2.78E+07	2.06E+09	-1.06E+10
17	1.68E+05	-8.95E+05	6.41E+05	-2.77E+07	7.81E+08	-6.78E+09
18	1.34E+04	-1.51E+06	5.51E+05	-3.21E+07	-7.91E+08	-6.52E+09
19	-3.57E+04	-1.54E+06	4.41E+05	-2.28E+07	-1.62E+09	-3.23E+09
20	5.58E+04	-8.44E+05	3.34E+05	-4.20E+06	-1.62E+09	3.42E+09
21	2.73E+04	-8.08E+05	1.69E+05	-4.10E+06	-1.59E+09	5.96E+09
22	-1.11E+05	-1.12E+06	8.00E+03	-1.52E+07	-1.43E+09	4.23E+09
23	-1.11E+05	-2.47E+05	-2.40E+04	-3.30E+06	-5.23E+08	4.70E+09
24	-1.20E+03	1.14E+06	3.80E+04	2.57E+07	5.57E+08	6.35E+09
25	-7.70E+03	1.08E+06	6.00E+04	3.09E+07	6.90E+08	2.87E+09
26	-8.53E+04	-2.00E+04	3.40E+04	7.90E+06	1.34E+08	-3.50E+09
27	-2.91E+04	-1.11E+05	4.00E+04	-7.50E+06	-1.04E+08	-5.05E+09
28	9.17E+04	7.93E+05	6.40E+04	-1.90E+06	-5.20E+07	-2.36E+09
29	7.37E+04	9.05E+05	5.30E+04	3.30E+06	-2.69E+08	-1.80E+09
30	-1.67E+04	-6.00E+03	5.50E+04	-2.40E+06	-4.42E+08	-3.02E+09
31	2.20E+03	-5.84E+05	1.25E+05	-6.70E+06	-7.40E+07	-1.21E+09
32	5.85E+04	-4.72E+05	1.74E+05	-5.80E+06	2.92E+08	2.35E+09
33	-4.10E+03	-3.57E+05	1.02E+05	-5.70E+06	2.70E+07	2.92E+09
34	-9.13E+04	-2.24E+05	-2.20E+04	-2.00E+06	-3.16E+08	1.39E+09

35	-4.50E+04	2.17E+05	-6.40E+04	8.80E+06	-1.50E+07	1.22E+09
36	4.42E+04	3.47E+05	-2.50E+04	1.13E+07	4.76E+08	1.08E+09
37	2.57E+04	-2.24E+05	3.00E+03	-3.70E+06	4.08E+08	-1.20E+09
38	-2.50E+04	-5.02E+05	8.00E+03	-1.51E+07	4.40E+07	-2.58E+09
39	1.03E+04	1.93E+05	2.70E+04	-4.00E+06	-3.90E+07	-4.60E+08
40	4.91E+04	7.63E+05	4.50E+04	1.31E+07	-1.70E+07	1.54E+09
41	-3.30E+03	1.95E+05	2.20E+04	1.08E+07	-2.10E+08	1.10E+08
42	-4.83E+04	-6.05E+05	-1.50E+04	-4.50E+06	-3.11E+08	-1.57E+09
43	8.00E+02	-4.20E+05	-2.60E+04	-1.01E+07	-6.40E+07	-2.00E+08
44	3.91E+04	2.74E+05	-1.50E+04	-3.00E+06	1.50E+08	1.48E+09
45	-1.22E+04	4.01E+05	2.00E+03	4.00E+06	7.10E+07	4.60E+08
46	-4.51E+04	5.30E+04	3.30E+04	5.90E+06	3.60E+07	-9.20E+08
47	1.21E+04	-1.48E+05	6.00E+04	3.90E+06	1.80E+08	-1.90E+08
48	4.82E+04	-2.03E+05	3.60E+04	-3.30E+06	1.06E+08	6.40E+08
49	-6.90E+03	-2.13E+05	-2.70E+04	-9.60E+06	-2.38E+08	-1.00E+08
50	-4.54E+04	7.80E+04	-5.40E+04	-3.70E+06	-3.15E+08	-3.70E+08
51	1.20E+03	4.44E+05	-2.30E+04	9.30E+06	3.30E+07	6.50E+08
52	3.72E+04	1.91E+05	1.40E+04	9.70E+06	2.88E+08	5.30E+08
53	1.90E+03	-4.70E+05	2.90E+04	-4.50E+06	1.73E+08	-1.07E+09
54	-2.34E+04	-4.69E+05	4.00E+04	-1.16E+07	-1.10E+07	-1.06E+09
55	5.00E+03	2.73E+05	3.50E+04	-1.50E+06	-9.70E+07	8.70E+08
56	1.48E+04	5.91E+05	-1.50E+04	9.10E+06	-2.13E+08	1.26E+09
57	-1.60E+04	3.10E+04	-6.80E+04	5.60E+06	-2.26E+08	-5.40E+08
58	-1.46E+04	-4.67E+05	-5.00E+04	-3.40E+06	8.80E+07	-1.18E+09
59	2.38E+04	-2.44E+05	2.80E+04	-5.60E+06	3.92E+08	2.90E+08
60	1.87E+04	1.80E+05	7.20E+04	-2.10E+06	1.99E+08	9.30E+08

K_{11} means the retardation function for surge coupled by surge (e.g. no coupled in this case) in the degree of freedom and so on for K_{22}, K_{33}, K_{44}, K_{55} and K_{66}.

Table 4.3 Retardation function (coupled)

Time	K_{13}	K_{15}	K_{24}	K_{26}	K_{35}	K_{46}
0	7.65E+05	3.80E+08	2.16E+08	1.45E+08	1.27E+08	4.97E+08
1	3.19E+05	2.48E+08	1.38E+08	8.21E+07	7.45E+07	3.92E+08
2	-4.24E+05	-8.95E+06	-1.52E+07	-3.23E+07	-2.19E+07	1.32E+08
3	-5.61E+05	-1.53E+08	-1.08E+08	-7.83E+07	-6.31E+07	-1.48E+08
4	-1.10E+05	-1.35E+08	-1.02E+08	-4.45E+07	-3.59E+07	-3.11E+08
5	2.24E+05	-8.06E+07	-5.99E+07	-8.17E+06	-2.37E+06	-3.19E+08
6	1.55E+05	-6.72E+07	-3.29E+07	-8.32E+06	1.49E+06	-2.34E+08
7	1.19E+04	-6.09E+07	-1.27E+07	-1.44E+07	-4.67E+06	-1.31E+08
8	2.24E+04	-3.13E+07	1.26E+07	-3.14E+06	-2.34E+06	-2.60E+07
9	3.62E+04	-6.33E+06	2.74E+07	8.29E+06	-1.45E+06	7.71E+07
10	-4.06E+04	-2.04E+06	2.27E+07	6.91E+06	-8.37E+06	1.41E+08
11	-6.84E+04	6.23E+06	1.43E+07	5.27E+06	-1.07E+07	1.38E+08
12	8.39E+03	2.70E+07	1.42E+07	9.95E+06	-3.05E+06	9.74E+07
13	5.41E+04	3.56E+07	1.37E+07	1.01E+07	3.44E+06	6.36E+07
14	1.30E+04	2.50E+07	5.42E+06	3.06E+06	2.53E+06	3.84E+07
15	-1.10E+04	1.72E+07	-3.14E+06	7.00E+04	1.24E+06	1.34E+06
16	1.94E+04	1.98E+07	-5.60E+06	2.53E+06	3.07E+06	-3.80E+07
17	2.13E+04	1.58E+07	-6.09E+06	5.60E+05	2.86E+06	-5.29E+07
18	-1.94E+04	1.55E+06	-7.21E+06	-5.59E+06	0.00E+00	-4.53E+07
19	-2.49E+04	-7.18E+06	-5.57E+06	-5.90E+06	-1.20E+05	-3.83E+07
20	8.72E+03	-7.28E+06	-2.17E+06	-7.40E+05	2.05E+06	-3.60E+07
21	8.97E+03	-1.03E+07	-2.28E+06	3.40E+05	1.19E+06	-2.56E+07
22	-2.22E+04	-1.52E+07	-4.14E+06	-2.86E+06	-1.69E+06	-6.13E+06
23	-2.00E+04	-1.05E+07	-1.15E+06	-2.64E+06	-1.50E+06	1.18E+07
24	7.61E+03	1.00E+04	4.95E+06	7.20E+05	6.20E+05	2.50E+07
25	3.27E+03	2.96E+06	6.03E+06	1.18E+06	2.70E+05	3.49E+07
26	-1.81E+04	1.40E+05	1.73E+06	-3.00E+04	-1.12E+06	3.53E+07
27	-4.80E+03	2.20E+06	-6.30E+05	1.66E+06	-6.00E+04	2.35E+07
28	2.10E+04	6.21E+06	1.08E+06	3.29E+06	1.17E+06	8.30E+06
29	1.10E+04	2.94E+06	1.96E+06	6.30E+05	-3.60E+05	-3.87E+06
30	-7.14E+03	-2.86E+06	4.00E+04	-1.95E+06	-1.35E+06	-1.82E+07
31	1.10E+04	-1.58E+06	-1.75E+06	3.60E+05	1.12E+06	-3.35E+07
32	2.86E+04	2.07E+06	-2.16E+06	2.66E+06	2.75E+06	-3.47E+07
33	-2.96E+03	-9.40E+05	-2.14E+06	-3.50E+05	-1.50E+05	-1.60E+07
34	-4.16E+04	-5.55E+06	-8.90E+05	-3.83E+06	-3.00E+06	6.81E+06

35	-2.51E+04	-2.62E+06	1.83E+06	-1.85E+06	-1.02E+06	1.92E+07
36	1.81E+04	3.37E+06	2.60E+06	1.72E+06	2.25E+06	2.40E+07
37	2.42E+04	3.62E+06	-3.70E+05	1.23E+06	1.69E+06	2.49E+07
38	1.15E+03	8.60E+05	-2.73E+06	-7.50E+05	-7.90E+05	1.41E+07
39	-7.15E+03	1.25E+06	-6.70E+05	-6.00E+04	-1.11E+06	-9.35E+06
40	-2.72E+03	1.68E+06	2.42E+06	9.50E+05	-1.50E+05	-2.72E+07
41	-6.02E+03	-1.68E+06	1.73E+06	-3.30E+05	-1.50E+05	-2.37E+07
42	-3.28E+03	-3.70E+06	-1.13E+06	-9.30E+05	4.00E+04	-5.50E+06
43	1.40E+04	-5.10E+05	-1.76E+06	8.30E+05	1.11E+06	1.04E+07
44	1.51E+04	2.03E+06	-1.20E+05	1.16E+06	7.40E+05	1.61E+07
45	-1.13E+04	-1.80E+05	9.90E+05	-1.14E+06	-1.29E+06	1.24E+07
46	-2.34E+04	-1.57E+06	9.10E+05	-1.56E+06	-1.55E+06	1.73E+06
47	6.00E+02	1.32E+06	3.70E+05	1.18E+06	6.60E+05	-9.53E+06
48	2.04E+04	2.55E+06	-7.50E+05	2.08E+06	1.64E+06	-1.15E+07
49	5.86E+03	-1.10E+06	-1.63E+06	-5.80E+05	5.00E+04	-2.73E+06
50	-1.24E+04	-3.28E+06	-4.10E+05	-1.99E+06	-9.60E+05	6.51E+06
51	-4.73E+03	-1.40E+05	1.85E+06	-5.00E+04	-8.00E+04	7.08E+06
52	7.85E+03	2.73E+06	1.61E+06	1.19E+06	3.20E+05	9.50E+05
53	1.94E+03	1.23E+06	-1.16E+06	-8.00E+04	-3.70E+05	-4.25E+06
54	-6.27E+03	-7.50E+05	-2.23E+06	-6.50E+05	-2.00E+04	-4.27E+06
55	-5.60E+02	-3.80E+05	2.00E+04	4.10E+05	1.01E+06	-3.70E+05
56	4.31E+03	-4.40E+05	1.97E+06	2.90E+05	2.50E+05	3.01E+06
57	-1.88E+03	-1.62E+06	9.80E+05	-9.00E+05	-1.41E+06	2.47E+06
58	-3.73E+03	-5.50E+05	-9.20E+05	-9.00E+04	-8.40E+05	-2.40E+05
59	5.14E+03	2.12E+06	-1.18E+06	1.67E+06	1.19E+06	-9.10E+05
60	7.32E+03	1.75E+06	-2.70E+05	6.60E+05	1.20E+06	1.60E+05

K_{13} means the retardation function for surge coupled by heave (e.g. coupled in this case) in the degree of freedom and so on for K_{15}, K_{24}, K_{26}, K_{35} and K_{46}.

The non zero values of the restoring coefficients C_{jk} given in Eqs. (3.6) and (4.1) can be calculated from the following equations:

$$C_{33} = \rho g A_W \tag{4.3}$$

$$C_{44} = \rho g \nabla \cdot GM_T \tag{4.4}$$

$$C_{55} = \rho g \nabla \cdot GM_L \tag{4.5}$$

$$C_{35} = C_{53} = \rho g \int x \cdot B(x) dx = \rho g \cdot \bar{x} \cdot A_W \tag{4.6}$$

where $\bar{x}$ is the longitudinal distance of the centroid of the waterplane area A_W from the origin of the global coordinate system and other parameters are defined in Section 2.2.

4.4 Motion Responses and Motion Spectra by Time-Domain Motion Simulations

The results of the time series of the motions at the attachment points of the mooring lines and of the FPSO in six degrees of freedom in the extreme wave condition of significant wave height 16 m and mean period 14.5 sec at three different heading angles as obtained by Eq. (4.1) are introduced in Figures 4.6~4.17 inclusive and are to be compared with the results from the fast time-domain analyses shown in Figures 3.29~3.68 inclusive. It is noted that these motions are induced by the first- and second-order wave excitations and the nonlinear restoring forces and moments from the mooring system are considered in a quasi-static manner. Since the motions of the FPSO vessel obtained by Eq. (4.1) are referred to the origin of the global coordinate system, the motions at the attachment points can be calculated by some transformation as given in Appendix B.

These motion results are arranged for surge mode in Figures 4.6 to 4.8, for sway in Figures 4.9 to 4.11, and for heave in Figures 4.12 to 4.14. The surge motions predicted by the time-domain simulations based on the retardation function are much the same as the combined first- and second-order surge motions obtained by the previous fast time-domain analyses as shown in Figures 3.47 to 3.49 while the sway and heave motions in the present time-domain simulations are much larger than those in the previous fast time-domain simulations. These differences may be caused by complex phenomena that some coupled effects could influence on the results in the time domain simulations.

Figures 4.15 to 4.17 illustrate the results of roll, pitch and yaw motions of the FPSO predicted by the present time-domain technique in the 100 year sea state in various wave directions and are compared with those by the previous fast time-domain method in Figures 3.56 to 3.58. The roll and pitch motions of the FPSO obtained by the present time-domain method are also larger than those by the previous fast time-domain technique but the yaw motions of the FPSO are similar from both methods. This may due to the coupling effects in the matrix form for the coefficients that could lead to some significant differences.

The spectra of the time series of the motions given in Figures 4.6 to 4.17 have been obtained from the Fourier transform and are shown in Figures 4.18 to 4.21. The corresponding motion spectra obtained from the fast time-domain method are given in Figures 3.59 to 3.62. The motion spectra for sway, heave, roll and pitch motions obtained by the present time-domain motion simulations are larger in magnitude than those by the fast time-domain method while the

surge and yaw motion spectra are shown in relatively reasonable good agreement between the two methods. Such reasonable correlation between the two methods for the motion spectra reflects that the corresponding motion responses obtained by the two methods are similar to each other.

Table 4.4 compares the values of mean, minimum, maximum and standard deviation of the motions of the FPSO obtained by the present time-domain method and fast time-domain technique for 100 year sea state in three different wave heading angles. It is noted that these motions are induced by both the first- and second-order wave excitations in the time-domain motion simulations based on the retardation functions but are the combination of the first- and second-order motions in the fast time-domain analysis. The motions of sway, roll and yaw are significantly reduced with increase in the incident wave angle from 150 to 180 degrees while surge, heave and pitch motions are unchanged. The differences in maximum and minimum values of the FPSO motions except surge mode obtained from the two different time-domain analyses may be due to the fact that one time-domain method considers the memory effects of the convolution integral of the retardation function with the velocity while the other does not.

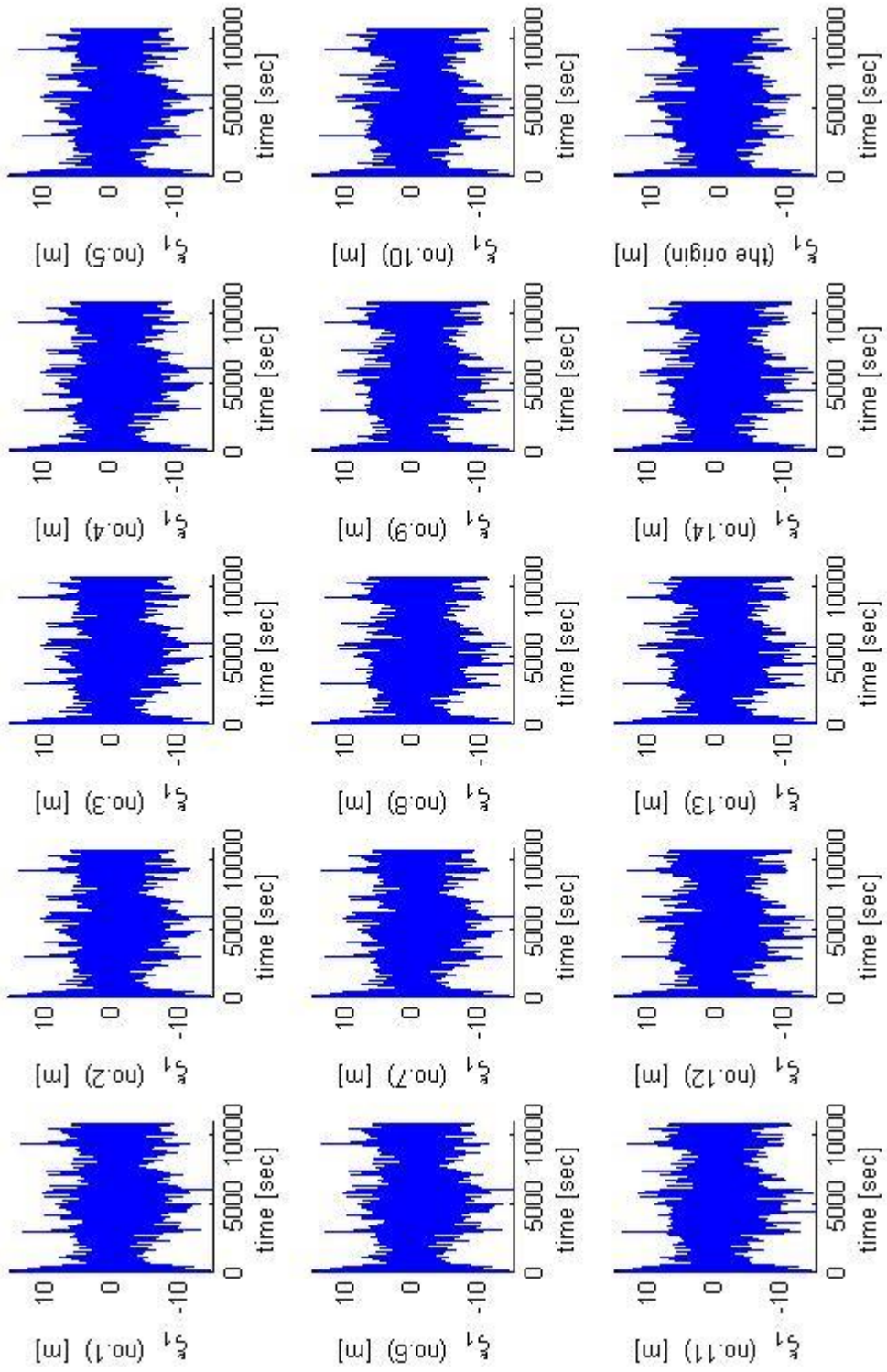

Figure 4.6 Time series of surge displacements at the mooring line attachment points and origin (β=150 degrees)

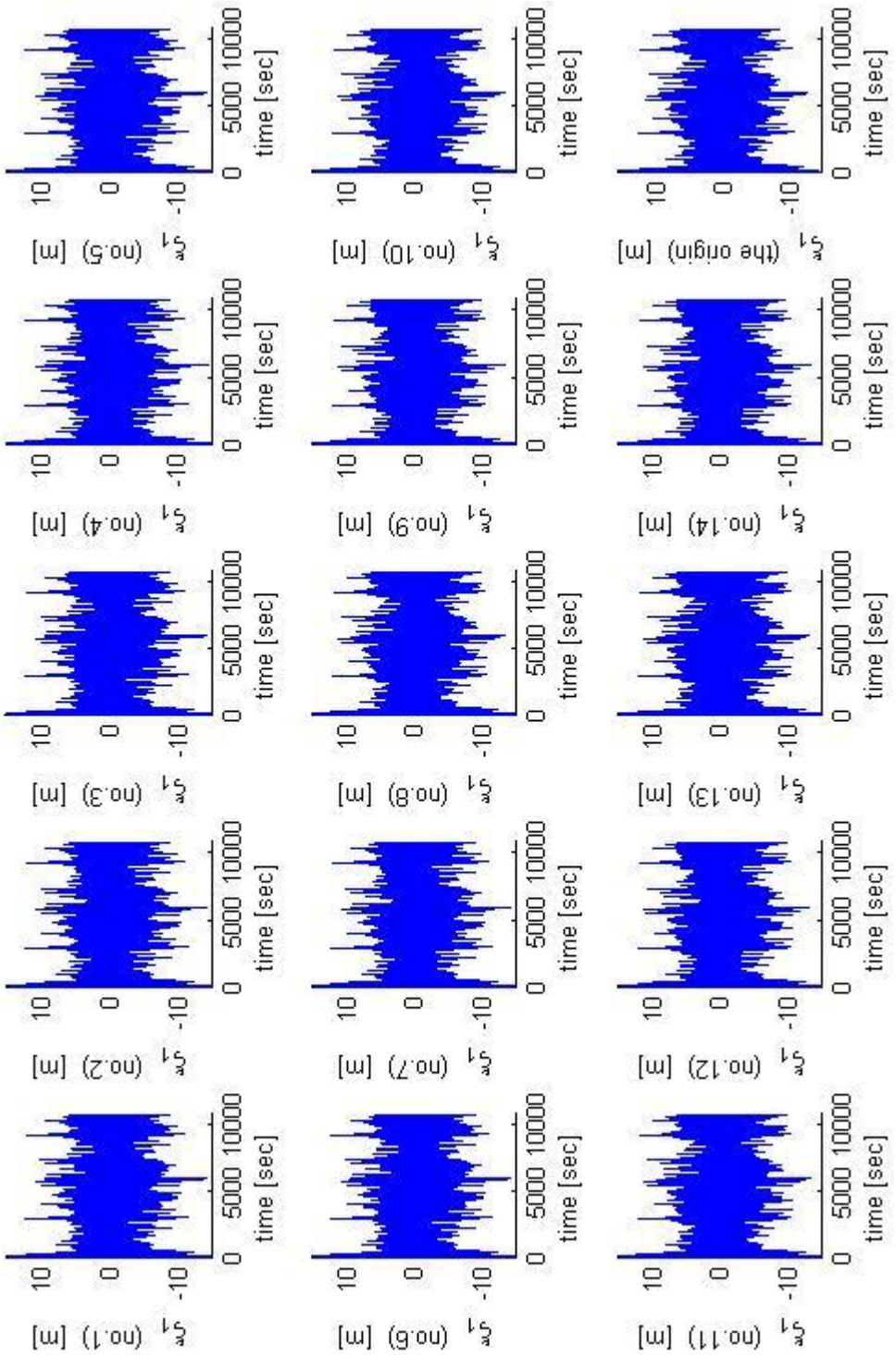

Figure 4.7 Time series of surge displacements at the mooring line attachment points and origin (β=165 degrees)

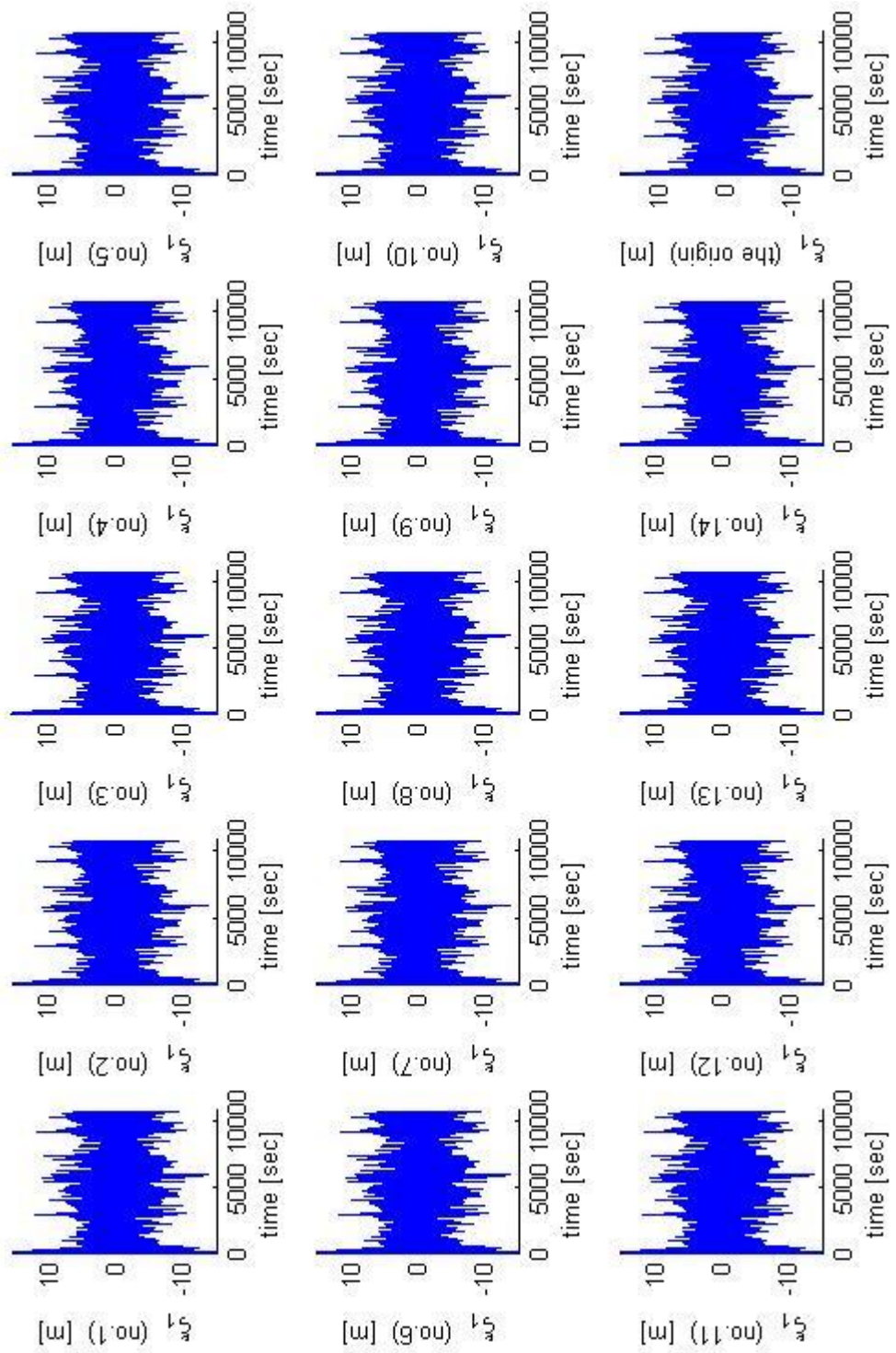

Figure 4.8 Time series of surge displacements at the mooring line attachment points and origin (β=180 degrees)

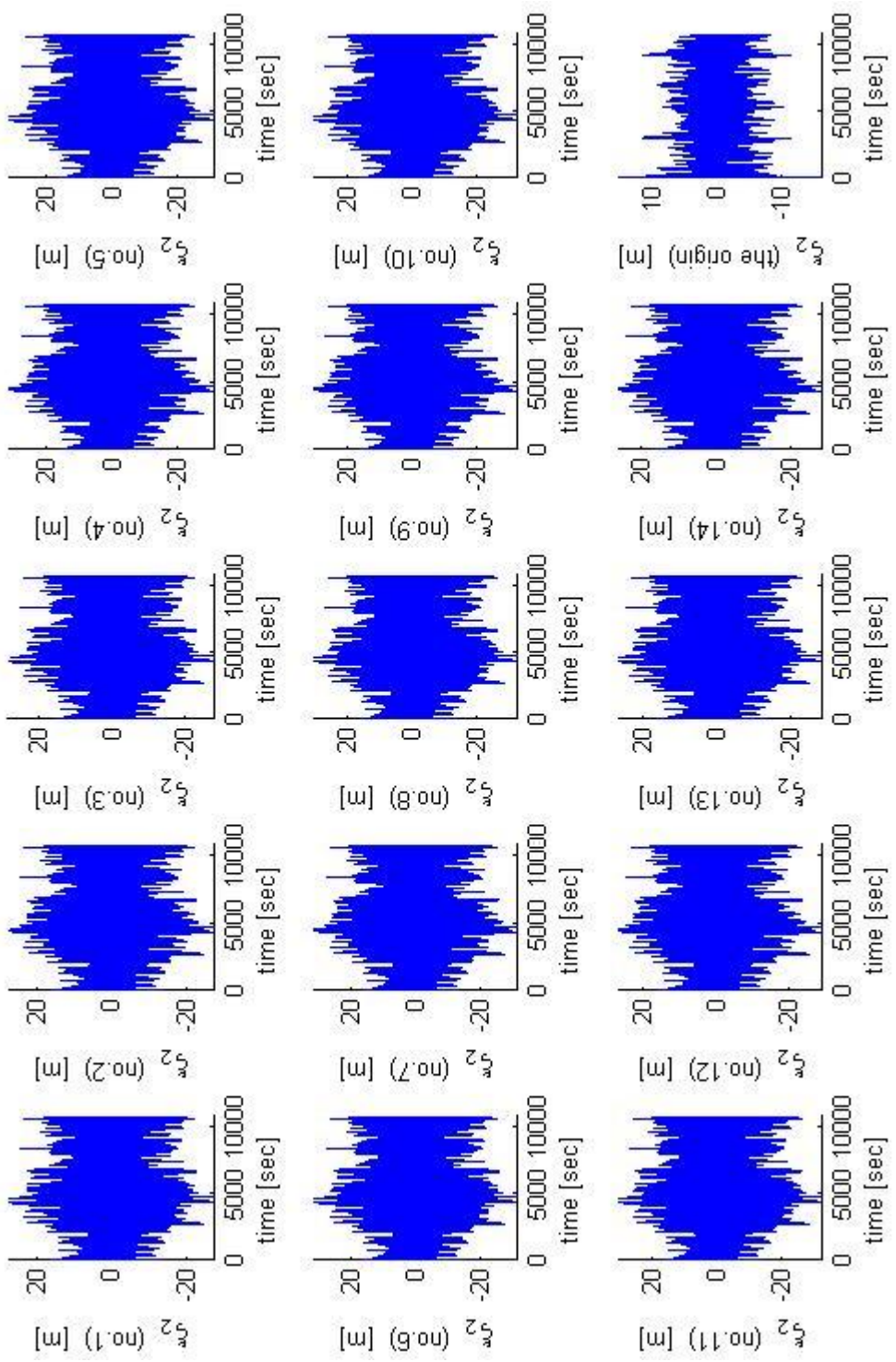

Figure 4.9 Time series of sway displacements at the mooring line attachment points and origin (β=150 degrees)

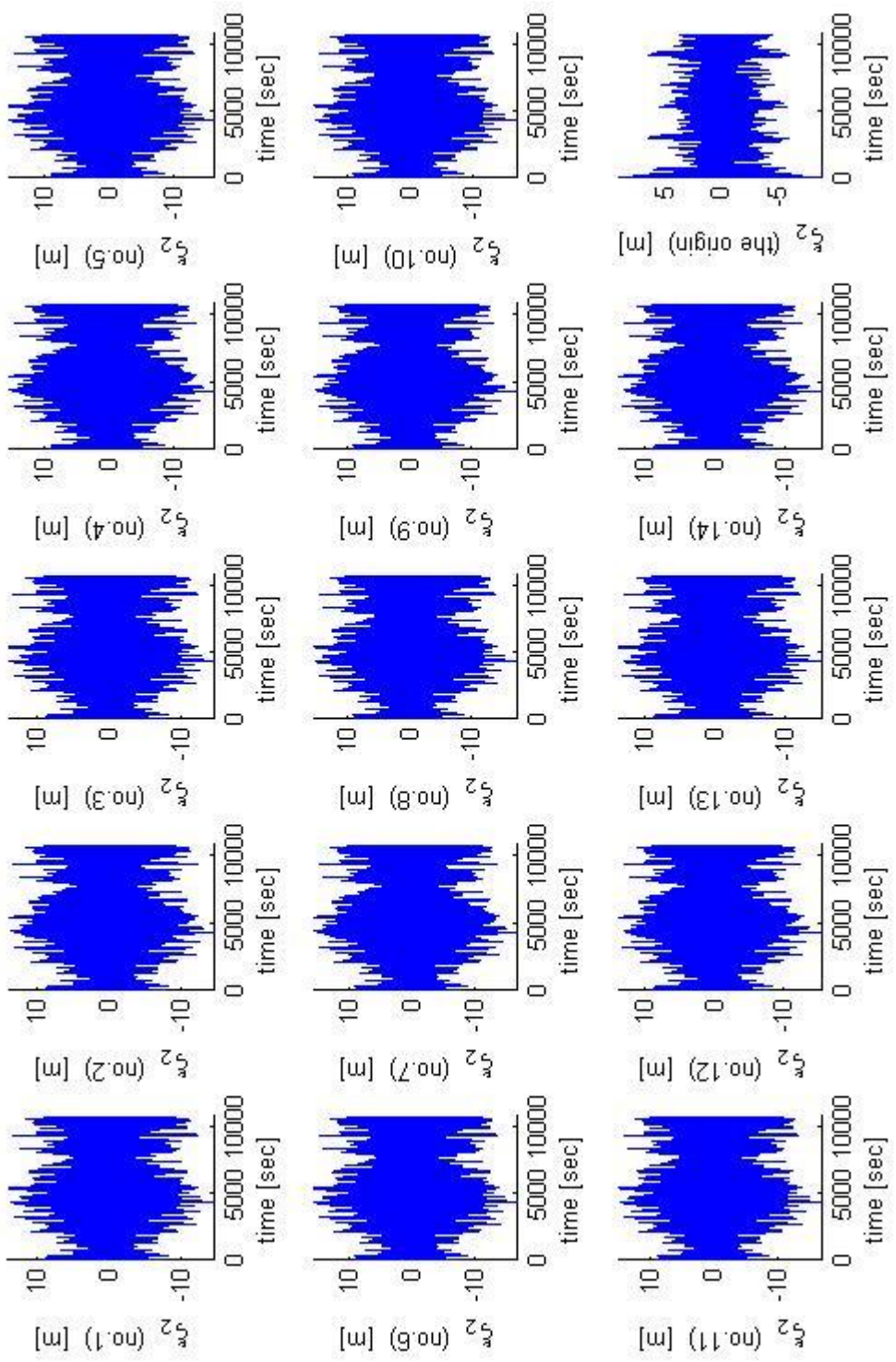

Figure 4.10 Time series of sway displacements at the mooring line attachment points and origin (β=165 degrees)

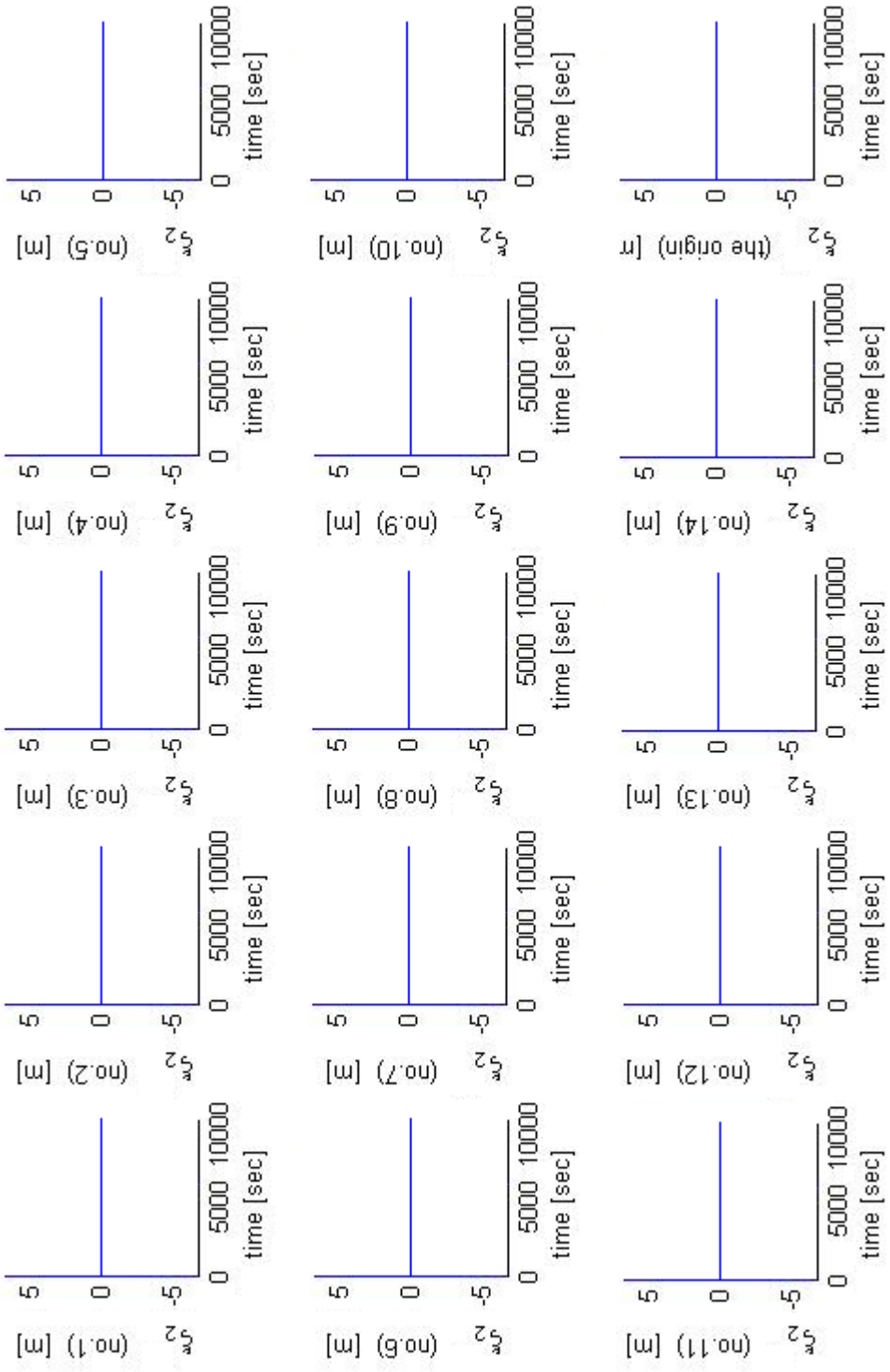

Figure 4.11 Time series of sway displacements at the mooring line attachment points and origin (β=180 degrees)

(The values of sway are zero in the head sea condition, β=180)

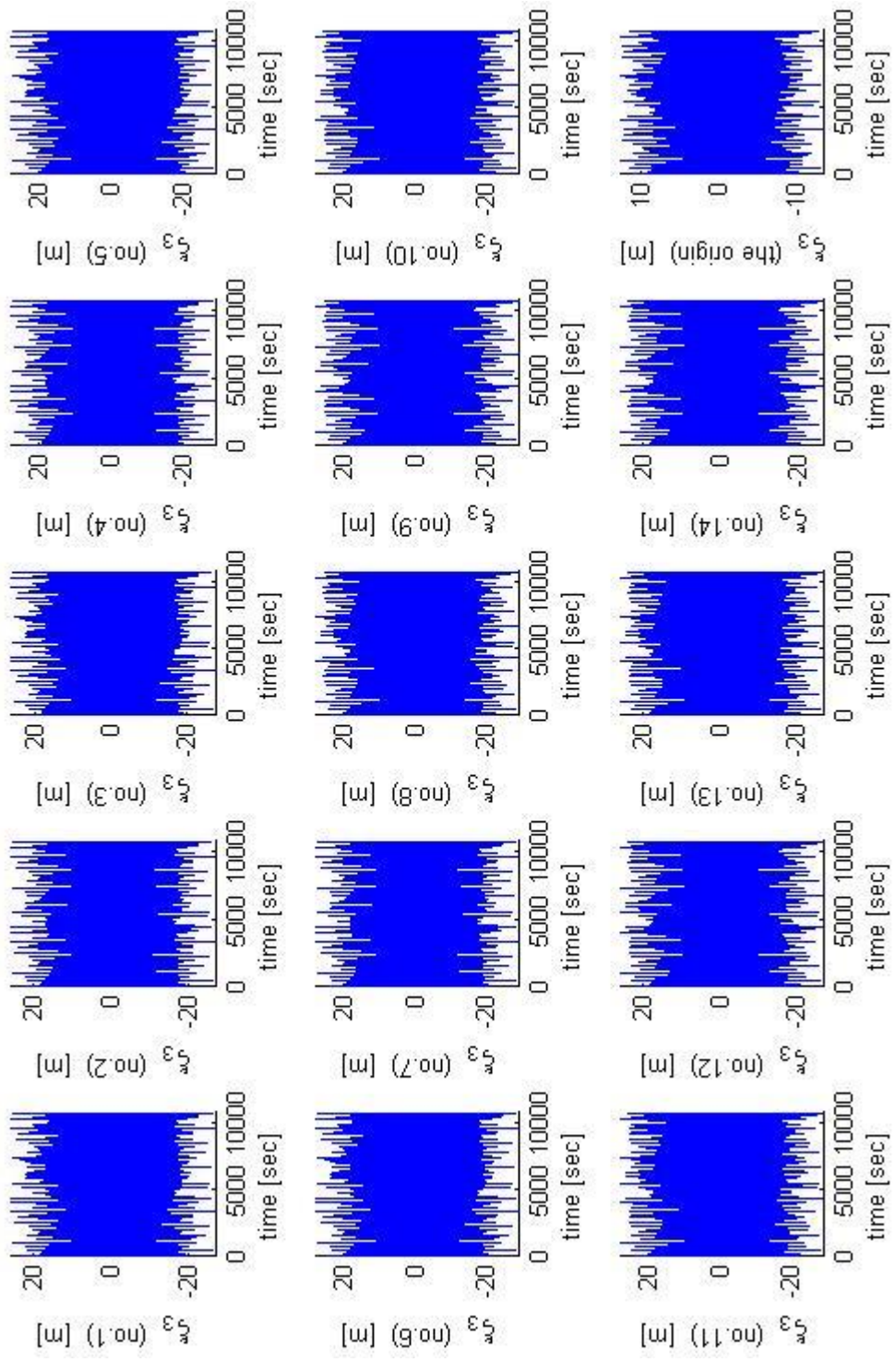

Figure 4.12 Time series of heave displacements at the mooring line attachment points and origin (β=150 degrees)

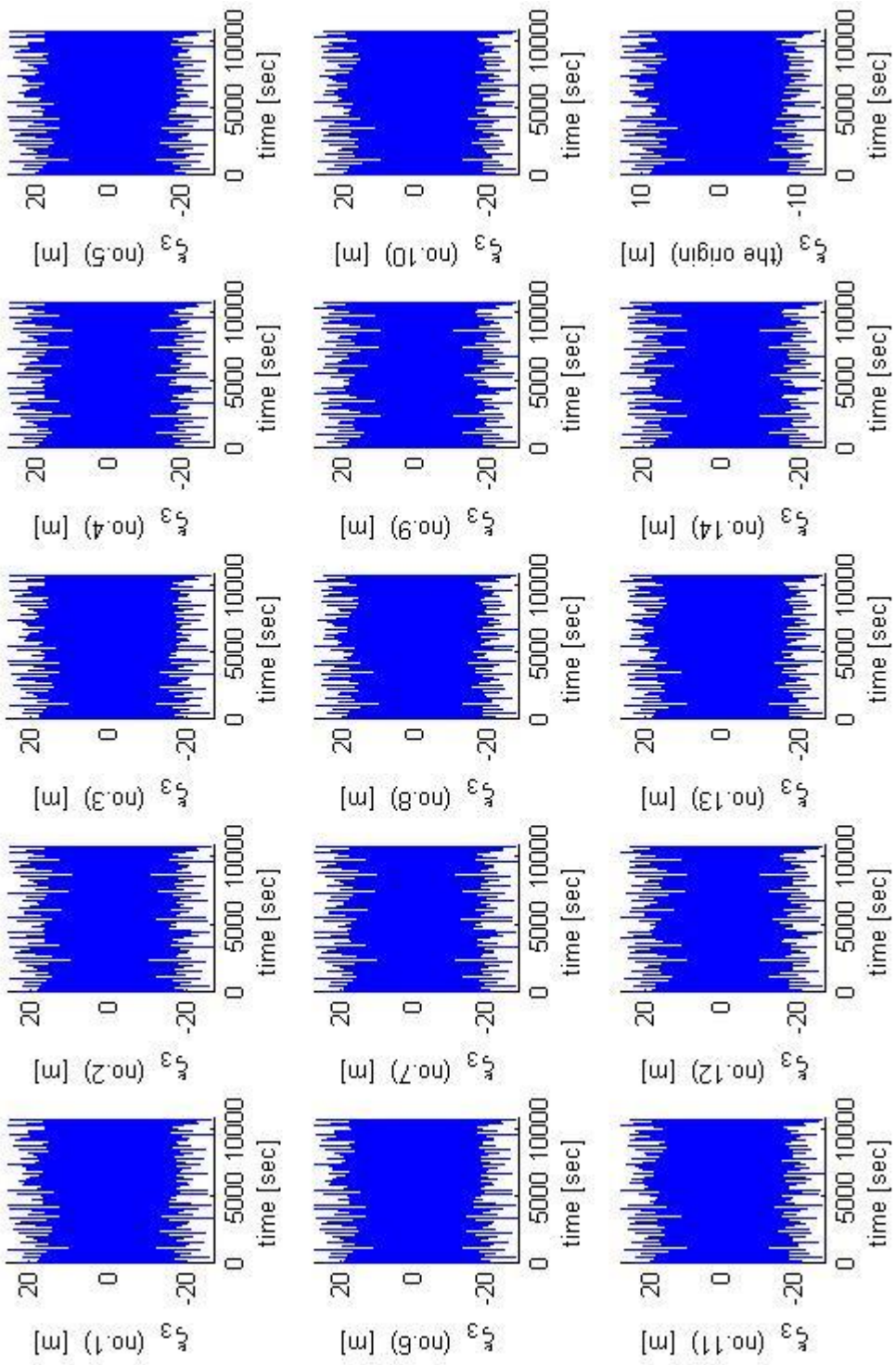

Figure 4.13 Time series of heave displacements at the mooring line attachment points and origin (β=165 degrees)

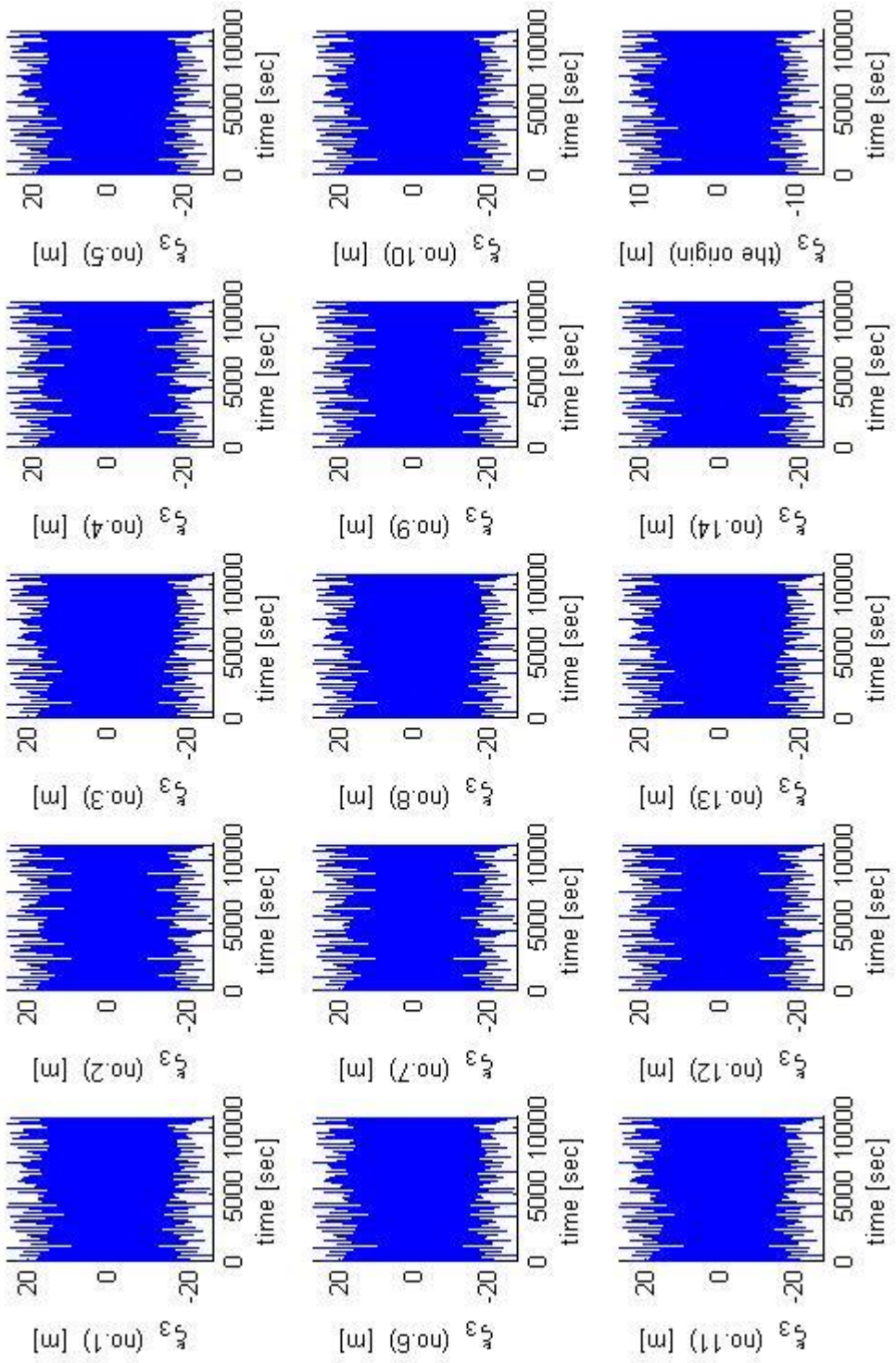

Figure 4.14 Time series of heave displacements at the mooring line attachment points and origin (β=180 degrees)

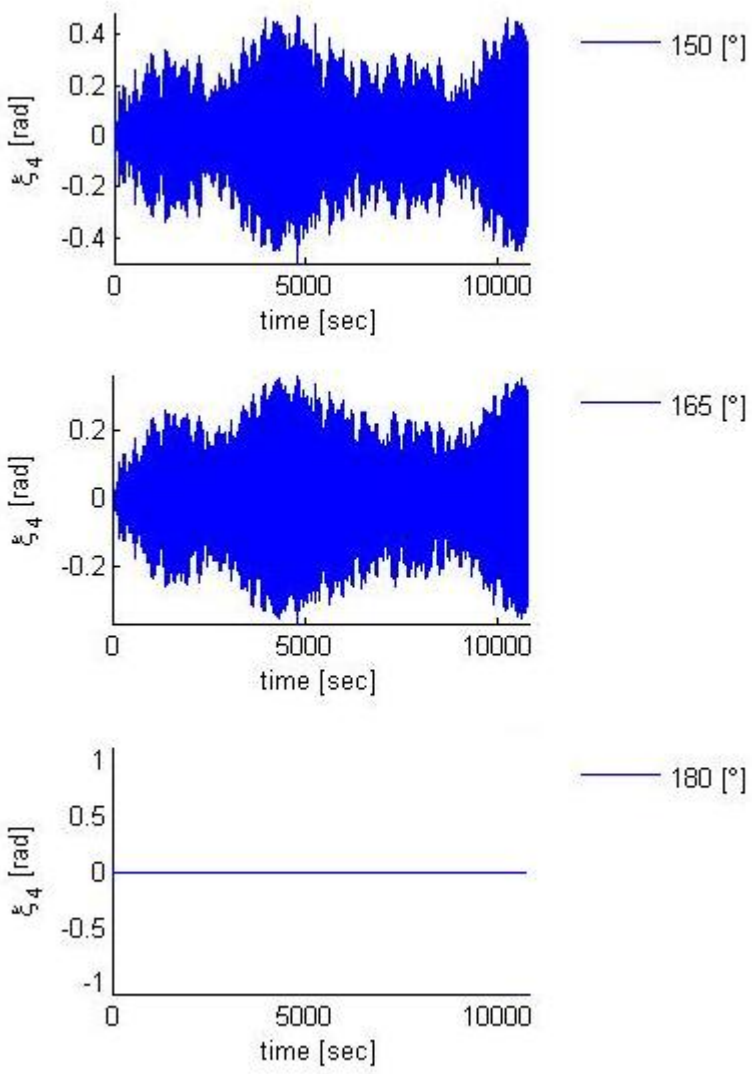

Figure 4.15 Time series of roll displacement

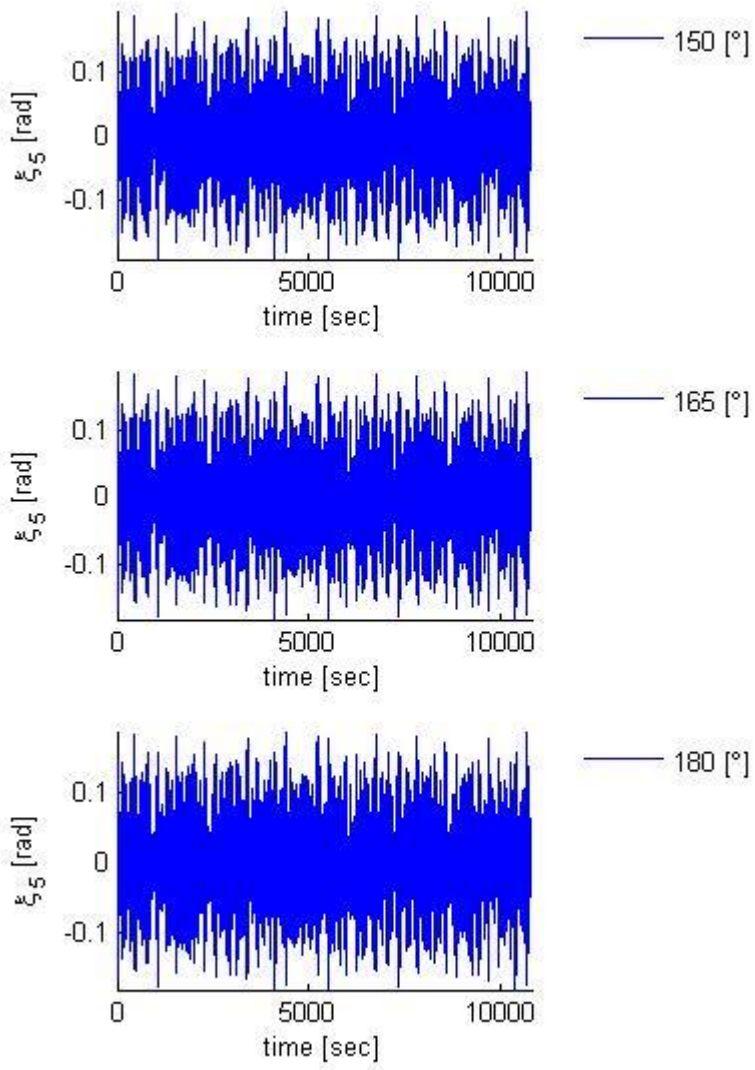

Figure 4.16 Time series of pitch displacement

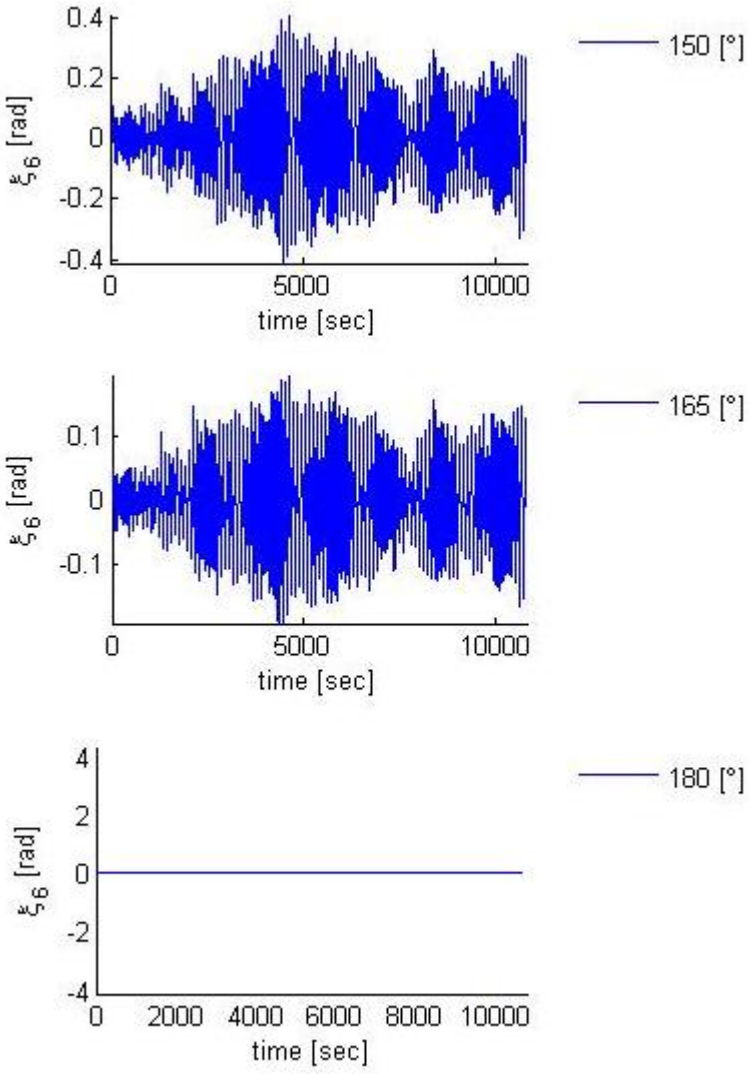

Figure 4.17 Time series of yaw displacement

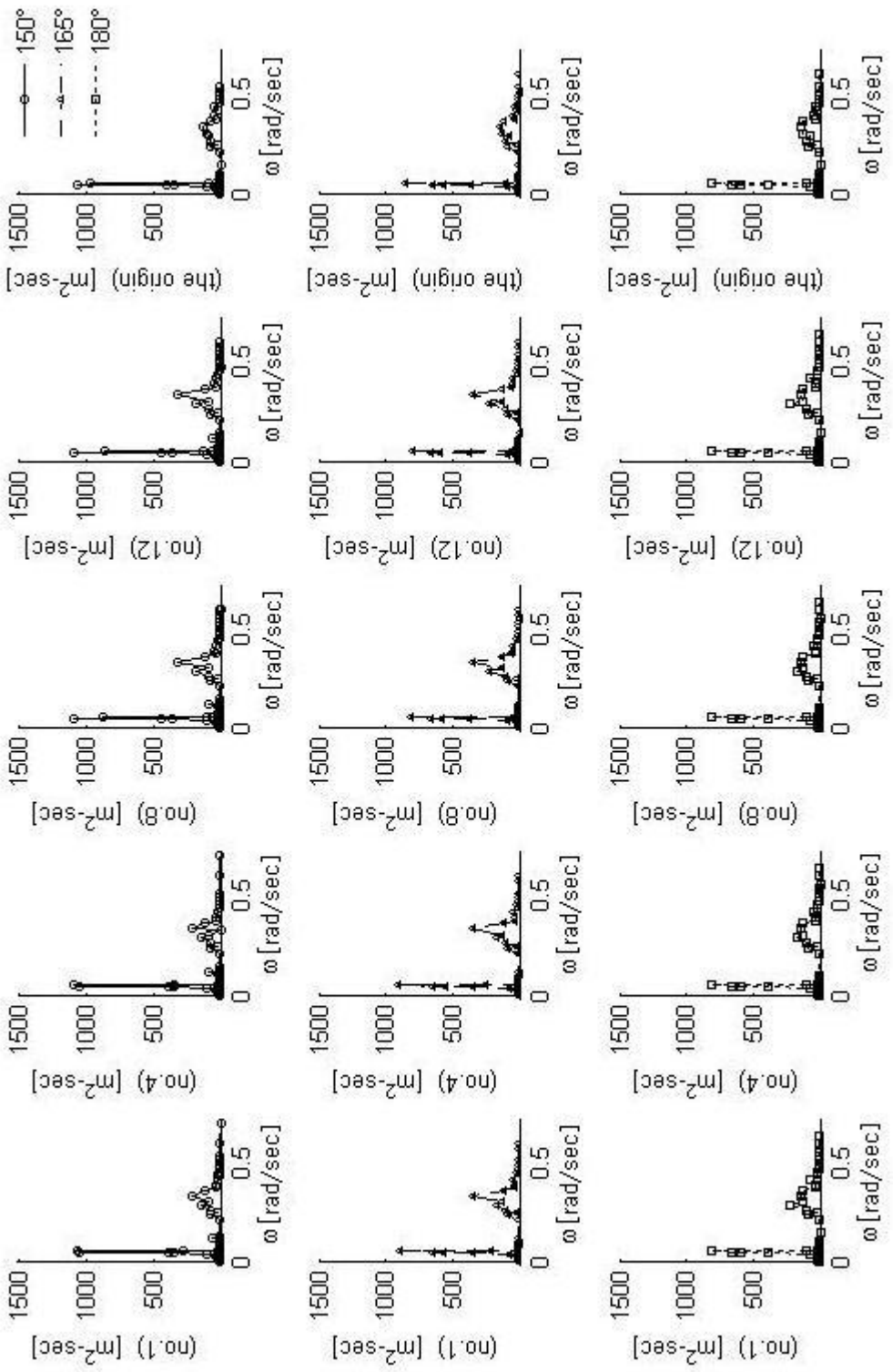

Figure 4.18 Surge motion spectra

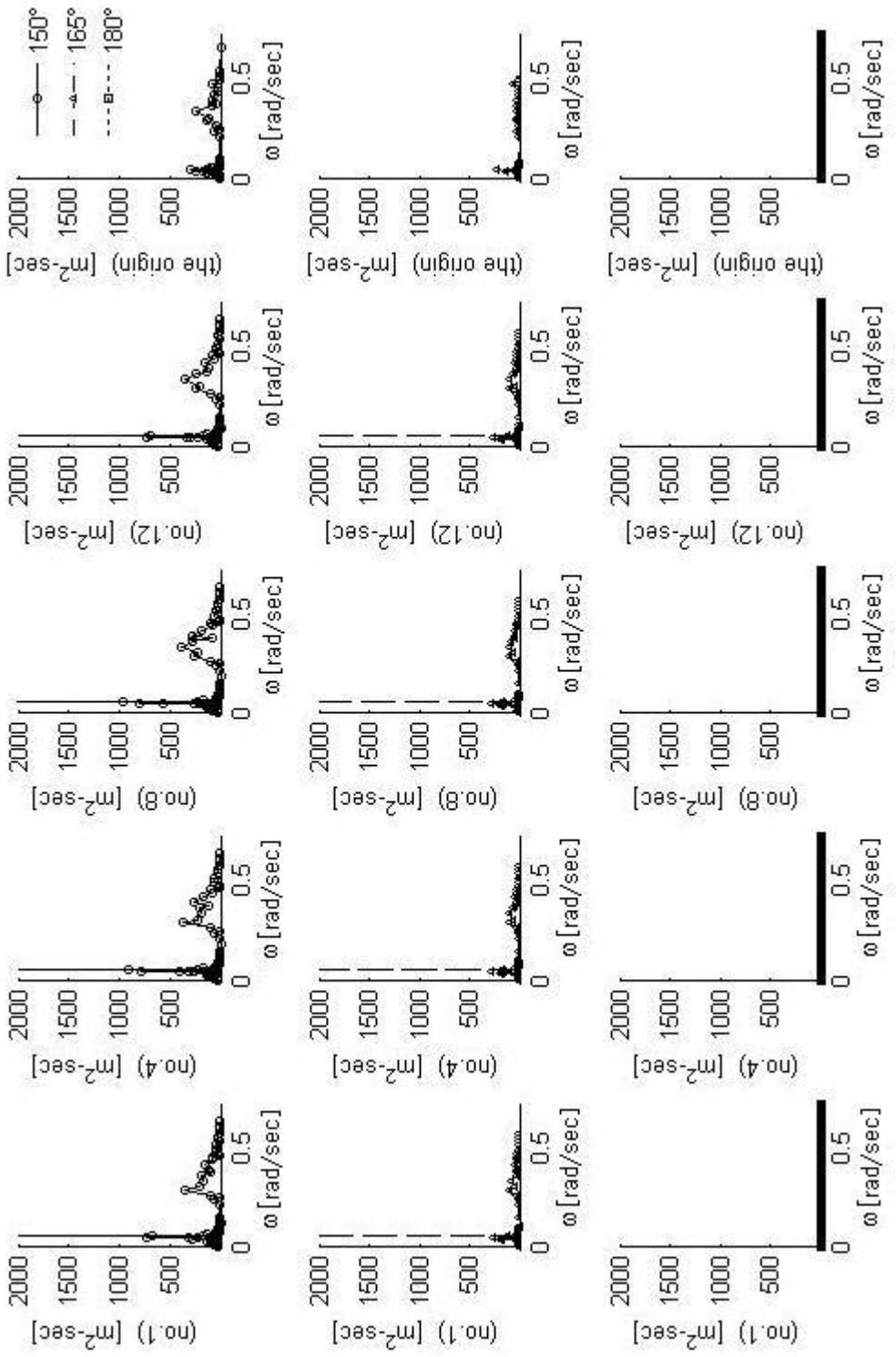

Figure 4.19 Sway motion spectra

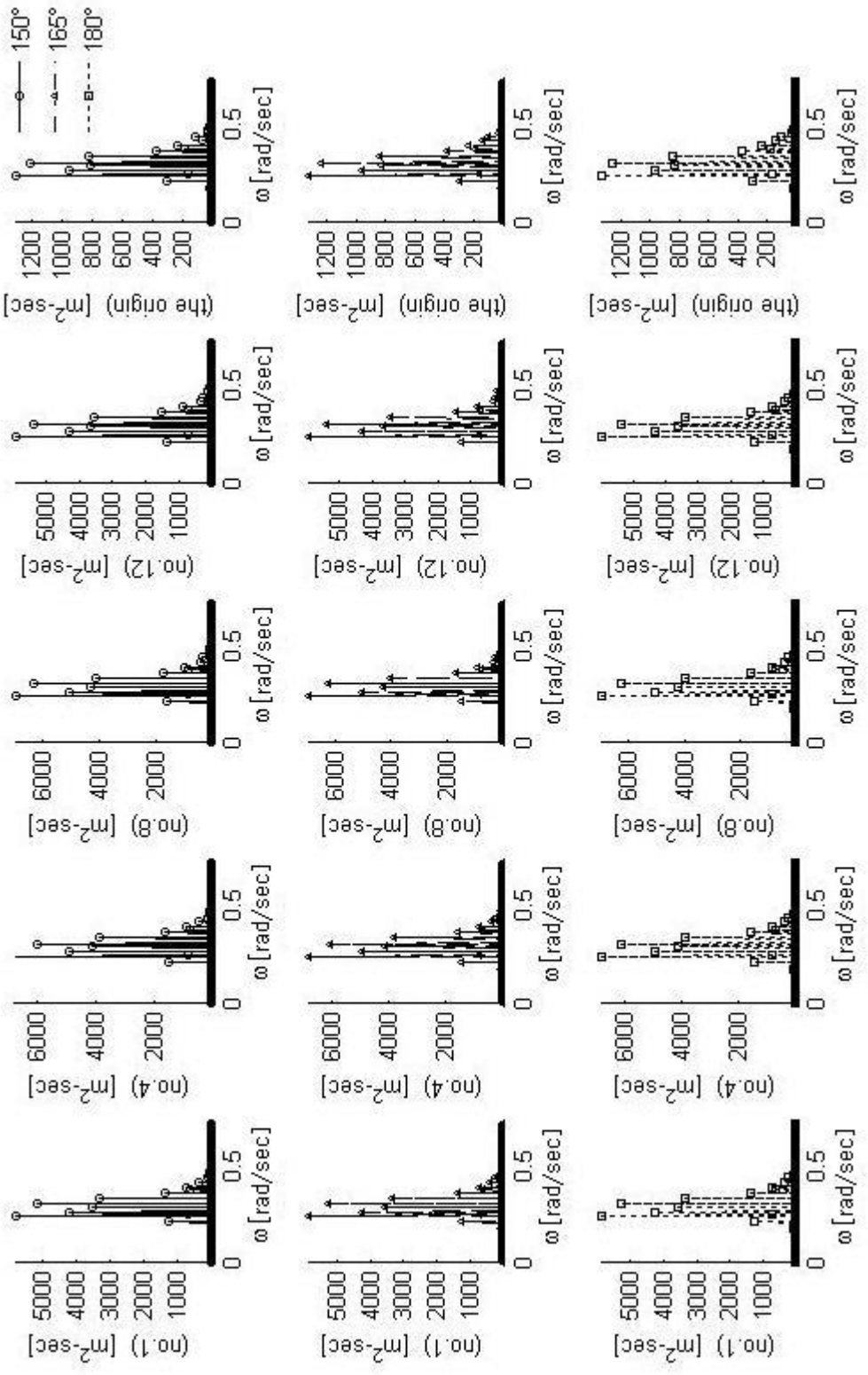

Figure 4.20 Heave motion spectra

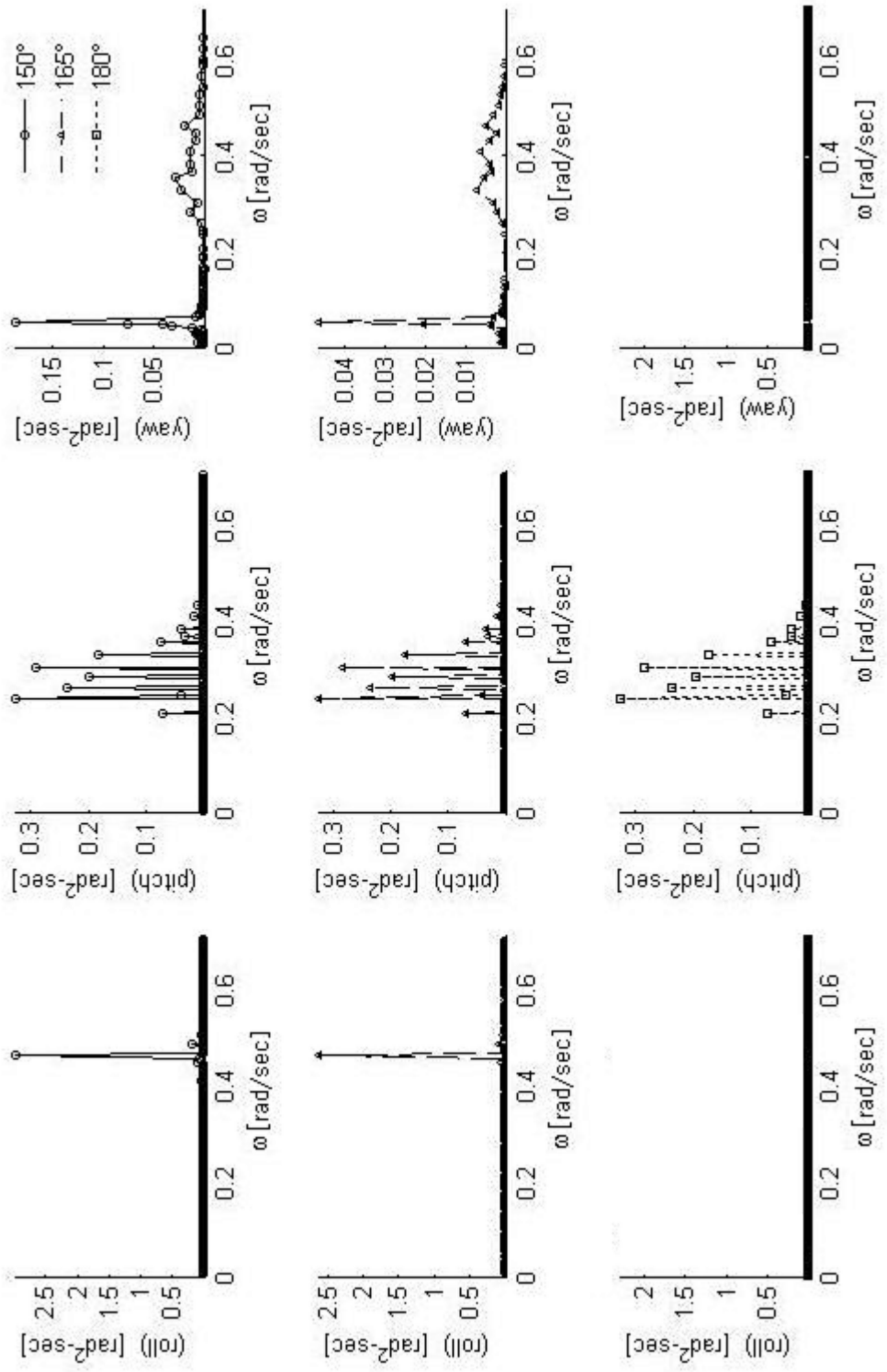

Figure 4.21 Roll, pitch and yaw motions spectra

(The values of roll and yaw are zero in the head sea condition, β=180)

Table 4.4 FPSO motions computed by two different time-domain methods

		FAST TIME DOMAIN				TIME DOMAIN			
		MEAN	MIN	MAX	STD	MEAN	MIN	MAX	STD
SURGE [m]	150°	-0.149	-16.925	16.880	6.363	0.042	-14.478	15.618	4.139
	165°	-0.910	-16.987	15.204	5.852	0.038	-14.639	15.828	4.002
	180°	-0.357	-17.225	14.669	5.765	0.035	-14.721	15.972	4.002
SWAY [m]	150°	0.854	-10.757	11.045	3.944	-0.042	-16.306	15.465	2.376
	165°	0.616	-5.606	5.642	1.984	-0.022	-8.960	9.266	2.069
	180°	0.000	0.000	0.000	0.000	0.000	0.000	0.000	0.000
HEAVE [m]	150°	0.001	-9.289	9.236	2.766	-0.007	-13.309	12.620	4.662
	165°	0.002	-8.477	8.169	2.546	-0.009	-13.334	12.727	4.688
	180°	0.002	-8.292	7.835	2.478	-0.010	-13.588	12.840	4.701
ROLL [rad]	150°	0.000	-0.114	0.124	0.039	0.001	-0.502	0.478	0.186
	165°	0.000	-0.069	0.069	0.024	0.000	-0.368	0.363	0.157
	180°	0.000	0.000	0.000	0.000	0.000	0.000	0.000	0.000
PITCH [rad]	150°	0.000	-0.128	0.130	0.039	0.001	-0.190	0.194	0.071
	165°	0.000	-0.130	0.128	0.038	0.001	-0.183	0.188	0.070
	180°	0.000	-0.132	0.128	0.038	0.001	-0.182	0.186	0.070
YAW [rad]	150°	0.001	-0.388	0.390	0.128	0.002	-0.412	0.410	0.144
	165°	0.001	-0.180	0.175	0.061	0.001	-0.194	0.195	0.074
	180°	0.000	0.000	0.000	0.000	0.000	0.000	0.000	0.000

4.5 Quasi-Static Frequency-Domain Mooring Analysis

Since a sea wave environment is continuously changing, a motions response and mooring analysis requires a large number of variations covering all possible wave directions, not only in regular waves but also in irregular waves. Within the framework of assumed linearization the responses of a floating body to irregular waves can be considered as the summation of the responses to combinations of regular waves of all heights and frequencies. Thus, a stochastic analysis can be carried out in order to predict the various statistical characteristics of dynamic motion responses. This section presents some statistical properties of spectrum analysis to be used in order to predict the maximum and significant values of the first-order and second-order wave induced FPSO motions at the attachment points of the various mooring lines. Then the maximum tension, within a given period of wave environment exposure, in each line can be calculated by displacing its attachment point with a predicted maximum horizontal distance in the direction of alignment of the individual line from its initial static equilibrium position and through the load-excursion characteristics given by Eq. (2.13) for a slack single component mooring line or by the equations associated with different configurations of a multi-component line given in Section 2.4.

The maximum excursions of the attachment point (x, y, z) of a mooring line in the j-th mode may be obtained by combination of the first-order wave-induced motion with second-order motion in accordance with the following empirical equation (DNV 1996):

$$X_j = \bar{\xi}_j + \hat{\xi}_j^{(2)} + \xi_{j1/3}^{(1)} \quad \text{when,} \quad \hat{\xi}_j^{(2)} > \hat{\xi}_j^{(1)} \tag{4.17}$$

$$X_j = \bar{\xi}_j + \hat{\xi}_j^{(1)} + \xi_{j1/3}^{(2)} \quad \text{when,} \quad \hat{\xi}_j^{(2)} < \hat{\xi}_j^{(1)} \tag{4.18}$$

where $\bar{\xi}_j$ is the mean offset due to mean second-order force $\bar{F}_j^{(2)}$. $\xi_{j1/3}^{(1)}$ and $\hat{\xi}_j^{(1)}$ are the significant and most probable maximum values of the first-order motion in the j-th mode respectively while $\xi_{j1/3}^{(2)}$ and $\hat{\xi}_j^{(2)}$ are respectively the significant and most probable maximum values of the second-order motion in the j-th mode. They can be obtained by means of spectral analysis with the application of the following equations:

$$\bar{\xi}_j = \frac{2\int_0^\infty \bar{F}_j^{(2)} S(\omega) d\omega}{K_{jj}} \quad \textbf{(4.19)}$$

$$\xi_{j1/3}^{(1)} = 2\sqrt{m_o} \quad \textbf{(4.20)}$$

$$\hat{\xi}_j^{(1)} = \sqrt{2m_o \ln(N)} \quad \textbf{(4.21)}$$

$$\xi_{j1/3}^{(2)} = 2\sigma_j \quad \textbf{(4.22)}$$

$$\hat{\xi}_j^{(2)} = \sigma_j \sqrt{2\ln(3600T/T_{jn})} \quad \textbf{(4.23)}$$

$$m_o = \int_0^\infty \left|\xi_j(x,y,z,\omega,\beta)\right|^2 S(\omega) d\omega \quad \textbf{(4.24)}$$

$$m_2 = \int_0^\infty \omega^2 \left|\xi_j(x,y,z,\omega,\beta)\right|^2 S(\omega) d\omega \quad \textbf{(4.25)}$$

$$N = 3600 T n' \quad \textbf{(4.26)}$$

$$n' = \frac{1}{2\pi}\sqrt{\frac{m_2}{m_o}} \quad \textbf{(4.27)}$$

where m_0 and m_2 are respectively the area and second moment of area of the first-order motion response spectrum. $|\xi_j(x,y,z,\omega,\beta)|$ is the first-order wave-induced motion amplitude operator at an attachment point (x, y, z) at wave frequency ω and heading angle β. $S(\omega)$ is the wave spectral density. T is the duration of storm in hours, N is the number of responses in a given storm and n' is the average number of a motion response per unit time. T_{jn} is the natural period of the FPSO in the j-th mode. The standard deviation σ_j of the low frequency motion in the j-th mode can be written as (Pinkster, 1979):

$$\sigma_j^2 = \int_0^\infty \frac{S_{Fj}(\mu)}{\left\{K_{jj} - (M + A_{jj})\mu^2\right\}^2 + B_{jj}^2\mu^2} d\mu \quad \textbf{(4.28)}$$

in which S_{Fj} is the spectral density of the low frequency drift force in the j-th mode, A_{jj} and B_{jj} are respectively the added mass and damping at the natural frequency of the j-th mode motion. In the present investigation, the damping B_{jj} was taken as 10 % of the critical damping. The spectral density S_{Fj} of the low frequency part can be determined from Pinkster's approximation (Pinkster 1975) as:

$$S_{Fj}(\mu) = 8\int_0^\infty S(\omega)S(\omega+\mu)\left(\frac{\bar{F}_j^{(2)}(\omega+\mu/2)}{\zeta_a^2}\right)^2 d\omega \qquad \textbf{(4.29)}$$

where $\bar{F}_j^{(2)}(\omega+\mu/2)$ the mean second-order force in the j-th direction for frequency $\omega+\mu/2$ and can be calculated by Eqs. (3.7) to (3.9) for surge, sway and yaw modes respectively.

Table 4.5 shows the comparisons between the surge and sway excursions obtained by the present frequency domain method and the fast time-domain technique for the FPSO in 100 year sea state with waves coming from three different directions. The first- and second-order motions can be calculated separately in the fast time-domain method described in Chapter 3 and in the present frequency-domain analysis, but the motions of the FPSO excited by the first- and second-order wave forces in the time-domain motion simulations based on retardation functions are mixed with both first- and second-order motions. Thus, the results of the latter time-domain motion simulations are not shown in Table 4.5.

The values of the significant and most probable first-order and second-order surge motions are greater than those for the first-order and second-order sway motions as predicted by both the frequency- and the fast time-domain methods. This phenomenon is also observed in the surge and sway RAOs presented in Figure F.1 (Appendix F). The first-order motions and mean offsets predicted by the frequency-domain method are larger than those obtained in the fast time-domain analysis. This means that the wave frequency motions are reliable between frequency domain and fast time-domain method however low frequency motions are not due to the difficulties finding exact values that are as follows with respect to critical damping.

The values of total surge motions predicted by both methods are similar order while the total sway motions estimated by the frequency-domain method are larger than those by the fast time-domain technique. This is due to the differences for the values of the first and second order motions and the combination for the use of them.

Table 4.5 Surge and sway excursions of the FPSO

Unit [m]			FAST TIME DOMAIN			FREQ DOMAIN		
			150°	165°	180°	150°	165°	180°
MAX	Wave freq	Surge	6.684	7.022	7.138	6.913	7.242	7.335
		Sway	3.858	2.021	0.000	4.042	2.012	0.000
	Low freq	Surge	13.795	13.109	13.073	14.906	14.224	14.150
		Sway	9.336	4.854	0.000	11.762	5.182	0.000
SIG	Wave freq	Surge	3.776	3.967	4.034	3.881	4.070	4.124
		Sway	2.211	1.094	0.000	2.265	1.129	0.000
	Low freq	Surge	9.324	8.296	8.054	8.763	7.980	7.897
		Sway	6.713	3.484	0.000	6.570	2.895	0.000
MEAN OFFSET		Surge	-0.150	-0.910	-0.358	-1.565	-1.480	-1.456
		Sway	0.854	0.617	0.000	2.855	1.245	0.000
TOTAL		Surge	17.420	16.166	16.749	17.222	16.814	16.819
		Sway	12.402	6.564	0.000	16.883	7.556	0.000

Once the values of surge excursion X_1 and sway excursion X_2 from the initial equilibrium position are obtained from Eq. (4.17) and (4.18), the resolved maximum horizontal distance X can be calculated and input to Eq. (2.13) in order to determine the maximum tension in the specific mooring line. The results of the frequency-domain quasi-static mooring analysis for some selected lines are shown in Table 4.7 and are discussed in Section 4.7. It should be noted that this quasi-static approach is conservative since the maximum surge and sway excursions may not occur simultaneously.

It is noted that the most probable maximum values of the first-order motion $\hat{\xi}_j^{(1)}$ and most probable maximum values of the second-order motion $\hat{\xi}_j^{(2)}$ may also be calculated by means of the equations proposed by DNV (1996) as given in Appendix G.

4.6 Line Tensions and Tension Spectra by two different time-domain approaches

Figure 4.22 shows the selected specifically analyzed mooring lines which are depicted in bold printed lines in the three alternative assumed groups of wave angles approaching the FPSO vessel. The principal wave group directions are the heading angles for the starboard quarter as shown, but could be on the port quarter. However the mooring line arrangement and the vessel are symmetric and thus the results of tensions in the mooring lines on the port side are expected to be the same as those on the starboard side.

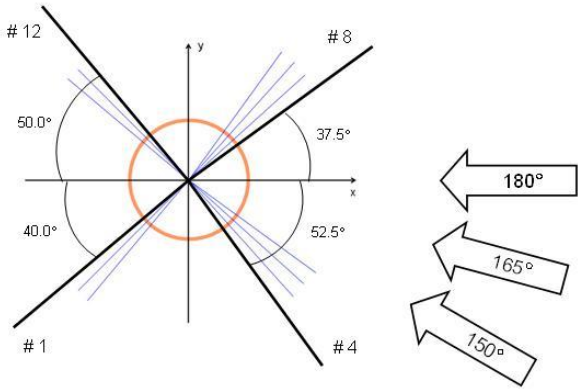

Figure 4.22 Arrangement of the mooring lines No.1, 4, 8, 12

The time series and corresponding spectra of line tensions at the attachment points of the selected lines obtained in the fast time-domain motion analysis are shown in Figures 4.23 to 4.25 for the three different wave heading angles. The largest line tension occurs on line No.8 as this line in the windward side of the turret experiences the farthest extension than other selected lines. The second and third largest tensions are in line No.1 and line No.4 respectively. However, the smallest tension occurs on line No.12 in the fast-time domain analysis. This is an anticipated result as line No.12 is on the leeward side of the turret in the travelling direction of the propagating waves and so it becomes more slack. The low frequency component is more appreciable than the wave frequency component in the tension spectrum for line No.12 in the cases of both 150 and 165 degrees heading angles. This is because the slackened line is less sensitive to small first-order wave frequency motions than to large second-order low frequency motions. The first order component of tension spectral density for line No.12 shows smaller values than for the other lines in most wave directions considered. The wave frequency tension component is much more dominant in line No.8 than in line No.12, as shown in Figure 4.23 for 150 degree seas and this phenomenon is also shown in the wave angle of 165 degrees, because

line No. 8 is situated to react to the maximum surge and sway excursions due to the first-order wave excitations. Line No. 8 also experiences significant wave frequency tensions in head seas than other lines as this line is in the windward side of the turret and more inclined to the incoming head waves.

Generally speaking, the low frequency tension spectral density is significant in the case of 150 degrees heading angle, while the tension spectral density in the wave frequency region has the same order of magnitude in the low frequency range for the wave directions of 165 and 180 degrees. The maximum excursion is found to create the largest tension in a mooring line and this generally occurs when the vessel moves to the maximum surge and sway distances concurrently. Both the maximum combined surge and sway excursions are expected to occur in oblique waves around 150 degrees but only surge displacements exist in head seas. This is the reason that the magnitude of the low frequency tension spectral density for head waves is smaller than that for 150 degree waves. However, the low frequency component of tension spectral density is significantly reduced in the case of β=165 degrees against β=150 degrees seas. This phenomenon can be applied to an optimization of the mooring system against the dominant direction of incident waves.

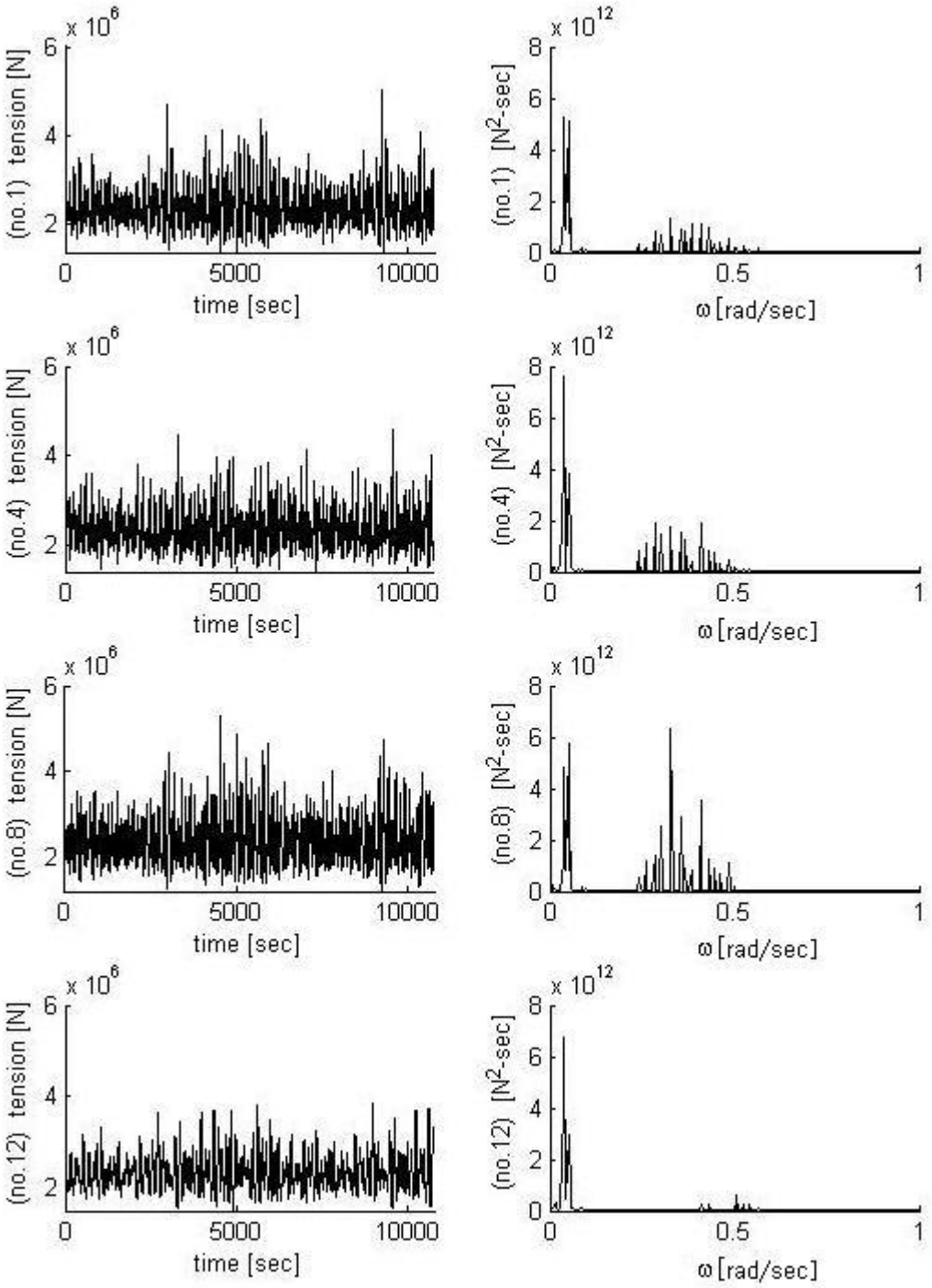

[Tension] [Spectrum]

Figure 4.23 Line tensions and spectra by fast time-domain analysis (β=150 degrees)

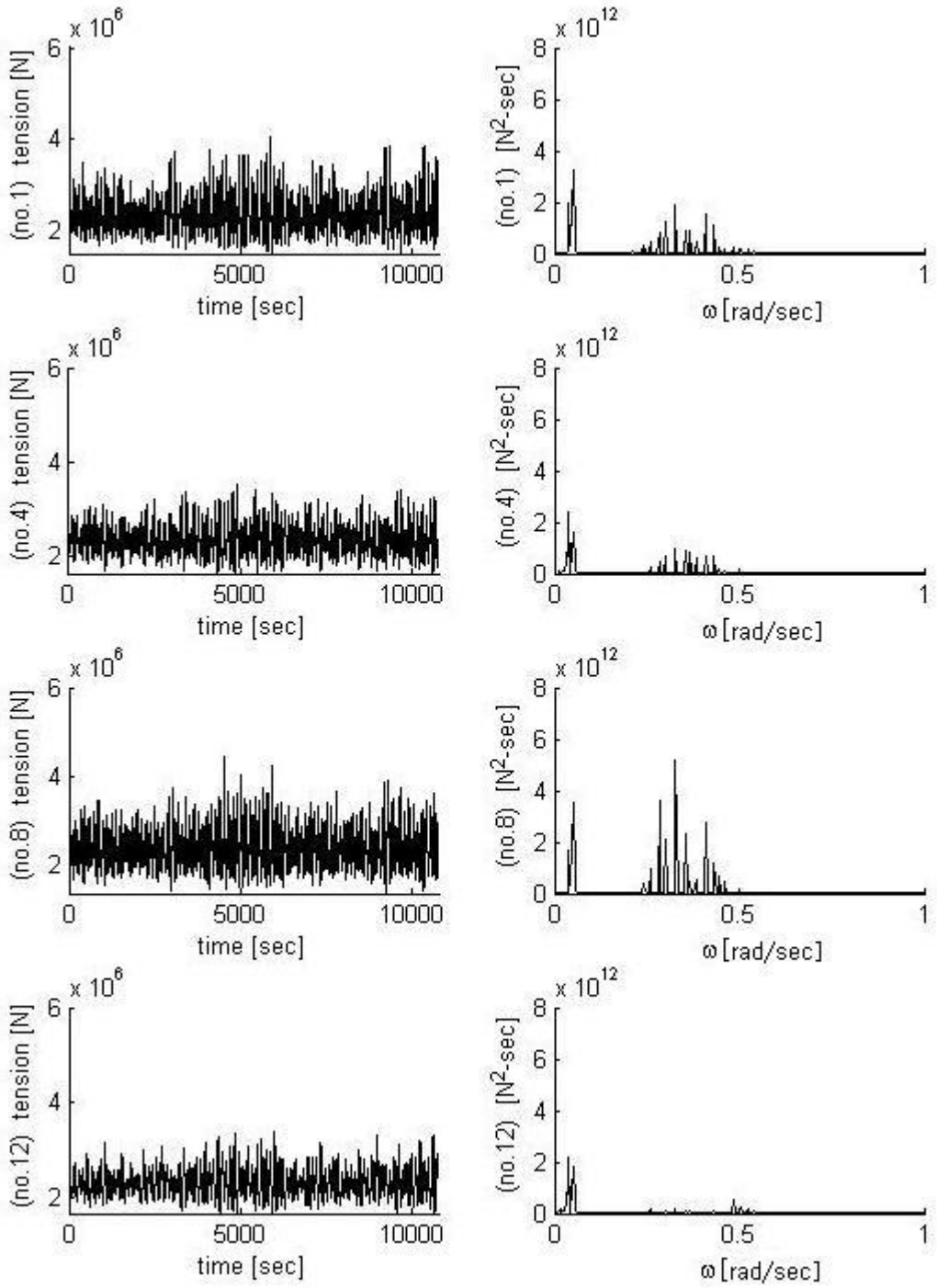

[Tension] [Spectrum]

Figure 4.24 Line tensions and spectra by fast time-domain analysis (β=165 degrees)

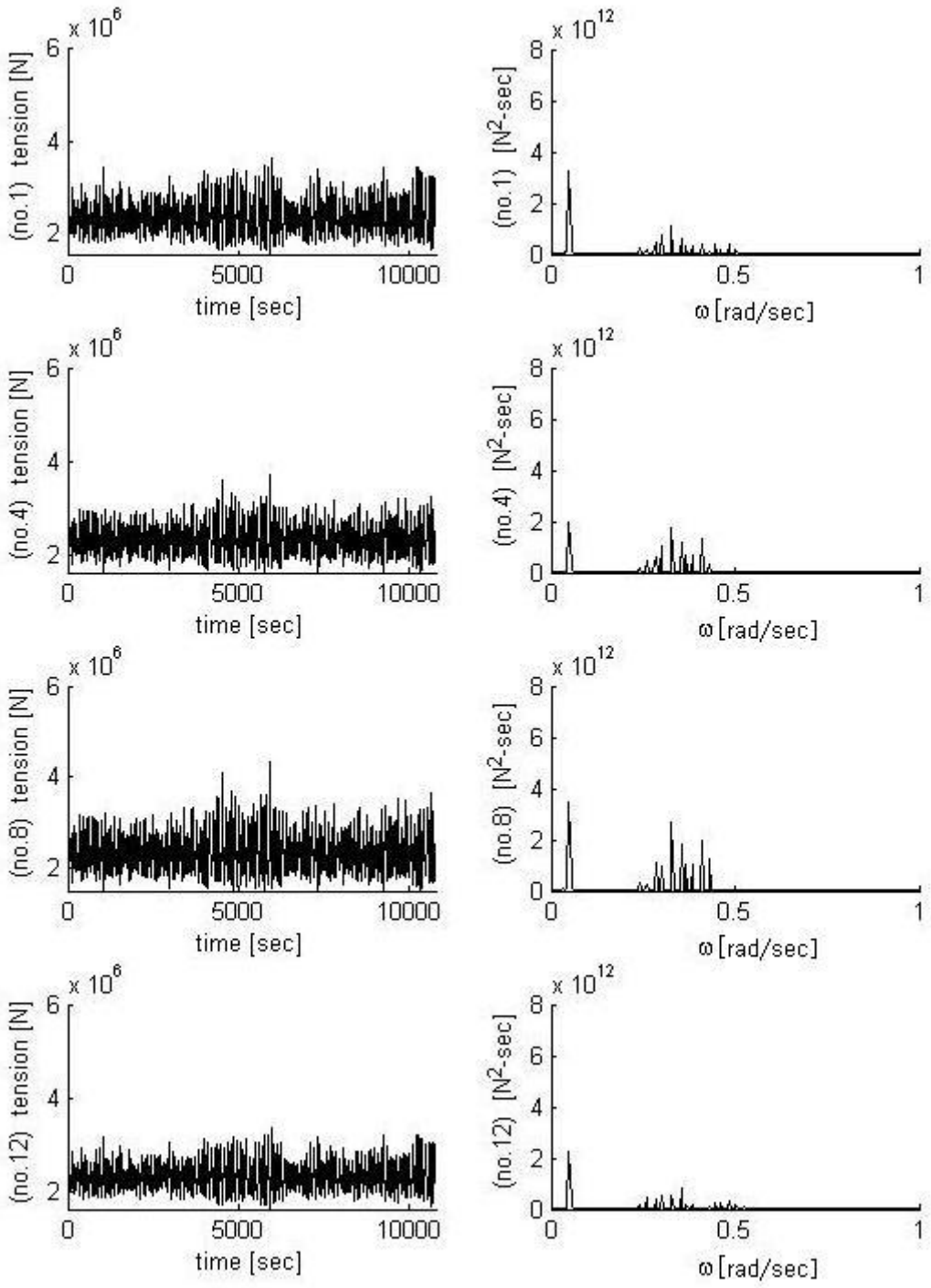

[Tension] [Spectrum]

Figure 4.25 Line tensions and spectra by fast time-domain analysis (β=180 degrees)

The line tensions and tension spectra of the four selected lines calculated by means of the time-domain motion simulations based on the retardation functions are shown in Figures 4.26 to 4.28 respectively for the wave heading angles of 150, 165 and 180 degrees, and are to be compared with those shown in Figures 4.23 to 4.25 obtained in the fast time-domain analysis. The differences in tensions for various wave directions are due to the differences in surge and sway motions mainly and may also be caused by heave, roll and pitch motions in head waves as shown in Tables 4.4 and 4.5. The low frequency tension spectral densities obtained in the time-domain motion analysis for the wave angles of 150 and 165 degrees are larger than those calculated by means of the fast time-domain method. This may be due to the difference in slow drift motions predicted by these two methods. However, the low frequency tension spectral density obtained by the time-domain technique in the case of head seas is similar to that by the fast time-domain method as the heave and pitch motions are dominant. There are still some discrepancies in tension spectral densities predicted by these two time-domain approaches in the frequency region of about 0.2~0.5 rad/sec. This indicates that the motions obtained in the present time-domain analysis are larger than those by the previous fast time-domain method for the specific mooring lines that are subject to the highest tensions.

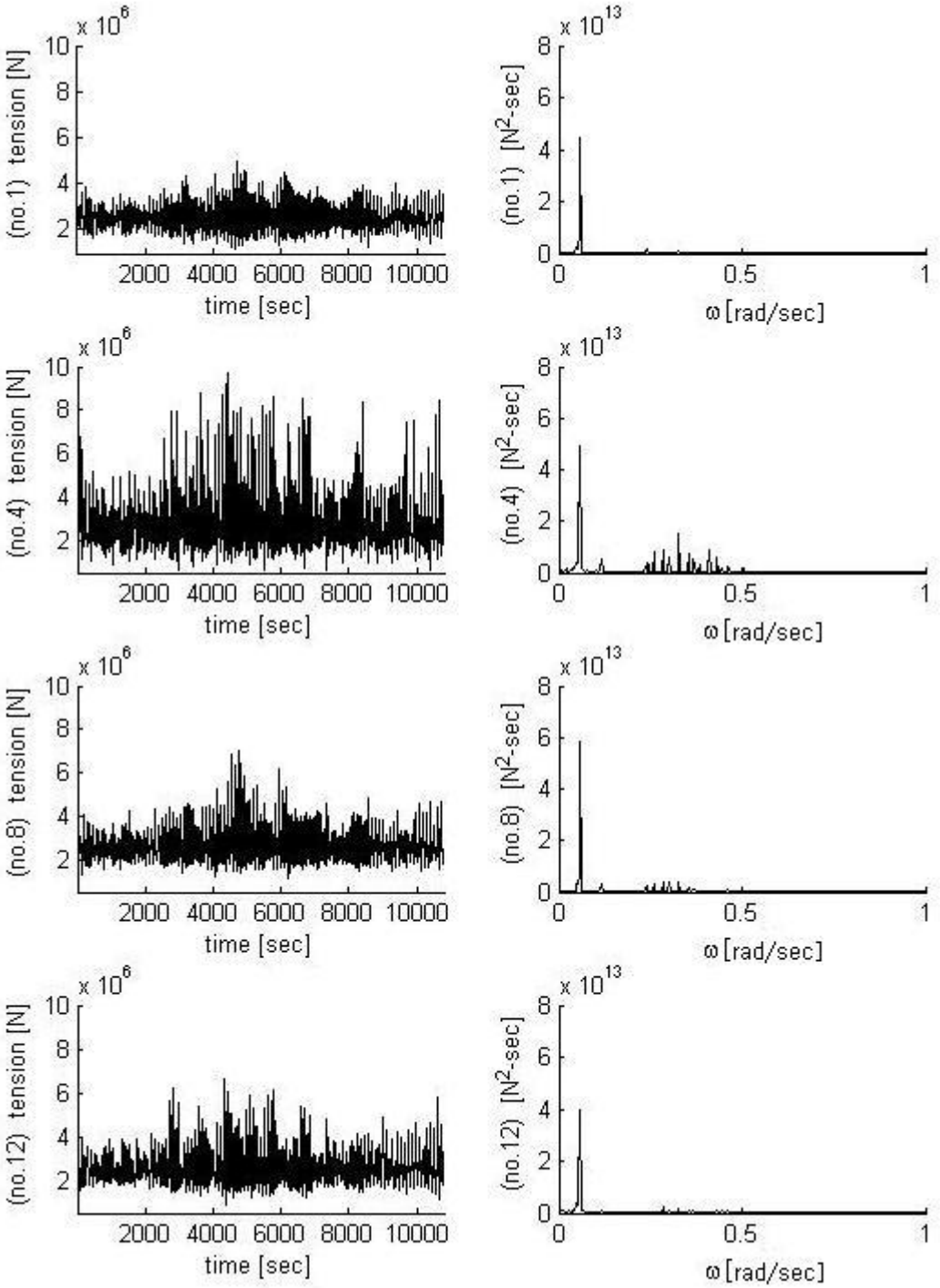

Figure 4.26 Line tensions and spectra by time-domain motion analysis (β=150 degrees)

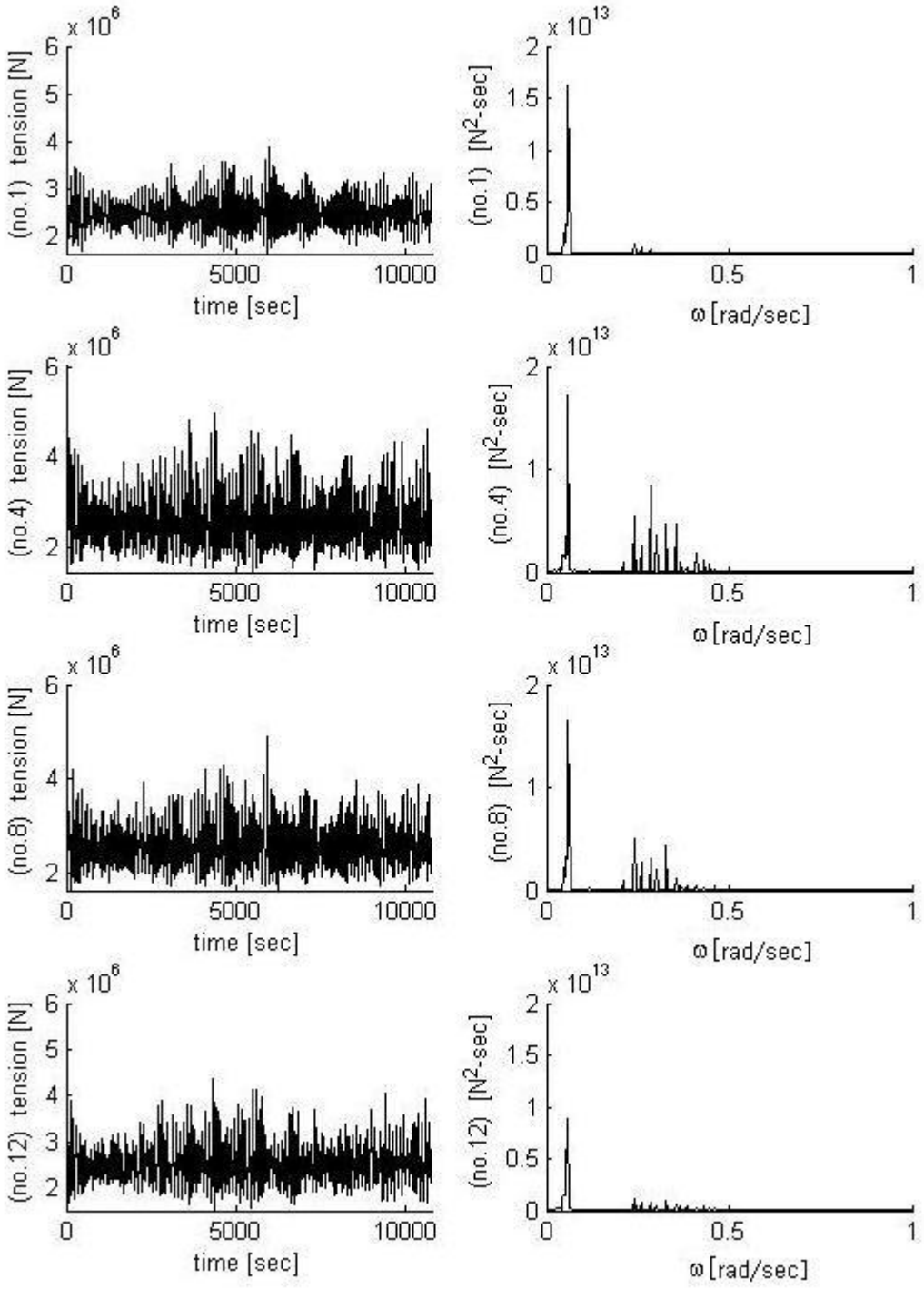

Figure 4.27 Line tensions and spectra by time-domain analysis (β=165 degrees)

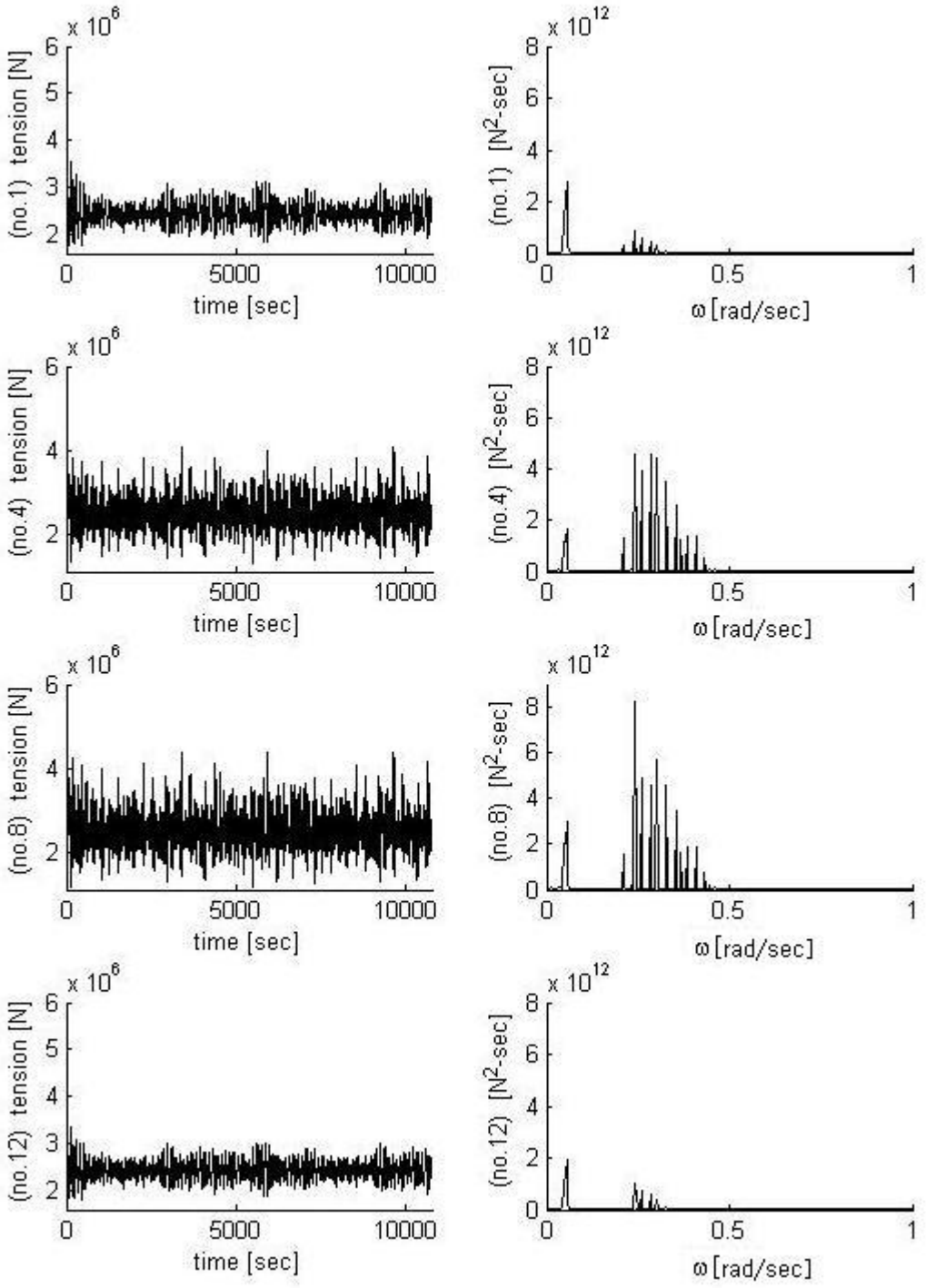

[Tension] [Spectrum]

Figure 4.28 Line tensions and spectra by time-domain analysis (β=180 degrees)

Table 4.6 compares the values of the mean, maximum, minimum and standard deviation of line tensions in four selected mooring lines calculated by means of the fast time-domain technique and the present time-domain motion simulation method. As predicted by the fast time-domain method, the maximum tensions in lines No.1 and No. 8 are larger than those in lines No.12 and No.4 respectively. Moreover, line No. 8 experiences the largest tension among the selected lines as it is in the direction of the incoming waves and has a more acute angle than other lines. Furthermore, line No. 12 encounters the least maximum tension as it is in the leeward side of the turret. These phenomena are not found in the results obtained in the present time-domain motion simulations for oblique waves. As predicted by the present time-domain technique, the maximum tensions in lines No. 4 and No. 12 in oblique seas of 150 and 165 degrees are greater than those in lines No.8 and No.1 respectively.

The minimum tensions in line No.1 and No. 8 of the present time-domain motion simulation method are larger than those of the fast time-domain technique. This result may be estimated by the large sway motions of the present time-domain motion simulation method however the mooring arrangement is influenced by the combination of the motions of the 6 degrees of freedom thus it may be difficult to regulate a reason. The standard deviation of line No. 4 has larger value in the present time-domain motion simulation method than the fast time-domain technique. This means that line No. 4 has larger scatter data for the present time-domain motion simulation method than the fast time-domain technique. The mean values are larger in the present time-domain motion simulation method than the fast time-domain technique for all line No. 1, No 4, No 8 and No 12 and all wave heading angle 150, 165 and 180 degrees. This means that the present time-domain motion simulation method is exaggerated for the mean values of the mooring line tensions than the fast time-domain technique. The present time-domain motion simulation method has the larger value of sway and yaw and this is directly liable to affect those mean values.

Table 4.6 Selected mooring line tensions by fast time-domain and time-domain quasi-static analyses

Unit [N]		Heading Angle 150°		Heading Angle 165°		Heading Angle 180°	
		Fast time domain	Time domain	Fast time domain	Time domain	Fast time domain	Time domain
LINE 1	MEAN	2,155,800	2,327,400	2,143,500	2,292,900	2,134,700	2,280,500
	MIN	1,162,000	1,166,900	1,310,500	1,448,400	1,346,700	1,598,500
	MAX	4,826,600	4,797,000	3,837,900	3,668,500	3,445,000	3,580,900
	STD	439,000	552,030	378,500	336,200	333,700	226,470
LINE 4	MEAN	2,150,300	2,555,700	2,123,400	2,367,000	2,120,500	2,300,200
	MIN	1,215,000	1,095,700	1,415,100	1,267,800	1,417,600	1,488,800
	MAX	4,406,600	9,237,800	3,293,500	4,772,400	3,501,400	3,578,200
	STD	424,600	996,930	305,100	512,840	288,700	292,420
LINE 8	MEAN	2,168,700	2,456,600	2,147,100	2,346,200	2,137,600	2,312,500
	MIN	1,017,600	1,355,700	1,141,100	1,422,200	1,305,400	1,381,200
	MAX	5,094,200	6,798,200	4,213,100	4,672,400	4,123,500	4,009,100
	STD	497,200	675,310	413,900	415,680	374,400	346,440
LINE 12	MEAN	2,145,800	2,413,000	2,126,300	2,317,700	2,123,100	2,277,200
	MIN	1,314,600	972,400	1,490,200	1,323,100	1,432,600	1,665,500
	MAX	3,672,800	6,580,600	3,201,200	4,171,500	3,162,500	3,374,800
	STD	379,500	779,030	289,800	417,420	276,300	199,190

4.7 Observation of Mooring Line Dynamics

The line tensions at the attachment points of the selected mooring lines discussed in the previous section were calculated by means of the quasi-static mooring analyses based on two different time domain approaches. This section presents the results of the line tensions at the attachment points of the four selected mooring lines by line dynamic analyses. Using the lumped mass method described in Chapter 2, the dynamic cable analyses were carried out based on the motions of the attachment points predicted in the present time-domain motion simulations. The large size of the FPSO against the water depth and the effect of the added mass effects of the mooring lines leaded to about 8 percent increase of the maximum tensions for the cable dynamics against the quasi-static cable analysis.

Figures 4.29 to 4.31 present the time series and corresponding spectra of line tensions in the four selected mooring lines with the effect of mooring line dynamics and are to be compared with those in Figures 4.26 to 4.28 without the line dynamic effect. The differences in the wave frequency components of line tensions with and without the line dynamic effect are observed in Figures 4.27 and 4.30 for the wave angle of 165 degrees.

Comparisons between the maximum tensions in the four selected lines obtained from the frequency-domain and two different time-domain quasi-static mooring analyses and the line dynamic analysis are shown in Table 4.7. The dynamic cable analysis predicts larger maximum tensions in line No. 4 for 150 degrees wave angle, in lines No. 4 and No. 8 for 165 and 180 degrees wave directions than the quasi-static cable analyses. Nevertheless, the maximum tensions in lines No.1 and 12 calculated by the lumped mass method are smaller than those by the quasi-static mooring analyses. This reveals that the line dynamics increases the tension in tautened line in the windward side of the turret but decreases the tension in slackened line in the leeward side, when the tensions in the four selected lines are compared with and without the effect of line dynamics. In other words the maximum line tension in tightened line with the inclusion of the cable dynamics is larger than that without the effect of line dynamics. In the present investigation, the effect of line dynamics on line tension leads to 8 percent increase in maximum line tension for the Schiehallion FPSO operating in the water depth of about 400 m and in the 100 year sea state of significant wave height 16 m and mean period 14.5 sec.

The frequency-domain and two different time-domain quasi-static mooring analyses give different results of line tensions in the wave direction of 150 degrees while they predict relatively similar results in head seas. The discrepancies for the case of oblique waves may be attributable

to the level of complexity in these analyses. The frequency-domain method is the most conservative since it estimates the largest maximum tensions among the quasi-static mooring analyses. This is not surprised because the maximum values of surge and sway excursions are used in the frequency-domain quasi-static mooring analysis. They do not take place concurrently in reality. As the sway motion vanishes in uni-directional head seas, the frequency-domain method predicts similar maximum tensions as the two different time-domain approaches. However, the maximum tensions in lines No. 8 and No. 12 obtained by the frequency-domain technique for 150 degrees wave angle are similar to those by the time-domain motion simulations based on the retardation functions. It is difficult to consider that the frequency-domain method is as good as the time-domain technique because they predict quite different maximum tensions in lines No. 1 and No.4.

Finally, the maximum tensions in the four selected lines calculated by means of the present time-domain motion simulations and the line dynamic analysis are in similar order since the motions of the attachment points in the dynamic analysis were based on those from the time-domain motion simulations. However, it is advised that a line dynamic analysis should be carried out as the line dynamics has significant effect on line tensions, in particular, for the mooring lines in the windward side of the turret.

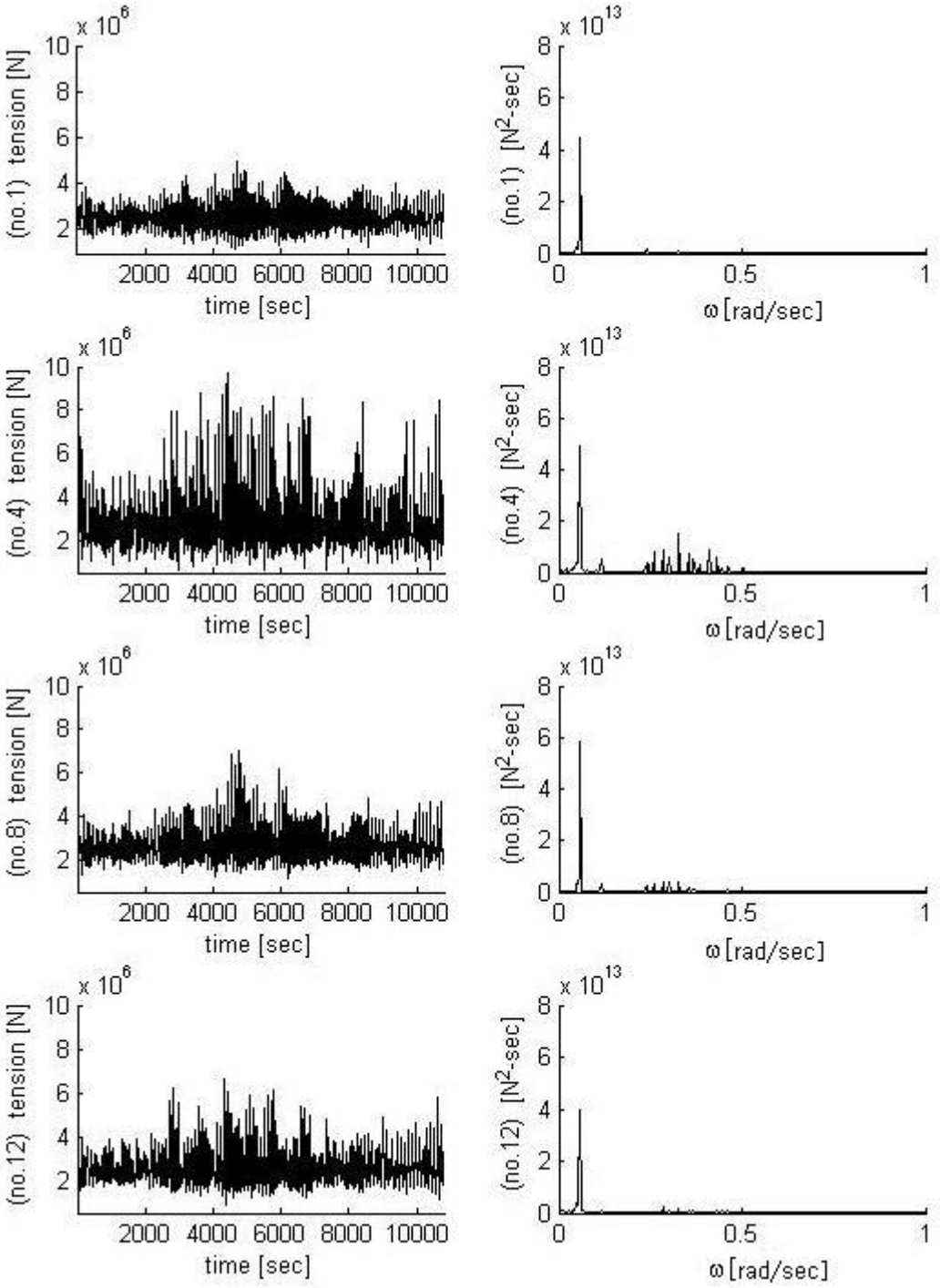

Figure 4.29 Line tensions and spectra by line dynamic analysis (β=150 degrees)

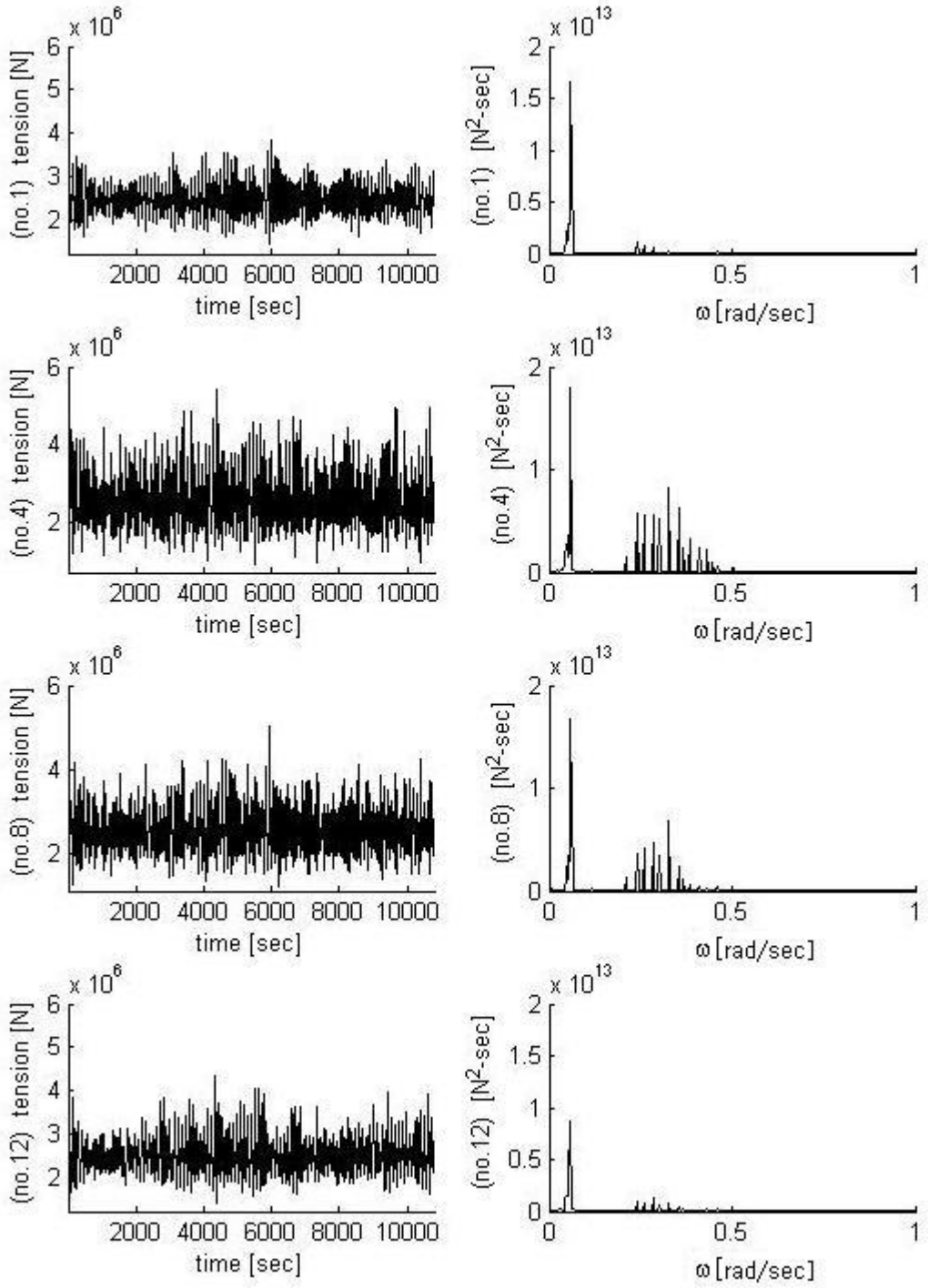

[Tension] [Spectrum]

Figure 4.30 Line tensions and spectra by line dynamic analysis (β=165 degrees)

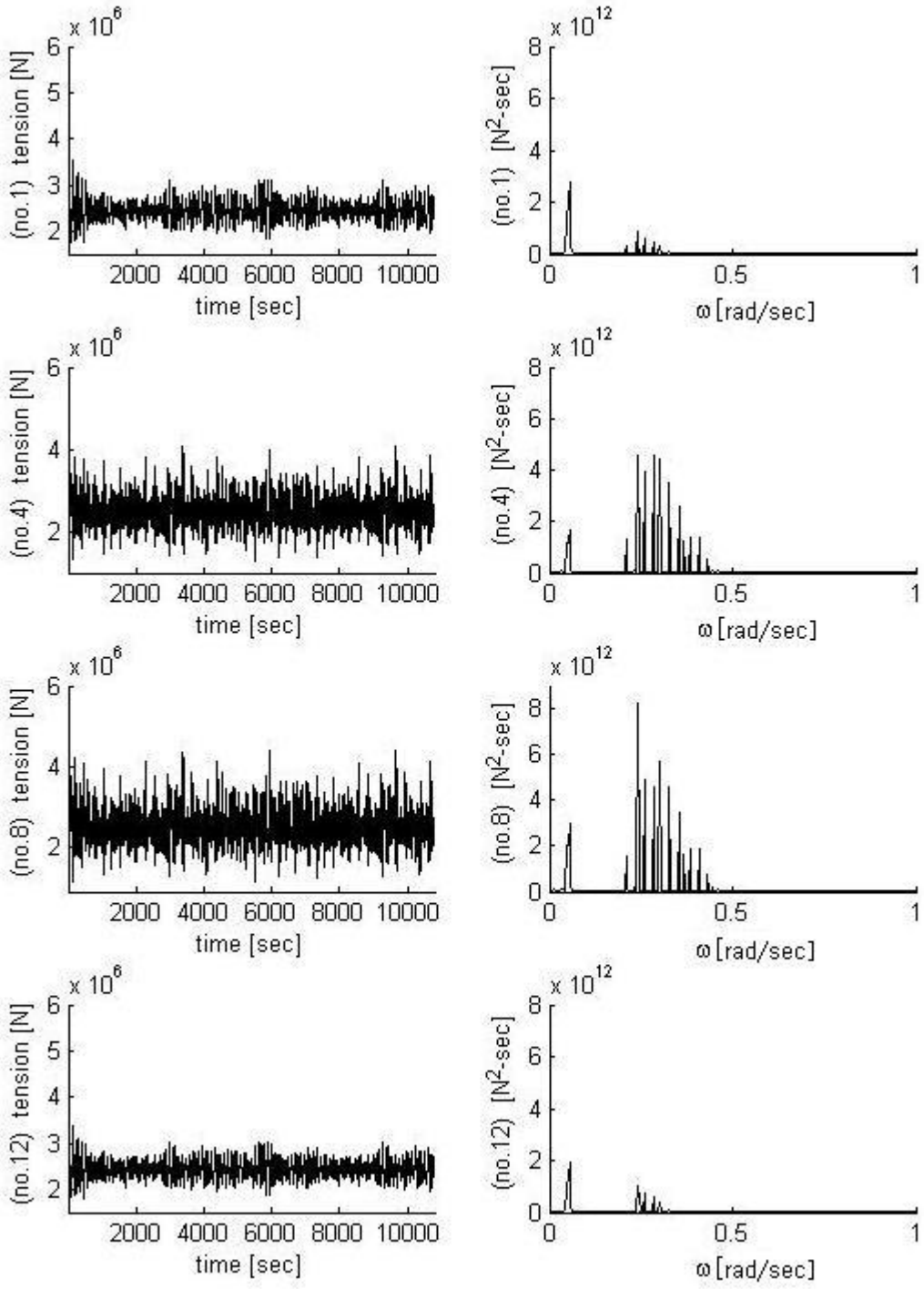

[Tension] [Spectrum]

Figure 4.31 Line tensions and spectra by line dynamic analysis (β=180 degrees)

Table 4.7 Maximum tensions in selected lines by different analyses

Unit [N]	LINE	FAST TIME DOMAIN	FREQUENCY	TIME DOMAIN	DYNAMIC ANALYSIS
150°	1	4,826,600	6,762,400	4,797,000	4,748,900
	4	4,406,600	6,697,900	9,237,800	9,464,000
	8	5,094,200	6,722,000	6,798,200	6,775,300
	12	3,672,800	6,746,200	6,580,600	6,449,000
165°	1	3,837,900	4,750,500	3,668,500	3,631,900
	4	3,293,500	4,408,300	4,772,400	5,205,300
	8	4,213,100	4,799,100	4,672,400	4,813,800
	12	3,201,200	4,487,000	4,171,500	4,132,000
180°	1	3,445,000	3,759,300	3,580,900	3,515,500
	4	3,501,400	3,345,500	3,578,200	3,869,900
	8	4,123,500	3,837,300	4,009,100	4,177,300
	12	3,162,500	3,429,000	3,374,800	3,321,200

4.8 Concluding Remarks

All of the behaviours of site-fixed floating structures, except for dynamically positioned vessels, depend on the mooring method, the environmental conditions such as wind, waves and currents, the properties of the mooring lines and the characteristics of the vessel's motions. The reliability of the mooring lines can be regulated by the correct decision of adequate proof and breaking loads to be obtained by carefully selecting the material, particularly its strength, weight, extensible ratio and durability. Nonetheless, the breaking strength of the mooring lines must be greater than the extreme line tensions anticipated in the life time of the structures.

In conclusion, FPSOs are installed at sea with an appropriate mooring arrangement considering wave heights, wave directions, water depth, etc. The mooring lines are also installed

according to their characteristics as unit weight of the line under water, material, shape, etc. The mooring lines should not be broken during the anticipated time span of operation at sea for the production of oil even in the harsh conditions from the range of sea-states during at least a 100 year return period, as recommended by Rules of Classification of Mobile Offshore Structure (DNV 1996). The tensions in mooring lines are mainly due to the excursions of the FPSO. Hence the body motion analysis is directly connected with the mooring line analysis as the resulting mooring line tensions are caused by the wave and wind induced motion responses of the FPSO.

A motion analysis may be performed either in the frequency domain or in the time domain. The frequency-domain motion and mooring analyses are linear while the time-domain motion and mooring analyses may be either linear or nonlinear depending on the treatment of hydrodynamic forces and restoring forces. In the present study, the linear frequency-domain motion analysis has been carried out. Furthermore, the quasi-static mooring analyses have also performed by means of the frequency-domain method and two different time-domain techniques. One is the fast time-domain technique presented in Chapter 3 and the other is the time-domain motion simulations based on the retardation functions. The first- and second-order motions can be separately calculated by the fast time-domain method but they are mixed in the present time-domain motion simulations. The first-order motion responses of the FPSO vessel in six degrees of freedom to irregular waves are coupled to each other through their phases with respect to each individual wave components but the second-order motions are uncoupled in the fast time-domain motion simulations. On the other hand, the motions of the FPSO vessel excited by both the first-order and second-order wave forces and moments are coupled to each other in the present time-domain motion simulations.

The results of surge and sway excursions predicted by the frequency-domain method and fast time-domain technique have been presented and discussed. It is found that the total surge motions obtained by these two methods are in good agreement for the wave directions of 150, 165 and 180 degrees while the total sway motions are much different in 150 degrees and this is mainly due to the maximum values of the sway motions being greater than the significant values used in the combination.

The time series of motion responses and the corresponding spectra at the attachments of points of the mooring lines and at the origin of the global coordinate system obtained by the present time-domain method have been presented and compared with those by the fast time-domain technique. The maximum values of surge and yaw motions obtained by these two

different time-domain methods are similar while the maximum values of sway, heave, roll and pitch motions show some discrepancies that the present time-domain method predicts larger values than the fast time-domain. The discrepancies may be due to larger differences in the first-order values than in the second-order values that can be observed in the motion spectra.

The mooring analyses carried out by the fast time-domain method and the time-domain technique are quasi-static and nonlinear since the nonlinear characteristics of line tension against excursion and the first- and second-order wave induced motions are considered. The time series of line tensions and the corresponding spectra for the four selected lines calculated by means of the two different time-domain approaches have been presented and discussed. The maximum line tensions estimated by the time-domain technique are larger than those by the fast time-domain method in wave directions of 150 and 165 degrees. These discrepancies are mainly due to the differences in the sway motions as the differences in the maximum tensions are significantly reduced in uni-directional head seas which have no effects of sway motion.

In this study, the mooring line dynamics was modelled by means of the lumped mass method described in Chapter 2 and the wave induced motions at the attachment points of the four selected lines were obtained from the present time-domain method and used in the line dynamic analysis. It is noted that the line dynamics in the present study did not have an effect on the FPSO motions as the lumped mass method was not coupled with the time domain motion simulations. However, the effects of line inertia, nonlinear drag damping and nonlinear line stiffness on line tensions were considered. It is evident that the effects of line dynamics on line tensions increase the maximum line tensions of tautened lines in the windward side of the turret but decrease those in slackened lines in the leeward side.

CHAPTER

5

Validation, Verification and Safety Factor of the Numerical Model

5.1 Introduction

This chapter plans to describe the validation of mooring system for FPSO at the Schiehallion oil field. The main criterion is based on the results from the fast time domain which is validated method to be considered in the comparison with other methods.

Four FPSO motion and mooring line tension analyses are studied with the frequency domain analysis, fast time domain analysis for quasi-static analysis, time domain analysis by 6-coupled motion equation for quasi-dynamic analysis and dynamic analysis for mooring dynamics of the mooring system. The provided mooring arrangement is composed of fourteen mooring lines and the pretensions are assumed at the equilibrium position and the maximum tensions are obtained at the fairlead which is the attachment point for each mooring line. Simulation was carried out for three heading angles (150, 165 and 180 degrees) to find out 6-DOF motions and mooring line tensions. For each wave heading angle, the most critical mooring line can be found in the selected mooring lines for the comparison.

The fast time domain analysis can be regarded as authenticated method because the database is obtained from 3-D panel method directly and applied in the calculation (Ch 3.4) without any disturbance. The numerical results were obtained in the intact condition. The applied mooring line arrangement and characteristics are allowable for the operation of Schiehallion FPSO with the compliance of safety factor by API and BV.

5.2 Reliable Hydrodynamic Analysis for Motion and Mooring System

The FPSO is almost a barge shaped vessel with no propulsion system with a turret mooring system connected by catenary mooring lines. The response amplitude operators (RAOs) of the FPSO in the form of the wave frequency motions and quadratic transfer functions (QTFs) with Newman's approximation method as the low frequency motions are obtained from the standard radiation/diffraction problem solution with the developed program (Chan 1992). The theory is 3D linear hydrodynamic method to determine RAOs in six degrees of freedom and QTFs in plane motion (surge, sway and yaw). This calculation requires the adequate element size and shape for the 3-D model to reach the reasonable solution. The hydrodynamic added mass and damping coefficients obtained from 3-D panel source distribution method can be applied to the analysis of the motion equation for the Schiehallion mooring system. 3-D panel method is also used to compute the first-order motions combined with the first-order exciting forces and also the second-order drift forces. RAOs and QTFs are main input database for the fast-time domain method.

The response motions of the FPSO obtained in the fast-time domain, frequency domain, time domain (6-DOF coupled motion equation) and mooring dynamic analyses are compared Furthermore mooring line tensions are also investigated from the static and dynamic analysis without any model experiment. Due to the absence of the experimental results of Schiehallion FPSO, damping coefficients were obtained from the retardation function (Ch 4.3) which transforms the frequency dependent term to the independent term for the solution of the 6-DOF coupled motion equation. Instead of the drift damping coefficients that can be calibrated from free-decay model tests for surge, sway and yaw for the second-order motions, the wave drift damping is found on the circular frequency value which is the same as the natural period of surge, sway and yaw in Table 2.2 to be used in the fast time domain method for the low frequency motions. Therefore, the linear low frequency damping coefficients are performed using the frequency dependent damping value from the radiation damping problem of the 3-D panel source method for the second order motions. This method is much reasonable than the other simplified method as the percentage of critical damping because the values are obtained by the direct calculation of the real hull form.

The viscous damping coefficient of a mooring line is obtained in the previous experiment (Nakajima et al 1982) for the mooring line dynamic calculation as shown in Eq. (2.40). The effect of mooring lines in the FPSO motions is regarded as restoring forces in the horizontal

direction and the stiffness coefficients of the mooring system for the direction of surge, sway and yaw can be obtained by the catenary mooring equation combined with mooring line tensions. The pretension of 2,297 kN is the initial static tension in each mooring line corresponding to the equilibrium position of the present mooring system because the stiffness of mooring line is determined at the equilibrium position except for environmental forces.

5.3 Authentic Design Application for Mooring System

The 3-D panel method was applied for the verified motion and mooring analysis. This method is based on the standard methodology to find out hydrodynamic coefficients and forces. Fast time domain method is a proven analysis accounting for the first-order exciting forces and response amplitude operators (RAOs) for the first-order motions and second-order forces for the low frequency motions.

Fourteen mooring lines are designed to maintain the Schiehallion FPSO on the operational area. The parametric data of the extreme condition recommended by DNV has been followed (Table D.1). This condition represents the extreme environmental condition for the 100 year return period at sea. Three different heading angles (150, 165 and 180 degrees) in the 100 year extreme condition are considered. The wave spectrum based on 100 year environmental condition to generate irregular waves can represent an extreme environmental sea state.

5.3.1 Methodology for Mooring System Calculation

The 6-motion coupled analysis for moored FPSO was also carried out by solving the time domain motion equations for the comparison with the fast-time domain analysis. This comparison is for the verification of the results in both motion responses including mooring line tensions as the fast time-domain method is a verified methodology.

The following analyses are used in the present research.

- Quasi-Static analysis of the fast time domain is considered with 1^{st} and 2^{nd} order motions in the random waves that are generated to be applied for the wave and low frequency exciting forces. Fast time domain methods can be a verified methodology to the resulting motions and tensions, however, frequency domain analysis is compared for the validation of the quasi-static analysis alternatively.

- The quasi-dynamic analysis takes into account the behaviours of the attachment point at fairleads depending on the first- and second-order forces that change according to the time histories. The fairlead motions depend on the vessel's resulting motions by 6-coupled motion equations.

- The dynamic analysis takes into account mooring line dynamics including the added-mass and drag coefficients of the mooring line by lumped mass method (Ch 2.5). The dynamic analysis also accounts for the dynamic behaviour of a mooring line determined by the motions at an attachment point.

- The safety factor is based on the American Petroleum Institute (API) for quasi-static and the Bureau Veritas (BV) for quasi-dynamic (dynamic) using the recommended tension safety factors.

5.3.2 Safety Factor for Mooring Design Criteria

The safety factor needs to be considered at an initial design stage of the mooring configuration. The attachment point of the mooring line should be checked for safety as fairlead is the position with the maximum tension in a catenary mooring line and the tension given at the fairlead should be limited by a safety factor.

The maximum excursion is the total combined wave and low frequency displacement. The maximum surge and sway motions are required to be within an allowable excursion in the provided working condition with safety factor to prevent a mooring line from breaking. The safety factor according to the classification rules is a criterion for the design of the mooring lines. This safety factor also allows for marine growth, abrasion and corrosion. The marine growth consideration is for the effect on the hull with a large added-mass and area. Abrasion is due to the contact on seabed with wear problem and corrosion is taken into account as chain can be weakened in its fatigue problem for a chain.

The safety factor is defined as follow:

$$Safety\ \ Factor = \frac{Minimum\,Breaking\ Load}{Applied\,Tension} \tag{5.1}$$

The applied tension is the maximum design tension in the mooring line and the minimum breaking load which depends on the material and size of the mooring is 19,652kN in the present mooring system.

API RP 2SK and BV (Bureau Veritas) are applied for the safety factor. API RP 2SK is based on the quasi-static analysis. In the quasi-static and quasi-dynamic analysis, the obtained mooring line tensions are calculated as static line responses to the vessel's behaviours and static loads are considered by the external forces. The reference load for the evaluation of safety factor is the minimum breaking strength (MBS) of the mooring line component (NI 493 DTM R00 E). The safety factor is defined as the ratio between the catalogue breaking load of the mooring line component and the maximum tension occurring over its length when the design tension is applied to the fairlead. At any point of the line, the safety factor should be greater than or equal to those specified in the Classification of BV (NI 461 DTO R00 E). The required minimum safety factor for mooring line components are specified in Table 5.1.

Table 5.1 Minimum safety factors for mooring line

Minimum safety factors	Quasi-static (API)	Quasi-dynamic (BV)	Dynamic (BV)
Intact condition of system	2.00	1.75	1.67
Allowable maximum tension	9,826 kN	11,230 kN	11,768 kN

The 100 year return period condition was considered for the calculation of safety factor. The applied maximum line tensions presented in Table 4.7 are used with the minimum breaking load of the mooring line for the safety factors. The safety factors in different mooring lines at three different heading angles (150, 165 and 180 degrees) are shown Table 5.2.

Table 5.2 Safety factor in selected mooring lines

Unit [N]	LINE	FAST TIME DOMAIN	FREQUENCY	TIME DOMAIN	DYNAMIC ANALYSIS
150°	1	4.07	2.91	4.10	4.14
	4	4.46	2.93	2.13	2.08
	8	3.86	2.92	2.89	2.90
	12	5.35	2.91	2.99	3.05
165°	1	5.12	4.14	5.36	5.41
	4	5.97	4.46	4.12	3.78
	8	4.66	4.09	4.21	4.08
	12	6.14	4.38	4.71	4.76
180°	1	5.70	5.23	5.49	5.59
	4	5.61	5.87	5.49	5.08
	8	4.77	5.12	4.90	4.70
	12	6.21	5.73	5.82	5.92

The quasi-static analysis can be performed by means of the frequency and fast time domain methods. The value of safety factor 2.0 which is the minimum safety factor for the quasi-static analysis by API is met for the operation of Schiehallion FPSO as the minimum safety factor is 2.91 in both frequency and fast time domain analyses. The quasi-dynamic analysis can be carried out by means of the time domain method by solving the 6-coupled motion equations. The minimum applied safety factor 2.13 obtained in the time domain analysis is satisfactory as the value of the safety factor for the quasi-dynamic analysis is 1.75 recommended by BV. The safety factor for dynamic analysis recommended by BV is 1.67, which is also satisfied since the results of dynamic analysis give the minimum safety factor of 2.08.

5.3.3 Maximum displacement for surge and sway

The displacement to water depth ratio is considered as the displacement of the maximum surge and sway affects the mooring line tensions. The extreme environmental condition for the 100 year return period has been used to calculate the maximum surge and sway of FPSO with the maximum tension of mooring lines. The frequency domain method is based on the POSITION MOORING by DNV (Appendix G.4). The fast time domain results can be estimated by two different approaches. One follows the DNV Rule as estimated in the frequency domain analysis, and the other is obtained from the time series directly. It is shown that the excursion obtained

from the DNV Rule approach is likely to be larger than that from the time series data in this comparison. The excursions calculated by 6-coupled time domain motion equations and in the dynamic analysis are the same because there is no coupling between FPSO and the mooring lines. However, the line dynamic analysis considers the dynamic effects of inertia and damping in the mooring line.

The excursion ratio is defined as follow:

$$Displacement\ \ Ratio = \frac{Displacement}{Water\ Depth} \times 100 \qquad \textbf{(5.2)}$$

The water depth is about 400m at the Schiehallion oil field.

The results of the displacement ratios for surge and sway are shown in Table 5.3.

Table 5.3 Displacement ratio for surge and sway

Unit [m]		MAXIMUM SURGE AND SWAY [m]			DISPLACEMENT RATIO [%]		
		150°	165°	180°	150°	165°	180°
FAST TIME (DNV)	Surge	17.420	16.166	16.749	4.36	4.04	4.19
	Sway	12.402	6.564	0.000	3.10	1.64	0.00
FREQUENCY (DNV)	Surge	17.222	16.814	16.819	4.31	4.20	4.20
	Sway	16.883	7.556	0.000	4.22	1.89	0.00
FAST TIME (Time Series)	Surge	16.880	15.204	14.669	4.22	3.80	3.67
	Sway	11.045	5.642	0.000	2.76	1.41	0.00
TIME DOMAIN & DYNAMIC (Time Series)	Surge	15.618	15.828	15.972	3.90	3.96	3.99
	Sway	15.465	9.266	0.000	3.87	2.32	0.00

The maximum excursions are estimated in the case of the extreme environmental condition in order to determine the displacement ratio. The maximum surge under 100 year exposure conditions with intact mooring lines is 17.42m (4.36% water depth) in Table 4.5 in the case of fast time domain method. For frequency domain method, the maximum surge was 17.22m (4.31% water depth) that is smaller than the fast time domain method. All the other values are also smaller than 20.0m (5% water depth) for the time domain and dynamic analysis.

The compared values given in Table 5.3 are the most critical case among the mooring lines. The mooring system of Schiehallion FPSO is concluded to be safe to maintain 5% coverage of water depth for surge and sway at the operational site in a 100 year return period wave condition.

5.4 Concluding Remarks

Four numerical analyses have been carried out for the motion responses of Schiehallion FPSO and tensions in the mooring lines. Frequency (quasi-static), time domain (quasi-dynamic) and dynamic analysis have been performed for intact condition. The fast time domain analysis is selected to verify the mooring system solution as the wave frequency motions are obtained from RAOs that is found from 3-D panel source method directly and the low frequency motions are calculated by second order forces by using Newman's approximation method. The wave frequency motions are mainly calculated from the first-order motion RAOs linearly from the wave frequency area. The low frequency motions are caused by non-linear interaction between vessel's motions and irregular waves. The reason why the fast time domain analysis stands for the validation is that no disturbance is applied to obtain the resulting motions of FPSO obtained from the 3D panel source method (Ch 3.4). As the fast time domain analysis appears to be calculated quickly and is the quasi-static analysis for the mooring system, corresponding quasi-dynamic and dynamic analyses are compared for the further research and the frequency domain analysis is also compared for the verification of the fast time domain method. Consequently, four (4) mooring analyses are checked for the maximum displacement and tensions.

The quasi-static analysis estimates the line tensions as static line responses against external forces and vessel's behaviour because static loads are taken into account for the application. The quasi-dynamic analysis considers the dynamic vessel's responses and the line tensions are calculated from the fairlead motions. The quasi-dynamic analysis contains the dynamic effects like added-mass, damping and second order forces on FPSO but the dynamic effects of the mooring line are excluded in the process. However, the dynamic analysis of mooring lines takes into account the inertia and drag damping forces of the mooring line components affecting acceleration and velocity of the behaviour of mooring lines. The coupling effects between FPSO and mooring lines are not considered in the dynamic analysis as all the motions of the attachment point are determined by the 6-coupled motion equations apart from the behaviour of the mooring lines in the time process for the simulation. However, the dynamic analysis is carried out to verify the maximum tensions in the mooring lines from the resulting motions of the quasi-

dynamic analysis. The axial elasticity of the mooring line is also included in the dynamic analysis while quasi-static and quasi-dynamic analysis are not, however, the effect of the axial elasticity is insignificant in the case of chain that is used for the mooring lines (Ch 2.5).

The safety factor of the mooring system is examined by means of API guidelines (Quasi-Static) and BV rules (Quasi-Dynamic and Dynamic) in the case of the intact condition. The mooring system is to keep the position within an allowable limit for the surge and sway motions of the FPSO in an extreme condition at sea. The maximum surge and sway are calculated as the sum of mean offset, wave and low frequency excursions of the FPSO. The maximum horizontal excursions of surge and sway were estimated within 20.0m (5.0 % of water depth) in condition that the average water depth is about 400m for the Schiehallion oil field.

It is concluded that the 14 mooring lines of Schiehallion FPSO are able to sustain the extreme environmental condition in the designed mooring arrangement at site.

CHAPTER

6

Conclusions and Recommendations for Further Study

6.1 Introduction

This chapter draws the conclusions that have been reached from the various analyses undertaken in the present study. This research was to investigate and compare the motion responses of the turret moored FPSO to irregular waves of 100 year return period and the resulting line tensions predicted by means of the frequency-domain method, the fast time-domain technique and the time-domain motion simulations based on the retardation functions with and without the effects of line dynamics.. Based upon the knowledge obtained during the overall programme of research, recommendations for further study are made.

6.2 Conclusions

The aim of this study was to make a floating production storage and off loading (FPSO) vessel possible to maintain her position by a mooring system at the oil field in extreme weather conditions during her life time. In order to achieve the aim and objectives of the present research, computer programs using MATLAB have been developed to perform respectively the frequency-domain, fast time-domain, retardation function based time-domain motion and quasi-static mooring analyses, and the line dynamic analysis.

Schiehallion FPSO which was selected for this research operates in the north east Atlantic ocean approximately 140km NNE of Cape Wrath to the west of the Orkney Islands. The huge vessel, Schiehallion FPSO, is anticipated to experience a 100 year sea state with a significant wave height of 16m and mean time period of 14.5sec, which occurs in the nearby Brent field and is recommended by the DNV Rules as shown in Appendix D. For such harsh sea condition, the

mooring lines attached from the sea bottom to the turret of the FPSO must be designed to withstand the wave induced motions of the FPSO and the resulting line tensions.

The role of the mooring system is to keep and control the excursions of the FPSO vessel within the allowable operational envelop of risers. The estimation of the possible range of vessel excursions and associated mooring line tensions is essential at the initial design stage. The characteristics of line tension against excursion can be formulated based on the catenary equations as a mooring line is made up of chain or cable where bending stiffness is negligible. There are different equations used for a slack single component mooring line and multi-component mooring line with various configurations. These different catenary equations can be applied for a static mooring analysis or a quasi-static analysis. Since the Schiehallion FPSO operates in the deep water of about 400 m, the effects of line dynamics on line tension will be significant and need to be considered in the mooring design and analysis. In the present study, the lumped mass method has been present and implemented for a line dynamic analysis.

Although a frequency-domain motion analysis provides practical results, it is linear and cannot capture nonlinear behaviour of line tension against excursion. Therefore, a time-domain motion and mooring analysis is needed in order to capture this behaviour. A time-domain motion simulation is quite time consuming especially for irregular wave condition because six coupled motion equations are integrated for a storm duration of at least three hours. Instead of solving the coupled first-order motion equations in the time domain, a fast time-domain technique based on the principle of superposition has been presented and developed. Since irregular waves can be simulated by summing the various amplitudes of wave components at different frequencies, the first-order motion responses of the FPSO to random waves can also be computed by summing the first-order motion response amplitude multiplied with the corresponding wave amplitude at different frequencies. On the other hand, the second-order motions of the FPSO can easily be calculated by solving uncoupled second-order motion equations based on Newman's approximation to the second-order wave excitations. Then the first- and second-order motions can be combined at each time step and used for a quasi-static or dynamic time-domain mooring analysis. In the present study the first-order motion response amplitudes and their phases, the first-order wave exciting forces and moments and their phases, and the mean second-order forces and moments on the FPSO vessel were calculated based on the source distribution method. The advantages of the fast time-domain technique are not only that the first- and second-order motions are calculated separately in an efficient manner but also that the time series of the combined motions can be used in a quasi-static or dynamic mooring analysis. The motion spectra

of the combined motions in surge, sway and yaw modes reveal that the first-order motions of the FPSO vessel are significant at wave frequency above 0.2 rad/sec but the second-order motions are dominant in long waves. Nevertheless, the motion spectra of the combined motions in heave, roll and pitch modes are contributed from the first-order motion components. As the first- and second-order motions calculated by the fast time-domain technique are separate, their significant and most probable extreme values can be calculated and compared with those by the frequency-domain analysis. It is found that the values of the significant and most probable first-order and second-order sway motions of the FPSO are smaller than those for the first-order and second-order surge motions as predicted by both the frequency- and the fast time-domain methods. The first-order motions and mean offsets predicted by the fast time-domain method are smaller than those obtained in the frequency-domain analysis. The values of total surge motions predicted by both methods are similar order while the total sway motions estimated by the frequency-domain method are larger than those by the fast time-domain technique.

Despite the advantages of the fast time-domain technique this method is lack of memory effect due to wave damping on ship motions. In order to consider this effect the retardation function based time-domain motion equations are needed. The retardation function is a memory function of time obtained by the cosine transform of frequency dependent wave damping. It is evident that the retardation functions are reduced rapidly and the memory effects affect very near past of the response motions of the FPSO vessel. The coupled motions of the FPSO vessel induced by the first- and second-order wave excitations are integrated in time with the memory effect and nonlinear effects of the mooring lines. The six coupled differential equations of motion are solved by means of the Runge-Kutta method. The time series of motion responses and the corresponding spectra at the attachments of points of the mooring lines and at the origin of the global coordinate system obtained by the present time-domain method have been presented and compared with those by the fast time-domain technique. The sway, heave, roll and pitch motions predicted by the time-domain method are larger than those by the fast time-domain motion simulations with the first-order wave frequency motions being dominant in the spectra.

The quasi-static mooring analyses performed by the frequency-domain method and two different time-domain approaches reveal that the frequency-domain method is the most conservative since the maximum values of surge and sway excursions are employed concurrently. Both the first- and the second-order motions have significant effects on line tensions as shown in the time series of line tensions and their corresponding spectra for the four selected mooring lines. Furthermore, the line tensions in the windward lines are larger than those in the leeward

lines as predicted by the quasi-static time-domain analyses. This phenomenon is more significant in the line dynamic analysis based on the lumped mass method. The effects of line dynamics on line tensions lead to increases in line tensions for the tautened lines in the windward side of the turret but to decreases in line tensions for the loosened lines in the leeward side. It is concluded that a line dynamic analysis is necessary for a moored vessel in deep water.

This research aims to validate the mooring system of the Schiehallion FPSO provided in the four mooring analyses that are the fast time domain, frequency, quasi-dynamic and dynamic methods. The main results are presented in Table 4.7 for maximum tensions and Table 5.2 for safety factors. Results obtained in the designed mooring system are based on the maximum excursions presented in Table 4.4 for the quasi-static and quasi-dynamic analyses and Table 4.5 for the frequency domain analysis. The safety factors for the selected mooring lines at three different heading angles have been calculated for different mooring analyses.

The effect of different mooring line modelling methods on the required safety factor from API and BV is presented and the minimum safety factor is shown in line No.1 for quasi-static analysis while it is in line No.4 for quasi-dynamic analysis. It is noted that the non-linear coupling effects more affect the sway for the 6 DOF coupled time domain analysis and all the minimum safe factors occur when the heading angle is 150 degrees rather than 165 and 180 degrees because the coupling effects are dominant when the wave heading angle is close to the bow sea condition than head sea condition.

The minimum value of safety factor calculated in the frequency domain analysis is 2.91 in the heading angle 150 degrees and meets the required minimum safety factor 2.0 by API while the minimum safety factor obtained in the fast time domain analysis for the same mooring line 1 in 150 degrees is 4.07 that is closer to the quasi-dynamic analysis than the frequency domain method. The time domain analysis gives the minimum safety factor of 2.13 in the case of the heading angle 150 degrees and this value also satisfies the required safety factor 1.75 by BV. The minimum safety factor from the dynamic analysis is 2.08 which is acceptable for the required safety factor 1.67 in Table 5.1.

It is noted that all the minimum safety factors are found in condition that the wave heading angle is 150 degrees caused by the combination of surge and sway, and the safety factor becomes higher when the heading angle is changing to the 180 degrees. This result represents the characteristics of the turret mooring system for the FPSO that the heading angle 180 degrees is safer than the heading angle 165 and 150 degrees.

The safety factor obtained in the mooring dynamic analysis shows smaller values than that in the quasi-static analysis. However there are not so much differences against the quasi-dynamic analysis. This is the reason why the mooring dynamic analysis can be carried out separately without the interaction of the vessel's motions. This result has been found because the mooring line is made of chain which has no much difference for the elastic effect.

In addition to the safety factor, the displacement ratios for surge and sway have been estimated for different numerical models. The allowable excursion is estimated as 5% of water depth for surge and sway. The way to find the surge and sway directly influences the mooring line tensions as the maximum offset is composed of the sum of the surge and sway in the plane area. The maximum surge and sway are found in 150 degrees heading angle rather than 165 and 180 degrees for the quasi-static and quasi-dynamic analyses as shown in Table 5.3. However, the dynamic analysis and quasi-dynamic analysis give similar results.

About three hours of the time series of motion responses and the resulting tensions are investigated for 100 year extreme conditions on the mooring system of the Schiehallion FPSO numerically. The maximum displacements and tensions obtained at three different wave heading angles are compared among the four different methodologies. The frequency and fast time domain analyses show a clear difference relatively than the quasi-dynamic analysis that can be disturbed in the process of second order forces for the slowly varying low frequency motions by the Newman's approximation method. The mooring dynamic analysis also gives different results in the safety factors since the dynamic behaviours of the mooring lines are affected by the acceleration and velocity of the lines while the static analysis of the mooring lines is not. However, the effect of the axial elasticity is not noticeable in the dynamic analysis and this can be presumed from the fact that the chain material has not so much influence on the axial elasticity for the catenary mooring lines in case that the water depth is not very deep as applied in this study about 400m.

The application of random phasing in FFT analysis was to generate the irregular waves for 3 hours representing 100 year return period of an extreme environmental conditions and transform the time series to the frequency domain with wave, motion and tension spectrum. The effective way to arrange the irregular frequencies is to set up the values in the limited values that are calculated down to three decimal places in this research. By this way, the statistic approach in calculating the FPSO's motions and mooring line tensions can be processed for the transformation of the data from the time series data to the frequency dependent data. Therefore,

the spectrum could be calculated correctly without any errors while handling the data in the calculation. This is important because if we do not know about the places of decimals for the frequency data, the exact numerals have to be assumed to be rounded off the data below the decimal point and this way could lead to an accumulated error in the analytical process. All this knowhow can be used for any time series data as motions and tension in time domain.

The surge motions calculated by the fast time domain method are well agreed with the frequency domain analysis while the sway motions are not. However, the time domain analysis shows relatively good correlation in both surge and sway motions. This is deduced from the fact that the sway motions are much more affected by the coupling effects with non-linear effects when the heading angles are 150 and 165 degrees rather than 180 degrees.

The maximum tensions depend on the FPSO's motions induced by the external environmental forces that are the first- and second-order wave forces. The tensions are mainly controlled by the position of the attachment point connected to the fairleads, and this means that the tensions largely depend on the surge and sway in the catenary mooring system. This is the reason why we need to investigate the quasi-dynamic analysis rather than the quasi-static analysis as coupled dynamic effects can be important for the exact 3-D motion analysis. In this respect, it is noted that the quasi-dynamic analysis is more realistic than the quasi-static analysis especially when the floating vessel faces bow sea conditions such as 165 or 150 degrees rather than the head sea condition as 180 degrees because the non-linear coupled dynamic effects are liable to affect the ship-shaped floating structures.

The dynamic effect of the mooring lines which is considered by the mooring dynamic analysis are also affecting the axial tensions in the mooring line by inertia and drag forces as the mooring lines contain the added mass and damping effects. However, these effects are not significant in the case that the mooring line is made of chain in the shallow water relatively against deep and ultra-deep water in this study. The water depth and the material are important for the elastic effect on the mooring line as the elongation is used to make an extension by that reason. The axial elasticity of mooring line in the quasi-static approach was not considered. Nevertheless, its effects may not be obvious as the chain used for the mooring lines has not so much effects on the elongation. The maximum tensions predicted by the dynamic analysis are somewhat different but not remarkable compared with the quasi-dynamic analysis in this study despite the elastic effects are included in the mooring dynamics in fact that the chain material of the mooring line had not much effect on the mooring lines.

The original contribution of this research is the studied four approaches in different heading angles (150, 165 and 180 degrees) within 100 year extreme environmental condition. All the approaches are compared for the practical application of the FPSO mooring system analysis. The fast-time domain analysis stands for the quasi-static analysis which is proven method to expect the resulting motions and tensions of the mooring system by using the data from RAOs for the first-order motions, the hydrodynamic coefficients from the radiation problem and the first- and second-order forces from the diffraction problem in the 3-D panel source method. Alternatively, the frequency domain method can be used to verify the fast-time domain analysis as the static analysis. The quasi-dynamic analysis was performed with the 6-DOF coupled effects for the added-mass, damping and stiffness coefficients. The developed methodology was accomplished to validate the fast time domain analysis in the same environmental condition. The further dynamic analysis was to verify the difference between non-dynamic and dynamic mooring line analysis. The resulting motion and tension data, also produced spectrum for each case, could contribute to the offshore industry in the practical application for the purpose of the safe operation correlated with the estimated safety factors.

In this research, the four procedures for the mooring systems have been examined with three heading angles (150, 165 and 180 degrees) with required safety factors. It is author's belief that the examinations of these four methodologies could contribute to the development of the offshore industry from the present research.

6.3 Recommendations for Further Study

The frequency-domain method, fast time-domain technique and retardation function based time-domain motion simulation method are shown to be powerful and practical tools for motion and mooring analyses with and without the effects of line dynamics. Continue efforts and developments on this line of research are very worthwhile.

6.3.1 Further Improvement of Weathervane Manner in Response

If the winds and waves are changing in directions, then the turret-moored FPSO vessel will rotate about the turret by an amount depending on the strength of the winds and waves. Normally waves and winds tend to have similar directions, but this will change with time as the seas persist after the wind changes direction. On the other hand, currents and tide will not be related to wave

directions. Therefore, the vessel will swing about the fixed turret in a weathervane manner in response to the system of environmental loads. Although head waves are an ideal condition, there are two aspects to consider:

- The confused seas will not be approaching the FPSO at a fixed heading angle, and there will be a spread of wave energy around the principal heading angle even after the FPSO has weathervaned.
- The FPSO has inertia and it will respond slowly to forces that try to rotate it about the turret.

6.3.2 Failure Conditions

It is necessary to prevent moorings from several possible failure modes, such as line failure, and the dragging or uplift of an anchor. A failure of the mooring system may put the FPSO in danger when, for example, one anchor looses holding strength as the behaviour will be much different in comparison with the intact condition. An advanced program could also be developed for the coupled analysis of FPSO, mooring and riser system. The stresses in the risers would be analysed on each time step and the potential fatigue failure of the mooring lines could be an extended subject. That will result in a total comprehensive analysis of the mooring system for a realistic situation. A background of models and methodology would then be available for reliability and risk assessment studies. There are numerous variations of these failure conditions as if the number of the disconnected mooring lines will be dissimilar from each other. There are several failure case studies that could be undertaken to determine an optimum mooring system.

6.3.3 Draught Changes

Although the changes in vessel draught will have little still water effect on the forces in the mooring lines, draught changes will affect vessel motions in waves. For example, draught changes will be negligible compared with water depth while the motion responses will be much different when the vessel's draught changes due to changes in amount of crude oil on-board and any ballasting, etc. It may be the worst condition that when all of the cargo tanks are full or when the vessel is in a lightship condition. The FPSO operator may also have a ballasting plan that is used when heavy seas are anticipated.

6.3.4 Effects of Damping Devices on Mooring Lines

A method should be developed to examine the effects of damping devices attached to lines that will lead to the considerable different motion responses and also the mooring line tensions according to the passage of time, in particular, for a line dynamic analysis.

6.3.5 Coupled Dynamic Analysis in Multi-Component Mooring Lines

As computing power is increasing year by year, the line dynamic analysis of mooring lines can be coupled to the motion analysis of a turret-moored FPSO subject to current, wind, and waves in the time domain to investigate whether this coupled effect is significant or not.

6.3.6 Safety Factor in damage condition

Although this research carried out different motion and mooring analyses in intact conditions, the tensions are much different in damage conditions that have different safety factors in the same environmental conditions. In damage condition, the safe factor is smaller than intact condition when one or two mooring lines are broken in the operational period. The FPSO's motions and the mooring line tensions can be newly verified and compared in intact and damage conditions. The permanent or transient failure condition can be applied in the same process of the intact condition in case that one or two line failure happens for the broken mooring line conditions. The lower safety factor will be applied for these worst environmental conditions followed by maximum displacement of FPSO and maximum tension of mooring line.

6.3.7 Safety Factor in the Updated Modeling

The FPSOs are to produce oil and gas by risers that affect the equilibrium position of FPSO and the mooring line tensions. The safety factors can also be calculated with the consideration of the effect of risers. The equilibrium position can be estimated with risers in the concept that the loads affect to the floating vessel horizontally by a riser for the plane motion (surge, sway and yaw). The tensions of the mooring lines can also be calculated with the initial riser arrangement. The analysis of an updated model which includes a new mooring line components and risers can be valuable for further research. A mooring analysis may be performed by means of the present methodology. However, it can appear to require different safety factors in condition that all the provided environmental data and mooring characteristics are newly calculated to the updated

mooring system. The safety factors may not be good enough to be applied in some mooring arrangement and then the parametric alternations will be necessary for the optimization of the mooring system to meet the required safety factor.

6.3.8 Ultra Deep Water Analysis for the Elastic Effects on Mooring Lines

The FPSOs can operate in deep and ultra deep water with a catenary mooring system. The elastic effects are much more important in the case of a deeper water depth condition than relatively a shallow water condition. The oil and gas development is likely to move to the ultra deep water in accordance with the exhaustion of oil and the advanced technology of the offshore industry. The mooring line components of the ultra deep water development are multiple to lessen the weight of the mooring lines and the other materials (elastic fiber or polyester) can be considered for the components. Thus, the effects of the axial elasticity will be much more important in this configuration.

6.3.9 Comparison with Commercial Software and Experimental Data

A comparison with simulation results (or experimental measurement) by commercial software will be valuable for a further study. The condition is to be within the same modelling in the exact scale among the numerical models (or reduced scale for an experimental model). The scaled model by Froude number may be good enough to verify the estimated motion responses and mooring line tensions in the allowable error range. This further study is recommended for the fully coupled analysis that could deal with the interaction between FPSO and its mooring lines for the resulting motions.

References

Abkowitz, M. A. (1972), “Stability and motion control of ocean vehicles,” MIT Press, Cambridge, MA, 1972.

Alexandrov, M. (1971) "On the dynamics of cables with application to marine use," Marine Technology, vol 8, no 1, pp 84-92, 1971.

Ansari, KA (1980). "Mooring with Multi-component Cable Systems," J Energy Res Tech, vol 102, June, pp 62-69, 1980.

Ansari, KA, and Khan, NU (1986). "The Effect of Cable Dynamics on the Station-Keeping Response of a Moored Offshore Vessel," J. Energy Res Tech, vol 108, March, pp 52-58, 1986.

API RP 2SK, Recommended Practice for Design and Analysis of Station Keeping Systems for Floating Structures, 3rd Edition, October 2005.

Aryawan, I.D., Incecik, A. and Djatmiko, E.B. (2000), “Evaluation of low frequency motions of a turret moored FPSO system and their influence on hull girder loads,” Proceedings International Conference on Offshore Mechanics and Arctic Engineering, ASME, New York, 2000.

Aryawan, I. D., Incecik, A. and Djatmiko, E. B. (1999), “Simple and accurate approach for the prediction of loads and motions of turret moored FPSO vessels,” Proceedings of the 18th International Conference on Offshore Mechanics and Arctic Engineering. ASME, NY, 1999.

Baltrop, N.D.P. (1998), “Floating Structures: a guide for design and analysis” CMPT publication, 1998.

Bernitsas, M. M., Matsuura, J. P. (2005), “Revealing nonlinear dynamics phenomena in mooring due to slowly-varying drift," Proceeding of 24th International Conference on Offshore Mechanics and Arctic Engineering, Halkidiki, Greece, 2001.

Bernitsas, M. M., Matsuura, J. P. and Andersen, T. (2002), “Mooring dynamics phenomena due to slowly-varying wave drift,” Proceedings International Conference on Offshore Mechanics and Arctic Engineering, Oslo, Norway, 2002.

Bernitsas, M. M., Garza-Rios, L. O and Kim, B. K. (1999), “Mooring design based on catastrophes of slow dynamics,” Proceedings of the 8th Offshore Symposium, Texas Section of the Society of Naval Architects and Marine Engineers, Houston, Texas, February 25-26, pp 76-123, 1999.

Bernitsas, M. M. and Kim, B. K. (1988) “Effect of Slow-Drift Loads on Nonlinear Dynamics of Spread Mooring Systems,” Journal of Offshore Mechanics and Arctic Engineering, vol. 120, No. 4, pp 201-211, 1988.

Bernitsas, M. and Matsuura, J. (2004), “Mooring dynamics phenomena due to slowly-varying wave drift,” Journal of Offshore Mechanics and Arctic Engineering, vol. 126, pp 280-286, 2004.

Berteaux, H. O. (1976) “Buoy Engineering,” John Wiley & Sons, 1976.

Bhattacharyya, S. K. and Panneer Selvam, R. (2003), “Parameter identification of large moored floating body under random ocean waves by R-MISO method,” Journal of Offshore Mechanics and Arctic

Engineering, vol. 125, pp 81-86, 2003.

Bhattacharyya, R. (1978), ”Dynamics of Marine Vehicles,” A Willey-Inter Science Publication, 1978.

Blagoveshchensky, S.N. (1962), “Theory of ship motions,” vol. 1, Trans, Dover, 1962.

Boom, W.C. de, (1987) "Turret mooring for tanker based FPSOs," Proc Workshop on Floating Structures & Offshore Operations, Wageningen, Netherlands, pp 143-152, 1987.

Buchner, B. (1998), “A new method for the prediction of non-linear relative wave motions,” Proceedings of the 17th International Conference on Offshore Mechanics and Arctic Engineering. ASME, NY, 1998.

Buchner, B. (1999) "Numerical simulation and model test requirements for deepwater developments," Proc Deep & Ultra Deepwater Offshore Technology, Newcastle upon Tyne, UK, 1999.

Bureau Veritas NI 461 DTO, Quasi-dynamic analysis of mooring systems, Recommended practice, Tentative issue, May 1998.

Bureau Veritas NI 493 DTM, Classification of mooring system for permanent offshore units, Guidance note, June 2004.

Chakrabarti, S. K. (1997), “Deep water floating moored systems and their numerical and physical simulation,” Proc. of the JNOC Workshop, OMAE '97, Yokohama, Japan, pp 147-187, 1997.

Chakrabarti, S.K. (2005), “Handbook of Offshore Engineering,” Elsevier Publication, 2005.

Chakrabarti, S.K. (1987), “Hydrodynamics of offshore structures,” Computational Mechanical Publications Southampton Boston, 1987.

Chakrabarti, S.K. (2002), “The theory and practice of hydrodynamics and vibration,” Offshore Structure Analysis, World Scientific, 2002.

Chan, HS (1992). “Dynamic Structural Responses of a Mono-hull Vessel to Regular Waves,” Int Shipbuilding Progress, vol 39, pp 287-315, 1992.

Chan, H.S. (1993), “Prediction of motion and wave loads of twin-hull ships,” Marine Structures, 6, 75-102, 1993.

Chan, H.S., Atlar, M. and Incecik A. (2002), “Large-amplitude motion responses of a Ro-Ro ship to regular oblique waves in intact and damage conditions,” Journal of Marine Science and Technology, vol. 7, 2002, pp. 91-99, 2002.

Chan, H.S. (2003), “Global wave loads on intact and damaged Ro-Ro ships in regular oblique waves,” Marine Structures, 2003, vol. 16, No. 4, 323-344, 2003.

Chan, H. S. and Ha, T. P. (2008), “Numerical methods for the analysis of mooring systems in deep water,” Proceeding of the International Offshore and Polar Engineering Conference, Vancouver, British Columbia, 2008.

Chung, J. S. and Bernitsas, M. M. (1997), “Hydrodynamic memory effect on stability, bifurcation, and chaos of two-point mooring systems,” Journal of Ship Research, vol. 41, No. 1, pp 26-44, 1997.

Clayton, B. R. and Bishop, R. E. D. (1982) “Marine vehicles,” J. W. Arrowsmith Ltd, Bristol, 1982.

Couliard, P.Y. and Langley, R. S. (2001), “Nonlinear dynamics of deep-water moorings," Proceeding of 20th International Conference on Offshore Mechanics and Arctic Engineering, 2001.

Cozijn, J. L and Bunnik, T. H. (2004), “Coupled mooring analysis for a deep water calm buoy,” Proceedings International Conference on Offshore Mechanics Arctic Engineering, Vancouver, British Columbia, 2004.

Dean, Robert G. (1984)and Dalrymple, Robert A., “Water wave mechanics for engineers and scientists,” Prentice-Hall Inc., 1984.

DNV (1996). Part 6 Chapter 2, Position Mooring (POSMOOR), Rules for Classification of Mobile Offshore Units, Det Norske Veritas, 1996.

DNV (2008). Part 6 Chapter 2, Position Mooring (POSMOOR), Rules for Classification of Mobile Offshore Units, Det Norske Veritas, 2008.

D’Souza, R., Dove, P.G.S., Hervey, D.G. and Hardin, D.J. (1992), “The design and installation of efficient deepwater permanent moorings,” Marine Technology, 29 (1), pp. 25-35, 1992.

Elsimillawy, N. & Miller, N.S. (1986) "Time simulation of ship motions: A guide to the factors degrading dynamic stability," SNAME Trans, vol 94, pp 215-240, 1986.

Faltinsen, O.M. (1990), “Sea loads on ships and offshore structures,” Cambridge University Press, 1990.

Faltinsen, O.M., Kjaerland, O., Liapis, N. and Walderhaug. (1979), “Hydrodynamic analysis of tankers at single-point mooring systems,” Proceedings BOSS '79 Conference, paper 59, pp 117-206, London, 1979.

Floating Production Systems Report, (2000) "Assessment of the outlook for FPSO vessels, production semis, TLPs and spars", International Maritime Associates, Inc. Washington, DC USA, 2000

Fonseca, N. and Guedes Soares, C. (1998), “Time-domain analysis of large-amplitude vertical motions and wave loads,” Journal of Ship Research, vol. 42, No 2, pp 100-113, 1998.

Fonseca, N. and Guedes Soares, C. (1998), “Time-domain analysis of large amplitude vertical motions and wave loads,” J. Ship Res., 42, pp 100-113, 1998.

Fonseca, N. and Guedes Soares, C. (1998), “Nonlinear wave induced response of ships in irregular seas,” Proceedings of the 12th International Conference on Offshore Mechanics and Arctic Engineering. ASME, NY, 1998.

Fossen T. I. and Smogeli, O. N. (2004), “Nonlinear time-domain strip theory formulation for low-speed maneuvering and station-keeping,” Modelling Identification and Control, vol. 25, No. 4, 2004, pp 201-221, 2004.

Garza-Rios, L. O. and Bernitsas, M. M. (1998), “Slow motion dynamics of turret mooring system and its approximation as single point mooring,” Applied Ocean Research, vol. 20, No. 6, 1998.

Guedes Soares, C., Fonseca, N. and Pascoal, R. (2001), “Experimental and numerical study of the motions of a turret moored FPSO in waves,” Proceedings International Conference on Offshore Mechanics and Arctic Engineering, Rio de Janeiro, Brazil, 2001.

Guedes Soares, C. and Schellin, T. E. (1998), “Nonlinear effects on long-term distributions of wave-

induced loads for tankers,"Journal of Offshore Mechanics and Arctic Engineering, vol. 120, no. 2, pp 65-70, 1998.

Guedes, C., Fonseca, N. and Pascoal, R. (2005), "Experimental and numerical study of the motions of a turret moored FPSO in waves," Journal of Offshore Mechanics and Arctic Engineering, vol. 127, pp 197-204, 2005.

H. de Groot., Lenting, A. and Peer, B. (2005), "Weather routing and motion monitoring in heavy transports," Marine Heave Transport & Lift, London, UK, Sept 2005.

Hess, JL, and Smith, AMO (1962). "Calculation of non-lifting potential flow about arbitrary three-dimensional bodies," Douglas Aircraft Company Report No. ES40622, 1962.

Hogben, N. and Standing, R.G. (1974), "Wave loads on large bodies," Proceedings International Symposium Dynamic Marine Vehicles and Structures in Waves, International Mechanics Engineering, 1974.

Hooft, J. P. (1982) "Advanced dynamics of marine structures," Maritime Research Institute Netherlands - Wageningen - The Netherlands, John Wiley & Sons, Inc, 1982.

Incecik, A., Bowers, J., Mould, G. and Yilmaz, O. (1998), "Response-based extreme value analysis of moored offshore structures due to wave, wind and current," Journal of Marine Science and Technology, pp 145-150, 1998.

ISSC, (1985) "9th International Ship and Offshore Structures Congress", Proceedings, Genova, Italy, 1985

ITTC, (1984) "17th International Towing Tank Conference", Proceedings, Göteborg, Sweden, 1984

Jiang, T. and Schellin, T.E. (1990), "Motion prediction of a single-point moored tanker subjected to current, wind and waves,"Journal of Offshore Mechanics and Arctic Engineering, vol. 112, pp 83-90, 1990.

Jordan, D.D. and Smith, P. (1999), "Nonlinear ordinary differential equations - an introduction to dynamical systems," Third edition, Oxford Applied and Engineering Mathematics, Oxford University Press, 1999.

KAIST (1985), "Development of design technology of offshore platforms for offshore oil production," Ministry of Korean Science and Technology, vol. 3, Jacket Structure Design, 1985.

KAIST (1985), "Development of design technology of offshore platforms for offshore oil production," Ministry of Korean Science and Technology, vol. 6, Transportation and Installation, 1985.

Kat, J.O. de & Dercksen, A. (1993) "The influence of spectral wave characteristics on the dynamics of a turret mooring system," 12th Intl Conf Offshore Mechanics & Arctic Engineering, Glasgow, UK, pp 167 - 174, 1993.

Kato, S., Saito, M. and Takase, S. (1994), "Nonlinear response of moored floating structures in random waves and its stochastic analysis," Ship Research Institute, Tokyo, Japan, vol. 31, No. 1, 1994.

Kim, C. H., Frank-S, Chou. and David, Tien. (1980), "Motions and hydrodynamic loads of a ship advancing in oblique waves," SNAME Transactions, vol. 88, 1980, pp. 225-256, 1980.

Kim, M. H. (2004), "Dynamic analysis tool for moored tanker-based FPSO's including large yaw motions," OTRC Industry Consortium, 2004.

Li, X., Yang, J. and Xiao, L. (2006), "Research on motion response of soft yoke mooring FPSO system," Proceeding of the International Offshore and Polar Engineering Conference, San Francisco, California, USA, pp 181-186, 2006.

Liu, Yingzhong and Miao Guoping (1998), "Theory of motion of ships on waves," Shanghai Jiao Tong University Press, 1998.

Liu, F. and Brown, D.T. (1998), "Turret moored floating production system response with varying turret location and wind direction," Proceeding of the 17th International Conference on Offshore Mechanics and Arctic Engineering, ASME, New York, 1998.

Lloyd, A.R.J.M. (1989) "Ship behaviour in rough weather," John Wiley & Sons, 1989.

Low, M.Y. and Langley, R. S. (2006), "A comparison of time domain and frequency domain approaches for the fully coupled analysis of deepwater floating systems," Proceedings International Conference on Offshore Mechanics and Arctic Engineering, 2006.

Low, M.Y. and Langley, R. S. (2006), "Time and frequency domain coupled analysis of deepwater floating production systems" Applied Ocean Research, vol 28, issue 6, pp 371-385, 2006.

Luke, J. C. (1967), "A variational principle for a fluid with a free surface," Journal of Fluid Mechanics, 27, pp 395-397, 1967.

Luo, Y. and Baudic, S. (2006), "Predicting FPSO response using model tests and numerical analysis," Proceedings International Offshore and Polar Engineering Conference, Honolulu, Hawaii, USA, pp 167~174, 2006.

Maruo, H (1960). "The Drift, a Body Floating on Waves," J Ship Research, vol 4, pp 1-10, 1960.

Matsuura, J.P.J. and Bernitsas, M.M. (2004), "Routes to large amplitude motions of mooring systems due to slowly-varying drift," Proceedings of the 23rd International Conference on Offshore Mechanics and Arctic Engineering, Vancouver, Canada, 2004.

Matsuura, J.P.J., Nishimoto, K., Bernitsas, M.M, and Garza-Rios, L.O. (2000), "Comparative Assessment of Hydrodynamic Models in Slow Motion Mooring Dynamics," Journal of Offshore Mechanics and Arctic Engineering, pp 109-117, 2000.

Mei, C. C. (1989), "The applied dynamics of ocean surface waves," vol. 1 of Advanced Series on Ocean Engineering, World Scientific, NJ, 1989.

Morandi, C. (2004), "Marine transportation of large floating production units: Key design aspects," 13th SNAME Offshore Symposium: The Application of Emerging Technologies Offshore, Houston, 2004.

Muga, B. J. and Wilson, J. F. (1970), "Dynamic analysis of ocean structures," Plenum, New York, 1970.

Nakajima, T. (1981) "A Study of the Mooring Dynamics of Various Types by Lumped Mass Method," Ph.D Thesis, Univ. of Tokyo (1981)

Nakajima, T., Motora, S. and Fujino, M. (1982). "On the Dynamic Analysis of Multi-Component

Mooring Lines," Offshore Technology Conference, OTC 4309, pp 105-120, 1982

Nakamura, M., Kajiwara, H. and Inada, M. (2007), "Automatic mooring system for ship," Proceeding of the International Offshore and Polar Engineering Conference, Lisbon, Portugal, pp 1039-1046, 2007.

Newman J. N. (1977), "Marine hydrodynamics," MIT press, 1977.

Newman, JN (1967). "The Drift Force and Moment on Ships in Waves," J Ship Research, vol 11, pp 51-60, 1967.

Newman, J.N. and Sclavounos, P.D. (1988), "The computation of wave loads on large offshore structures," Proceeding International Conference on the Behaviour of Offshore Structures, BOSS88, vol. 2, pp 605-622, 1988.

Newman, JN (1974). "Second Order Slowly-varying Forces on Vessels in Irregular Waves", Proc Int Symp On the Dynamics of Marine Vehicles and Structures in Waves, University College, London, 1974.

Nienhuis IU. (1968), "Simulation of low frequency motions of dynamically positioned offshore structures," vol 7, The Royal Institution of Naval Architects, London, 1968.

Nishimoto, K., Aranha, J.A.P., Matsuura, J.P.J., Kaster, F., Namba, H. and Masetti, I.Q. (1997), "Full scale decay test of a moored tanker : measurement procedure of surge damping," Proceeding of the ASME 16th International Conference on Offshore Mechanics and Arctic Engineering, vol. I-A, Yokohama, Japan, April, pp 81-90, 1997.

Obokata, J. (1987), "On the basic design of single point mooring systems," J. Soc. Naval Arch, pp 183-195, 1987.

Ochi, Michel K. (1998), "Ocean waves." Cambridge University Press, 1998.

Oortmerssen, G. V. (1976), "The motions of a moored ship in waves," Ph.D Thesis, Delft University of Technology, 1976.

Ormberga, H. and Larsenb, K. (1998), "Coupled analysis of floater motion and mooring dynamics for a turret-moored ship" Applied Ocean Research, vol 20, issues 1-2, pp 55-67, 1998.

Panneer Selvam, R. and Bhattacharyya, S. K. (2006), "System identification of a coupled two DOF moored floating body in random ocean waves," Journal of Offshore Mechanics and Arctic Engineering, vol. 128, pp 191-202, 2006.

Patel, M. H. (1989), "Dynamics of offshore structures," Butterworth, 1989.

Patel, M. H. (1991), "Compliant offshore structures," Butterworth Heinemann, 1991.

Pin Yu Chang and Walter D. Pilkey (1973), "Static and Dynamic Analysis of Mooring Lines", vol. 7, no. 1, Hydronautics, 1973.

Pinkster, J.A. (1975) "Low frequency phenomena associated with vessels moored at sea". Soc Petroleum Engineers AIME J, vol 15, no 6, pp 487-494, 1975.

Pinkster, JA (1979). "Mean and Low Frequency Wave Drifting Forces on Floating Structures", Ocean Engineering, vol 6, pp 593-615, 1979.

Pinkster, J.A. and Oortmerssen, G. van (1976), “Computation of first and second order wave forces on bodies oscillation in regular waves,” Proceedings 2nd International Conference Ship Hydrodynamics, Berkeley, 1976.

Pinkster, J.E. & Wichers, J.E.W. (1987) “The statistical properties of low-frequency motions of nonlinearly moored tankers,” Offshore Technology Conference(OTC), 1987.

Prislin, I., Blevins, R. D., and Halkyard, J. E. (1998), "Viscous Damping and Added Mass of Solid Square Plates," Proceedings Offshore Mechanics and Arctic Engineering Conference, Lisbon, Portugal, 1998.

Rao V. Dukkipati, M. Ananda Rao. and Rama Hhat. (2000) "Computer Aided Analysis and Design of Machine Elements" New Age International Ltd., Publishers, pp 122-125, 2000.

Rawson, R. J. and Tupper, E. C. (1983) “Basic ship theory,” vol 1, Longman, 1983.

Sadeghi, K. (2006), “An approximate model for the first and second order dynamic response analysis of truss SPAR platforms,” Proceedings International Conference on Offshore Mechanics Arctic Engineering, Hamburg, Germany, 2006.

Sadeghi, K. (2005), “Classical and approximate methods in the dynamic response analysis of a truss spar in waves,” Ph.D Thesis, Newcastle University, 2005.

Salvesen, N. (1974), “Second-order steady-state forces and moments on surface ships in oblique regular waves,” Proceedings Symposium of Dynamics Marine Vehicle Structure In Waves, IMechE, 1974.

Salvesen, N., Tuck, E.O. and Faltisen, O. (1970), “Ship Motions and Sea Loads,”Trans. Soc. Naval Archit and Mar. Eng., vol. 78, pp 250-287, 1970.

Sandvik P. C. and Ormberg H. (2005), “Dynamic analysis and simulation of offshore marine operations,” Marine Heavy Transport & Lift London, UK, Sept. 2005.

Sarpkaya, T. (1981), “Mechanics of Wave Forces on Offshore Structures”, Van Norstrand Reinhold Company, 1981.

Schellin, TE, Scharrer, M, and Mathies, HG (1982). "Analysis of Vessel Moored in Shallow Unprotected Waters," Offshore Technol. Conf., OTC-4243, 1982.

Senra, S.F., Correa, F.N., Jacob, B.P., Mourelle, M.M., Masetti, I.Q. (2002), “Towards the integration of analysis and design of mooring systems and risers, Part II: Studies on a DICAS system,” Proceedings of the 21st International Conference on Offshore Mechanics and Arctic Engineering, vol. 1, pp. 291–298, 2002.

Simos, A. N., Tannuri, E. A. and Pescc, C. P. (1998), “Dynamics of a turret FPSO system and Hydrodynamic models,” Proceedings of the 17th International Conference on Offshore Mechanics and Arctic Engineering(OMAE), Lisbon, Portugal, 1998.

Skop, R. A. and O'Hara, G. J. (1969), “The Static Equilibrium Configuration of Cable Arrays by Use of the Method of Imaginary Reactions,” NRL-6819, Naval Research Lab., Washington, D.C., 1969.

Sluijs, M. F. van. and Blok, J. J. (1977) "The dynamic behaviour of mooring lines,". Offshore Technology Conference, 1977.

Takatsu, W. and Ikebuchi, T. (2000), “Experimental and Numerical study on deep sea mooring of ocean observation platform,” Proceeding of the Tenth International Offshore and Polar Engineering Conference, Seattle, USA, pp 73-79, 2000.

Tannuri, E. A. and Simos, A. N. (2001), “Directional wave spectrum estimation based on moored FPSO motions,” Proceedings International Conference on Offshore Mechanics Arctic Engineering, Rio de Janeiro, Brazil, 2001.

Tannuri, E. A. and Simos, A. N. (2007), “Directional wave spectrum estimation based on a vessel 1st order motions : field results,” Proceeding of the International Offshore and Polar Engineering Conference, Lisbon, Portugal, pp 1938-1944, 2007.

Thiagarajan, K.P. and Finch, S. (1998), “A preliminary investigation into the effect of turret mooring location on the vertical motions of a FPSO vessel,” Proceedings of the 17th International Conference on Offshore Mechanics and Arctic Engineering, ASME, New York, paper OMAE98-0554, 1998.

Van Oortmessen, G. Pinkster, J.A. and van den Boom, H.J.J. (1986), “Computer simulation of moored ship behaviour," Journal of Waterway, Port, Coastal and Ocean Engineering, vol. 112, No.2, 1986, pp 296-308, 1986.

Veststad, T.M. (1998), “A preliminary investigation into the effect of turret mooring location on the vertical motions of a FPSO vessel,” Proceedings of the 17th International Conference on Offshore Mechanics and Arctic Engineering, ASME, New York, paper OMAE98-0554, 1998.

Walton, J.S. and Polachek, H. (1959), “Calculation of Transient Motions of Submerged Cables”, Mathematics of Computation, vol. xiv, 1959.

Wichers, J. E. W. and Sluijs, M. F. van (1979) "The influence of waves on the low-frequency hydrodynamic coefficients of moored vessels," Offshore Technology Conference, 1979.

Yilmaz, O. and Incecik, A. (1996), “Hydrodynamic design of moored floating platforms,” Marine Structures 9, pp 545-575, 1996.

Yonghe, X. and Runpei, Li. (2005), “A numerical and experimental study on motion and wave load response of very large FPSO in restricted water depth,” Proceedings International Offshore and Polar Engineering Conference, Seoul, Korea, pp 176~181, 2005.

Zambrano, T., MacCready, T., Kiceniuk Jr, T., R. Roddier, D. G. and Cermelli, C.A. (2006), “Dynamic modelling of deepwater offshore wind turbine structures in Gulf of Mexico storm conditions,” Proceedings International Conference on Offshore Mechanics Arctic Engineering, Hamburg, Germany, 2006.

Appendix A
FOURIER TRANSFORM

$$c_0 = |a_0| \tag{A.1}$$

$$c_n = \sqrt{a_n^2 + b_n^2} \tag{A.2}$$

$$a_0 = \frac{1}{2L}\int_0^{2L} g(x)dx \tag{A.3}$$

$$a_n = \frac{1}{L}\int_0^{2L} g(x)\cos\frac{n\pi x}{L}dx \tag{A.4}$$

$$b_n = \frac{1}{L}\int_0^{2L} g(x)\sin\frac{n\pi x}{L}dx \tag{A.5}$$

$$\omega_0 = \frac{\pi}{L} \tag{A.6}$$

$$2L = period \tag{A.7}$$

c_0 is the initial value of the amplitude spectrum and c_n is the harmonic amplitude. a_0 is the Fourier coefficient which is the mean value of the provided time series data. a_n is the cosine component of the Fourier series and b_n is the sine component of the Fourier series. Thus a function, even irregular, can be expressed as the serial sum of the sine and cosine as in Fourier integration. For example, a function f(x), a time series data, can be expressed as the sum of a_0, a_n and b_n term. ω_0 is the frequency in the spectrum.

This Fourier transform can be utilized to transform the time series of motion and line tension into their respective spectra. The amplitude spectrum can be expressed by setting the frequencies $n\omega_0$ on the horizontal axis while the harmonic amplitude c_n is on the vertical axis. The amplitude spectrum is to determine that how much which amplitude of the frequency components contribute for the motion responses and mooring line tensions, and so it is easy to understand that how much a certain frequency component contributes to the time series data.

Appendix B
GEOMETRIC TRANSFORMATION

The position of a mooring line attachment point is transformed to another coordinate system according to the following method for the rotations.

$$Roll: \begin{bmatrix} 1 & 0 & 0 & 0 \\ 0 & \cos\theta & -\sin\theta & 0 \\ 0 & \sin\theta & \cos\theta & 0 \\ 0 & 0 & 0 & 1 \end{bmatrix} \begin{bmatrix} x \\ y \\ z \\ 1 \end{bmatrix} \qquad Yaw: \begin{bmatrix} \cos\theta & -\sin\theta & 0 & 0 \\ \sin\theta & \cos\theta & 0 & 0 \\ 0 & 0 & 1 & 0 \\ 0 & 0 & 0 & 1 \end{bmatrix} \begin{bmatrix} x \\ y \\ z \\ 1 \end{bmatrix} \tag{B.1}$$

$$Pitch: \begin{bmatrix} \cos\theta & 0 & \sin\theta & 0 \\ 0 & 1 & 0 & 0 \\ -\sin\theta & 0 & \cos\theta & 0 \\ 0 & 0 & 0 & 1 \end{bmatrix} \begin{bmatrix} x \\ y \\ z \\ 1 \end{bmatrix} \qquad Translation: \begin{bmatrix} 1 & 0 & 0 & \Delta x \\ 0 & 1 & 0 & \Delta y \\ 0 & 0 & 1 & \Delta z \\ 0 & 0 & 0 & 1 \end{bmatrix} \begin{bmatrix} x \\ y \\ z \\ 1 \end{bmatrix}$$

The transformation is necessary in two methods for all that the required translational (surge, sway, heave) and rotational (roll, pitch, yaw) transformations. The matrix forms of these translations are easy to apply for the change of coordinate system. The motion responses of the FPSO are represented as surge, sway, heave, roll, pitch and yaw with respect to the origin of the global coordinate system. Thus, the translational motions at an attachment point on the turret depend on the behaviour of the FPSO. Therefore, the motions at the attachment point can be made by using these transformation matrices to take into account the FPSO motions in six degrees of freedom.

Appendix C
DRAG COEFFICIENT

The Beam-draught ratio for a rectangular cross-section is introduced as follows (O. M. Faltinsen, 1990) :

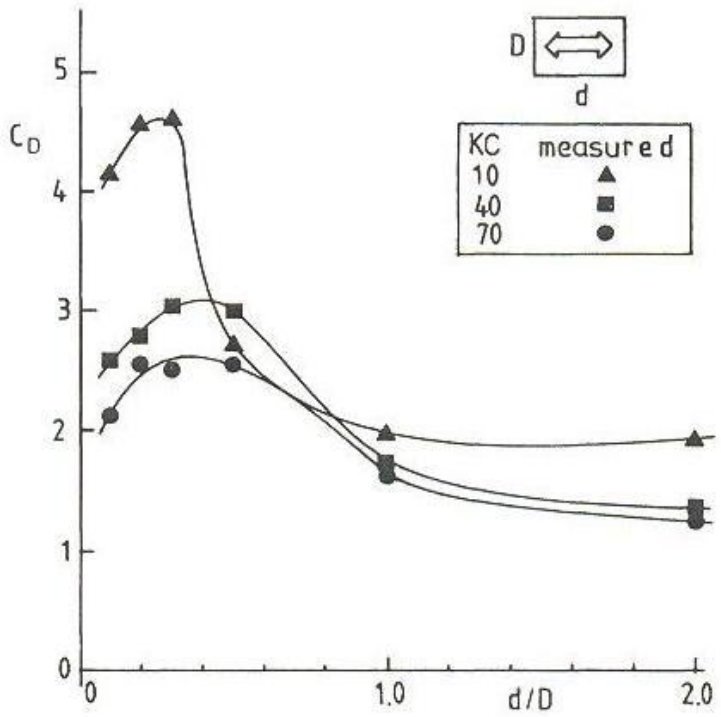

Figure C.1 Drag coefficient

The drag coefficient, $C_{D,}$ as a function of aspect ratio d/D is about Rectangular cylinders with sharp corners. D = Projected width. ($KC = U_M T/D$, U_M = forced harmonic velocity amplitude of the cylinder, T = oscillation period.) (Tanaka et al., 1982.)

The hull envelope below the water line can be approximate by a series of rectangular cross-section forms and for which the drag coefficient, C_D, can be determined.

Appendix D
EXTREME WEATHER CONDITION

Environmental weather conditions are shown the Table D.1 for different locations in the North Sea. A range of H_S and wave periods T_Z, each combination representing a 100 year return period, should be considered in the mooring analyses where low frequency motion is an important part of the total motion (DNV 1996). The schiehallion oil field in latitude 60 degrees North and in longitude 4 degrees West is similar to the Brent location with respect to the features that are the significant wave height of 16m and a mean time period of 14.5sec in the North East Atlantic area.

Table D.1 Extreme weather conditions

Location		*Waves*	
Field	Position	H_S (m)	T_Z – range (s)
Beryl	59°36'N 1°30'E	16	11,0—14,5
Brent	61° 4'N 1°21'E	16	11,0—14,5
Ekofisk	56°32'N 3°15'E	14	10,0—13,5
Frigg	59°54'N 2°8'E	16	11,0—14,5
Maureen	58°5'N 1°45'E	15	10,5—14,0
Statfjord	61°13'N 1°55'E	16	11,0—14,5
Valhall	59°16'N 3°13'E	14	10,0—13,5
Viking	53°30'N 2°20'E	10	8,5—12,5
Haltenbanken	65°7'N 8°E	17	11,0—15,0
Tromsøflaket	71°19'N 20°E	17	11,0—15,0

Appendix E
GENERAL SCHEME

E.1 Time and Frequency Domain Analysis

The general scheme that was developed in this study for undertaking fast-time domain, coupled (motion equation with 6x6 matrix m, c, k coefficients) and frequency domain analyses is as follows:

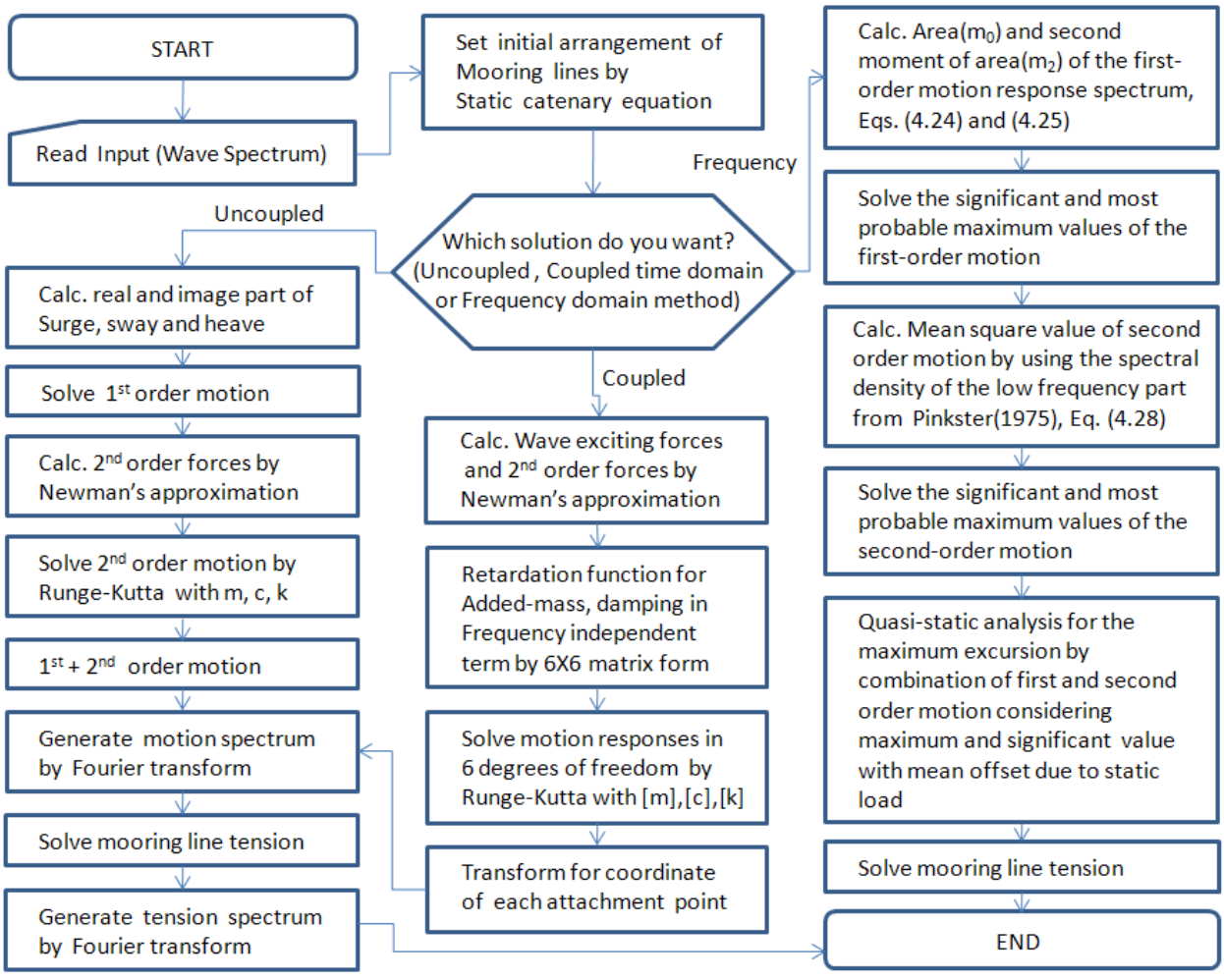

Figure E.1 General scheme for the time and frequency domain analyses

E.2 Mooring Line Dynamics

The computational procedures for solving the dynamic tensions in the mooring lines are as follows, in a general scheme and with regard to the time domain analysis:

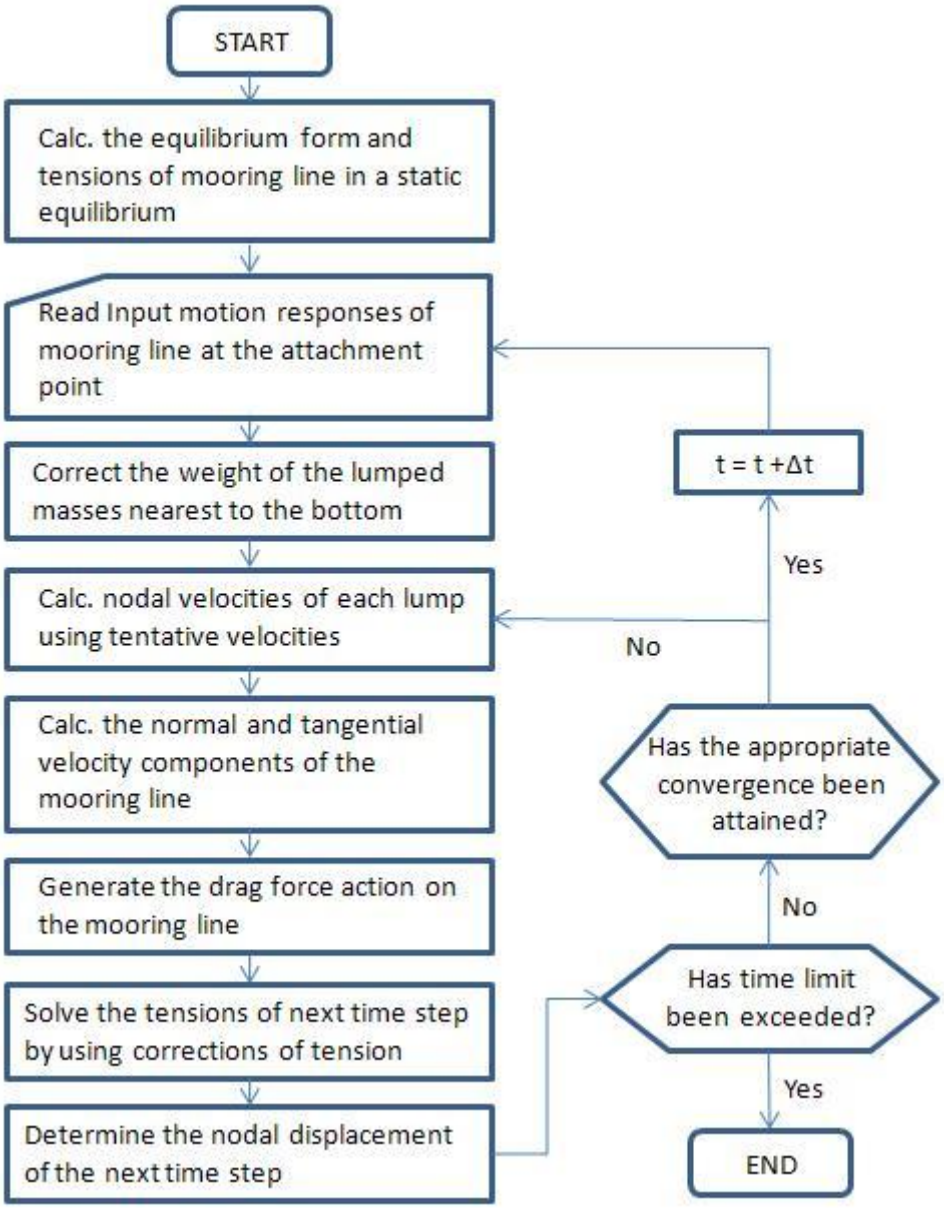

Figure E.2 General scheme for mooring line dynamics

Appendix F
HYDRODYNAMIC FORCES AND COEFFICIENTS

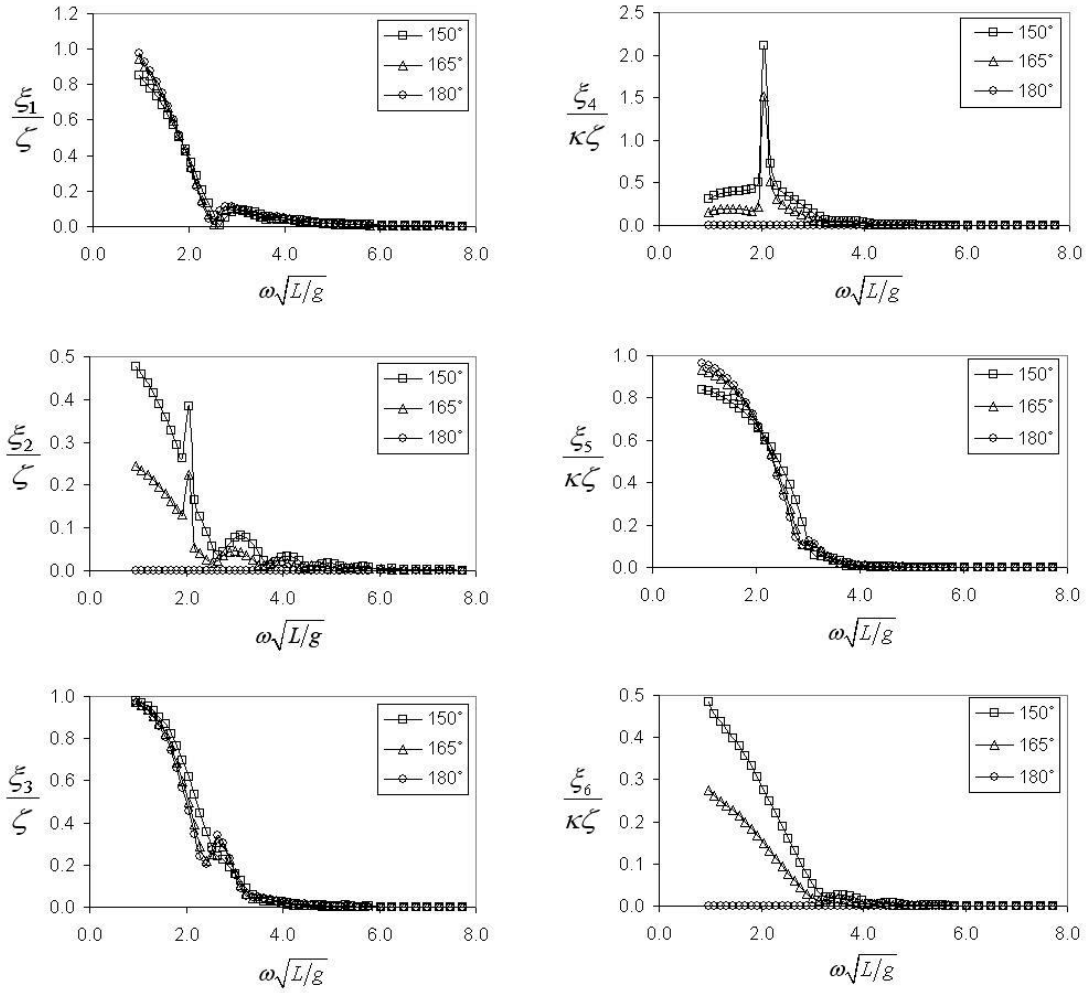

Figure F.1 MTA (Motion RAO)

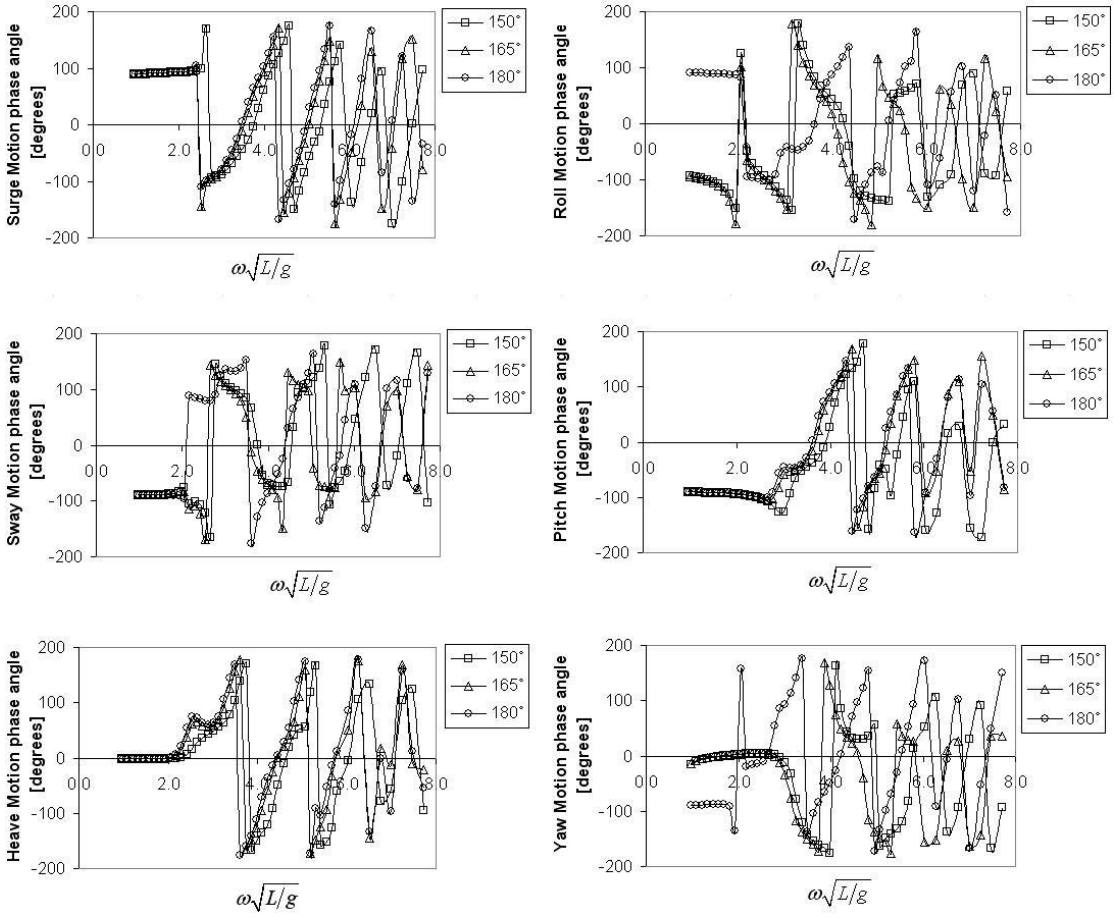

Figure F.2 MTP (Motion phase angle)

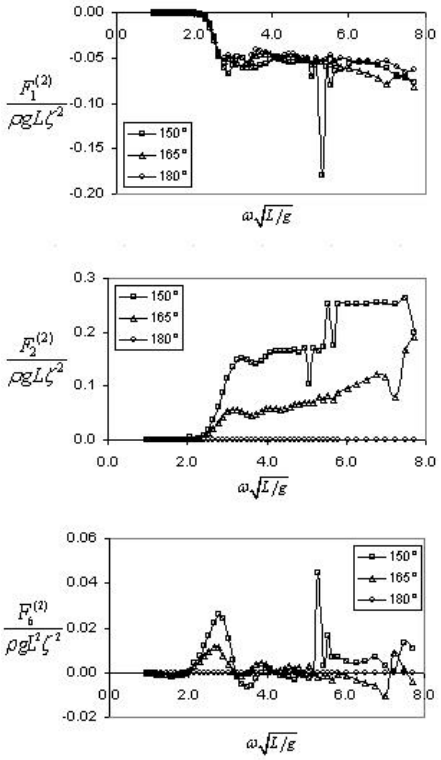

Figure F.3 MSF (Mean 2nd order force)

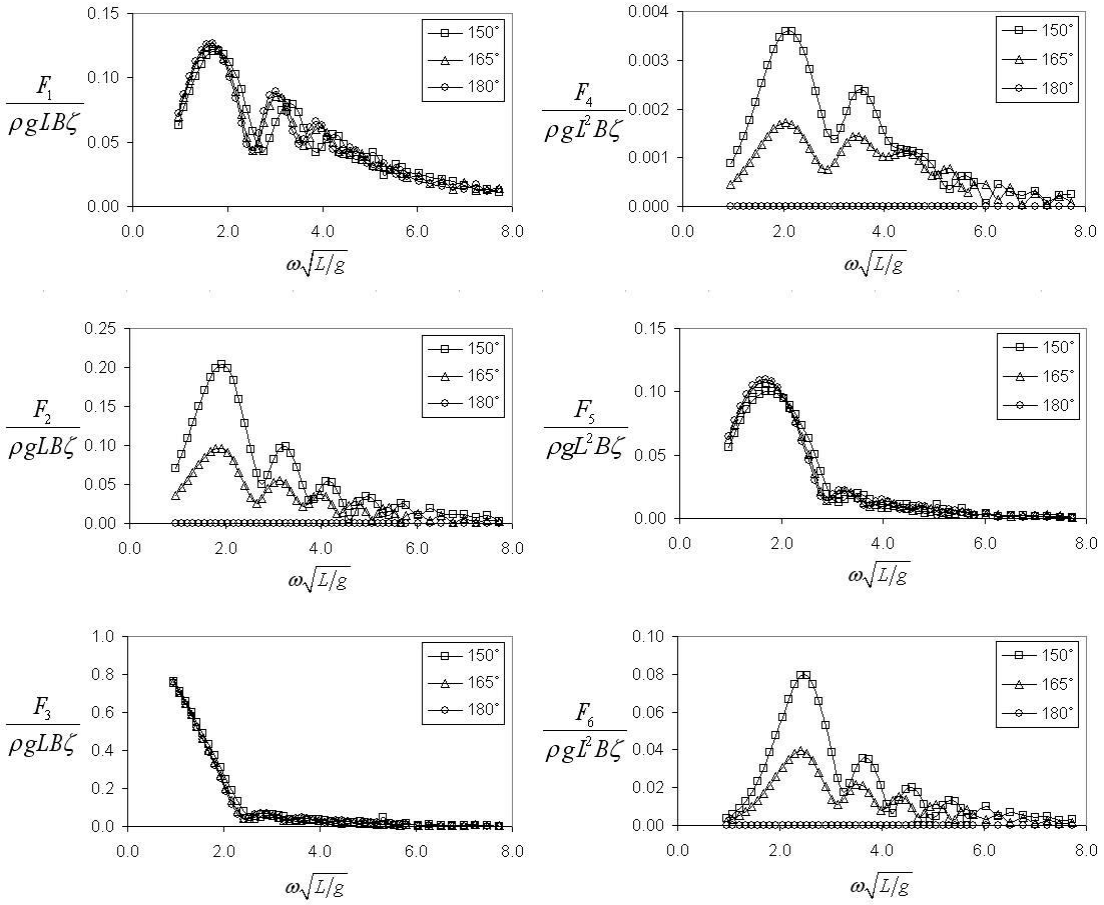

Figure F.4 WEF (Wave exciting force)

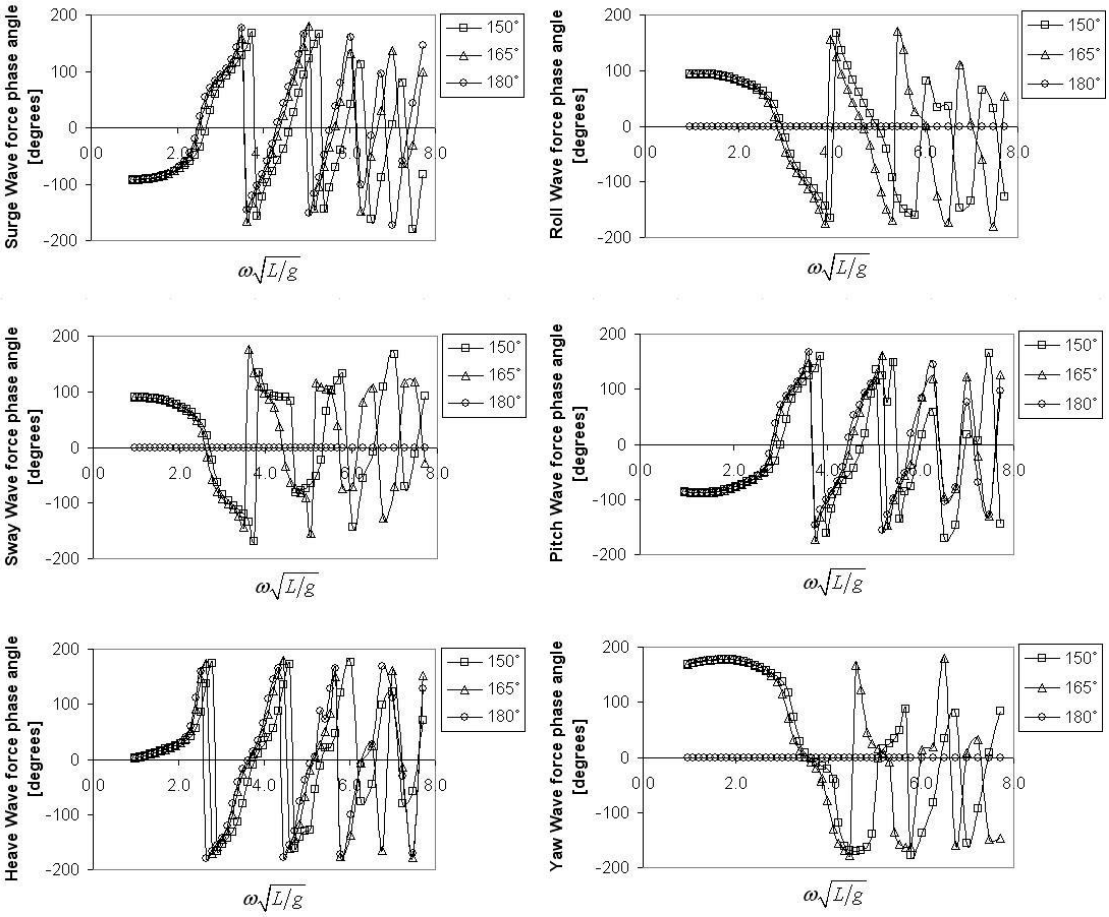

Figure F.5 WEP (Wave exciting phase angle)

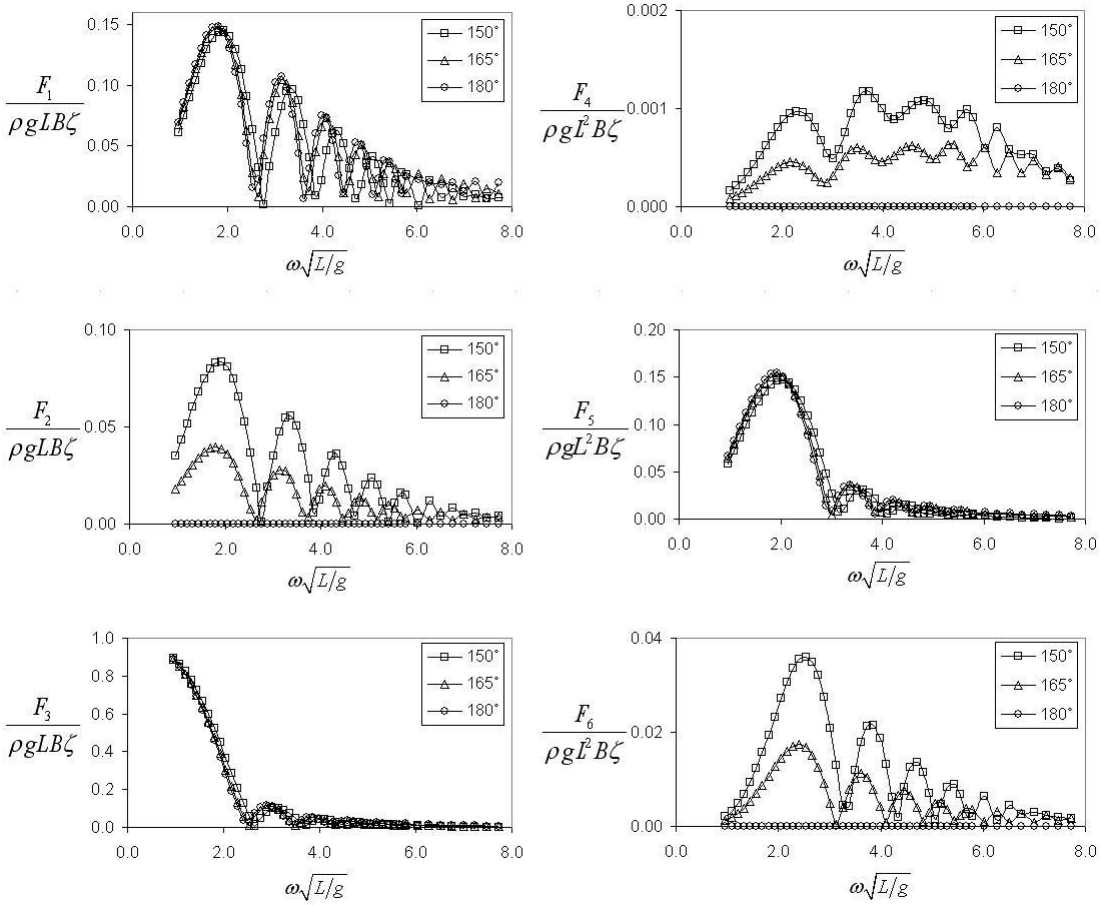

Figure F.6 FKF (Froude-Krylov force)

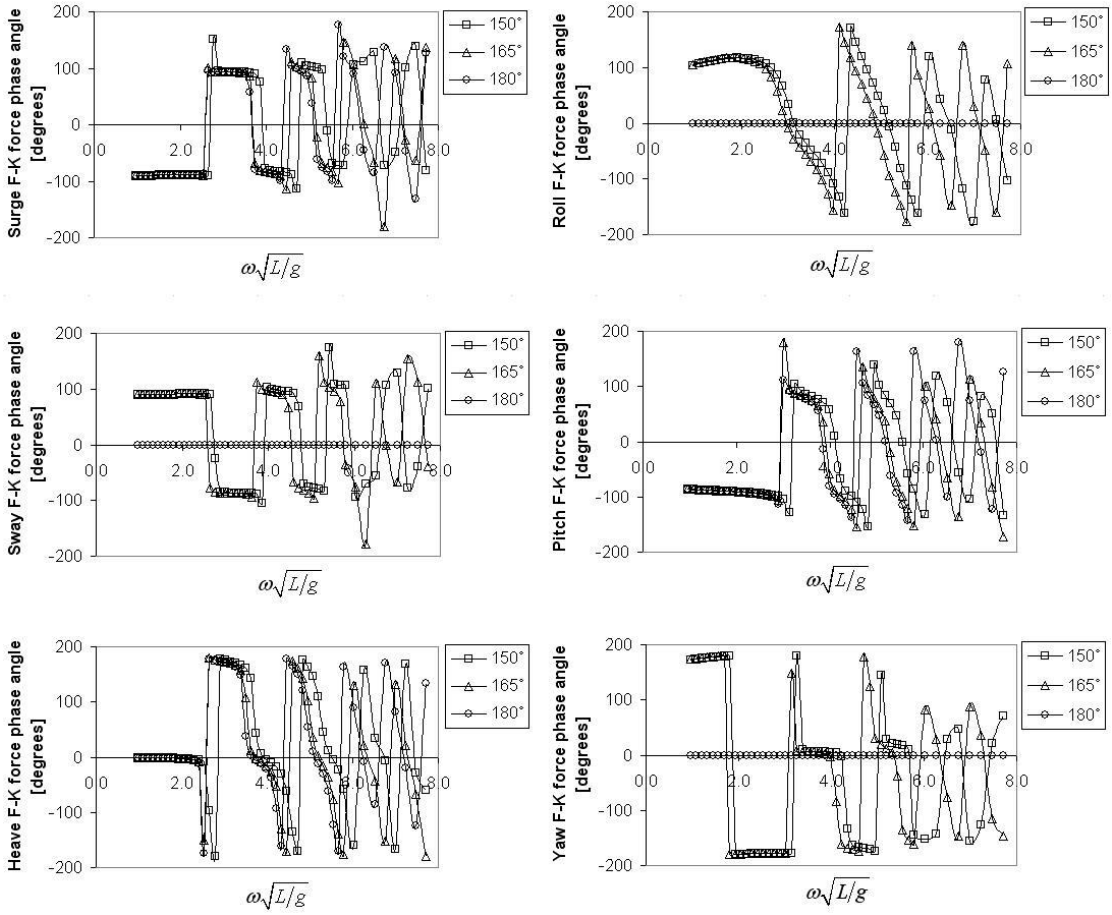

Figure F.7 PKP (Froude-Krylov phase angle)

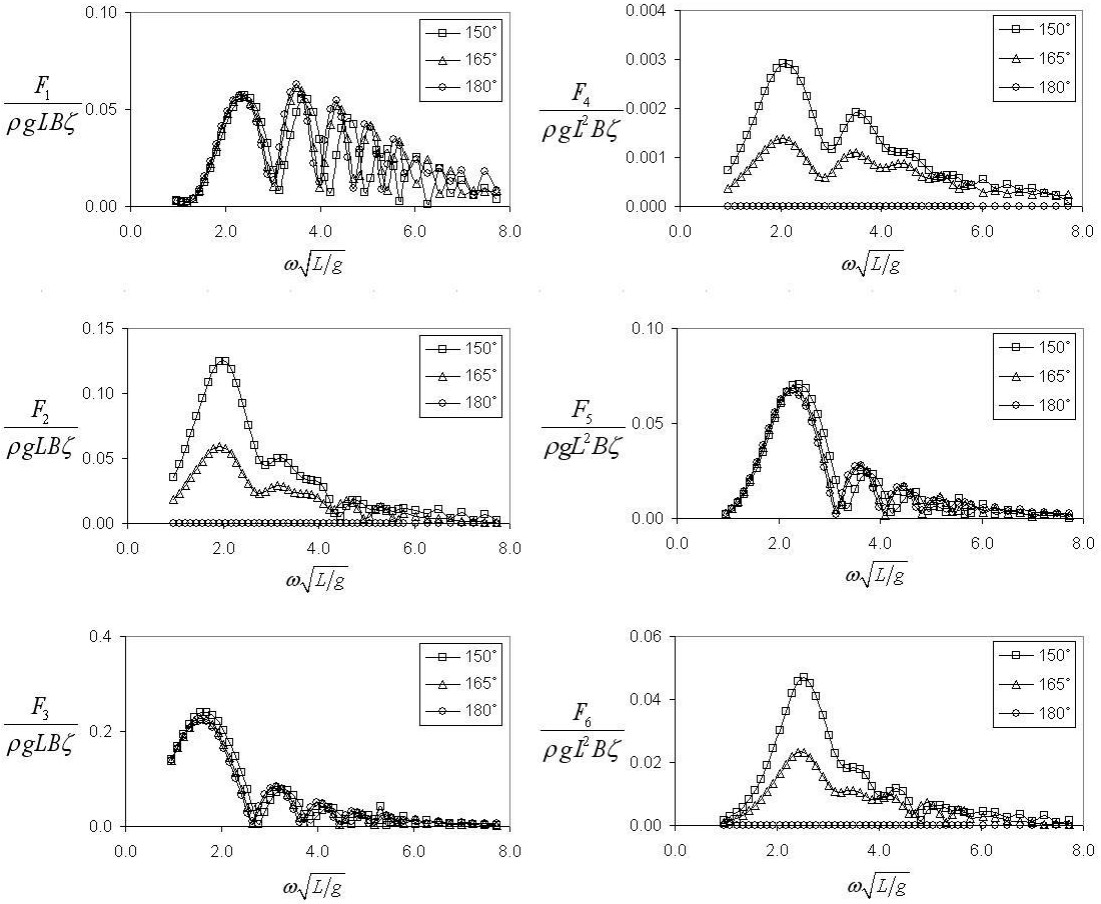

Figure F.8 DFF (Diffraction force)

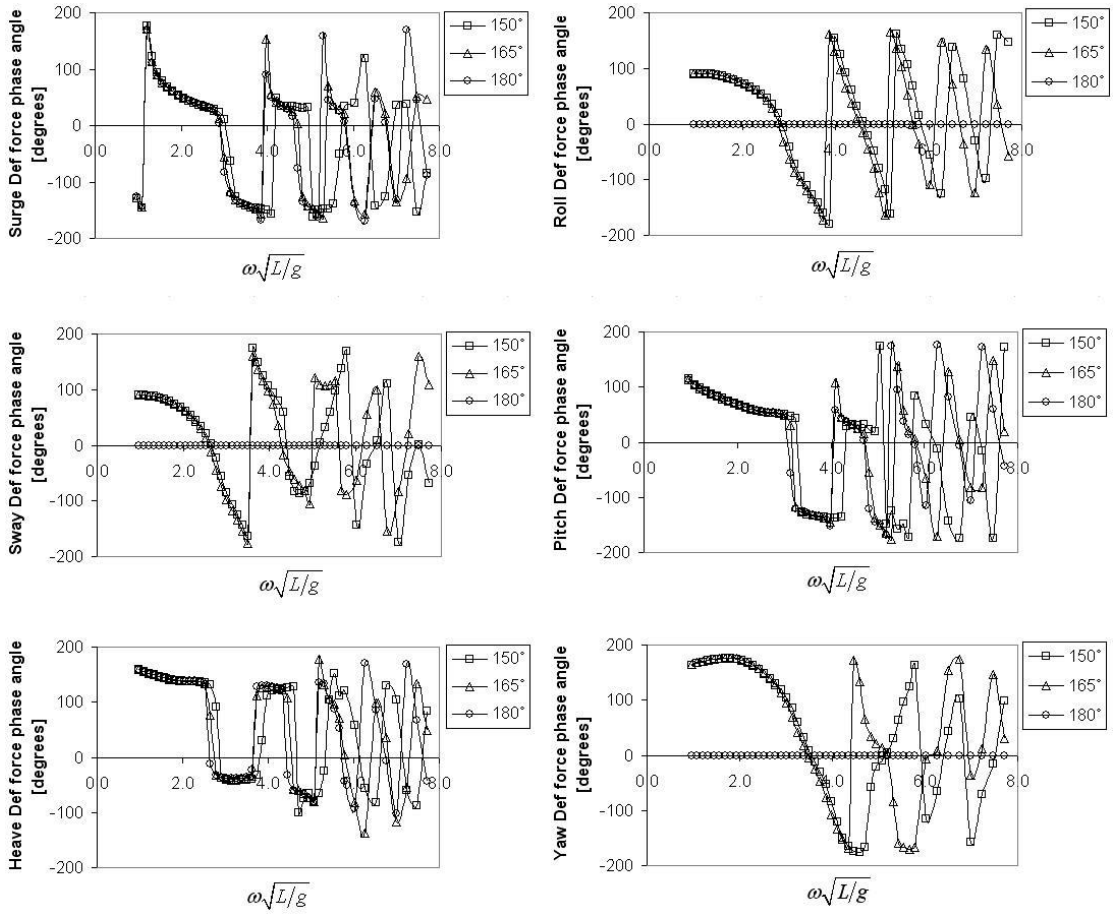

Figure F.9 DFP (Diffraction force phase angle)

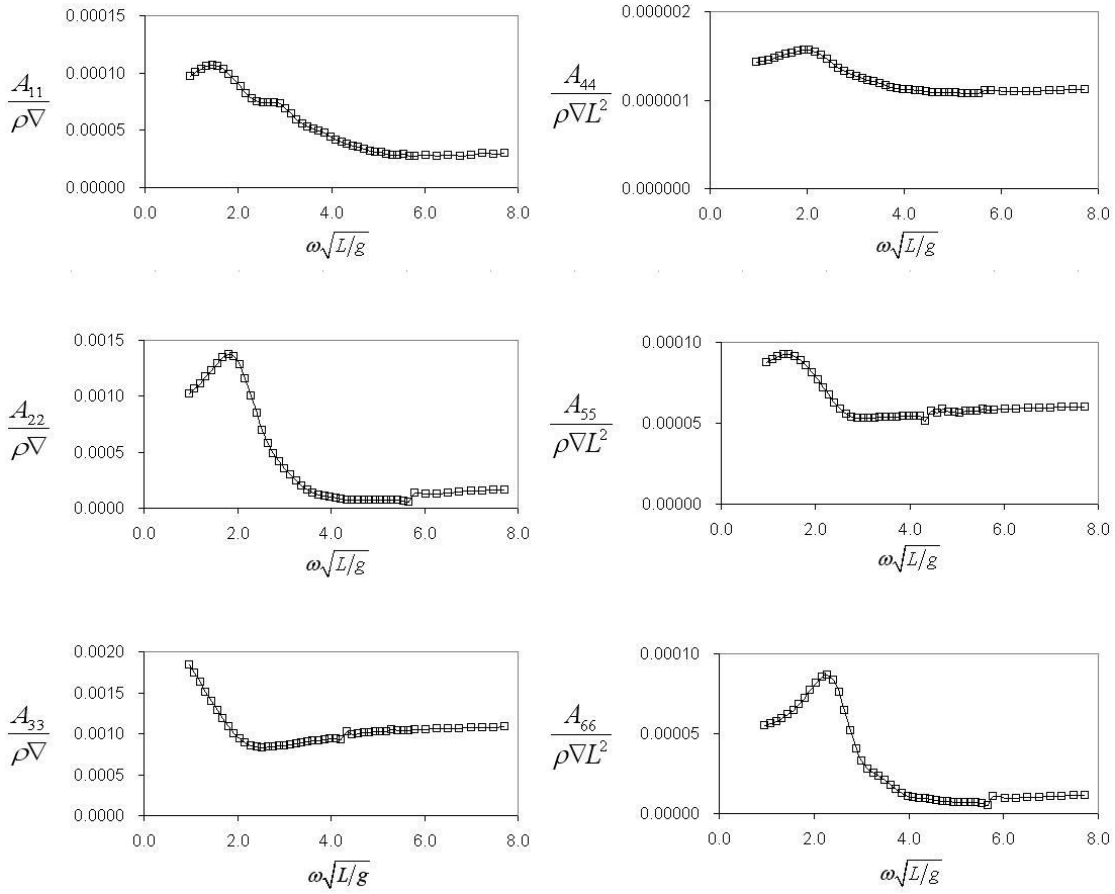

Figure F.10 AMS (Added mass)

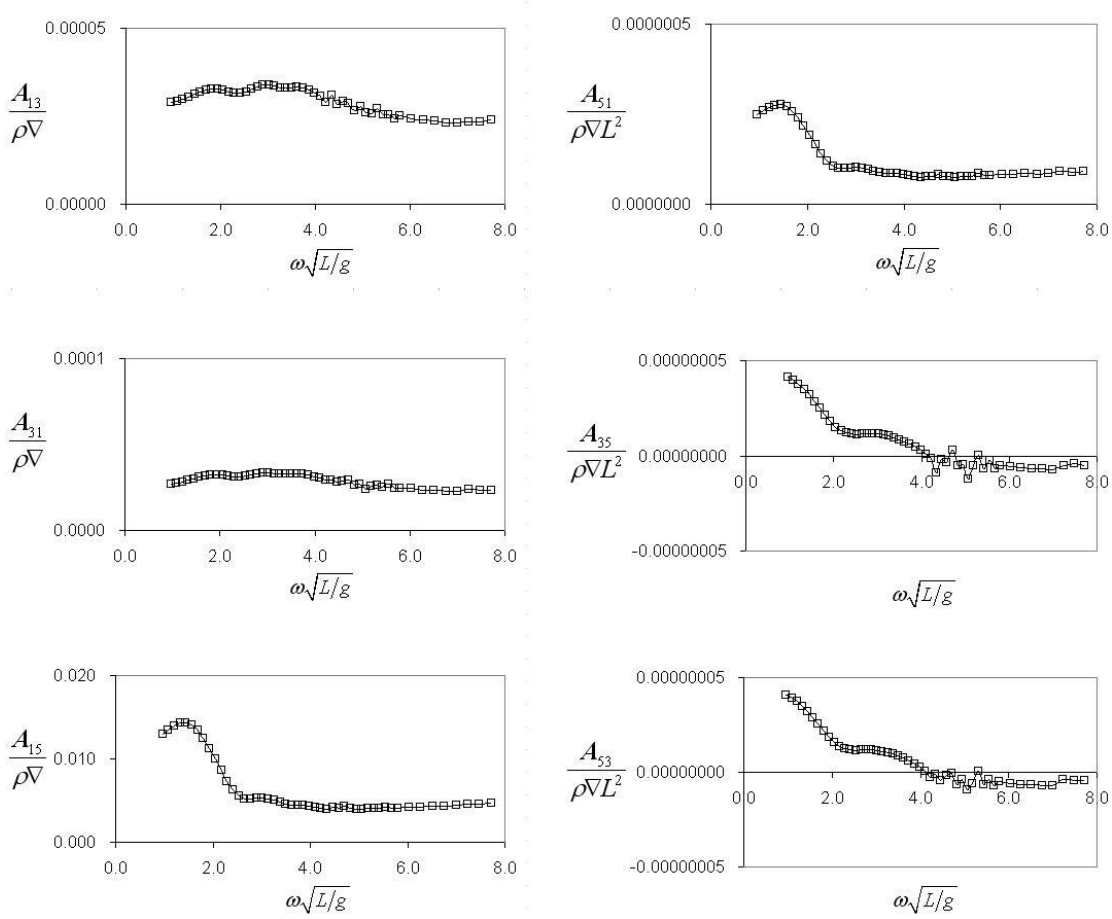

Figure F.11 (Coupled added mass)

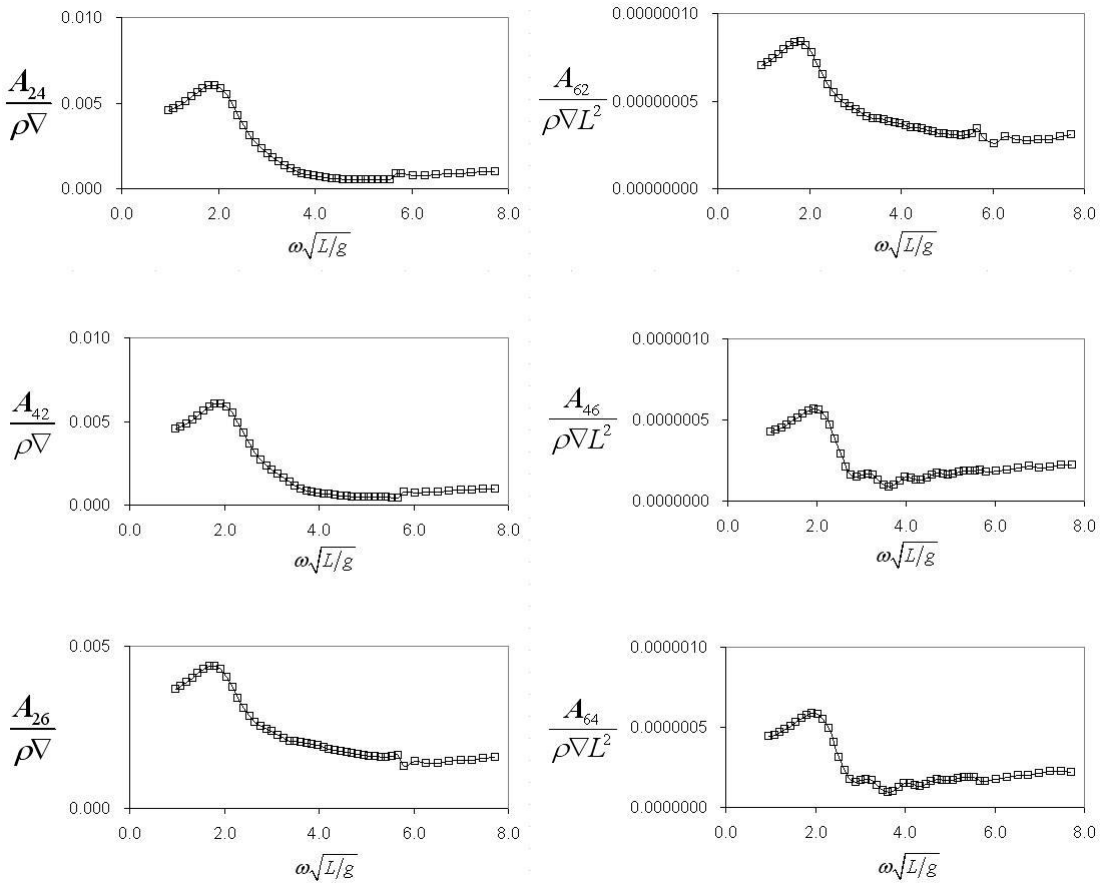

Figure F.12 (Coupled added mass) - Additional

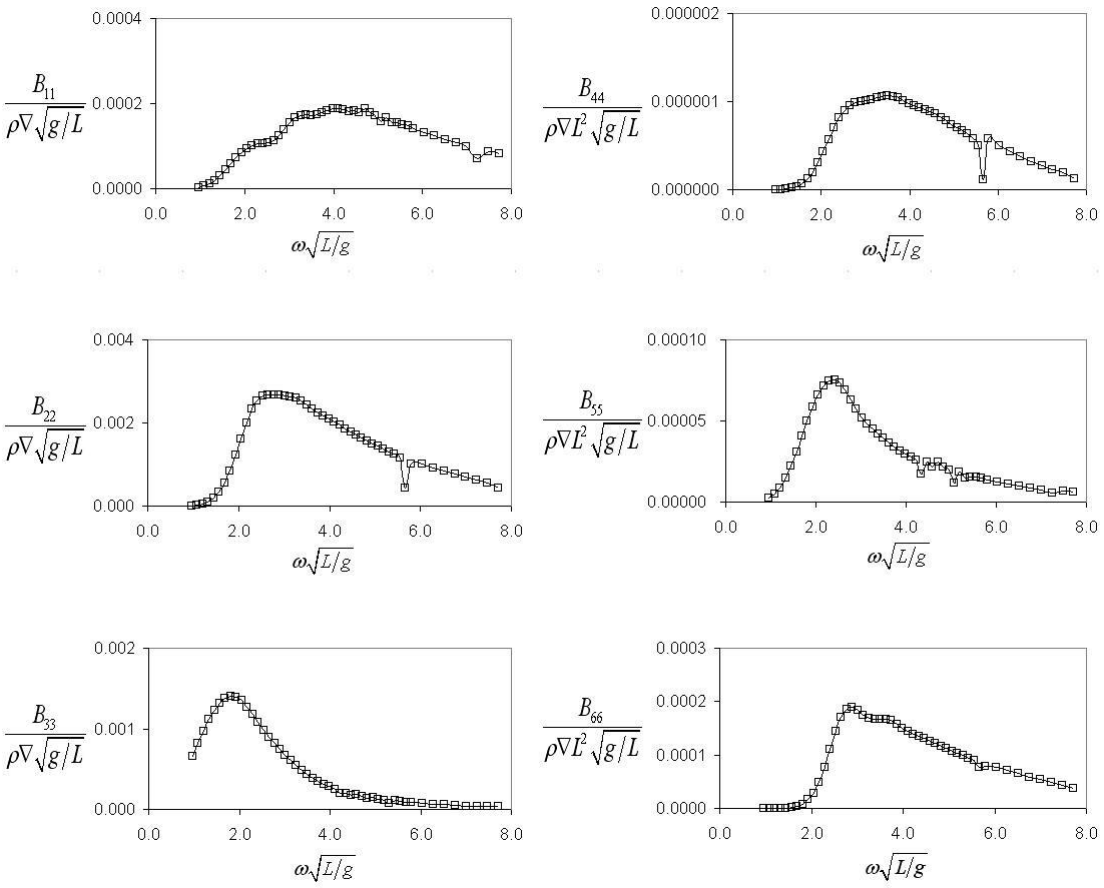

Figure F.13 DMP (Damping)

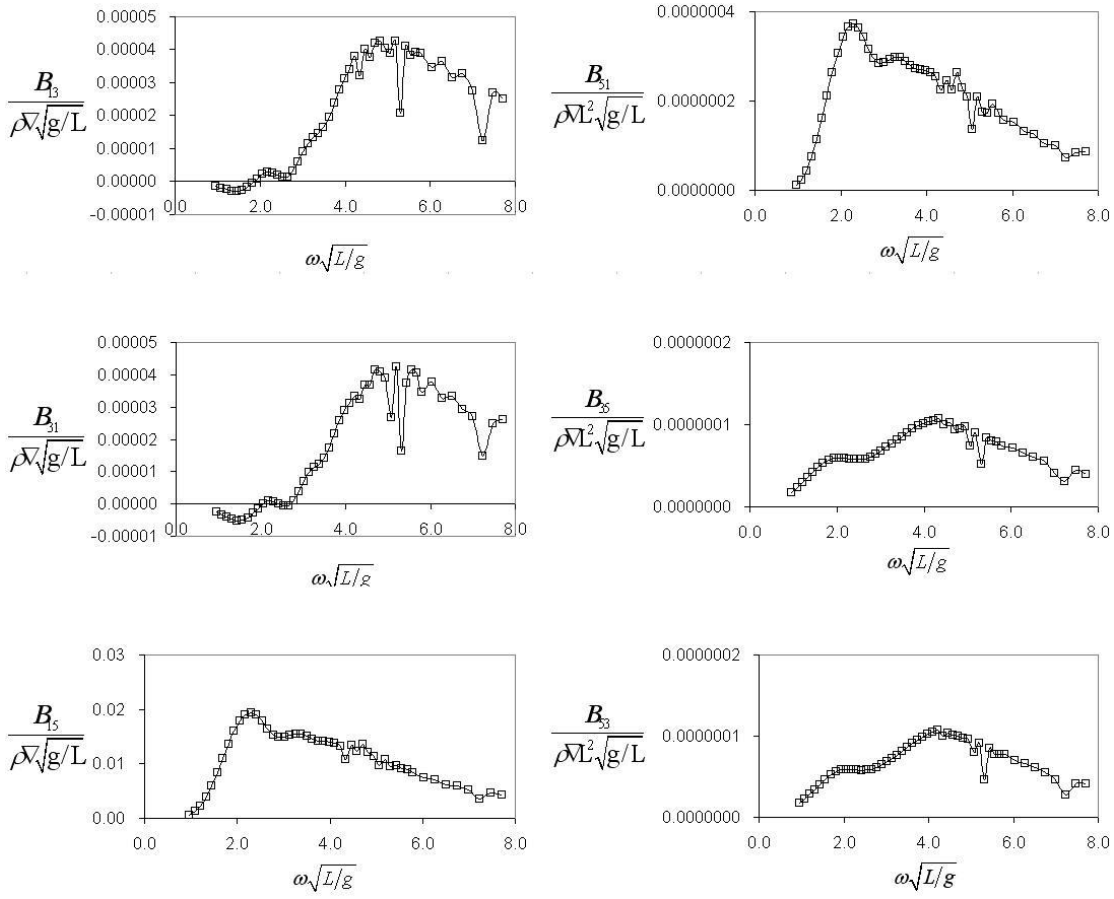

Figure F.14 (Coupled damping)

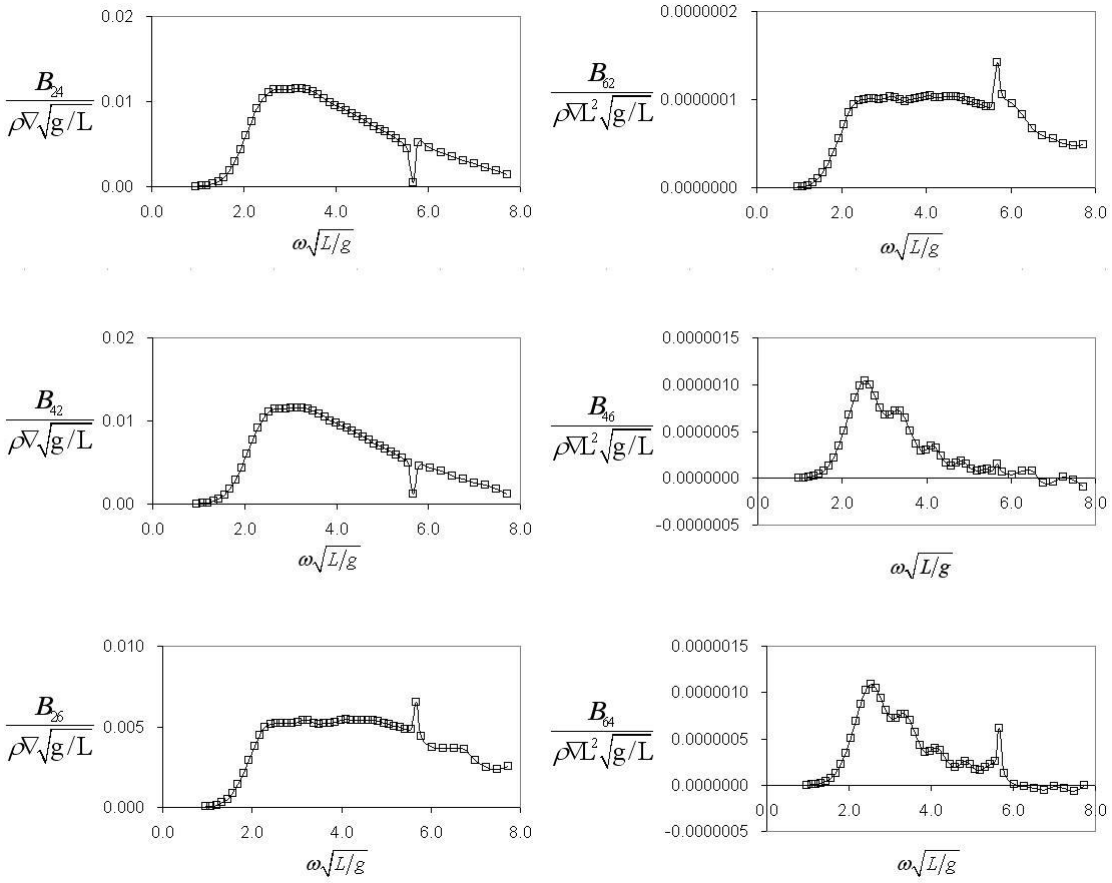

Figure F.15 (Coupled damping) - Additional

Appendix G
POSITION MOORING

The quasi-static analysis for a mooring system is introduced as following theory given by POSMOOR (DNV, POSITION MOORING, PART6 CHAPTER2) :

G.1 Introduction

The general requirements for a spread point mooring system are to be installed on the FPSO which is a ship-shaped vessel relying on a catenary mooring system for station keeping. Design decisions are made for ensuring the reliability and safety of the mooring system when waves are acting on the FPSO. The equilibrium position is assumed when the static environmental force is equal to the collective restoring force of the mooring system. The waves are assumed to have a return period of 100 years at the operational site and the wave frequency motion is considered as a linearly-excited motion mainly in the wave frequency range of the significant wave energy. The necessary requirements are environmental induced loads and motions of the unit in design conditions and the resulting corresponding restoring forces and maximum line tensions are determined. Where low frequency motion is an important part of the total motion, a range of significant wave heights and wave periods, each combination representing a 100 year return period, should be considered in the mooring analysis. Wave drift forces can be calculated according to recognized theory (e.g. diffraction theory, Newman’s approximation) or based on model testing but is not to be taken for a period less than 3 hours. High-frequency motions of the unit are also can be determined by recognized theory or model testing (Rules for Classification of Mobile Offshore Units by DNV).

G.2 First Order Motion

The first-order motion is as follows :

$$X_{HF}^{\max} = \sigma_{WF}\sqrt{2\ln N} \quad \text{(G.1)}$$

Where,

$X_{HF}^{\max}$ = the probable largest wave frequency motion response

σ_{WF} = standard deviation of wave frequency motion response

$N = t/T_Z$ (t is the specified storm duration in seconds and is to be at least 3 hours.

T_Z is the zero up-crossing wave period.

G.3 Low Frequency Motion

Stansberg's distribution method is used for the most probable largest low frequency(LF) motion, and given by :

$$X_{LF}^{\max} = \sigma_{LF} A(\ln N + B) \quad \text{(G.2)}$$

σ_{LF} = standard variation of low frequency motion response

$$A = \frac{2\sqrt{M}}{M+1} \quad \text{(G.3)}$$

$$B = \left(\frac{(M-1)}{M+1}\right)(0.3M - 0.5) \quad \text{(G.4)}$$

$$N = t/T_{LF} \quad \text{(G.5)}$$

(Specified storm duration in seconds / T_{LF} resonance period of the low frequency motion)

The M is given in the case that the resonance period is 100-150 seconds in Table G.1.

Table G.1 M value relating to critical damping

M	% critical damping
13	9
7.5	14
4.5	21

The critical damping can be determined by $2\sqrt{(M+m)k}$.

where,

m = unit mass including added mass in kg

k = overall mooring system stiffness in N/m taken at the vessel's mean position

A logarithmic distribution is shown by a conservative approach :

$$X_{LF}^{\max} = \sigma_{LF}\sqrt{\ln N} \tag{G.6}$$

The damping coefficient is less than 5% in the case of a weakly damped system.

G.4 Quasi-Static Position

Mooring system analysis is undertaken as follows with the assumption that the maximum excursion may be obtained by combination of second order motion with the first order wave induced motion as given Eqs. (G.7) and (G.8) :

$$X_{TOT} = X_{mean} + X_{LF}^{\max} + X_{WF}^{sign} \quad when,\ X_{LF}^{\max} > X_{WF}^{\max} \tag{G.7}$$

$$X_{TOT} = X_{mean} + X_{WF}^{\max} + X_{LF}^{sign} \quad when,\ X_{LF}^{\max} < X_{WF}^{\max} \tag{G.8}$$

where,

X_{TOT} = quasi-static position of the unit at which the line tensions are calculated

X_{mean} = mean offset (equilibrium position) due to quasi-static loads caused by waves

$X_{LF}^{\max}$ = maximum low frequency motion from waves

$X_{WF}^{\max}$ = maximum wave frequency motion

X_{LF}^{sign} = significant low frequency motion from waves

X_{WF}^{sign} = significant wave frequency motion

The maximum value of the motion can be found from the combination with wave and low frequency motions in the extreme condition for 3 hours of continuous storm exposure.

In the quasi-static analysis, the maximum excursions depend on the stiffness of the lines and are related to the tensions.

The generation of the irregular waves are made from the wave spectrum having the characteristics of the North East Atlantic extreme sea state for the period of 3 hours covering long term analysis. In a long term mooring analysis that is to be taken to be the required operating lifetime of the FPSO installation, it is recommended that the process is to generate a time series of the motions (6 DOF) for at least 3 hours to be used in the analysis of the dynamic mooring line tensions. The process is extrapolated from a storm exposure condition (e.g. 3 hours) to the required design life time with the significant wave height and mean time period, and thus these combinations represents a 100 year return period. An extreme weather condition can thus be determined by considering in the mooring analysis from short term 3 hours to the lifetime in a specified number of years.

$$X_{TOT} = \tilde{X}_{LF} + X_{HF}^{\max} \tag{G.9}$$

Where,

$\tilde{X}_{LF}$ is the quasi-static offset

$X_{HF}^{\max}$ is maximum high frequency motion

X_{TOT} is the total excursion of the line

WEB REFERENCE LIST

http://www.offshore-technology.com/projects/northatlantic_gallery.html

http://www.offshore-technology.com/contractors/installation/gallery.html

http://www.offshore-technology.com/projects/schiehallion/

http://www.ramnas.com/scripts/dimensions.php

http://www.gasandoil.com/goc/company/cne80566.htm

http://www.offshore247.com/news/art.aspx?id=15125

http://www.radarpages.co.uk/oral/dbarrett/schiehallion.htm

http://www.marin.nl/web/Ships-Structures/Merchant-vessel-Work-boat/Shuttle-Tankers.htm

http://www.bp.com/liveassets/bp_internet/globalbp/STAGING/global_assets/downloads/U/uk_asset_schiehallion.pdf